UNIVERSITAT POLITÈCNICA
DE CATALUNYA
BARCELONATECH

PhD Thesis

Virtually Synchronous Power Plant Control

Andrés Tarrasó

Terrassa (Barcelona) February 2022

Virtually Synchronous Power Plant Control

Author:

Andrés Tarrasó Martínez

Supervisor:

Dr. Jose Ignacio Candela

Dr. Joan Rocabert Delgado

Disertation submitted to the PhD Doctorate Office of the Universitat Politecnica de Catalunya in partial fulfillment of the requirements for the degree of Doctor of Philosophy by the

UNIVERSITAT POLITÈCNICA DE CATALUNYA

UNIVERSIDAD DE SEVILLA

UNIVERSIDAD DE MALAGA

UNIVERISDAD DEL PAIS VASCO/EUSKAL ERRIKO UNIBERTSITATEA

Joint Doctoral Programme in Electric Energy Systems

FEBRUARY 2022

Virtually Synchronous Power Plant Control

Printed in Catalunya by the DEE-UPC
June 2021

UNIVERSITAT POLIT´ECNICA DE CATALUNYA (UPC)

Electrical Engineering Department (DEE)
Research Center on Renewable Electrical Energy Systems (SEER)
Gaia Building, 2nd floor
Rambla de Sant Nebridi, 22
08222 Terrassa, Barcelona, Spain.

Project: R+D+I competititu

FlexiGRID

RTI2018-100921-B-C21

Project: TSO-DSO-Consumer INTERFACE aRchitecture to provide innovative grid services for an efficient power system -INTERRFACE (http://www.interrface.eu/)

GA nº 824330

Research Project: This work was supported in part by the European Commission under Project FLEXITRANSTORE-H2020-LCE-2016-2017-SGS-774407.

Those who search for different results, do not always follow the same path.

Acknowledgement

First of all, I would like to thank my supervisor, Prof. Ignacio Candela for his endless support in my research. His critical thinking challenged my work in every step of the way. I can only be grateful, as his constant curiosity and enthusiasm towards my work kept me motivated to develop new ideas. I only hope that someday I will be able to match his immense knowledge.

A paragraph is not enough to express my deepest gratitude to Prof. Álvaro Luna. He helped me, taught me, and offered his support regardless of the situation. He always found a way to encourage me, make me laugh, and give me the motivation I needed to continue pursuing the PhD.

Further on, I have to thank Prof. Pedro Rodriguez for his guidance during my PhD at SEER. He made me grow as a professional and, most importantly, as a person. Giving me opportunities that I was not expecting and believing in me, and my knowledge, from the very beginning. Also, thanks to Prof. Joan Rocabert who designed and built most of the equipment I used throughout my PhD at SEER. Without all his work, I could not have tested all the crazy control ideas I showed him.

I also want to thank all my teammates in the lab, especially Borja Garcia, with whom I shared most of my time during my research. Thank you for all the spiritual guidance you gave me on the way, especially in the hardest times. It made me realize what is truly important in life, and I could never thank you enough for that. I would like to express as well my deepest appreciation to my friend Ngoc Bao Lai. Even though we rarely see each other, his endless support and encouragement kept me going throughout all these years of research.

To my family and friends, who have supported me through all these years. It has been a tough journey but as it happens to all paths, it eventually comes to an end. I learned that true happiness cannot be achieved unless you are surrounded by those who appreciate you, Cristian, Marc, Roger, Sergio, Jesus, Victor, Gemma, Cristina, I thank you for making everyday enjoyable in the office.

I cannot end this section without acknowledging my brother, Jaime. I know you did your best to fight against my poor wrting skills, my fundamental lack, of understanding on how, commas work, and my special way of mixing ideas in the same grid-following.

Abstract

During the last century, the electrical energy infrastructures have been governed by synchronous generators, producing electrical energy to the vast majority of the population worldwide. However, power systems are no longer what they used to be. During the last two decades of this new millennium the classical, centralized and hierarchical networks have experienced an intense integration of renewable energy sources, mainly wind and solar, thanks also to the evolution and development of power conversion and power electronics industry. Although the current electrical system was designed to have a core of generation power plants, responsible of producing the necessary energy to supply end users and a clear power flow, divided mainly into transmission and distribution networks, as well as scalable consumers connected at different levels, this scenario has dramatically changed with the addition of renewable generation units. The massive installation of wind and solar farms, connected at medium voltage networks, as well as the proliferation of small distributed generators interfaced by power converters in low voltage systems is changing the paradigm of energy generation, distribution and consumption.

Despite the feasibility of this integration in the existing electrical network, the addition of these distributed generators made grid operators face new challenges, especially considering the stochastic profile of such energy producers. Furthermore, the replacement of traditional generation units for renewable energy sources has harmed the stability and the reliable response during grid contingencies. In order to cope with the difficult task of operating the electrical network, transmission system operators have increased the requirements and modified the grid codes for the newly integrated devices.

In an effort to enable a more natural behavior of the renewable systems into the electrical grid, advanced control strategies were presented in the literature to emulate the behavior of traditional synchronous generators. These approaches focused mainly on the power converter relying on their local measurement points to resemble the operation of a traditional generating unit. However, the integration of those units into bigger systems, such as power plants, is still not clear as the effect of accumulating hundreds or thousands of units has not been properly addressed. In this regard, the work of this thesis deals with the study of the so-called virtual synchronous machine (VSM) in three control layers. Furthermore, an in-depth analysis of the general structure used for the different virtual synchronous machine approaches is presented, which constitutes the base implementation tree for all existent strategies of virtual synchronous

generation. In a first stage, the most inner control loop is studied and analyzed regarding the current control on the power converter. This internal regulator is in charge of the current injection and the tracking of all external power reference. Afterward, the synchronous control is oriented to the device, where the generating unit relies on its local measurements to emulate a synchronous machine in the power converter. In this regard, a sensorless approach to the virtual synchronous machine is introduced, increasing the stability of the power converter and reducing the voltage measurements used. Finally, the model of the synchronous control is extrapolated into a power plant control layer to be able to regulate multiple units in a coordinated manner, thus emulating the behavior of a unique synchronous machine. In this regard, the local measurements are not used for the emulation of the virtual machine, but they are switched to PCC measurements, allowing to set the desired dynamic response at the power plant level.

Contents

List of Figures

List of Tables

Nomenclature

AC	Alternating current.
ACCB	ac circuit breaker.
AC/DC	ac to dc conversion.
ANN	Artificial neural network.
CB	Circuit breaker.
CT	Current transducer.
DC	Direct current.
DC/AC	dc to ac conversion.
DCCB	dc circuit breaker.
DG	Distributed generator.
HIL	Gardware in the loop.
Inst.	Instantaneously.
MRA	Multi-resolution analysis.
MVDC	Medium-voltage dc.
O/C	Over current.
PCC	Point of common coupling.
PG	Pole to ground.
PP	Pole to pole.
PV	Photovoltaic.
RES	Renewable energy system.
SSCB	Solid-state circuit breaker.
TMD	Time margin of the differential-based backup zone.
VSC	Voltage source converter.

Chapter 1. Introduction

During the last years, energy systems around the globe have been transitioning towards a more sustainable and greener scenario, based on the use of renewable energy sources. In this journey, that should bring mankind to a more decarbonized and sustainable energy system, the creation of large power plants using renewable energies is of great importance. These plants should be a trustable alternative to the traditional generation plants, which are still responsible for covering the vast majority of the energy demand, based most of them on fossil fuels. Nevertheless, the naked truth is that traditional units offer a higher reliability and a larger generation capacity in front of renewables, which are tight by the stochastic and variability of the green resources themselves.

No matter these barriers, the evolution towards a generation system with a higher proportion of non-traditional energy sources, such as solar or wind power, has been very important in the last two decades. Just to provide some facts, the installation of renewable energy based plants was beyond 200 gigawatts (GW) in 2019 [1]. Wind and solar energy have become two of the most installed and cost-competitive energies for power plant integrations all around the world, where wind power has reached a 93GW of installed power capacity in 2020, representing a 53% increase in respect to the previous year, whereas around 115GW of solar PV was integrated worldwide in 2019. In this regard, the evolution of renewable energy towards its integration into the electrical power system has been increasing, especially during the last few years where 32 different countries reached an installed capacity of at least 10GW. Investments in renewable energy kept increasing during the year 2019, which obtained much more investment than any other electricity-generating technology, where, for the first time since 2009, the investment in wind energy exceeded solar power.

The installed renewable energy capacity provided approximately 27,3% of the global electricity generation during 2019. The vast majority of energy was generated from hydropower, with 58% of estimated generation, but closely followed by wind and PV power, with a total of 22% and 10% approximately. Over the last decade, Europe experienced a huge growth in renewable electricity generation, which increased from 19% in 2019 to 35% in 2020.

In northern European countries, for example in Denmark or the United Kingdom, the increase was even more drastic, reaching more than 30% in renewable electricity generation.

Despite the high growth in energy integration, renewable electricity has continued to face great challenges in increasing its impact on global energy generation. Some countries have been revising the grid connection and the market rules to allow more actors to participate in some of the ancillary services, thus enabling a more flexible operation of the electrical system. Furthermore, some countries have upgraded and modernized their grid infrastructure to allow higher levels of renewable generation. In this regard, a number of projects centered on the topic of hybrid systems, composed of at least two renewable energy technologies, were announced for countries all around the world, with the Netherlands, Australia, China or the United States as the leading forces.

There are different technologies which grow in parallel with the integration of renewable energies into the power system, such as energy storage or electrical vehicle technology.. These technologies permit the introduction of certain flexibility for managing changes in the supply and the demand, enhancing the grid stability transmission losses during partial or total outages.

To increase the power system flexibility the market is promoting new business models associated to provide grid balancing services. Conventional generation systems with low integration of renewable energy provide flexibility by adjusting the output of the generators to follow the demand. As the share of renewable energy increases, flexibility can be also obtained from sources such as demand or energy storage systems. In addition to flexbility those technologies can contribute to provide grid support services, such as frequency control, inertial response, power oscillation damping, or voltage regulation. In this regard, grid operators are procuring packed flexibility services that link generation, energy storage assets, and demand response. Demonstrators installed all around the globe have presented some innovative approaches to provide flexibility services. In 2019, a virtual power plant (VPP) was created in the Australian Renewable Energy Agency (ARENA), by connecting a large number of solar battery storage systems to deliver a coordinated power regulation and frequency control. In Finland, a demonstrator combined loads from buildings and renewable energy generators with battery storage systems integrating innovative forecasting technologies.

1.1. Challenges in the integration of renewable energy into the power system

These newly integrated sources may vary in their scale, going from big power plants to microgrids, connected to the electrical networks at different levels, from high-voltage transmission systems to low voltage distribution networks. To operate such a complex hybrid configuration, considering traditional and non-traditional generation units with multiple renewable energy systems, the regulation approaches have to be examined and redefined to undertake the new operation challenges of the electrical power system.

During the last century, the electric power system has relied on synchronous generators to regulate the power exchange in the electrical grid, adjusting its output power to respond to voltage and frequency disturbances. One of the main challenges is the transition from conventional fuel generation to renewable energy generation systems, such as wind or PV, is the stochastic profile of generation in the latter. The maximum energy production of such technologies depends gratly on the weather conditions, either by the average wind, the solar irradiance, or even the presence of clouds. This variability in the generation constitutes already a challenge for the power system stability itself, that should guarantee the instantaneous balance between generation and demand. Furthermore, the location of large-scale PV and wind systems are, most of the times, far away from the main demand zones or even from the transmission system infrastructure.

These challenges in the operation and the location of the renewable energy systems have led to two different types of generation. On the one hand, large-scale renewable power plants have gathered a lot of attention during the last years. This approach accumulates the harvested energy from a wide area and injects it into the transmission system through a unique point. On the other hand, a utility-scale generation, composed of small units in the distribution system, produces energy for a limited area. This approach is feasible for residential photovoltaic or battery storage systems connected to the distribution low voltage network, or also small power plants located close to a demand zone connected to the transmission system.

Apart from the location challenges and the stochastic profile of energy production, the high integration of renewable energy interfaced by power converters has harmed the stability of the grid. The replacement of some of the traditional generation units to renewable systems, interfaced by power converters, has reduced the overall stored kinetic energy. This transition leads to further challenges in the operation of these non-synchronous generation units, given the intermittent generation profile and the inexistent rotational mass, which could give rise to larger power oscillations in the system and an increase in the rate of change of frequency (RoCoF). This inertia loss has been historically pointed out by transmission system operators worldwide as one of the main drawbacks that power electronic based devices introduced in the energy system [2]. The reduction of synchronous inertia give rise to faster frequency changes in case of a mismatch between supply and demand, which leads to the activation of protection relays, creating further distortion and possible damage to equipment.

During the last few years, synchronous inertia has fostered attention regarding the definition of the lowest allowable synchronous inertia for the system to withstand a high RoCoF deviation, especially considering that the turn off and on of power plants modifies the amount of inertia available.

The use of power converters to interface renewable energy sources into the electrical grid has been widely used all over the world as the key factor to enable sustainable energy growth, thus partially reducing the usage of fuel and nuclear generation systems. Nowadays, most of the

power converter-based generation units integrated in large renewable power plants and in utility-scale systems use phase-locked loops (PLLs) to regulate the power delivered, giving rise to a grid-following type of generation. Although this solution has been extended in most power electronic based power conversion applications to provide power supply to the electrical grid, the lack of operability under certain fault circumstances highly reduces their impact on the power system stability.

Grid-connected power converters have integrated most of the traditional regulation services for primary frequency and voltage regulation. However, inverter-based generation does not include an inherent behavior to reduce the df/dt of the system, which finally does not contribute to guarantee the security of the grid [3], [4]. To ensure a safe and reliable operation of the system most generators must be able to provide RoCoF withstand capability in terms of synthetic inertia. This limitation is used to avoid the inertia constant (H) going below the target value. In the initial stage of a frequency contingency, the synthetic inertia can significantly reduce the RoCoF, especially during the first deviation. However, if the synthetic inertia is aggressively tuned for different units, it may lead to a second frequency swing in the power system.

Even though synthetic inertia may be requested soon to all generators, microgrids have been in operation for decades with zero or little inertia reserve. As the integration of renewable energy into the power system is gaining huge interest, the reliance on inertia may be the result of a legacy of the experience using synchronous generators. In this regard, there are discussions of how much inertia is required for the proper operation of the power system, when considering the high controllability of power converters [5]. It is a reality that synthetic inertial response can be integrated in power converter's control firmware without investing a high technological effort. However, even though it is feasible to generate synthetic inertia, the path to a 100% renewable energy penetration relies on the capacity to generate and regulate a grid, which is hardly achievable by grid-following power converters. The inability of the grid-following systems to create a grid makes it unsuitable for the future electrical grid power system scenario, where dynamic support will be the key to the flexible operation of the electrical grid. One of the most common approaches in grid-following converters to generate synthetic inertia is the usage of the mathematical derivative term of frequency measurement. However, depending on the implementation, it can give rise to failures during hard frequency contingencies or even instability issues due to the derivative nature of the signal used for inertia emulation.

To overcome the issues of the grid-following generation units, researchers around the world have been presenting different approaches to enhance the control methods of such units to emulate the behavior of traditional generation units. This kind of operation is generally referred to as a grid-forming control strategy, which provides seamless integration of renewable energy systems to the electrical grid while providing a natural response during faults, similarly to a synchronous generator. This control approach enables the system to operate under high-inertia

and low-inertia systems, providing dynamic support to either voltage and frequency deviations. In general, the grid-following and the grid-forming control strategies can be distinguished by Table 1.

Grid-following	Grid-forming
▪ PLL-based control strategy. ▪ Stationary reference frame current control to inject power to the grid. ▪ Decoupled control of P and Q. ▪ Needs a voltage to synchronize in order to deliver active and reactive power. ▪ Can not operate in island mode. ▪ Highly integrated into renewable energy power converters control.	▪ Uses a power synchronization algorithm to synchronize to the grid. ▪ Control the voltage and frequency magnitudes. ▪ Can provide virtual rotational mass inertia. ▪ Can black-start a power system. ▪ Can coexist with grid-feeding power converter in island mode. ▪ Not extended in many applications of renewable energy resources.

Table 1: Comparison between grid-following and grid-feeding approaches.

Apart from the capacity to naturally generate a synthetic inertial response, grid-forming power converters can generate and regulate their output voltage depending exclusively on its local measurements. This feature plays a crucial role in keeping the stability of the electrical grid and strengthening the grid with synthetic inertia, not only during grid-connected applications but also during the re-energization after partial or total blackoutsIn this regard, some grid codes, especially in large and small island power systems, are including re-energization as a system security service. For example in Great Britain it is being requested as a possible grid support service for re-energizing the grid after a shutdown [6].

This re-energization, also called black-start, is the capacity of a generator to start up an isolated grid without external support from the grid. During the last decade, most of the black-start capabilities were provided purely from synchronous generator-based power plants. However, the recent increase of grid-connected power converters and grid-forming strategies have raised a lot of interest in searching the potential capacity of those units into the black-start and island operation support. Even though some demonstrators have shown evidence of the feasibility of the grid-forming power converter black-start capacity, there are major aspects that were untested with a clear demonstration, such as the risk in the stochastic generation profile in PV and wind units, or the maximum time the generation units must provide rated power to ensure that the power supply and demand match.

Although grid-forming offers a practical solution for emulating the behavior of traditional generation units, the technology is still immature in terms of development and installation [7]. As a diffrence with microgrids, where the system is relatively small, larger power systems may interconnect thousands of power converter units in a wide generation area, which increases the

grid-forming operational challenges. In this regard, it will be necessary to coordinate the control of the grid-forming power converters to ensure a stable operation of the grid, especially during faults. Although the grid-forming strategies based on the synchronous generator have a predictable current during contingencies, the physical limits of current injection are directly constrained by the electronic interfaces. This implies redefining the detection and mitigation of fault events, which will be more susceptible to undesired tripping events.

1.2. Scope and objectives of the PhD dissertation

This thesis presents the work performed during my PhD studies at SEER (Sistemas Eléctricos de Energía Renovable) research center, during a five-year period from 2016 to 2021. While working at SEER, I was involved in multiple European projects regarding the control of power converters to enable a more flexible grid operation. One of the projects was to increase the flexibility in smart transmission grids with storage entities and large penetration of renewable energy sources (FLEXITRANSTORE). This project had specific objectives towards a sustainable energy future, such as the increase of flexibility by integrating a BESS system to provide ancillary services close to stochastic generation, and to increase the flexibility of the transmission grid by performing congestion management and power flow redirection. The second project on which I was involved was an interface architecture to provide grid services for an efficient power system (INTERRFACE). This project was focused on the creation of an architecture able to connect market platforms, allowing market players to procure services and trade energy in a transparent manner.

This PhD dissertation is structured as follows. After this introduction:

Chapter 2 describes the state of the art of grid-forming strategies based on the virtual synchronous machine approach. Here, all the basic structures to implement a grid-forming converter will be presented. Later, they are used to conform to different virtual machine's implementations displaying different advantages and drawbacks that will be discussed at the end of each implementation.

Chapter 3 deals with the most inner control level of traditional power converters. For this, a modified proportional-resonant current controller to deal with active and reactive power couplings during step responses under weak grid conditions is proposed. This solution provides a natural structure to decouple different harmonic sequences, which can be used to separate the current controller for the positive and negative sequence of the fundamental frequency.

Chapter 4 presents synchronous services provided by generation units based synchronous power controller (SPC) virtual synchronous machine implementation. In this chapter, frequency and voltage regulation loops are presented based on specific requirements on the grid codes. Furthermore, an enhanced power quality control structure, based on harmonic current injection, is used to support voltage imbalances due to harmonic loads.

The detailes regarding the implementation of a synchronous power control oriented to the generating unit are treated in detail in Chapter 5. Here, the state space structure of one of the most common grid-forming strategies is presented, as well as additional structure for black start capabilities and island resynchronization to the grid. Apart from the traditional synchronous control structure based on local measurements of voltage and current, a sensorless system is introduced in this section. The path to achieve this sensorless synchronous control starts with the use of a traditional grid-following structure, which is later modified to a grid-forming one by the use of a virtual admittance.

In the same direction, Chapter 6 presents the synchronous control oriented to the system, enabling an area control focusing on the regulation of multiple units to achieve the emulation of a coordinated synchronous virtual machine at the PCC of a power plant. This system-oriented structure emulates the synchronous generator capacities at the plant level based on the communication link towards each generation unit. The control structure coordinates the different units regardless of the system configuration, dynamically adapting the active and reactive power based on a synchronous machine emulation.

Finally, in Chapter 7, the synthesis and conclusions of the ideas within the thesis, and the ideas for future works, are exposed.

1.3. List of publications

This thesis has resulted in the following publications:

A. Journal Papers:

JP1. **A. Tarraso**, N.-B. Lai, G. N. Baltas, and P. Rodriguez, “Power Quality Services Provided by Virtually Synchronous FACTS,” Energies, vol. 12, no. 17, p. 3292, Aug. 2019, doi: 10.3390/en12173292.

JP2. **A. Tarrasó**, N. B. Lai, C. Verdugo, J. I. Candela, and P. Rodriguez, “Design of Controller for Virtual Synchronous Power Plant,” IEEE Trans. Ind. Appl., vol. 57, no. 4, pp. 4033–4041, 2021, doi: 10.1109/TIA.2021.3075173.

JP3. W. Zhang, **A. Tarraso**, J. Rocabert, A. Luna, J. I. Candela, and P. Rodriguez, “Frequency Support Properties of the Synchronous Power Control for Grid-Connected Converters,” IEEE Trans. Ind. Appl., vol. 55, no. 5, pp. 5178–5189, 2019, doi: 10.1109/TIA.2019.2928517.

JP4. C. Verdugo, **A. Tarraso**, J. I. Candela, J. Rocabert, and P. Rodriguez, “Centralized Synchronous Controller based on Load Angle Regulation for Photovoltaic Power Plants,” IEEE J. Emerg. Sel. Top. Power Electron., pp. 1–1, 2020, doi: 10.1109/jestpe.2020.2995339.

JP5. N.-B. Lai, **A. Tarraso,** G. Baltas, L. V. M. Arevalo, and P. Rodriguez, "External Inertia Emulation Controller for Grid-following Power Converter," IEEE Trans. Ind. Appl., p. 1, 2021, doi: 10.1109/TIA.2021.3108350.

JP6. G. N. Baltas, N. B. Lai, L. Marin, **A. Tarrasó**, and P. Rodriguez, "Grid-Forming Power Converters Tuned Through Artificial Intelligence to Damp Subsynchronous Interactions in Electrical Grids," IEEE Access, vol. 8, pp. 93369–93379, 2020, doi: 10.1109/ACCESS.2020.2995298.

JP7. G. N. Baltas, N. B. Lai, **A. Tarraso**, L. Marin, F. Blaabjerg, and P. Rodriguez, "AI-Based Damping of Electromechanical Oscillations by Using Grid-Connected Converter," Front. Energy Res., vol. 9, p. 39, 2021, doi: 10.3389/fenrg.2021.598436.

JP8. M. Shahparasti, A. Rajaei, **A. Tarraso**, J. D. Vidal Leon Romay, and A. Luna, "Control and Validation of a Reinforced Power Conversion System for Upcoming Bioelectrochemical Power to Gas Stations," Electronics, vol. 10, no. 12, 2021, doi: 10.3390/electronics10121470.

JP9. M. Abdollahi, J. I. Candela, **A. Tarraso**, M. A. Elsaharty, and E. Rakhshani, "Electromechanical Design of Synchronous Power Controller in Grid Integration of Renewable Power Converters to Support Dynamic Stability," Energies, vol. 14, no. 8, 2021, doi: 10.3390/en14082115.

JP10. M. Shahparasti, P. Catalan, I. Garcia, J. I. Candela, **A. Tarraso**, and A. Luna, "Enhanced performance controller for high power wind converters connected to weak grids," IET Renew. Power Gener., vol. 14, no. 12, pp. 2058–2067, 2020, doi: 10.1049/iet-rpg.2019.1021.

B. Patents:

P1. J. Candela, **A. Tarrasó**, P. Rodríguez, and Bao, "Método de control síncrono para una unidad de conversión de potencia," 2020.

P2. A. Tarrasó, C. Verdugo, J. Candela, J. Rocabert, A. Luna, and P. Rodríguez, "Sistema y método de control síncrono agregado de una planta de potencia con múltiples estaciones de conversión de potencia," 2019.

C. Conference papers:

CP1. **A. Tarraso**, N. B. Lai, and P. Rodriguez, "Synchronous Fault Compensator for Voltage Sensorless Grid-Following Power Converters," in 2021 IEEE 12th International Symposium on Power Electronics for Distributed Generation Systems (PEDG), 2021, pp. 1–5, doi: 10.1109/PEDG51384.2021.9494205.

CP2 A. Tarraso, N. B. Lai, G. N. Baltas, and P. Rodriguez, "Voltage Sensorless Grid-Forming Power Converters," 2020 IEEE 21st Work. Control Model. Power Electron. COMPEL 2020, 2020, doi: 10.1109/COMPEL49091.2020.9265760.

CP3 A. Tarraso, L. Marín, N. B. Lai, and P. Rodriguez, "Enhanced Proportional-Resonant (PR) Controller with Negative Decoupling for Weak Grids," in 2020 IEEE 21st Workshop on Control and Modeling for Power Electronics (COMPEL), 2020, pp. 1–4, doi: 10.1109/COMPEL49091.2020.9265663.

CP4 A. Tarrasó, C. Verdugo, N. B. Lai, J. I. Candela, and P. Rodriguez, "Synchronous Power Controller for Distributed Generation Units," in 2019 IEEE Energy Conversion Congress and Exposition (ECCE), 2019, pp. 4660–4664, doi: 10.1109/ECCE.2019.8912667.

CP5 A. Tarraso, J. I. Candela, J. Rocabert, and P. Rodriguez, "Synchronous power control for PV solar inverters with power reserve capability," in IECON 2017 - 43rd Annual Conference of the IEEE Industrial Electronics Society, 2017, pp. 2712–2717, doi: 10.1109/IECON.2017.8216456.

CP6 A. Tarraso, J. I. Candela, J. Rocabert, and P. Rodriguez, "Proportional-resonant current controller with orthogonal decoupling on the αβ-reference frame," in IECON 2017 - 43rd Annual Conference of the IEEE Industrial Electronics Society, 2017, pp. 1453–1458, doi: 10.1109/IECON.2017.8216247.

CP7 A. Tarrasó, J. I. Candela, N. B. Lai, G. N. Baltas, and P. Rodriguez, "Virtual Admittance PLL Structure for Grid-forming Power Converters in Microgrids," in 2020 IEEE Energy Conversion Congress and Exposition (ECCE), 2020, pp. 5007–5011, doi: 10.1109/ECCE44975.2020.9235629.

CP8 N. B. Lai, **A. Tarrasó**, and P. Rodriguez, "Efficient Management of Energy Storage Systems using Competitive Controller," in 2021 IEEE 12th International Symposium on Power Electronics for Distributed Generation Systems (PEDG), 2021, pp. 1–3, doi: 10.1109/PEDG51384.2021.9494222.

CP9 A. Rón, **A. Tarrasó**, Á. Luna, and P. Rodríguez, "Analysis of Rapid Control Prototyping Performance for Power Conversion Applications," in 2020 IEEE Energy Conversion Congress and Exposition (ECCE), 2020, pp. 3225–3230, doi: 10.1109/ECCE44975.2020.9236009.

CP10 N. B. Lai, **A. Tarraso**, G. N. Baltas, L. Marin, and P. Rodriguez, "Inertia Emulation in Power Converters with Communication Delays," in 2020 IEEE Energy Conversion Congress and Exposition (ECCE), 2020, pp. 1665–1669, doi: 10.1109/ECCE44975.2020.9235379.

CP11 C. Verdugo, **A. Tarraso**, J. I. Candela, J. Rocabert, and P. Rodriguez, "Synchronous Frequency Support of Photovoltaic Power Plants with Inertia Emulation," in 2019 IEEE Energy Conversion Congress and Exposition (ECCE), 2019, pp. 4305–4310, doi: 10.1109/ECCE.2019.8913200.

CP12 N.-B. Lai, **A. Tarraso**, and P. Rodriguez, LMI-based Control Design to Enhance Robustness of Synchronous Power Controller. 2019.

CP13 L. Marin, **A. Tarraso**, I. Candela, R. Rye, and P. Rodriguez, Influence of the ICFF Decoupling Technique on the Stability of the Current Control Loop of a Grid-Tied VSC. 2019.

CP14 L. Marin, **A. Tarrasó**, I. Candela, and P. Rodriguez, "Stability Analysis of a Droop-Controlled Grid-Connected VSC," in 2018 IEEE Energy Conversion Congress and Exposition (ECCE), 2018, pp. 4161–4167, doi: 10.1109/ECCE.2018.8558126.

CP15 L. Marin, **A. Tarraso**, N. B. Lai, G. N. Baltas, and P. Rodriguez, "Small-signal Model and Analysis of a Grid-forming Power Converter based on the Synchronous Power Controller," 2020 IEEE 21st Work. Control Model. Power Electron. COMPEL 2020, 2020, doi: 10.1109/COMPEL49091.2020.9265712.

CP16 G. N. Baltas, N. B. Lai, L. Marin, **A. Tarraso**, and P. Rodriguez, "A Growing Self-Organising Maps Implementation for Coherency Identification in a Power Electronics Dominated Power System," in 2020 IEEE Energy Conversion Congress and Exposition (ECCE), 2020, pp. 1963–1967, doi: 10.1109/ECCE44975.2020.9235611.

CP17 G. N. Baltas, N. B. Lai, L. Marin, **A. Tarrasó**, and P. Rodriguez, "Grid-Forming Power Converters Tuned Through Artificial Intelligence to Damp Subsynchronous Interactions in Electrical Grids," IEEE Access, vol. 8, pp. 93369–93379, 2020, doi: 10.1109/ACCESS.2020.2995298.

Chapter 2.

Virtual synchronous machine state of the art

The upgrade of grid requirements for connection of power converter to the electrical grid during the last decade has made the researchers develop new approaches for the control of grid-connected units, intending to improve their interaction and response during grid events. Furthermore, special attention has been paid to massively integrate renewable energy resources interfaced by power converters without hindering the stability of the electrical network. In addition to the grid codes, other applications such as energy storage, microgrid, and especially grid-connected electrical vehicles have also reinforced the development of these new control solutions for power converters in the power system. In this regard, a lot of different approaches have been presented to improve the converter interaction with the electrical grid, where the virtual synchronous machine (VSM) has been one of the most extended. These controllers, inspired by the regulation of a synchronous generator, have gained high importance due to their grid-forming implementation potential and the beneficial effects when integrated into the power system.

Although there have been many different approaches to the virtual synchronous machine concept within the grid-forming implementation in the last years, all of them use the same principal characteristics of a traditional synchronous generator. In this way, the structure of a virtual synchronous machine can be fragmented into different structures, leading to an implementation mechanism for any kind of grid-forming power converter, where each implementation can have its features, advantages, and drawbacks.

In this section, the general concepts for the synchronous generator will be presented, which will be used as the base to develop the implementation tree of the virtual synchronous machine. The tree allows splitting the different controllers allocated in the power converter control by the specific action they fulfill. After the implementation tree is decomposed, some of the most well-known VSM implementations will be presented, fragmenting their control structure to compare them using the implementation tree.

2.1. Virtual synchronous machine concept

The VSM concept was born from the intention of emulating the behavior of the well-known synchronous generator. In general, the synchronous machine is composed of two general constructive elements, the mechanical shaft acting as the rotor and the electrical windings acting as the stator. In the rotor, there are two basic construction topologies, the salient and the non-salient poles, which can be used for power range from very few amounts of kW to a few GW. Although the power scale and the constructive elements can differ in each implementation, the equivalent electromechanical model can be applied in all the existing machines and is a universally recognized model through the literature [8]–[10]. The electrical part is composed of the windings in the stator, generating the output current, the damper windings, adding a damping coefficient to enlarge the stability of the mechanical system, and the excitation windings, to regulate the magnetic force in the generator. Each can be described by multiple equations to define their characteristics.

2.1.1. Electrical system

The electrical network is one of the most complex systems that humanity has ever created. Although the operation and control of this outstanding system is complex and highly dependant on multiple layers of restrictions, requirements, and controllers, it tries to fulfill three main objectives.

- To supply electrical energy to the end-consumer, while fulfilling the quality standards in power, voltage, frequency, and distortion.
- To ensure the reliability of supply, reducing the probability of failures that may give rise to partial or total outages.
- To comply with the energy demands of consumers and the safe operation of the grid, following cost-effectiveness criteria.

The electrical system has to face daily an immense amount of challenges to be able to achieve these objectives. The rapid detection and mitigation of the damage during system faults is one of the key elements to fulfill the electrical system objectives, which allow a fast separation of damaged parts from the rest of the grid. In this regard, the most common faults in the electrical systems are overcurrents, generally due to short-circuits, overvoltages, which may differ depending on the event that generated it, and other types of faults that can include disturbances such as electrical resonances, voltage sags, or even harmonics.

In a way to address all these electrical faults, the power system is equipped with many different types of protection relays, which are designed to ensure their activation when a fault is detected and disconnect the damaged part from the rest of the system, thus reducing the total outage of the power system. One of the most important actions to protect the power system is monitoring its behavior. With this approach, the system can estimate and analyze possible contingencies, taking corrective actions to operate the system most safely, minimizing thus the probability of partial outages in the demand or total blackouts of the system. The restoration

of this partial or total loss in power has to be achieved as quickly as possible, to keep the system under a stable operational state or to reach the steady-state in the minimum time having the fundamental magnitudes, frequency, and voltage, under operational ranges. The stability of the power system can be divided into three groups. First, the voltage stability is usually generated by reactive power imbalances between the demand and the generation system. Second, angle stability can be described as a loss of synchronization between different generators or grid areas. Finally, the frequency stability which is usually due to unexpected imbalances in active power between the demand and the generation.

2.1.2. The synchronous generator

The synchronous generator model can reach up to a 7th-order model if all the elements are considered. The electrical system is composed of three different windings: the stator, the damper, and the excitation winding, which can reach up to a 5th-order system. This model can be represented in many different ways, based on the equivalent reactance model representing the transient, sub-transient, and steady-state reactances, or based on inductances working on the static reference frame *abc* or in the synchronous reference frame *dq*. In general, to reduce the order of the equivalent model and simplify the complexity of the system, some hypotheses are made. First, the effect of the transient and sub-transient inductances of the generator, which mainly affect the short-circuit currents, are much higher than the rated current of a power converter, so for safety reasons they are not considered for the virtual generation model. In addition, the direct and quadrature inductances, which have a lot of impact on salient poles synchronous generators, are also ignored from the modeling. Although they influence the relationship between the rotor and the power, an effective model can be achieved by assuming a non-salient poles rotor. This model can be depicted in Figure 1, representing the equivalent system that has an accurate response from variations in voltage, frequency, and phase angle.

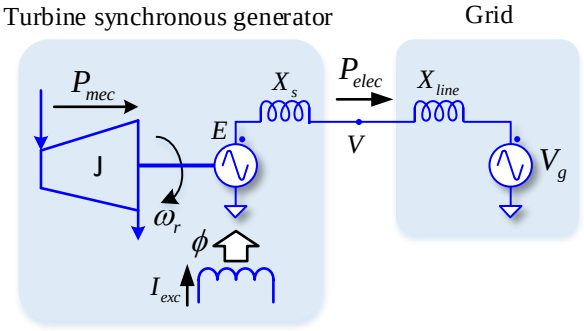

Figure 1: Turbine synchronous generator group scheme

The most important parameters of the reduced model are:

- J – The moment of inertia of the rotating mass $[kg \cdot m^2]$
- ω_r – The generator rotational speed $[\frac{rad}{s}]$
- P_{mec} – The mechanical power provided by the generator shaft $[W]$
- P_{elec} – The electrical power at the electrical grid $[W]$
- X_s – The equivalent reactance of the generator $[\Omega]$
- E – The electromotive force (emf) $[V]$
- V – The voltage at the point of connection $[V]$

The electrical circuit presented in Figure 1 can be represented as two voltage sources interconnected through an impedance, the value of the latter is generally inductive. The electromotive force amplitude of the generator can be controlled via the excitation system, whereas the frequency and the phase-angle are directly linked to the rotor rotational speed and position. The difference between the grid phase-angle and the rotor phase-angle creates the load angle, δ, that defines the quantity of active power delivered to the grid. On the other hand, the difference between the voltage magnitude at the grid side and the voltage magnitude at the generator terminals define the quantity of reactive power delivered to the grid. This exchange of electrical power at the generator terminals can be described by:

$$P = \frac{E \cdot V}{Z} \cdot \cos(\theta - \delta) - \frac{V^2}{Z} \cdot \cos(\theta) \tag{1}$$

$$Q = \frac{E \cdot V}{Z} \cdot \sin(\theta - \delta) - \frac{V^2}{Z} \cdot \sin(\theta) \tag{2}$$

As the impedance interconnecting both systems is mainly inductive, the phase angle θ can be considered as approximately 90 degrees. This assumption reduces the equations and can be rewritten as:

$$P = \frac{E \cdot V}{X_s + X_{line}} \cdot \sin(\delta) \tag{3}$$

$$Q = \frac{U}{X_s + X_{line}} \cdot (E \cdot \cos(\delta) - V) \tag{4}$$

From the previous equations, it can be defined that the load angle δ defines the active power flow in the system. Similarly, the reactive power exchange depends on the voltage difference between the electromotive force, *E*, and the grid voltage, *V*. It is worth mentioning that the load angle is generally shifting around values below 10 degrees and the voltage magnitude is normally within a 90% of nominal value. Consequently, even though in equations (3) and (4), the active and reactive power is coupled with *V* and δ, the variance is unsignificant and does not affect the power flow.

The inductive nature of the interconnection impedance can be considered valid for all lines on the transmission system. In a particular case, the low voltage distribution lines may not present a high inductance ratio in front of the resistance. However, the overall impedance can be considered mainly inductive due to the transformers and generators connected to these networks.

In general, the virtual synchronous generator is composed of two control loops, one focusing on the electromechanical behavior of the synchronous machine and the other one focused on the electromagnetic behavior.

On the one hand, the electromechanical loop defines the mechanical performance of the generator which can be modeled using the motion equation.

$$J\omega\frac{d\omega}{dt} = P_{mec} - P_{elec} \tag{5}$$

This equation can be written as a function of the mechanical and electrical power exchange, where P_{mec} represents the mechanical power at the shaft, and the P_{elec} represents the electromagnetic power at the stator. This electrical power depends on the load angle δ, which can be described as (6) for a generator with a single pair of poles.

$$\frac{d\delta}{dt} = \omega_r - \omega_{grid} \tag{6}$$

Where the value of ω_{grid} represents the grid frequency, and the value ω_r represents the angular speed of the machine.

Imbalances between electrical power and mechanical power generate a speed change in the generator, consequently modifying the load angle δ. This modification in the load angle gives rise to a variation in the output power of the generator as it can be determined by (3). In general, this process forces the generator to reach a new equilibrium point, which can be reached by modifying the mechanical power. For this reason, to complete de dynamical model of the machine it is needed to model some of the external regulators, such as turbines, drives, etc. The differential equation presented in (6) would present an oscillatory performance due to the lack of damping factor in the equations. Generally, to avoid this undesired performance in synchronous generators a damper winding is used, which can be modeled as:

$$J\omega\frac{d\omega}{dt} = P_{mec} - P_{elec} - k_d\left(\omega_r - \omega_{grid}\right) \tag{7}$$

Where the factor k_d is the damping coefficient. Using the equation presented in (7) the mechanical control of the synchronous machine can be modeled as in Figure 2.

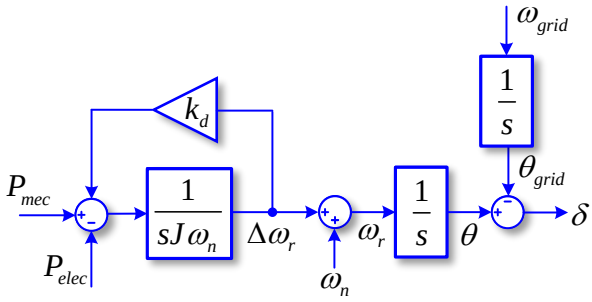

Figure 2: Synchronous machine mechanical loop model

The coefficient ω_n represents the nominal frequency of the system, θ is the phase angle of the synchronous generator, and $k_d$is the damping coefficient. Using Figure 2 as a reference, it can be concluded that the frequency may be different at different points on the network during power changes or transients events in the power flow, but in a steady-state, the frequency value should be the same in all buses of the grid.

On the other hand, the electromagnetic loop targets the electrical system emulation. As presented in the previous section, the synchronous generator model can reach up to a 7th-order model. However, to reduce the complexity of the system without hindering the electromagnetic response some assumptions are made. The stator impedance is reduced to a first-order system only composed of the subsynchronous impedance. In general, these values can be calculated based on the traditional values of the synchronous generator, which can reach up to a 0.3 pu for the inductance coefficient, and a 0.05 pu for the resistance parameter.

2.1.3. Control elements of a generation unit

To complete the synchronous generation unit model, some additional control elements are included that interact with the generator. The governor is devoted to keep the power delivered by the generator and maintaining the grid frequency close to the specified value. It also controls the turbine, which is responsible for providing mechanical power to the generator shaft. Another controller is the automatic voltage regulator (AVR), which is in charge of sending the necessary reference to the excitation system of the generator to keep the voltage level close to the nominal value during the operation. Figure 3 presents the control schematic of the generation unit.

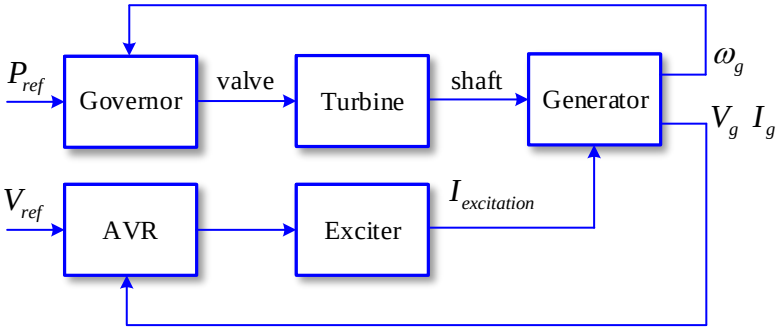

Figure 3: Block diagram of the generator

2.2. Implementation tree

The study of the synchronous generator can be an extensive and complex topic, the previous section presented a general overview of the elements inside the synchronous generator as an introductory section to highlight the advantages of the control, which offers natural support to regulate the electrical grid. This regulating capacity has permitted the expansion of the electrical network over the last century. The vast use of this generation system has made that power plants based on synchronous generation cover the majority of the electrical power needs, reaching satisfactory levels of stability and reliability, being until today the central pillar of the power system.

The exigent requirements for renewable energy generation have increased during the last decade, which has made the companies and researchers develop new methods for controlling grid-connected power converters to improve their integration and response in case of grid events. In addition, special attention has been focused on finding solutions that provide an effective massive integration in the grid without hindering the stability of the electrical network. In this regard, new controllers inspired by the synchronous generator operation have gained huge importance due to their high potential benefits when applied to the power system.

Even though there are different approaches for controlling a power converter as a virtual synchronous generation unit, all of them revolve around the same principal characteristics of the conventional generation. In this way, any implementation of a VSM can be studied through the analysis of each main functionality and its auxiliary regulation loops. This implementation tree provides the capacity to construct the VSM implementation by selecting the building blocks in each functional layer, where each combination gives rise to a particular implementation, with its features, advantages, and drawbacks.

Therefore, based on the generation unit key features detailed in the previous section, the structure of the virtual synchronous generator implementation tree is presented in Figure 4, where the general concepts are grouped in four main functional layers devoted to the

synchronization loop, the electromagnetic and the electromechanical interaction, and lastly the external loop controllers.

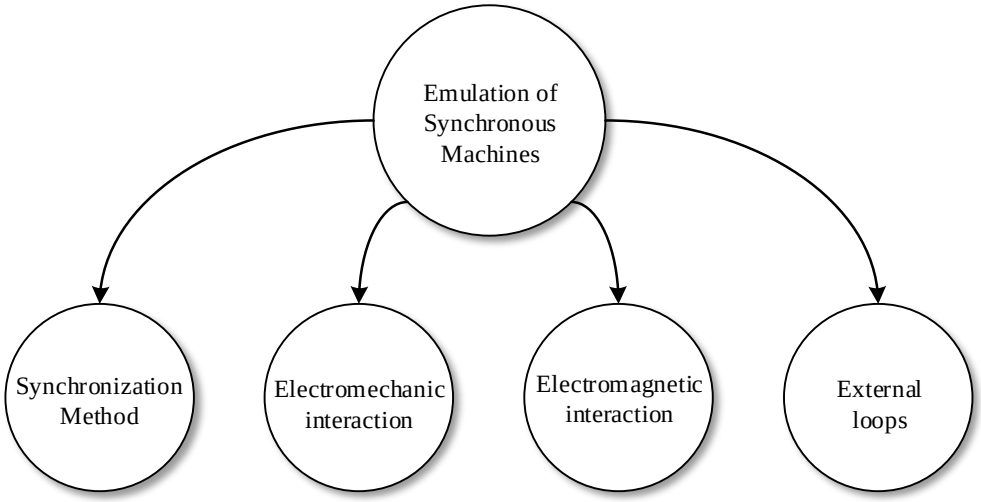

Figure 4: Virtual synchronous generation implementation tree

2.2.1. Synchronization method

The first group in the implementation tree presented in Figure 4 is the one related to the synchronization method. Regardless of the generation technology, the generation unit must be synchronized to the grid voltage to have a coordinated operation of the system. This grid synchronization entails forming a proper AC sinusoidal waveform, with a specified frequency and voltage level. The phase-angle of such AC waveform, together with additional elements, determine the current injected by the power converter into the grid, thus regulating the power exchanged with the power system. In addition, the dynamic response of the synchronization system sets the generation unit capacity for supporting the power system, as well as transients and instabilities, which is particularly important during grid faults.

2.2.1.1. Voltage-Based Synchronization

The voltage-base synchronization system is the most recognizable technique in the field of grid-connected power converter control since it is one of the most essential elements in most applications.

There are different approaches to implement a voltage synchronization based on the processing of the voltage at the point of common coupling (PCC) of the power converter. However, one of the most extended implementations is the phase-locked loop (PLL) synchronization, which by using the grid voltage measurement at the PCC its capable of detecting in real-time the amplitude, frequency, and phase-angle of the voltage. This

information of the phase and the amplitude will form the central pillar of the power converter control algorithms, adjusting the references and the measurements signals to inject or absorb the desired power according to the operating conditions. Figure 5 shows the diagram where the phase-locked loop (PLL) is processing the voltage measurement, $\boldsymbol{v_{abc}}$, at the output of the converter.

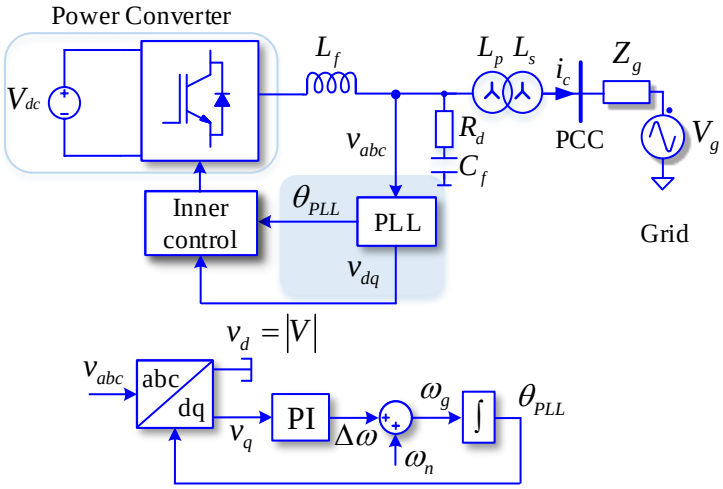

Figure 5: Classic PLL structure by voltage

As shown in the PLL structure in Figure 5, the voltage measurement is used by the PLL to determine the frequency, amplitude, and phase-angle of the input voltage. This is achieved by projecting the input voltage vector on a synchronous reference frame, which angular position is determined by the PLL closed-loop controller. In this way, by forcing the quadrature component in the synchronous reference frame "*q*" to zero, it is possible to match the input voltage vector phase-angle, which means that the direct component "d" represents the voltage vector amplitude. This synchronization algorithm is valid under balanced grid conditions. This hypothesis will be considered to reduce the complexity of the analysis.

The classical structure of a PLL can be presented as a 2nd order transfer function with configurable bandwidth and damping factor. The information detected by the PLL is sent to the inner control system, where it is used to determine the active and reactive power to be injected. In addition, this information provided by the PLL is generally used by other control layers, such as the grid supporting functions for voltage and frequency. Even though it is an extended method in the design of power converters, no matter the implementation, it is highly non-linear and does not respond as other elements in the electrical grid. This directly affects the performance of the power converter during transient conditions, which is one of the main weak points of this synchronization method. A voltage sag, where the voltage changes

dramatically may excite the second-order response of the PLL, which may harm the controllers stability. In addition, one case scenario that can be even more challenging for this synchronization method is the absence of grid voltage, leaving the power converter without a pattern to synchronize to.

2.2.1.2. Power-Based Synchronization

The power-based synchronization does not use the voltage vector at the power converter point of common coupling (PCC) to detect the phase-angle, but it establishes a power equilibrium point between the power converter and the rest of the elements in the grid. This synchronization method is the one used by synchronous generators since the creation of the power system, as it is synchronized to the grid by balancing its power exchange. However, the integration of this kind of method in the converter control is relatively new, as it was included with the appearance of the virtual synchronous operation of the power converter.

The concept of power exchange between sources was presented in the previous section, where the angle δ reaches a constant value when the power exchanged between the two sources is balanced. A simplified diagram presenting the implementation of the power-based synchronization in a power converter is presented in Figure 6. The measurement of power is compared with the reference of power, which creates the deviation processed by the motion equation block, creating in this way the necessary angular position for the power converter to achieve the equilibrium point, and thereby deliver the power to the grid. The synchronization dynamics are tuneable by the parameters of inertia and damping factor, which are compatible with the ones in a conventional generator.

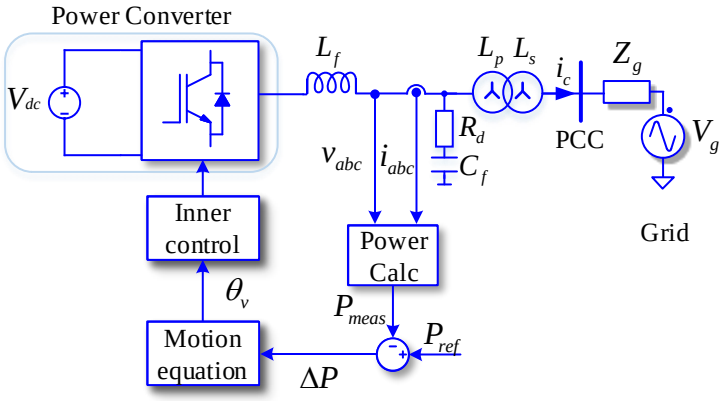

Figure 6: Power-based synchronization between two voltage sources

In this regard, a heavy mismatch in power can lead to a large overcurrent during transient periods, which is something that the synchronous machine can withstand but not the

electronics composing the power converter. This is a significant drawback that forces, in real implementations, to add additional elements such as current limiters.

It is worth mentioning that the power-based synchronization adds the grid forming functionality option, due to its self-synchronization feature introduced by the power synchronous modeling. In this regard, this synchronization method allows modifying the power converter control as a traditional voltage-dependent current-regulated unit to a generation unit able to form and regulate an electrical island just by adding simple frequency and voltage control loops.

2.2.2. Electromechanical interaction

The electromechanical model may be the most valuable characteristic of a VSM due to its capacity to emulate the behavior of the motion equation of a synchronous generator in a power converter. Figure 7 shows the two main approaches for electromechanical emulation in a VSM implementation. First, all the windings and mechanical elements are defined to emulate the dynamic equations of the synchronous generator and mimic its performance. Additional controllers can be used to enhance the performance of the electromechanical model, although its equations are not directly linked to the model of the rotating mass itself, they look for the enhanced closed-loop performance of the generation unit. These enhanced transfer functions, collect the effect of external regulators such as the governor or the PSS, to upgrade the performance of the unit under demanding conditions. Second, these dynamic equations can be simplified to the motion equation of a generic rotating mass adjusting the values of inertia and damping according to the desired performance.

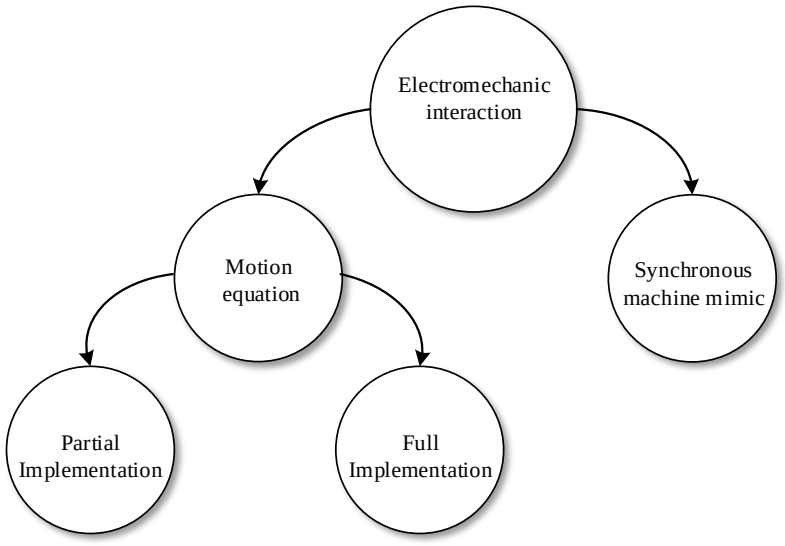

Figure 7: Electromechanic models for virtual synchronous machines.

2.2.2.1. Mimic of the synchronous generator

The electromechanical model of a synchronous generator [8] with the turbine model and the governor is presented in Figure 8. The representation includes the stator windings, the excitation winding, and the damping windings in the *dq* reference frame.

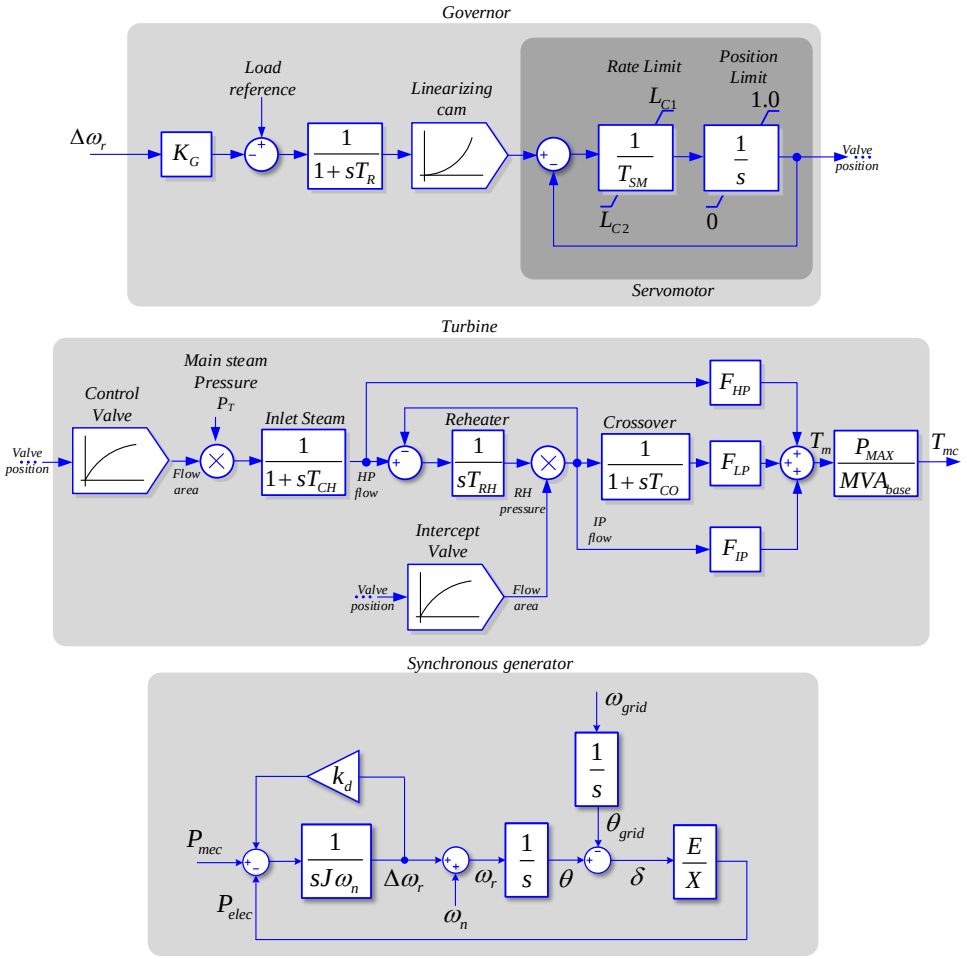

Figure 8: Model of a synchronous generator including a governor and a turbine.

The model describes the physical behavior of a synchronous generator. This can be exported and programmed in the power converter control to emulate precisely the behavior of an electrical machine. In this way, the benefits of the synchronous generator can be transferred to the power converter. However, the power converter is based on a fully controlled semiconductor that has an instantaneous response but limited robustness in terms of thermal

limitation and overcurrents. Hence, the mimic of a synchronous generator in a power converter may give rise to important drawbacks especially due to the hardware limitations of the power converter.

2.2.2.2. Simplified motion equation

A version of the motion equation (7) was presented in the previous section. Even though it is a simplified version of the synchronous machine emulation, it provides an operational implementation. Figure 2 showed the block diagram of the motion equation, where the moment of inertia is represented by *J* and the damping characteristic as k_d. This implementation differs from the mimicked approach, as this simplified strategy takes into account that, as a virtual system, the inertia and the damping factor may not match the ones of a real machine. However, the parameters can be modified dynamically, allowing more flexible operating conditions. In real machines, the damping is limited by the physical damping winding, but in virtual machines, there is no limit as the damping can be as high as necessary according to the needs of the system.

The motion equation can be implemented in as much detail as necessary. For example, the inertia and the damping of the system can be considered, which may also include the derivative, integral, and proportional relationship between the variation of the angular speed of the rotating mass and the exchanged power. However, the equation can be simplified to only consider the inertial response and the damping parameter, or even in its primal expression by considering only the effect of the damping factor.

2.2.3. Electromagnetic interaction

The electromagnetic interaction of the VSM to the electrical grid highly depends on the electrical model of the stator and the internal controllers of the power converter. The synchronous generator presents different values of impedance for the sub-transient, transient, and steady-state impedance of the generator. These values are dependant on the physical characteristic and the construction of the generator, and they set the performance of the unit under different operation points. In particular, the transient and sub-transient impedances determine the evolution and the magnitude of the currents during faults. Alternatively, the steady-state impedance influences the current sharing among generators working in parallel.

Although power converters have a high controllability margin, they have a reduced thermal and current limitation due to the electronic devices. Therefore, the transient response of the converter has to be accurately designed to ensure a safe operation under diverse operating conditions on the system. In addition, the modeling of the steady-state impedance is highly important as it is in charge of making the operation compatible with the rest of the elements in the grid.

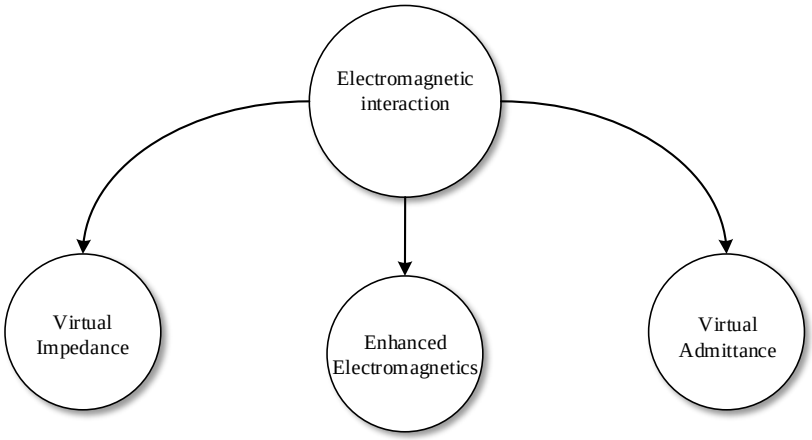

Figure 9: Electromagnetic models for VSM

2.2.3.1. Virtual Impedance

The simplified model of the connection between a synchronous generator interconnected to an external grid is presented in Figure 10. Based on the figure, it is possible to see that the electrical interaction in the steady-state between a synchronous generator and an external grid can be analyzed using a simple circuit that represents the AC voltage at the PCC, $\boldsymbol{v_{abc}}$, the internal electromotive force (emf), $\boldsymbol{e_{abc}}$, and the interconnection impedance of the generator, *R-L*.

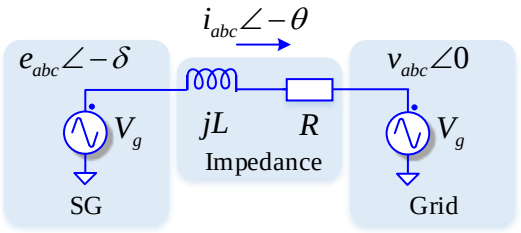

Figure 10: Simplified electrical diagram of the interconnection between a SG and an external grid

By using the Kirchhoff law, the dynamic performance of the system above can be represented as the following transfer function:

$$v(s) = e(s) - (R + Ls) \cdot i(s) \tag{8}$$

Therefore, by using the mathematical equation described in (8), the voltage that should be provided by a power converter emulating the response of a synchronous generator can be represented as:

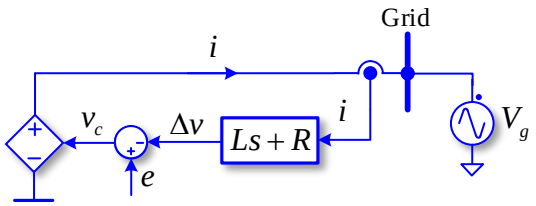

Figure 11: Virtual impedance implementation effect in a power converter

This implementation uses the current injected into the grid to calculate the voltage drop on the output impedance of the electrical machine. This straightforward application of the electromagnetic loop provides the voltage reference to the power converter. Although this implementation is feasible, a voltage controller is needed in the power converter control. Furthermore, the emulating effect of a series impedance as a voltage drop reference has a negative impact on the stability margin of the system due to the derivative term appearing in the inductive parameter. It is also important to note that the derivative term associated with the impedance will amplify any disturbance in the measurements.

2.2.3.2. Virtual admittance

Considering the same circuit presented in Figure 10, an alternative strategy can be used to implement the interconnection impedance. In this approach, the current flowing through the impedance is isolated from the equation (8), which gives rise to the following transfer function.

$$i(s) = \frac{1}{R + Ls}\left(e(s) - v(s)\right) \tag{9}$$

In this implementation, the current reference is set by the difference between the electromotive force of the machine and the voltage measurement at the point of connection, which is multiplied by the admittance value. It is worth noting that this variation in the structure of the electromagnetic link highly improves the stability of the system in case of perturbation, as the admittance acts as a first-order low-pass filter. Figure 12 present the simplified control schematic for the virtual admittance implementation approach. In this case, the converter behaves as a current source instead of as a voltage source.

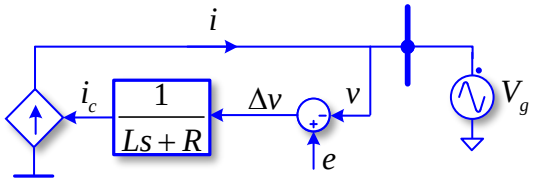

Figure 12: Virtual admittance implementation effect in a power converter

This implementation closely resembles the conventional control structure of the power converter, which is traditionally controlled as a current source, providing additional limitations to the current during faults. This is an advantage compared to the virtual impedance implementation since the majority of power converters work as a current-controller voltage source. In addition, the natural filtering by the virtual admittance provides better performance under noisy signals coming from the measurements.

2.2.3.3. Enhanced electromagnetics

The virtual implementation of a synchronous generator allows enhanced performances, which do not follow a direct mimic of the electrical circuit of the real synchronous machine. In general, synchronous generators have a unique inductance and resistance. However, in a virtual environment, this can be extended to have multiple electromagnetic blocks with different impedances, tuned for different sequence components or specific harmonics. In this regard, some research has been made to include parallel virtual impedances or admittances to regulate additional grid sequences. Figure 13 presents the control schematic approach for enhanced electromagnetic interaction. This multi-admittance/impedance approach provides additional controllability for harmonics and can be selected for different operating conditions.

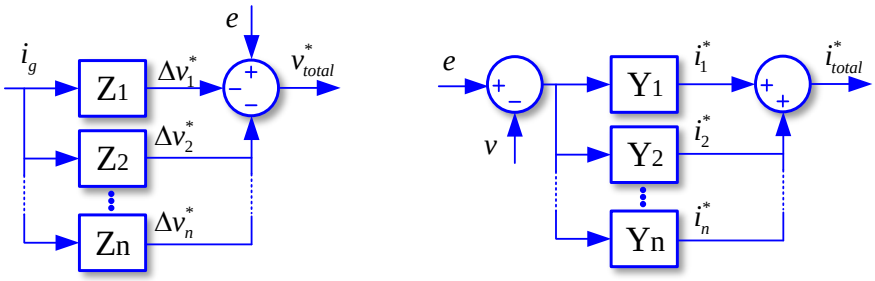

Figure 13: Implementation for parallel multi-admittance & multi-impedance loop

2.2.4. External loops

The synchronous generation units are traditionally equipped with external regulation loops when connected to the electrical grid. Although synchronous generators present inherent beneficial characteristics to operate in the electrical grid, their nature is not enough to guarantee that the frequency and voltage magnitude remain within safety operation margins. These safety margins are vital to guarantee that all elements connected work properly and follow the local standards.

The generator is equipped generally with two external regulators, the governor and the automatic voltage regulator (AVR). These controllers permit adjusting the response of the generator regulating its output within the desired boundaries. The external regulators can be

added as an external loop to the VSM implementation, which not only allows emulating perfectly the behavior of those controllers but also, as they are a virtual implementation, some alternative methods can be combined to enhanced its implementations.

2.2.4.1. Virtual governor

A governor is a device used to measure and regulate the speed of a machine. The most classic example of governor is the Watt or fly-ball governor used in steam engines. Its main function is to adjust the speed of the machine, making the governor capable of controlling indirectly the frequency of the power system. In applications with multiple generation units operating in parallel, the most convenient approach is the use of a droop-based governor, where the speed and the frequency decrease as the output power increases. Feasible implementation of a governor inside of a VSM is presented in Figure 14.

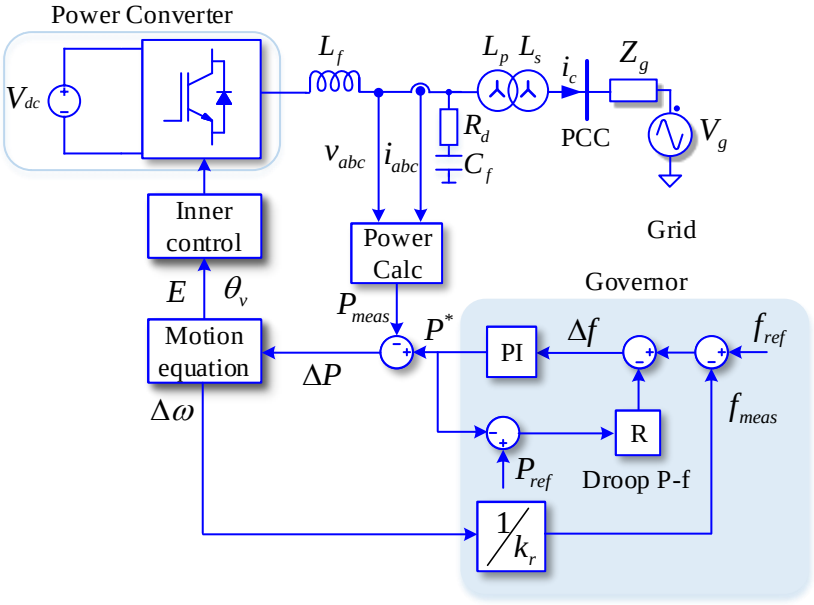

Figure 14: Implementation of a virtual governor

The conversion of the conventional structure of governor into a virtual governor is fully feasible. However, as it is necessary to consider that the power converter has a faster dynamic response, the virtual governor may have adapted features to offer an enhanced response in power converters.

2.2.4.2. Virtual automatic voltage regulator (AVR)

The synchronous generators require an excitation system for the energy transformation. It also fixes the generator output voltage and reactive power, which highly impacts the stability of the entire electrical grid. This excitation system is generally controlled by the automatic voltage regulator (AVR). Although it provides a very effective solution during steady-state operation, in case of sudden disturbances and frequency oscillations, it may have a negative impact on the damping system.

In this regard, the use of the AVR in the power converter control will be focused on regulating the output voltage of the electromotive force and the reactive power. Therefore, the equivalent AVR in a VSM will create the amplitude of the emf, without hindering the frequency of the power system. As in the governor subsection, it is convenient to use a droop-based AVR when multiple generation units are connected in parallel, to have a natural share of reactive power exchange. Figure 15 presents an implementation of an AVR in a VSM model.

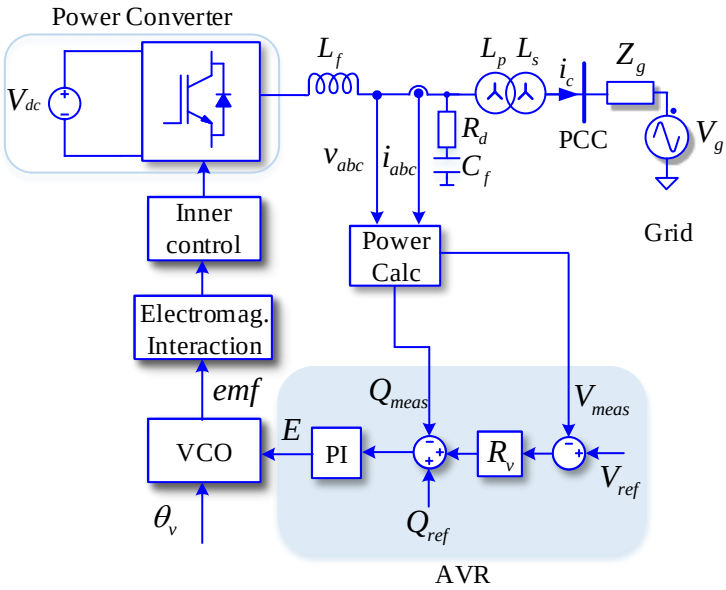

Figure 15: Implementation of an automatic voltage regulator

2.2.5. Inner control loops

Apart from the integration of the electromechanical, electromagnetic, and external regulators, the inner controllers fulfill an important role in the power converter control. The power converter is composed of switches that can generate a voltage output by using the dc-link as the voltage source. This voltage amplitude is regulated by the control duty, which is usually created by an inner control algorithm, a voltage controller, or a current controller, Figure 16.

On the one hand, the voltage controller can generate the necessary output duty for the power converter, however, during fast transients or short-circuits, the system is not able to regulate the output current of the converter. On the other hand, the current controller strategy provides a safer operation, as it acts as a limiter for the current delivered to the electrical grid. This limitation is necessary for electronic devices, as they cannot withstand more than nominal current.

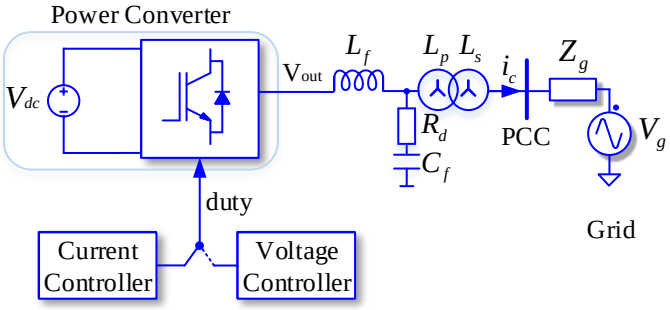

Figure 16: Power converter control with current or voltage controller.

The most typical power converter electrical composition is shown in Figure 16, where the output voltage, V_{out}, of the power converter is filtered by an LC or an LCL filter. To properly control the output current of the converter, the system needs to adjust the magnitude and the phase angle of the output voltage V_{out} in order to regulate the current being delivered by the power converter.

The need to determine the magnitude and phase angle of the utility grid before the connection of power converters to the grid has been one of the most studied issues during the last decade. The synchronization loop is, in most cases, the key factor for any power converter connected to the grid, as it is the one in charge of the detection of the grid phase and the amplitude in most of the power converter controllers. In this regard, PLL is the most extended synchronization system in power electronics connected to the grid, which uses the grid voltage to extract the magnitude and the phase angle using the synchronous reference frame (SRF). The general structure of the SRF-PLL is presented in Figure 17, which is composed by a Park transformation, to rotate the system from the stationary into the synchronous reference frame, a proportional-integral (PI) controller, to eliminate the voltage error in the q axis, and an integrator, to obtain the phase angle from the calculated grid frequency.

Where $\boldsymbol{v_{abc}}$ is the three-phase voltage measurement from the grid, $\boldsymbol{v_{dq}}$ expresses the synchronous reference frame of the grid voltage, $\Delta\omega$ defines the frequency deviation to adjust the voltage magnitude in the q axis to a value of zero, ω_r is the nominal frequency of the grid, and finally θ_g defines the detected grid phase of the system.

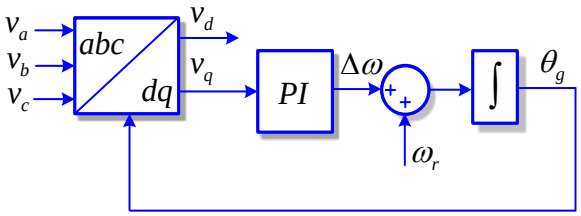

Figure 17: SRF Phase-locked loop traditional structure.

This phase angle is then used to rotate the grid voltage from the stationary into the synchronous reference frame to create two components that are static from the control point of view.

The PLL output phase has been used in many applications to shift the system from a static control in *abc* to the synchronous system in the *dq* frame. This synchronous reference frame is the most extended approach for power converter control, as it uses traditional PI controllers to regulate the current output of the power converter. Figure 18 presents the typical control scheme of a VSC converter using the synchronous reference frame. In this case, the PLL connected to the point of common coupling (PCC) of the power converter receives the voltage measurement of the three-phase signal and extract the phase and its magnitude, represented by θ_{PLL} , v_d and v_q respectively. The phase detection signal is then used to rotate the input signals of the current, $\boldsymbol{i_{abc}}$, into the *dq* synchronous reference frame, $\boldsymbol{i_{dq}}$, to use the PI controller to generate the voltage magnitude, $\boldsymbol{v^*_{dq}}$, and return these values into the stationary reference frame to be sent to the power converter control voltage, $\boldsymbol{v^*_c}$.

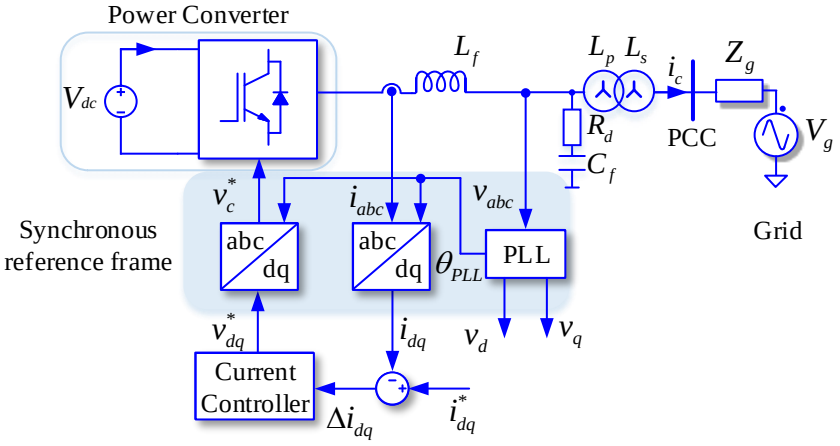

Figure 18: Traditional synchronous reference frame power converter current control

Even though the PI control structure is one of the most extended current control techniques for power converters connected to the grid, the performance and the stability margin of the controller are highly dependant on the strength of the electrical grid connection and the PLL dynamics. In this regard, other types of current control techniques have been researched and integrated into grid-connected power converters through the years. These new strategies are based on the use of the stationary reference frame, avoiding the use of a PLL to detect the magnitude and the phase of the grid voltage to be synchronized to the electrical grid.

2.2.5.1. Current controller structure

The synchronous reference frame which describes two continuous components is generally used to control the system with a PI controller for each component. In general, the system can be represented as Figure 19, in which, through the elimination of the error of current at the converter output, $\Delta \boldsymbol{i_{dq}}$, the system calculates the voltage reference for the power converter, $\boldsymbol{v_{dq}}$, to deliver the specified current, $\boldsymbol{i^*_{dq}}$.

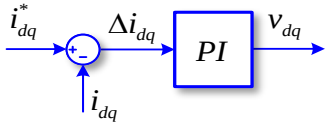

Figure 19: PI Controller in the *dq* reference frame

The transfer function of the PI controller can be expressed as (10), where the parameters k_p and k_i define the settling time and the stability of the current controller.

$$\mathbf{H}(\mathbf{s})_{PI,dq} = \begin{bmatrix} k_p + \frac{k_i}{s} & 0 \\ 0 & k_p + \frac{k_i}{s} \end{bmatrix} \tag{10}$$

Although the outstanding performance and the easy implementation of the PI controller, the synchronous reference frame still requires a PLL to detect the phase, to make the system rotate at the same speed as the grid. The use of the PLL is not necessary if the system is controlled in the stationary reference frame by terms of using a resonant controller, composed of two integrators in series which generates a 180 phase shift into a sinusoidal waveform. In this way, the system can eliminate the input error by subtracting the value from the integrators. One of the most used resonant control strategies is the second-order general integrator (SOGI). As shown in Figure 20, the main idea of the double integrator is to generate a 180-degree phase shift to the input signal to obtain the resonance characteristic, that will make the values of $\boldsymbol{v^*_{\alpha\beta}}$ increase until the quadrature variables, $\boldsymbol{qv^*_{\alpha\beta}}$, are able to eliminate the error in $\Delta \boldsymbol{i_{\alpha\beta}}$.

If the system is analyzed, the first branch is a pure integrator from the error, which leads to a 90-degree phase shift lag at the output. Once it is integrated a second time, the signal gets a 180-degree phase shift lag in respect to the input value, which is then subtracted to reduce the error at the input of the first integrator.

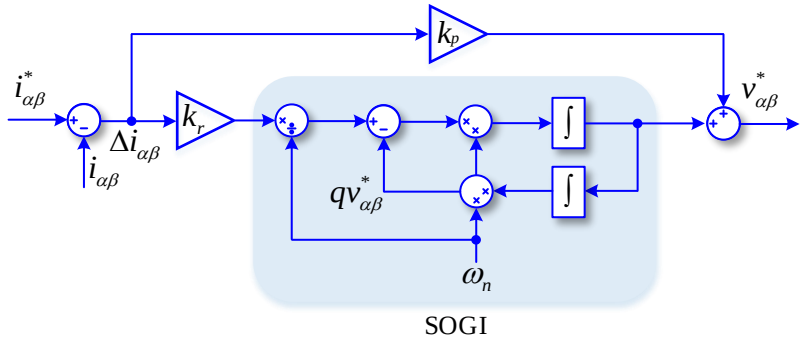

Figure 20: SOGI current controller structure

With infinite gain at the resonance frequency, ω_n, the second-order general integrator (SOGI) PR controller can reduce the steady-state error to zero. The equivalent transfer function can be described as (11).

$$\mathbf{H}(\mathbf{s})_{PR,\alpha\beta} = \begin{bmatrix} k_p + \dfrac{2k_r s}{s^2+\omega^2} & 0 \\ 0 & k_p + \dfrac{2k_r s}{s^2+\omega^2} \end{bmatrix} \tag{11}$$

Where the parameters k_p and k_r define the settling time and the stability of the current controller in the stationary reference frame.

2.2.5.2. Decoupling matrix

The effect of the output LC or LCL filter into the power converter control gathered much attention in the synchronous reference frame, which made the active and reactive power to couple during power steps and transients. The addition of a decoupling matrix is a method to decouple the active and reactive power at the output of the converter. The description of this principle can be analyzed by the voltage difference between two voltage sources through an impedance, Figure 21. This difference creates a circulating current depending on the magnitude and the phase difference.

To study the voltage variation at the first inductor, the system can be transformed into the synchronous reference frame to reduce the number of equations and to highlight the effect on each of the axes.

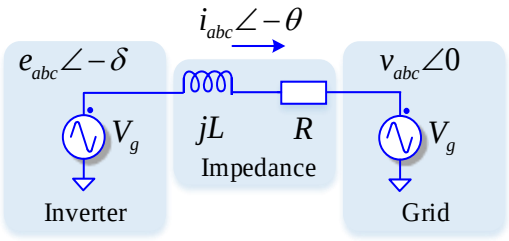

Figure 21: Current through and impedance between two voltage sources

Where equations (12) and (13) present the relationship between the current through the impedance, $\boldsymbol{i_{dq}}$, and the voltage variation, $\boldsymbol{\Delta v_{L_{dq}}}$.

$$v_d(s)-e_d(s)=(R+Ls)\cdot i_d(s)-\omega L i_q(s)=G_L(s)-\omega L i_q(s) \tag{12}$$

$$v_q(s)-e_q(s)=(R+Ls)i_q(s)+\omega L i_d(s)=G_L(s)+\omega L i_d(s) \tag{13}$$

To reduce the coupling terms appearing from the inductance in the system, the decoupling term, $j\omega_g L$, is introduced as a compensation factor in the current controller output, Figure 22. The resistive value of the inductance can be usually neglected as its value compared to the inductance is insignificant.

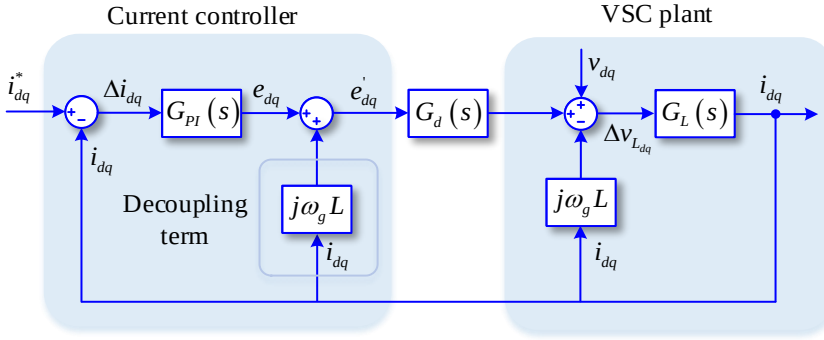

Figure 22: Transfer function diagram of the decoupling terms in the current controller.

This coupling component gives rise to a coupling between the active and reactive power at the output of the converter. For this reason, in case of the synchronous reference frame, *dq*, the output is generally forwarded with this decoupling term of the inductance value. Figure 23 presents the decoupling matrix integration into the *dq* current controller implementation, where the subtraction and the addition of the voltage deviation quadrature component are included in their respective axis.

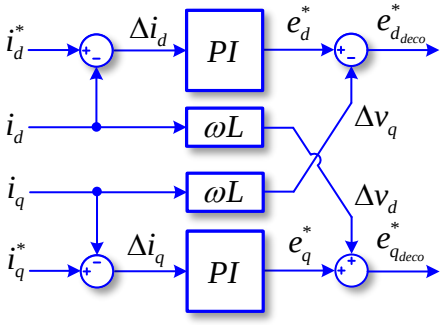

Figure 23: Synchronous reference frame decoupling matrix

On the stationary reference frame, the same mathematical procedure can be used to obtain the decoupling matrix. In this case, to obtain the coupled terms in the $\alpha\beta$ frame it is needed to consider that the magnitude of the current can vary with time. Taking into consideration equations (14) and (15) as the initial mathematical expression to evaluate the voltage drop at the inductor, the system can be linearized.

$$\frac{d\left(i_\alpha(t)\right)}{dt}\cdot L = v_\alpha(t) - e_\alpha(t) - R\cdot i_\alpha(t) \tag{14}$$

$$\frac{d\left(i_\beta(t)\right)}{dt}\cdot L = v_\beta(t) - e_\beta(t) - R\cdot i_\beta(t) \tag{15}$$

Where the linearization of the voltage drop at the inductor, considering that the magnitude varies sinusoidally with time at a frequency ω, the equation can be expressed as equations (16) and (17).

$$\Delta v_{L\alpha}(t) = v_\alpha(t) - e_\alpha(t) - R\cdot i_\alpha(t) + \omega\cdot L\cdot i_\beta(t) \tag{16}$$

$$\Delta v_{L\beta}(t) = v_\beta(t) - e_\beta(t) - R\cdot i_\beta(t) - \omega\cdot L\cdot i_\alpha(t) \tag{17}$$

Comparing the synchronous and the stationary reference frame mathematical equations and the equivalent transfer function, it is possible to see that the coupling existing during the transient in current through an inductor is equal in both reference frames, Figure 24.

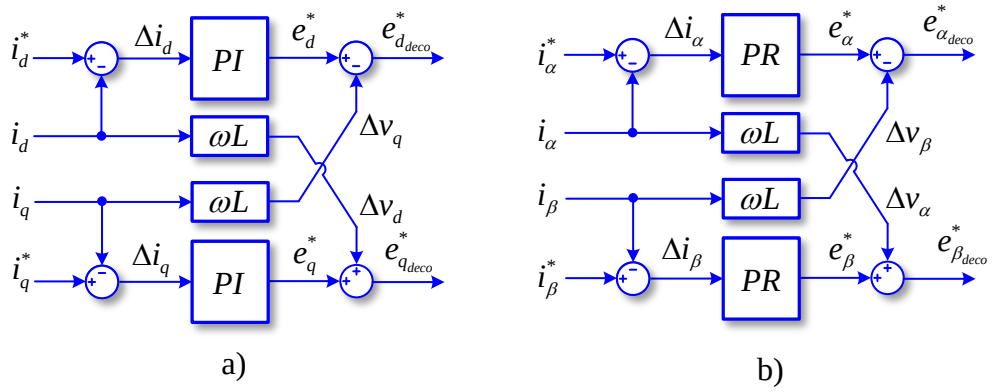

Figure 24: Decoupling matrix in a) Synchronous reference frame b) Stationary reference frame

2.2.5.3. Positive and negative decomposition

The synchronization unit is the key element to detect the phase angle, the magnitude, and the sequence of the electrical grid. As it was presented in the previous section, the PLL is a simple yet effective way to detect the phase angle and the magnitude of the input voltage. However, the traditional structure of the PLL only allows the detection of the positive sequence, rotating at the grid nominal frequency. Extensive work has been presented in the literature about how to enhance the PLL structure to detect and decompose the voltage into the positive and negative sequence for control purposes, adding also harmonic calculation. One of the used techniques in the synchronous reference frame is the decoupled double synchronous reference frame PLL (DDSRF – PLL) [11], which uses two synchronous reference frames, allowing the decoupling effect on the negative sequence in the positive angular speed, and the positive sequence in the negative angular speed.

In this regard, the SOGI structure has been used as an alternative synchronization system that focused on detecting the frequency. This synchronization method is called frequency locked-loop (FLL), and it uses the quadrature signal generator (QSG) natural resonant structure to generate an adaptive filter system, which replicates the input sinusoidal waveform voltage by generating a quadrature vector of the input [12]. This structure has been also widely used to decompose and extract the positive and negative sequence from the grid [13]. However, the need for algebraic equations at the output of the SOGI structure adds complexity to the solution.

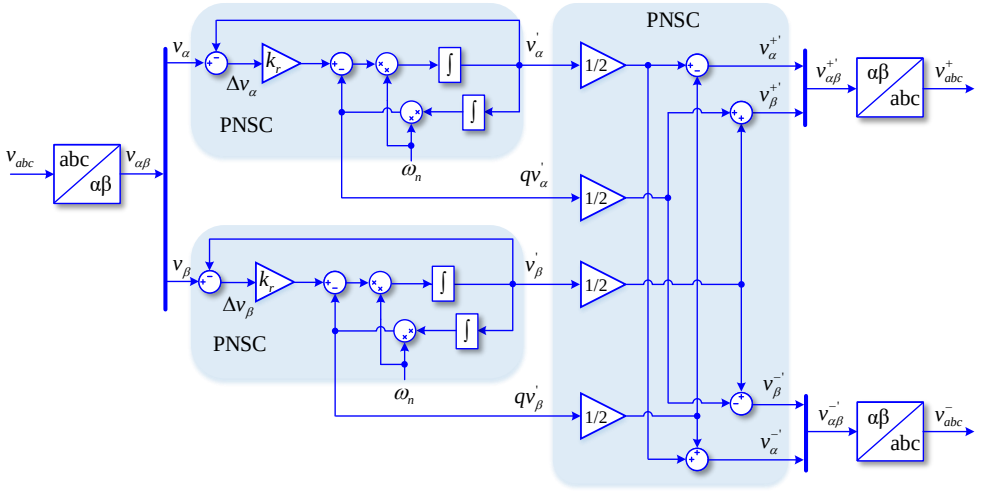

Figure 25: Positive negative sequence calculation

2.3. Virtual synchronous machines implementation

The combination of the blocks presented in the previous section gives rise to different implementation approaches, each one having its own advantages and drawbacks. During the last decade, many different proposals have been presented by research centers and private entities, although most of them are minor adjustments on the same idea. It is possible to identify six virtual synchronous machine implementation families, which are the central pillar for the rest of the proposals. In this section, each family will be structured with the functional blocks presented in the previous section. The general VSM implementation families are presented in Figure 26.

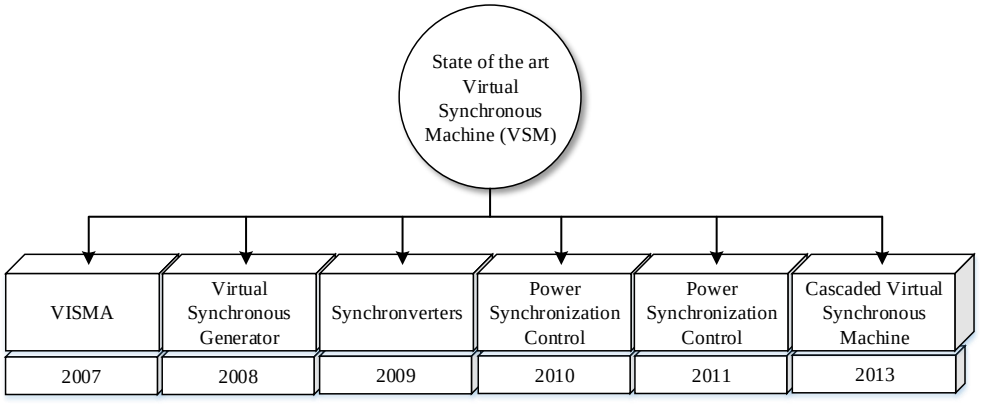

Figure 26: Main implementation approaches of a virtual synchronous machine.

2.3.1. VISMA

During the year 2006, several patents were presented in different countries, all of them with the first version of the VISMA model. There were some patents published beforehand, but it was not until 2007 that the VISMA was publicly presented [14]. In the first approach, the synchronous machine was emulated completely. The functional blocks used by this first VISMA approach are highlighted in the implementation tree in Figure 27.

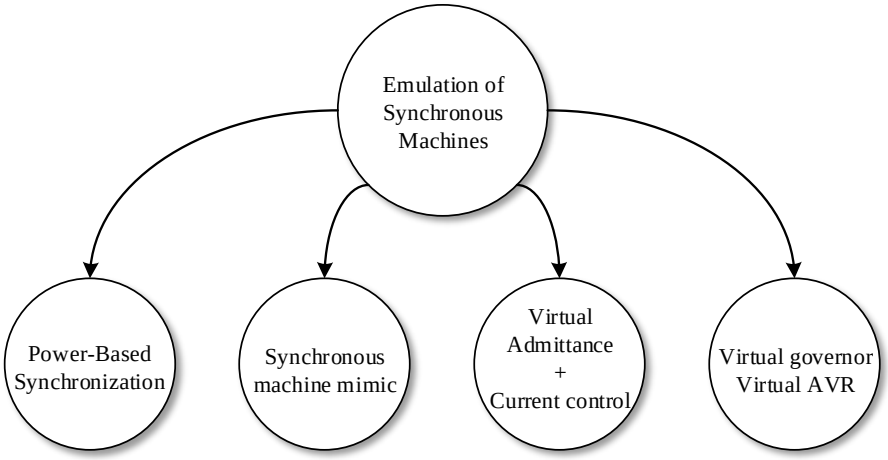

Figure 27: Implementation tree for the first version of VISMA.

The electromechanical layer is a mimic of the synchronous machine, which receives the mechanical torque and excitation as references to the model. This delayed model includes the swing and the flux linkage equations, which consider the stator, the damping windings, and the excitation winding. These equations define the current through the stator of the virtual synchronous machine as a function of the angle and the grid voltage parameters. This reference current is used for the current controller, which regulates the injected current of the power converter. Even though any kind of current controller loop may work for this application, a hysteresis current controller is used in this particular case of the VISMA implementation. In addition, following the traditional synchronous machine control, the excitation voltage and the input torque are provided by external frequency and voltage regulators. The resulting VISMA model can be implemented as in Figure 28.

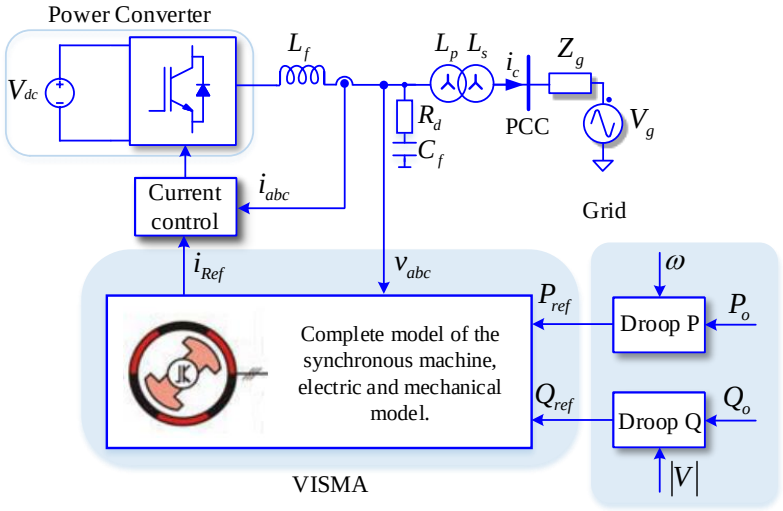

Figure 28: Basic VISMA model

The use of this VISMA model allows the elimination of the conventional grid voltage synchronization system and adds the capacity to generate electrical islands, even when the power converter based on VISMA is the only generator available. Although it is a feasible implementation, the model is rather complex as it requires the definition of constructive parameters of the electrical machine. On top of this, the synchronous machine inherits all the characteristics of the electromechanical and electromagnetic loops, along with its drawbacks, such as the weak damping factor or a slow response to excitation changes. This leads to reaching the same stability problems as in an electrical system with real synchronous machines. The VISMA model includes fast dynamics-related transients and sub-transient responses, which could lead to a stability problem in the real implementation of this control in a power converter, especially when considering low sampling and switching rates. The advantages and drawbacks of the VISMA implementation are presented in Table 2.

Advantages:	Drawbacks:
▪ The current reference can be supplied to any current control loop, which in addition has overcurrent protection. ▪ Mimic implementation of a synchronous machine ▪ No need for additional voltage synchronization (PLL) ▪ Allow network support and load sharing.	▪ The computation time is large ▪ Stability issues when connecting to the electrical grid.

Table 2: Advantages and drawbacks of VISMA implementation

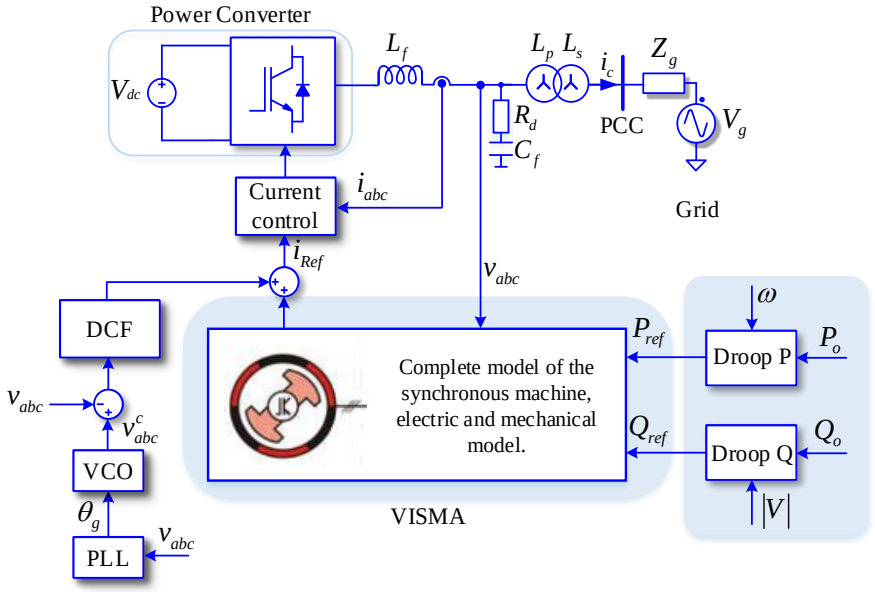

Figure 29: VISMA Model with harmonics compensation

Further implementations were added into the VISMA approach with the patent [15] and paper [16], where the same model for the synchronous machine was developed but with a parallel system devoted to harmonic compensation and voltage unbalance control. This compensation system works in a parallel branch with the VISMA model, modifying the current reference sent to the current controller. The structure uses a single-phase PLL to synchronize to the electrical grid, which modifies the dynamic of the virtual synchronous machine implementation, making it complex to operate in island mode. This additional control, based on a virtual admittance, uses the grid voltage detected by a PLL as an input reference, which is used to generate the voltage difference that determines the current reference to be injected into the grid through a virtual admittance. The reference value is then adjusted by a parameter called distortion compensation factor (DCF), Figure 29. However, there is not much information about how that parameter is adjusted in a real implementation.

A variation of the original VISMA implementation was presented in [17], where the electromechanical loop was simplified from a detailed model in the synchronous reference frame to a reduced model composed only of an L-R admittance at the output in the natural reference frame. In this publication, some experimental results regarding load sharing, frequency variations, and oscillation attenuation were presented, showing interesting results. In [18] and [19] additional experimental results based on this simplified model of VISMA were presented. In the first one, the paper presents results for power and voltage reference

variations, as well as parallelization of two VISMA systems, modifying the inertia and damping for different grid disturbances. In the second one, experimental results for the islanding operation of the VISMA system are presented, specifically the transition between the grid-connected to the island mode, and energizing an electrical island. However, the information about droop controllers was not included, even though it is stated that it is essential for maintaining the island operation.

2.3.1.1. Simplified voltage source – VISMA

In 2012, a new approach for the VISMA model was presented and studied in [20]. In this model, the power converter control is switched from a current controller to an open voltage loop controller, and the virtual admittance is modified to a virtual impedance. The implementation tree for this VISMA approach is presented in Figure 30.

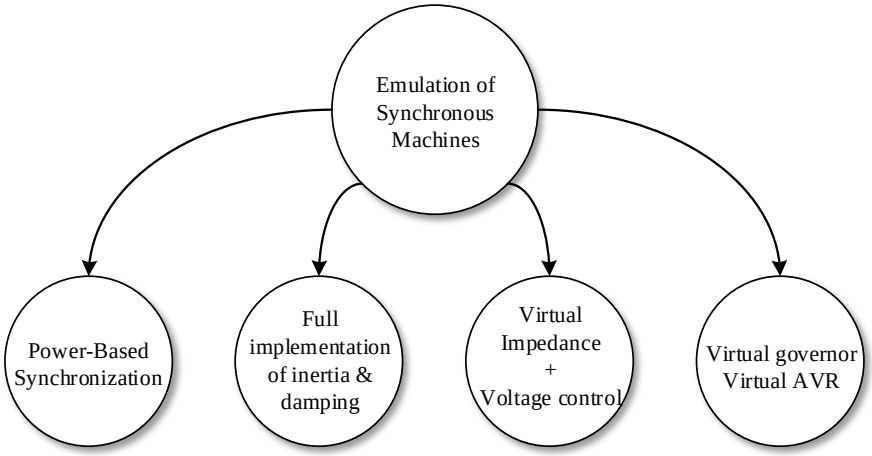

Figure 30: Implementation tree for the modified VISMA structure

In this modified implementation, as the inner controller is adapted to an open voltage controller, the virtual admittance is processed as a virtual impedance instead. Therefore, the measured current needs to be used to obtain the voltage difference. To achieve a noise-free signal, it is necessary to use a filter to remove high frequency from the derivative term of the inductor. However, the specifications of the filter are not defined in the paper. In the model, the *f(s)* function is used as a phase compensator for the mechanical loop, but there is not much information about the transfer function implemented. Although it is stated in [20] that the modified model is more stable operating in island mode compared to the previous model, the lack of protection against overcurrent in this implementation makes it less feasible to integrate into a power converter.

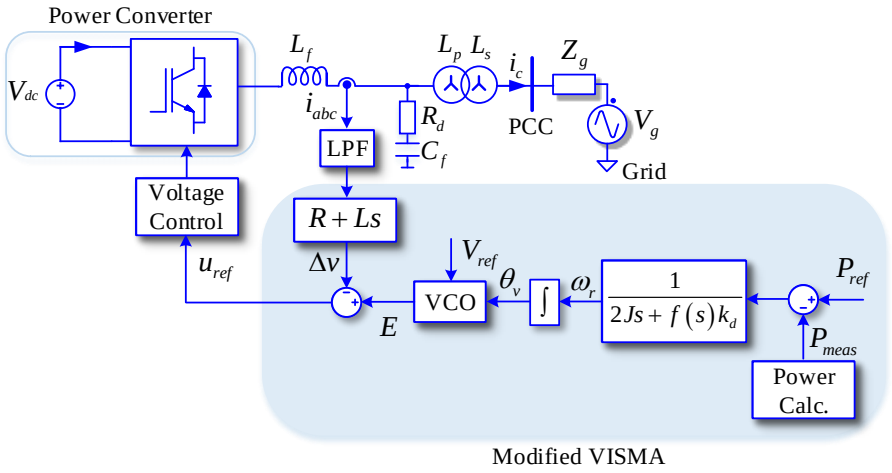

Figure 31: Modified VISMA model

2.3.2. Virtual synchronous generator - VSYNC Project

The European project "VSYNC", which started in October 2007, proposed an approach to emulate the synchronous generator behavior in distributed power converters by adding some energy storage capacity. The idea behind the emulation of the synchronous generator is to add a short-term energy storage system to the power converter to be able to provide inertia to the system, contributing in this way to the grid frequency stabilization.

The implementation tree for the VSYNC approach can be defined using the implementation tree architecture, where the specific methodology for synchronization, electromagnetic, electromechanical, and external loops are introduced.

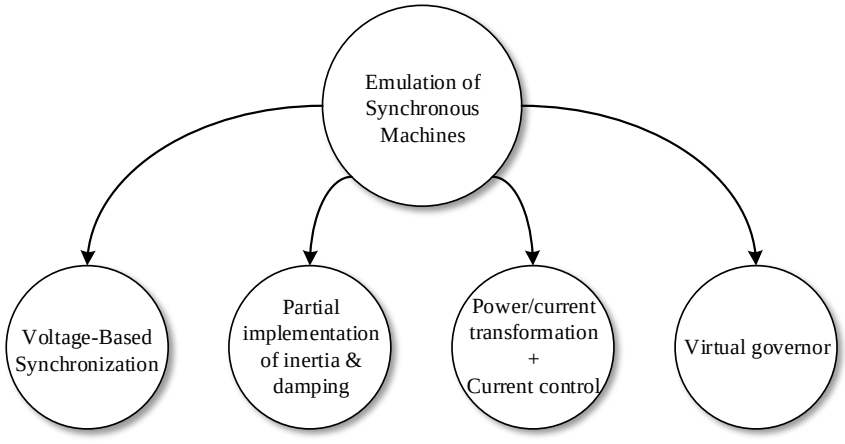

Figure 32: Implementation tree for the VSG approach – VSYNC Project

The VSYNC first publication dates from 2008 where papers [21] and [22] show the general concept for the virtual synchronous generator as an approach to emulate a virtual rotating mass to stabilize the grid. The VSG presented a solution to improve the power converter control by including the emulation of a synchronous generator, achieved by adding some energy storage capacity. Using the motion equation of the synchronous generator shaft, the initial approach was based on the modification of a PLL to match the motion equation dynamics. Such PLL was adapted to set the virtual electromechanical loop of the power converter control, making the system able to emulate inertia in case of transient grid events.

The first implementation of the control schematic for the VSG approach was presented in 2009, where the PLL to reproduce the swing equation dynamic was shown, presenting a similar behavior as the electromechanical loop in a synchronous generator [23]. The PLL does not only provide the frequency measurement, but also the power reference for the converter. Figure 33 shows the control scheme for the PLL implementation in the VSG, which enables the system to be synchronized to the grid, as well as emulating the inertia of a synchronous generator.

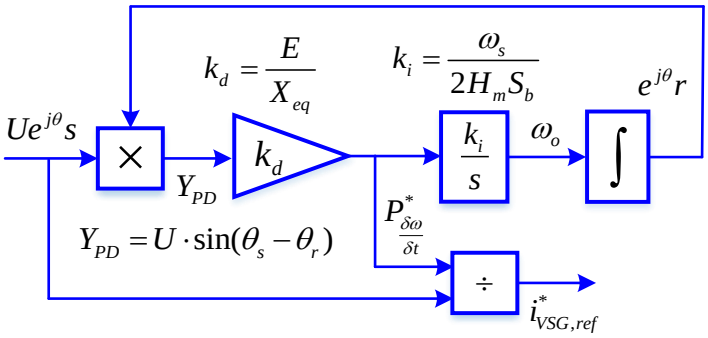

Figure 33: Implementation of the PLL in the VSG

In [24] the inertia emulation control was implemented at a high layer within the inverter control structure, which used a Linear Quadratic Gaussian (LQG) controller in the lower level to regulate the exchanged power between the converter and the grid. In this regard, results of such VSG-based power converter were tested under different case scenarios [25], including frequency regulation, micro-grid operation, or black-start of a microgrid. Even though the VSG initial approach consisted of the emulation of the inertia reproducing the swing equation dynamic on a PLL, other alternatives were proposed along with the VSYNC project. One of the proposals was obtained through the derivation of the frequency output of the PLL in addition to a gain parameter to emulate the effect of the inertia. Then, a droop regulator was included in the control scheme by using the error of frequency detected by the PLL to act as a damping winding in the VSG strategy, Figure 34.

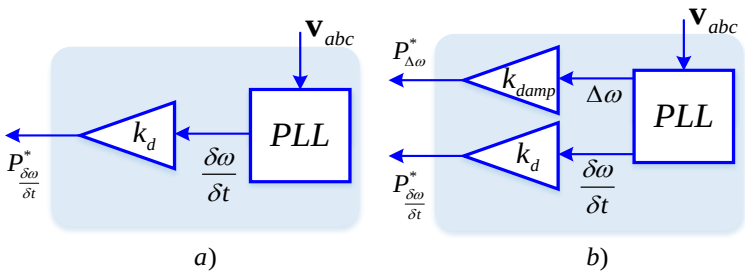

Figure 34: VSYNC project PLL implementation a) Inertia emulation b) Inertia and damping effect

In [26] an individual VSG and a coordinated VSG scheme were presented, and the results in the real-time simulation were presented in [27]. The latter control scheme allows multiple VSG units to coexist, even if they have different specifications, to evenly distribute the power among units during frequency deviations, and maintain the state of charge (SoC) of the energy storage within safety limits. This approach implemented in the VSYNC project can be classified as a voltage-based system, which relies on the PLL to set the interaction with the electrical grid. In addition, the SoC power control is included into the support strategy to limit the capacity of the battery storage system, Figure 35.

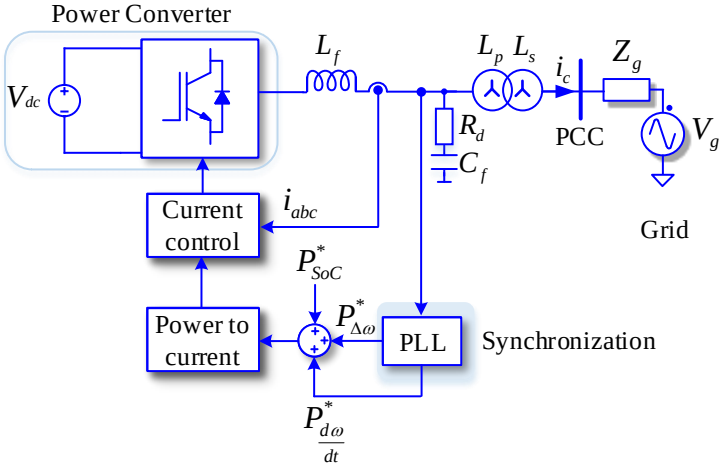

Figure 35: Virtual Synchronous Generator – VSYNC Project

This implementation was tested in two demonstrator sites. The first one is located in the Netherlands, where the experimental setup is composed of 10 VSG of 5kW rated power each [24]. The second experimental setup was located in the area of Romania, where a 100kVA power converter based on the VSG was installed as the main supply of a residential load. In addition to these two demonstrators, multiple VSG units were coordinated to provide

frequency stability in [28] [29]. The advantages and drawbacks of this implementation are presented in Table 3.

Advantages:	Drawbacks:
▪ The use of the current controller inherently provides overcurrent protection to the system ▪ Allows emulating inertia and damping of a synchronous machine.	▪ The electromechanical behavior is exclusively linked to the PLL dynamics ▪ The derivative term of the PLL can give rise to instabilities depending on the grid characteristics.

Table 3: Advantages and drawbacks of the virtual synchronous generator approach

2.3.3. Synchronverter

In 2009, the static synchronous generator was proposed by Qin-Chang Zhong and George Weiss under the name of synchronverter, to approach the emulation of the behavior of synchronous generators from the grid point of view [30]. In 2010, experimental results about the synchronverter, as well as in-depth analyses, were presented in [31] and [32], where the desired behavior and stable operation of the synchronverter were verified under power reference steps and grid frequency deviations. Due to this stable operation, this implementation soon found application in different systems, such as STATCOM [33], power system stabilizer [34], transformerless PV inverters [35], and electrical drives [36].

The modeling of the synchronverter is based on a simplification of the synchronous generator equations, in which the damping windings and the iron core saturation are neglected. The control layers of the synchronverter considering the implementation tree are shown in Figure 36. Even though in an initial stage the synchronverter was presented to synchronize by power balance during grid-operation, the PLL had an essential function during the start-up process. For the electromechanical loop, a complete mathematical model of the generator is adopted, excluding the damping windings and the saturation effects. Finally, a simplified version of the virtual governor and the virtual AVR are considered as frequency and voltage droops.

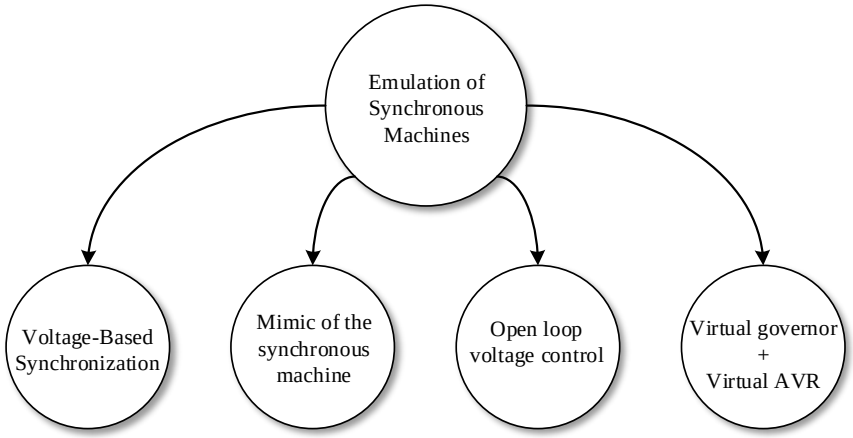

Figure 36: Implementation tree of the first version of the synchronverter

Although the concept of the synchronverter was convincing, the practical implementation remained an open question since limited results were presented in publications, Figure 37. Some concerns arise in this regard:

- The PLL is still needed for adjusting the converter during the start-up process and for the reactive power control.
- The damping windings are omitted which may affect the damping capability of the system
- The open-loop voltage control emulating the electromagnetic interaction may jeopardize the synchronverter stability, as the inductance of the power converter output is smaller than the one in a synchronous generator.

After the first implementation of the synchronverter, many researchers have made numerous attempts to validate and improve the synchroverter concept. Major improvements to the initial concept were made in all the layers of the implementation tree. In 2013, the voltage control loop was enhanced by adding a PI controller to compensate for inverter parameter mismatches, modifying the electromagnetic loop slightly [37]. In 2015 a comparison between the dynamic performance of the synchronverter and a synchronous generator was made, from the perspective of the electrical grid [38]. Concerning the synchronization method, there was a major upgrade in [39] which included the use of a virtual admittance and a PI controller to avoid the use of the PLL during the start-up process. Even though the use of switches to modify from a self-synchronization mode to a grid-connected mode operation, the synchronization method was enhanced to work only as a power-based synchronization system. The detailed model of the synchronverter with those modifications is presented in Figure 38.

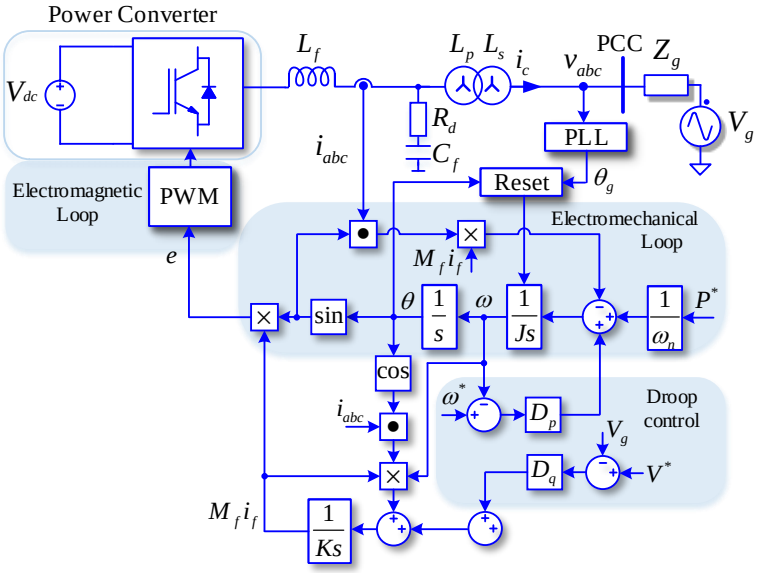

Figure 37: Synchronverter implementation with PLL

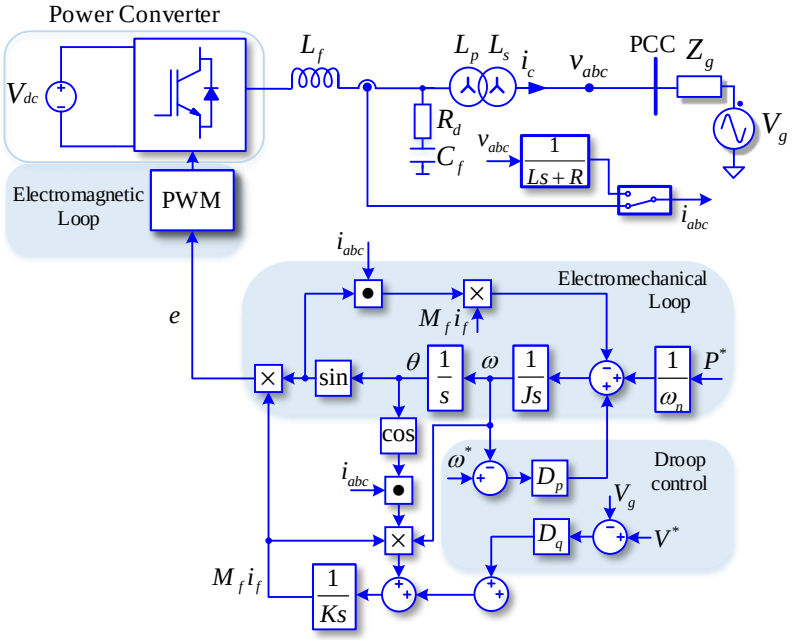

Figure 38: Synchronverter without the use of the PLL

Over the years, more applications of the synchronverter were found in the literature such, as multilevel modular converters [40], hybrid multi-terminal HVDC systems [41], and isolated micro-grids [42]. In the last two publications, an additional droop control was included in the control scheme to allow coordination among different synchronverter units. Apart from this research, additional stability and design aspects of these implementations were discussed in [43] and [44].

Related to the electromagnetic interaction of the synchronverter, [45] concluded that the control of the synchronverter was less stable than a synchronous machine of the same rating, due to the output inductance of the power converter filter, which is much smaller than the stator inductance of the machine. To overcome this problem, a virtual impedance was included in the voltage control loop to virtually increase the output impedance of the power converter. As another approach to further rise the stability margin of the synchronverter implementation, some modifications were made to the field current, to ensure that the frequency and the voltage magnitudes would stay within the given range [46]. In [47] an additional virtual admittance is set to improve the quality of the injected current during abnormal or distorted conditions in the grid, Figure 39. An alternative to [47] was presented in [48] where the system uses a virtual harmonic impedance.

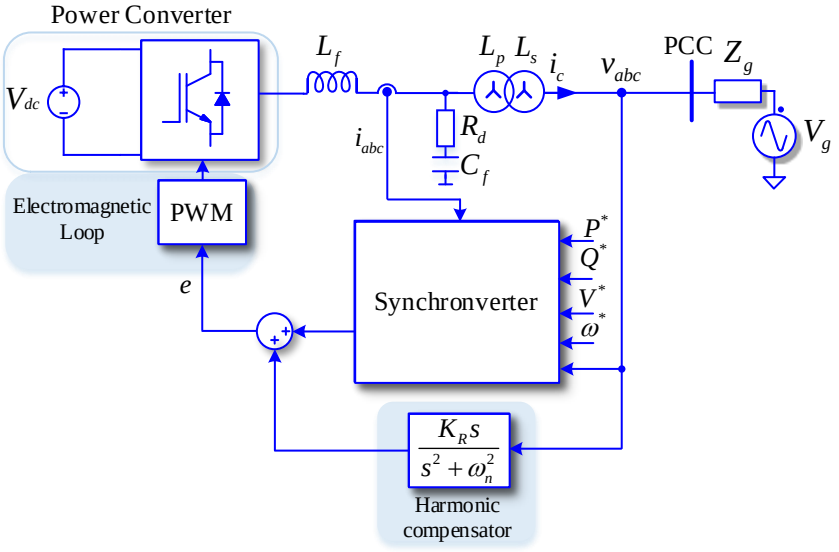

Figure 39: Synchronverter with virtual admittance for distorted conditions

The absence of current control in the implementation of the synchronverter gives rise to a potential issue related to the open-loop voltage regulation. The excessive-high inrush fault current is a big drawback which was confirmed in [49]. One of the most important

modifications in [49] was the use of a hysteresis current controller to limit the injected current during faults, which, in addition, included a fault detection algorithm. This allows the synchronverter to work as a voltage source during normal grid conditions. However, during grid faults the hysteresis current controller is activated and, at the same time, the power control loop is disabled forcing the power converter to be in a grid-feeding mode.

In 2017, the electromechanical loop of the synchronverter was further investigated in [50], where it was confirmed that using the damping factor dependant on the droop coefficient is not an optimal solution, since the response of the converter cannot be adjusted without affecting the steady-state droop characteristic. To adjust the damping factor independently, a correction on the damping loop was introduced in [50], which is based on the addition of the derivative term on the active power feedback, preserving the final droop characteristic. As consequence, the additional derivative term allows the synchronverter to be modified freely without interfering with the droop, however, measurement noises in active and reactive power can give rise to significant degradation in the performance of the synchronverter. To solve this issue, low-pass filters were used to reduce the high-frequency noise in the measurement signals in the damping correction fault as shown in Figure 40.

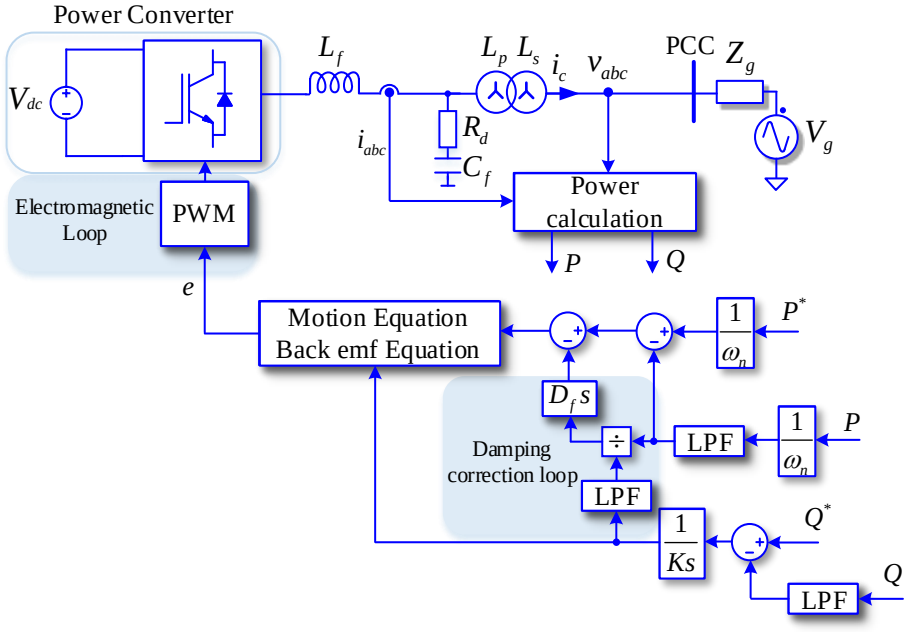

Figure 40: Synchronverter with damping correction loop

The advantages and drawbacks of the synchronverter implementation of a VSM are presented in Table 4.

Advantages:	Drawbacks:
▪ Straightforward implementation as it mimics the synchronous generator dynamic equations. ▪ No additional hardware is needed.	▪ In some implementations, a PLL is required for start-up ▪ The use of the inverter output filter reduces the stability margin. The implementation needed an additional virtual impedance or admittance. ▪ Reduced practical verification under grid faults.

Table 4: Advantages and drawbacks of the synchronverter implementation

2.3.4. Power Synchronization Loop

A first stage of the power synchronization loop (PSL) was presented in [51] by Lidong Zhang and Hans Peter Nee, linking the power synchronization to the operation of power converters, which was later extended in collaboration of Lennart Harnefors [52]. The PSL is oriented for high voltage dc systems (HVDC), however, the analysis presented can be extended for low voltage AC systems. The PSL can be shown using the control layers in the implementation block as shown in Figure 41.

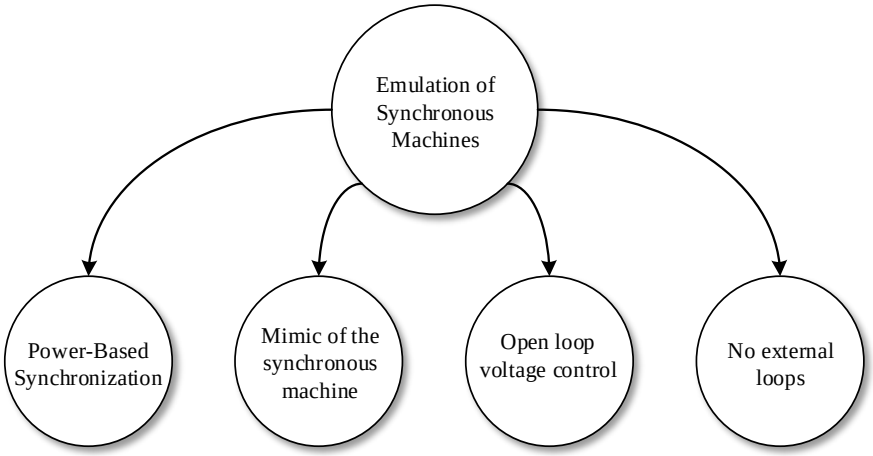

Figure 41: Implementation tree of the power synchronization loop

The PSL relies on the power balance between the reference power and the measured power on the power converter to synchronize to the electrical grid, regulating the load angle detected by the synchronization system. In the original proposal of the PSL, there was not a detailed description of how the electromechanical layer was implemented in the power converter. Regarding the electromagnetic layer in this implementation, instabilities and resonances in the

current are compensated by adding a high-pass filter in the current feedback signal in the voltage control loop, which acts as active damping for the electromagnetic loop.

The stability of power converters is an important factor in the large penetration of renewable energy in the electrical grid, especially in cases like microgrids, smart grids, HVDC systems, and electrical islands, which are characterized to be weak grids where large power converters should be connected to [53]. The low short-circuit ratio (SCR) in these systems generally gives rise to two issues in the stability of the power converter control. On the one hand, the PLL is highly affected by the grid voltage distortion created in weak grids, which can negatively affect the dynamic performance of the power converter, as well as reducing its stability margin [54]–[56]. On the other hand, the X/R ratio of the interconnection impedance highly influences the capacity of such a grid to operate in a stable range.

To provide a solution to this issue, in 2009 L. Zhang, H.P. Nee, and L. Harneforst presented the PSL approach for a VSM control [57], which was later patented in 2010 [58]. The main feature of this implementation is the development of the power-based synchronization, capable of improving the dynamic performance of the power converter under a weak AC system. This power loop is achieved by subtracting the power reference to the power measured by the converter, and then adding a controller gain to create the load phase angle deviation to synchronize the power converter as shown in Figure 42.

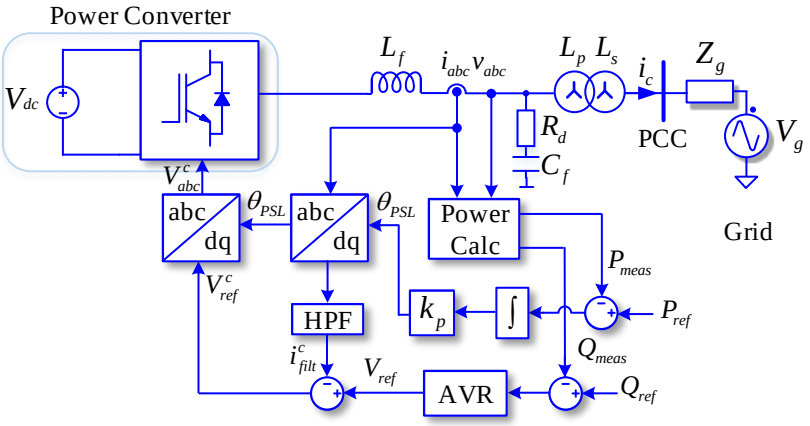

Figure 42: Control implementation scheme of the PSL approach

As it can be seen in Figure 42, the PSL does not implement the motion equation in the active power control loop. Instead, direct integration of the power error and the gain, k_p, are used to obtain the phase angle of the system, θ_{PSL}. This approach reduces the integrators used in the synchronization loop, reducing the regular motion equation into just one integrator, increasing

the stability margin of the power converter control but losing the physical meaning of the inertia provided by the active power during frequency deviations.

In [52] a modification on the voltage control loop was made, including the alternating-voltage controller (AVC) in the reactive power. This controller is implemented using a proportional controller with a first-order time delay, providing a droop characteristic in the voltage reference. In addition, during faults, a backup PLL is used to overcome high exigent operating conditions such as the start-up of the power converter or even grid faults. This transitory process related to the changes in the operation mode was studied in the PhD thesis [59]. It is worth mentioning that during demanding operating conditions where the PSL can not maintain the system under a stable operation, the PLL also loses control capacity to maintain the synchronism. Therefore, this use of the PLL may give rise to an even more undesired operation during faults, especially considering the change in the operation mode of the power converter. In 2011, the stability limits of the power were analyzed in [60], which was extended in [61], providing a wider analysis on the stability for the reactive power control, and considering the reactive power controller and the AVC block. In [57] the PSL approach was tested under weak grid conditions and voltage transients, and in [62] and [63] some results regarding the steady-state operation on wind farms and multi-terminal dc grids were reported.

The PSL implementation has not presented any major evolution since 2014, which compared to other VSM implementations is quite limited. Even though a pioneer on the power-synchronization loop, the limited capacity of emulating the swing equation reduces the capacity of providing adjustable virtual inertia to the system. On top of this, the voltage controller does not provide a major regulation advantage in front of the current controller, which in addition provides current limitation capacity.

As a summary, the advantages and the drawbacks of the PSL implementation of a VSM can be grouped as in Table 5.

Advantages:	Drawbacks:
▪ Simple implementation control algorithm ▪ The reduced integrator enlarges the stability margin in weak grids. ▪ The high-pass filter attenuates grid voltage resonances.	▪ A backup PLL is used for the start-up of the converter and in front of grid perturbances. ▪ The system does not present a beneficial control capacity during instabilities. ▪ The overcurrent protection is limited with the voltage controller implementation.

Table 5: Advantages and disadvantages of the PSL implementation

2.3.5. Synchronous Power Controller

The synchronous power controller (SPC) idea was patented in 2011 [64], [65], and [66], which was later published in 2013 in [67]. This implementation approaches the grid synchronization by using the power exchange principle, although it expands its functionalities by adding some upgraded algorithms that enable an enhanced response under exigent operation conditions. The control layer of the SPC can be defined using the implementation tree as shown in Figure 43.

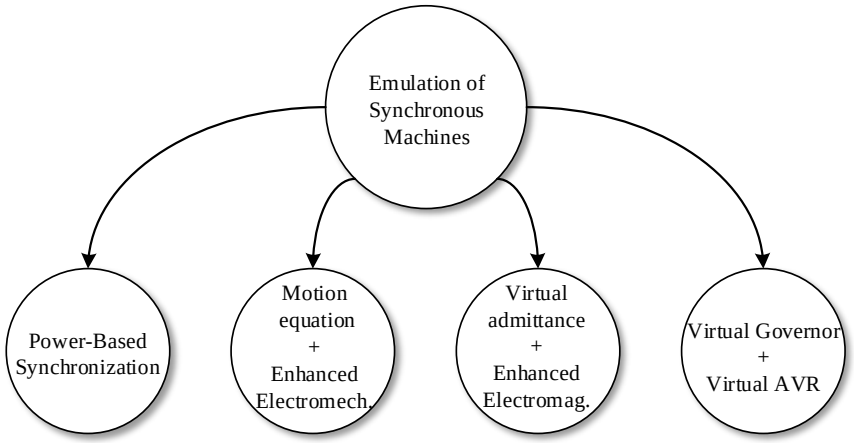

Figure 43: Implementation tree for the synchronous power controller (SPC)

The electromechanical layer in the SPC uses the power-based synchronization method, which guarantees the power balance in the converter and inherently synchronizes the system to the grid. Since the power loop controller (PLC) regulates the synchronization to the electrical grid, there is no need for any additional synchronization mechanism, such as the PLL. This controller enables a natural interaction of the power converter under all kinds of electrical networks including electrical islands and microgrids, by adjusting the virtual inertia and damping parameters depending on the grid operating conditions.

Regarding the electromagnetic layer, the SPC implements a virtual admittance that defines the current injected into the grid based on the impedance value, the measurement of the grid voltage at the PCC, and the internal electromotive force [66]. This reference current is used in the current control loop to regulate the response of the converter. In addition, considering the impedance in the generator is predominately inductive, it gives rise to a first-order low pass filter implementation, minimizing the voltage variability in the measurement [68].

The SPC first publication is dated 2013 [67], where experimental results of an SPC-based power converter connected to a PV system validated the VSM implementation. This first implementation is presented in Figure 44, where the electromechanical layer was mainly

controller by the motion equation integrated into the so-called PLC. In this block, the PLC adjusts the frequency deviation which is integrated to match the grid phase angle and provides the necessary active power demanded by the reference. The parameter of the PLC structure has to be properly defined to ensure optimum values for emulating inertia and damping in the power converter. The amplitude of the *emf* is controlled by a PI controller, which regulates the reactive power exchange. With those two magnitudes, the voltage-controlled oscillator (VCO) can generate the internal electromotive force which interacts with the grid through the virtual admittance.

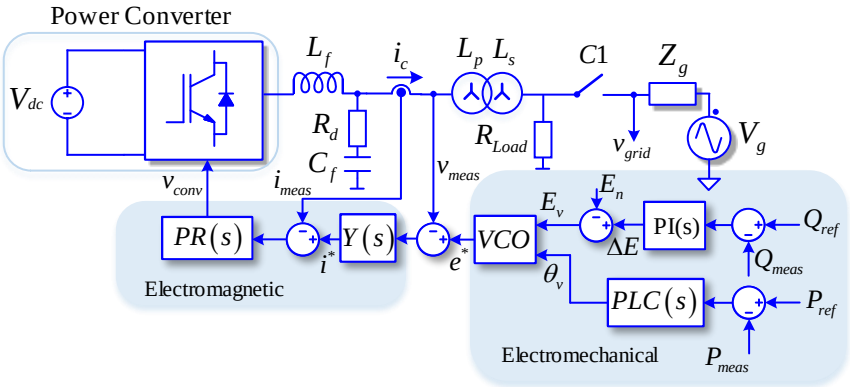

Figure 44: Synchronous power converter first implementation

The first PLC for the SPC implementation was presented in [65] and was based on a low-pass filter implementation. By adjusting the parameters k_c and ω_c, the inertia and damping of the electromechanical loop are defined. However, due to the implementation, this PLC structure results in a steady-state gain between the rotor frequency and the active power, giving rise to some interferences with the outer frequency droop control, deteriorating the steady-state support of the power converter. To provide the desired frequency support, the gain of the outer loop control has to be properly defined. In this regard, alternative structures for the PLC were analyzed in [69] and [70]. In [70] a comparison between different PLC structures was presented, where a PI structure for the PLC was presented to eliminate the inherent droop response of the initial PLC structure. In addition, a transfer function referred to as the configurable natural droop controller (CND) was presented, which had three configurable parameters, the inertia, the damping factor, and the steady-state droop gain, which can be independently adjusted.

An alternative control loop was presented in [71] for a STATCOM application, which added a PI controller to set the dc voltage to a specified value, whereas another PI controller regulates the AC voltage, controlling the reactive power exchange into the electrical grid. Another proposal for the electromechanical loop was presented in [72] and [73], where the virtual

inertia was stored as electrostatic energy in a capacitor connected to the same dc-bus of the power converter. In this proposal, the inertia was controlled from the dc-side by using a dc-dc power converter emulating the kinetic energy storage. In [74] a comparison between a conventional power converter controller based on a PLL approach and an SPC-based power converter was presented on the $\alpha\beta$ reference frame. This work proved the benefits of the SPC approach which considerably improved the performance of the system.

Grid support functionalities have been proposed in the literature for the SPC implementation. As an example, [75] presents an external droop controller to provide frequency and voltage support to the grid, where the parameters were adjusted according to the transmission system operator (TSO) requirements. Likewise, a variation of the electromagnetic loop in the SPC was presented in [68] to mitigate voltage harmonics at the grid side and providing support during grid voltage unbalances. In this work, the virtual admittance is split into several individual admittances working at a specific frequency range. The voltage used for each virtual admittance is extracted from a band-pass filter tuned to a given frequency and sequence. By adjusting the inductance and resistance, L_i and R_i for each virtual admittance, it is possible to set the dynamic performance of the SPC-based power converter for each harmonic frequency and sequence.

In [76] and [77] the SPC was used for an aggregated model of a distributed PV power plant, which proposed several power converters connected in parallel to PV strings to provide frequency and voltage restoration, as well as power oscillation damping. In addition, in [78] the stability of the distributed system was studied, focused on the ability of the system to maintain the supply during transmission blackouts. In this work, it was proved that the SPC approach in distributed generators improved the reliability of the system under disconnections of the grid. In [79] the impact of a hybrid solar power plant based on SPC-based power converters was presented. This work shows the harmonious interaction between the SPC system and an electromechanical generator supplied by thermal solar power. The analysis shows the increase in the damping of oscillations and the mitigating effect of frequency deviations.

The SPC has been implemented also in HVDC systems, wherein [80] a multi-area system was presented. This work analyzed the frequency stability in the HVDC links by providing inertia and damping emulation. In another work, the SPC was integrated into a modular multilevel converter, where simulation results validated the operation under voltage and frequency deviations. The SPC implementation has been proven to be an effective approach to be used in power converters as it presents a beneficial performance under stiff grids, weak grids, and in islanded mode. As a summary, the advantages and the drawbacks of the SPC implementation of a VSM can be grouped as Table 6.

Advantages:	Drawbacks:
▪ Easy implementation on traditional current-controlled power converters. ▪ Good performance during transients and steady-state operation. ▪ Enhanced behavior in the electromagnetic interaction to the grid. ▪ Good performance both in islanded and grid-connected operation.	▪ The PLC approach gives rise to an inherent frequency droop characteristic, which forces to retune the outer loop steady-state frequency controller.

Table 6: Advantages and drawbacks of the SPC implementation.

2.3.6. Cascaded virtual synchronous machine

In 2013, a conference paper presented another approach for a VSM implementation [81]. This initial work was later expanded in [82] and [83] where the implementation and development of the control model were further analyzed. This cascaded voltage-current control (CVCC) uses a power-based synchronization system, where the electromechanical loop is composed of the swing equation of the synchronous generator. For the electromagnetic loop, the system is based on the virtual impedance approach using a cascaded voltage-current controller in the inner loop. The implementation tree for the CVCC can be represented as Figure 45.

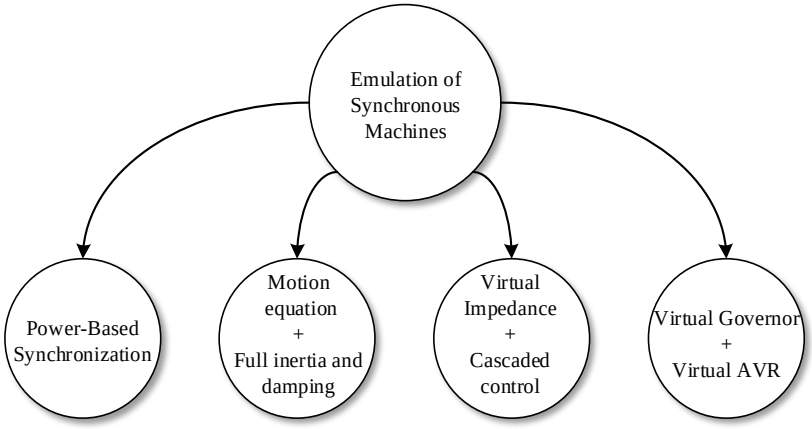

Figure 45: Implementation tree for the cascaded virtual synchronous machine

The CVCC implementation of the VSM includes the motion equation for damping and inertia, a two cascaded voltage and current control loop, and droop-based reactive power control [81] as presented in Figure 46.

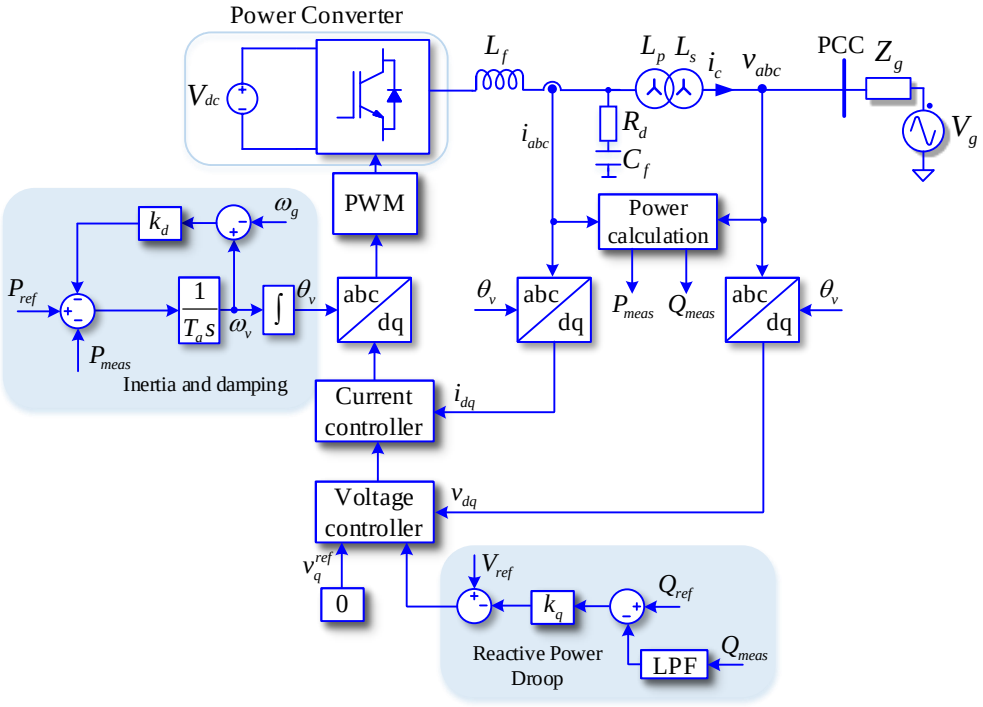

Figure 46: Control model of the cascaded virtual synchronous machine

This first approach of the CVCC integrates a droop-based reactive power controller similar to the ones generally used in microgrid systems. This reference is then processed by two cascaded controllers to generate the output voltage at the power converter. These controllers work on the *dq* reference frame set by the angular position of the virtual rotor. The swing equation is in charge of processing the power exchange of the power converter to determine the angular position of the rotor.

The cascaded controllers entail some limitations in terms of dynamics since they inherit cascaded delays, which need to have their bandwidth separated enough to avoid interactions between them. In [81] a guide to tune the system by the eigenvalue sensitivities of the linearized system was presented. This work also presents the interaction between the cascaded control loops for a low switching and sampling frequency, as well as the complex dependency of the system to the control parameters.

In [82] and [83] additional work to improve the initial proposal was presented. This extension showed an outer frequency droop control loop with a similar response to the steady-state operation of a synchronous generator. In addition, this work included a PLL to separate the damping effect in the swing equation from the one in the outer frequency control loop. The

addition of the PLL modifies the dynamic response of the electromechanical layer, because of that the PLL bandwidth has to be carefully selected. Moreover, the implementation of the CVCC included a virtual impedance in its control structure to regulate the power and frequency in resistive grids, Figure 47.

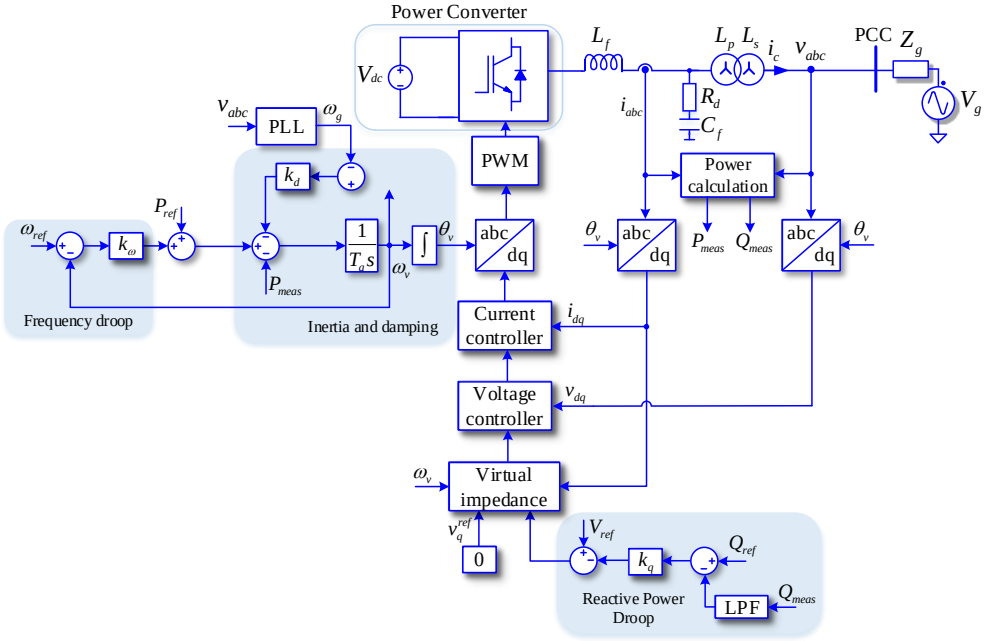

Figure 47: Enhanced version of the cascaded virtual synchronous machine

Several publications regarding the CVCC enhanced implementation were published, where the small-signal analysis was presented to study the stability of the system in [82] and [83], the operation of the CVCC in islanded mode [84], and the seamless reconnection of the power converter in [85].The advantages and the drawbacks of the CVCC implementation of a VSM can be grouped as Table 7.

Advantages:	Drawbacks:
▪ Easy implementation on traditional current-controlled power converters. ▪ Natural protection for short circuits with the current controller. ▪ Outer voltage and frequency loop regulation, to adjust the steady-state operation.	▪ The cascaded voltage and current loop reduce the bandwidth of the system. ▪ The parameter tunning is vital for the stability of the system. ▪ The fundamental frequency is exclusively used for the virtual impedance.

Table 7: Advantages and drawbacks of the CVCC implementation.

Chapter 3.

Modified current control for a voltage source converter

The grid codes are being reinforced including specific requirements to harmonize the integration of renewable energy resources into the electrical system. These incoming modifications are mainly oriented to modify certain operations on the RES systems influencing the dynamic at the most inner level of the power converter control, requiring them to be more stable, faster, and able to operate under a wide range of faults. To satisfy this, some enhancements to the inner control loops have to be made.

In order to guarantee the quality of supply to meet the required standards it is necessary that the power control structures improve their performance. The PI-based controller has been by far one of the most extended implementations in grid-connected power converters. This synchronous reference frame controller allows regulating the current to ensure a zero steady-state error, which can highly decouple the active and reactive power using a decoupling matrix considering the inductance value in the system. As an alternative, the proportional-resonant (PR) controller presents a well performing dynamic in grid-connected power converters due to its natural resonance behavior, avoiding in this way the use of a PLL to regulate the output current of the converter as it automatically control the current in the stationary reference frame.

This section will present one of the most extended structures to implement a PR controller by using the second-order general integrator (SOGI). Later in this chapter, this SOGI structure will be modified to avoid the positive and negative coupling during changes in the regulation. In addition, the mathematical expression of the decoupling matrix used in the synchronous reference frame to avoid the active and reactive power coupling will be transferred into the stationary reference frame to use it in the PR current controller.

3.1. General SOGI structure

The SOGI structure has been widely used in the control of power converters for the $\alpha\beta$-stationary reference frame. In general, this structure is composed of two integrators that create a virtual resonance for a specific input frequency. During the years this structure has been used as a bandpass filter to detect the positive and negative sequence of the grid voltage [86], as

well as to regulate the voltage or the current of the power converter in the stationary reference frame [87]. The structure of the SOGI is represented in Figure 48, which is composed of a double integrator creating the virtual resonance in one of the components.

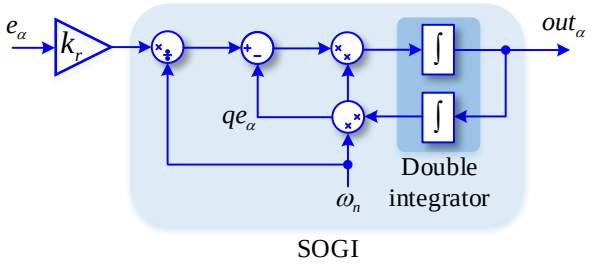

Figure 48: General implementation of the SOGI

As mentioned the most common use of this structure is in the inner voltage or current control loop. In the previous section, the traditional PR structure was presented in Figure 20, however, the digital implementation of this structure may give rise to some issues due to the infinite gain at the resonance frequency. For this reason, in many of the real implementations, a bandwidth regulation has been added to the SOGI structure to adjust and limit the resonance gain of the controller [88]. Figure 49 presents the structure for the bandwidth regulation of the controller, where the damping coefficient, $2\omega_c$, limits the gain at the resonance frequency of the controller.

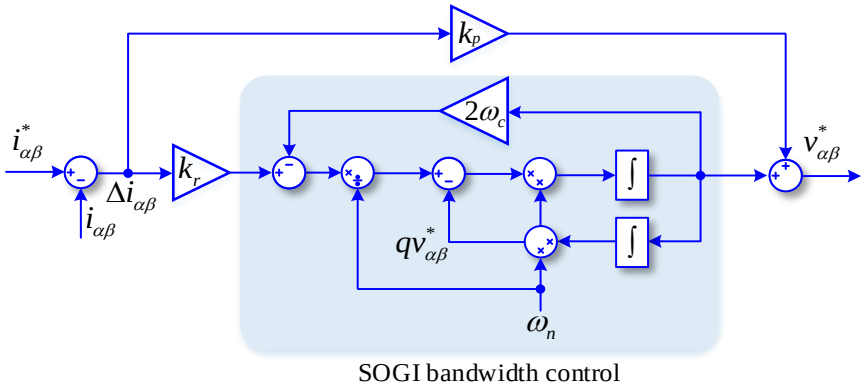

Figure 49: SOGI with bandwidth control applied in a PR-current control loop

Even though the two SOGI implementations have been widely used in the control of power converters, both present a very similar coupling effect between the negative and the positive-sequence due to the double integrator strategy. In this way, the parameter k_r is defining the

behavior of the controller for the positive and the negative sequence. The frequency response of the SOGI structure, presented in equation (11), can be represented as shown in Figure 50, which has the same resonance gain at the positive and the negative sequence.

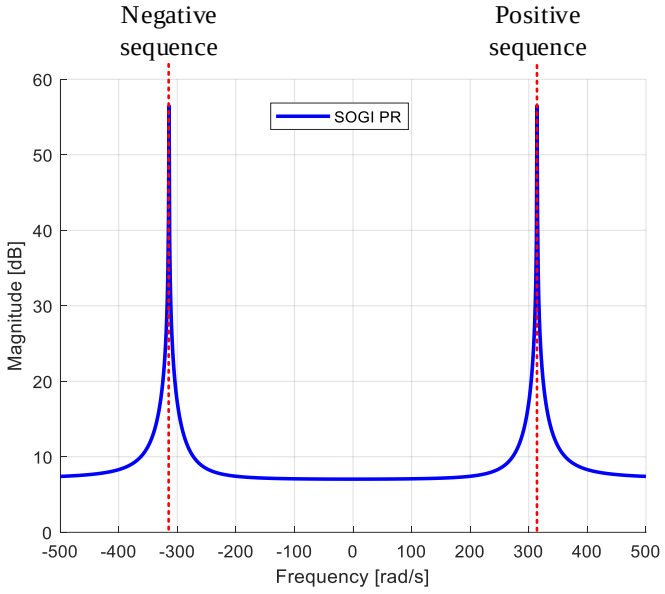

Figure 50: Frequency response of the SOGI PR controller

3.2. Modified resonant current control structure

The traditional structure allowed to split the positive- and the negative-sequence components using a double SOGI structure for the $\alpha\beta$-sequence components and algebraic calculations. The quadrature vectors obtained from the SOGI filter are described in Figure 51. The alpha component, α, creates a quadrature vector, $q\alpha$, -90-degree phase-shifted from the α-input vector due to the integrator. Similarly, the beta component, β, creates a quadrature vector, $q\beta$, phase-shifted from the input.

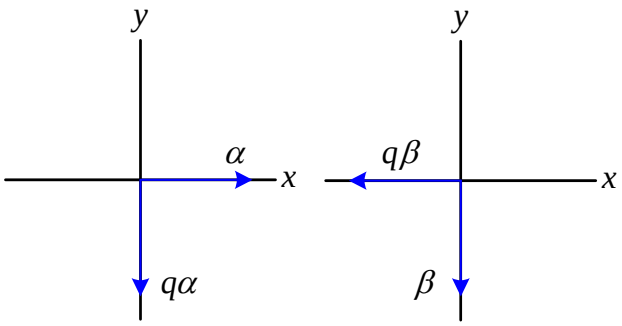

Figure 51: quadrature vectors of $\alpha\beta$ components

This capacity to generate quadrature vectors can be used to reorganize the terms of the SOGI structure to have a compact sequence separator that can extract separately the different sequences within a single structure [89]. To do this, the quadrature vector generation has to be redefined to couple both stationary reference frames. The proposed resonant structure, Figure 52, avoids the use of multiple integrators, just one per component. In this manner, the input error is amplified by the resonant gain coefficient, k_r, and then added to the quadrature component obtained from the β integrator. The α-sequence component is then integrated to obtain the specified sequence, which depends on the input value of the resonance frequency, ω_r, in this case, determining the positive sequence of the input. The α integrator output is used as the quadrature vector of the β-sequence component, subtracting its value to the error in the β-sequence component. Considering the αβ-sequence components are -90-degree phase-shifted between each other, the integration of their values will be 180-phase degree phase-shifted with respect to the quadrature component.

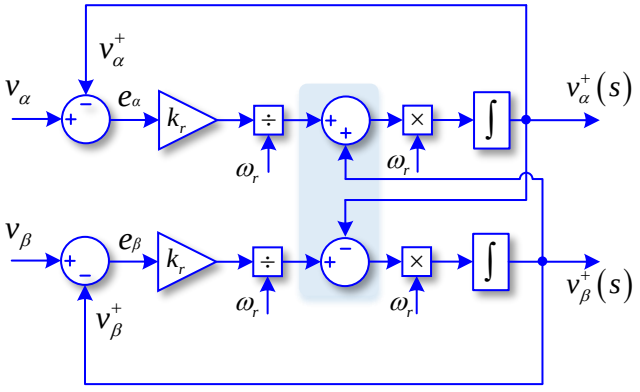

Figure 52: Proposed reduced resonant structure

This modified structure of the SOGI can be used to extract specific harmonic sequences from the input signal. The equivalent transfer function of the proposed reduced resonant strategy can be obtained as:

$$e_\alpha = \left(v_\alpha - v_\alpha^+\right) \tag{18}$$

$$e_\beta = \left(v_\beta - v_\beta^+\right) \tag{19}$$

$$v_\alpha^+ = \frac{\left(e_\alpha \cdot k_r + v_\beta^+ \cdot \omega_r\right)}{s} \tag{20}$$

$$v_\beta^+ = \frac{\left(e_\beta \cdot k_r - v_\alpha^+ \cdot \omega_r\right)}{s} \tag{21}$$

By combining equations (20) and (21) it is possible to create the transfer function of each of the branches, which can be expressed as:

$$v_\alpha^+ = \frac{\left(e_\alpha \cdot k_r \cdot s + \left(e_\beta \cdot k_r - v_\alpha^+ \cdot \omega_r\right) \cdot \omega_r\right)}{s^2} \tag{22}$$

$$v_\beta^+ = \frac{\left(e_\beta \cdot k_r \cdot s - \left(e_\alpha \cdot k_r - v_\beta^+ \cdot \omega_r\right) \cdot \omega_r\right)}{s^2} \tag{23}$$

If equations (22) and (23) are expressed in a matrix, it is possible to obtain a similar transfer function as the one implemented in the SOGI, equation (24). The main difference between the SOGI structure and the reduced resonant structure is the coupling terms on the transfer function depending on the bandwidth, k_r, and the resonance frequency, ω_r. In this specific case, the ω_r parameter is selected as positive, giving rise to a positive sequence regulator. If the value for the resonance frequency is selected as negative the output component would be regulating the negative sequence.

$$\begin{bmatrix} v_\alpha^+ \\ v_\beta^+ \end{bmatrix} = \begin{bmatrix} \frac{k_r \cdot s}{s^2 + \omega_r^2} & \frac{k_r \cdot \omega_r}{s^2 + \omega_r^2} \\ \frac{-k_r \cdot \omega_r}{s^2 + \omega_r^2} & \frac{k_r \cdot s}{s^2 + \omega_r^2} \end{bmatrix} \cdot \begin{bmatrix} e_\alpha \\ e_\beta \end{bmatrix} \tag{24}$$

This adapted structure of the SOGI can be used in a similar way to the traditional structure, with the advantage to have a reduced amount of integrators in the transfer function, and the capacity to split the positive and negative resonant gains independently from each other. In the case of using this structure as a band-pass filter, the performance is defined by the constant value of the central frequency of the filter, ω_r, and the value of the bandwidth of the controller, k_r, Figure 53.

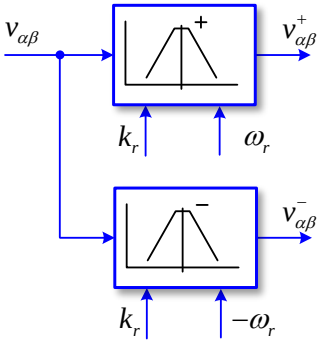

Figure 53: Positive and negative decomposition using the reduced resonant strategy

If the resonance gain, k_r, is equal for both positive and negative sequences, the structure presents a similar behavior as in the case of the SOGI structure, Figure 50. However, as the system can be independently tuned, the resonance gain can differ from the positive and the negative components, giving rise to an adjustable system able to regulate separately the harmonic components of the input signal, while regulating the coupling independently for each sequence. Figure 54 shows the open-loop gain margin and phase margin of the structure presented in Figure 53, where the resonant gain coefficient of the negative-sequence component has been reduced to 0.1 p.u with respect to the positive-sequence component, highly reducing the bandwidth of the negative component. It can be seen that the structure allows the separation of sequence and its control independently of each other, which is an advantage compared to the traditional SOGI structure.

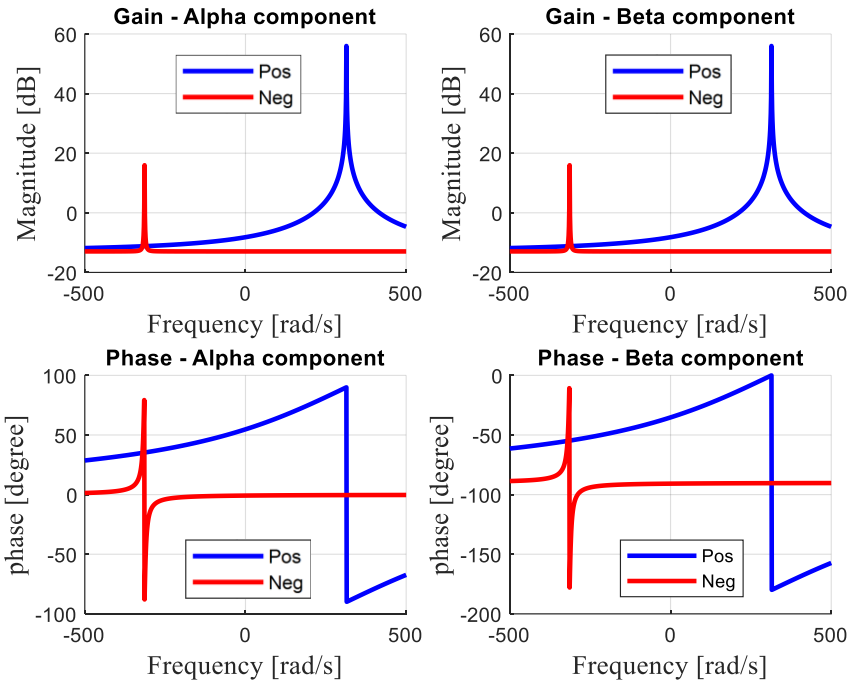

Figure 54: Modified resonant structure for independent regulation of harmonics. Positive sequence band-pass filter (Blue), negative sequence band-pass filter (Red)

3.3. Modified resonant control structure for grid-connected inverters

The structure of the SOGI resonant controller has been generally used in power converters connected to the grid because of its simplicity in controlling the output current of the converter and robustness in front of grid contingencies and harmonics. However, as it requires a double integrator structure, Figure 20, it may give rise to a coupling between the positive- and the negative-sequence component. For this reason, the reduced resonant structure has been adapted for the current control structure. In this way, the system can be decoupled and forced to control a single grid sequence.

The proposed modified PR structure is presented in Figure 55, which allows having a separated control for each sequence of the grid. The performance of the resonant controller depends on the resonant and proportional gains, k_r and k_p, and the central frequency of the resonance, ω_r.

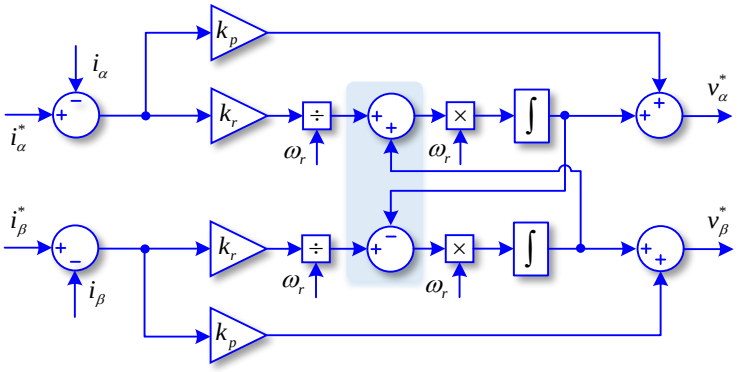

Figure 55: Modified PR-control structure

The equivalent transfer function of the proposed controller can be described as equation (25):

$$\boldsymbol{G_{PR}}(s)=\begin{bmatrix} \frac{k_r s}{s^2+\omega_r^2} & \frac{k_r \omega_r}{s^2+\omega_r^2} \\ \frac{-k_r \omega_r}{s^2+\omega_r^2} & \frac{k_r s}{s^2+\omega_r^2} \end{bmatrix}+\begin{bmatrix} k_p & 0 \\ 0 & k_p \end{bmatrix} \tag{25}$$

This transfer function can be also obtained from the PI controller rotated to the stationary reference frame by terms of using the park transformation. This transformation adds the coupling terms appearing in the $\alpha\beta$-reference frame [90].

3.4. Stability analysis

In this section, the three current controllers used in the simulation results are analyzed, and some of their interesting features are highlighted, especially considering the coupling between sequences during power steps or transients. The three controllers, the PI controller represented by equation (10), the SOGI-PR controller represented by (11), and the modified PR controller presented in (25), present similar resonance gain at the resonance frequency. In Figure 56(a) and Figure 56(b) , it is possible to see that the SOGI-PR controller and the modified PR controller show the same gain and bandwidth for the positive sequence. However, the SOGI PR controller has a negative sequence resonance gain which may give rise to a coupling between sequences, especially during transients where small negative components can be appearing in the grid current and voltage. In the case of the PI controller, Figure 56(c), the system is synchronized to the natural frequency of the grid, this leads to have a 0 Hz equivalent resonant frequency in the controller.

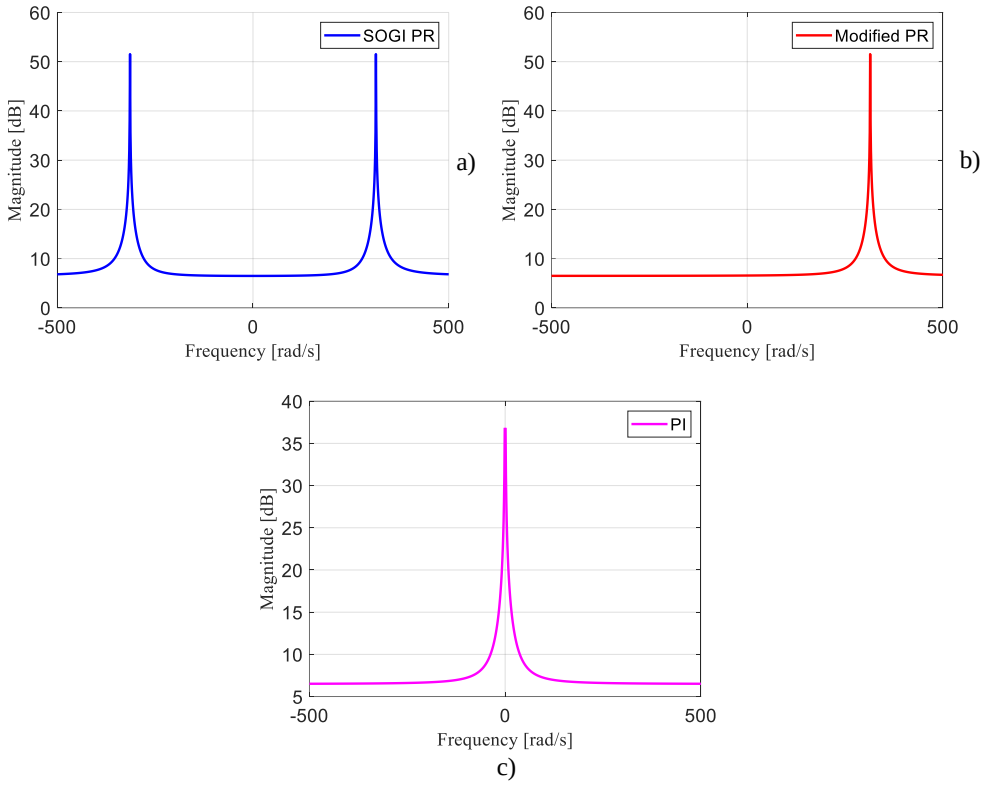

Figure 56: Bode gain plot of the different current controllers (a) SOGI-PR current controller open loop bode (b) Modified PR current controller open loop bode (c) PI current controller open loop bode.

If the rotation matrix is used for modifying the reference frame of the PI controller to the synchronous reference frame [90], it can be seen that the bandwidth and the gain of the controller match, giving rise to an equivalent dynamic performance between the PI and the PR controllers during steps and transients. Figure 57 shows the PI controller moved from the stationary reference frame, Figure 56, to the synchronous reference frame to match the modified PR controller.

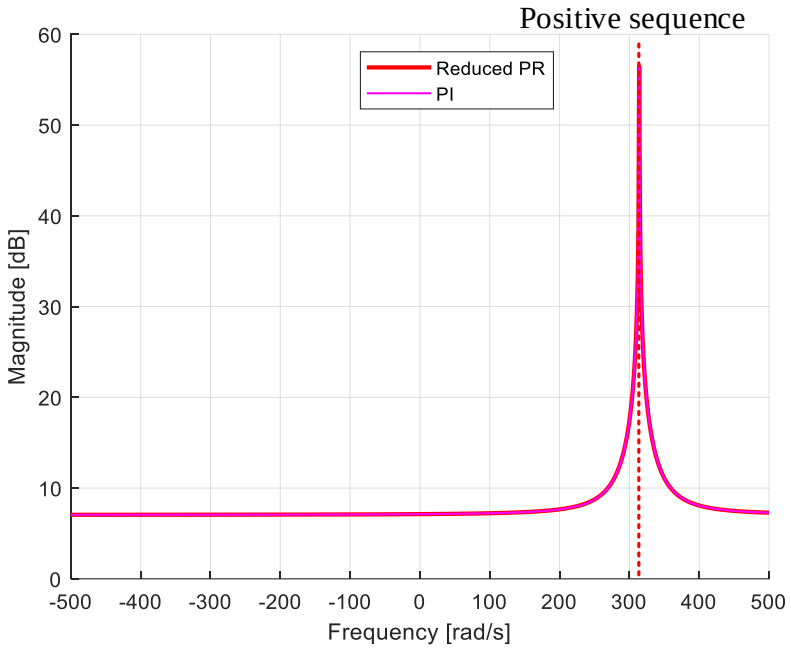

Figure 57: PI and modified PR controller frequency response

Although they present very similar frequency responses at the specified frequency, matching in bandwidth and gain, the coupling in the negative sequence regarding the SOGI-PR controller may have a huge impact during transients.

A simple close loop diagram can be represented as Figure 58, which is composed of the current controller, a time delay to emulate the effect of the pulse width modulation (PWM) on the power converter, and an output inductance filter.

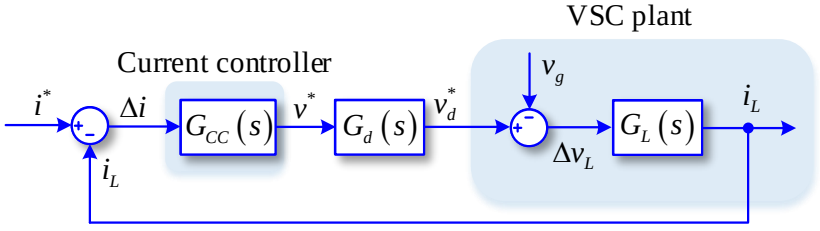

Figure 58: Simple closed-loop system of the current controller with an L-filter on the power converter

To make a comparison between the SOGI PR controller and the modified PR controller, both systems will be analyzed under the same model. The equations for the current controllers used

in the analysis are presented in (26) and (27) for the modified PR controller and the SOGI PR controller, respectively.

$$\boldsymbol{G}_{\boldsymbol{PR}_m}(\boldsymbol{s}) = \begin{bmatrix} \frac{k_r s}{s^2+\omega_r^2} + k_p & \frac{k_r \omega_r}{s^2+\omega_r^2} \\ \frac{-k_r \omega_r}{s^2+\omega_r^2} & \frac{k_r s}{s^2+\omega_r^2} + k_p \end{bmatrix} \tag{26}$$

$$\boldsymbol{G}_{\boldsymbol{PR\_SOGI}}(\boldsymbol{s}) = \begin{bmatrix} \frac{2k_r s}{s^2+\omega_r^2} + k_p & 0 \\ 0 & \frac{2k_r s}{s^2+\omega_r^2} + k_p \end{bmatrix} \tag{27}$$

In the digital implementation of current control, there are two types of delays, the computation delay, and the PWM. For this specific case, the sampling is updated twice during a switching period ($f_s = 2f_{s\omega}$), where f_s is the sampling frequency and $f_{s\omega}$ is the switching frequency. It is common to assume that the equivalent delay of the system, considering both the computation and the PWM delays, can reach 1.5 times the sampling time ($T_s = {}^1/_{f_s}$). Therefore, the output voltage of the power converter can be described as:

$$v_d^* = e^{-T_d s} \cdot v^* \tag{28}$$

Where the parameters T_d can be described as:

$$T_d = 1.5T_s \tag{29}$$

To approximate the time delay a second-order Padé approximation is used to rationalize the factor $e^{-T_d s}$.

$$G_d(s) = \frac{12 - 6T_d s + T_d^2 s^2}{12 + 6T_d s + T_d^2 s^2} \tag{30}$$

The output filter of the power converter has been simplified to a unique inductor filter to reduce the order of the model. This filter can be modeled in the $\alpha\beta$-reference frame as:

$$\boldsymbol{G}_L(\boldsymbol{s}) = \begin{bmatrix} \frac{1}{R_L + Ls} & 0 \\ 0 & \frac{1}{R_L + Ls} \end{bmatrix} \tag{31}$$

Where R_L represents the resistive part of the inductance, and the L the inductive part. To model the system the forward loop of the whole system can be expressed as:

$$\boldsymbol{G_{OL}}(\boldsymbol{s}) = \boldsymbol{G_L}(\boldsymbol{s}) G_d(s) \boldsymbol{G_{cc}}(\boldsymbol{s}) \tag{32}$$

The open-loop transfer function can be described for the modified-PR controller as:

$$\boldsymbol{G_{OL_m}}(\boldsymbol{s}) = \begin{bmatrix} \dfrac{K_p s^2 + K_i s + K_p \omega^2}{Ls^3 + R_L s^2 + (Ls + R_L)\omega^2} & \dfrac{K_i \omega}{Ls^3 + R_L s^2 + (Ls + R_L)\omega^2} \\ \dfrac{-K_i \omega}{Ls^3 + R_L s^2 + (Ls + R_L)\omega^2} & \dfrac{K_p s^2 + K_i s + K_p \omega^2}{Ls^3 + R_L s^2 + (Ls + R_L)\omega^2} \end{bmatrix} \cdot \left(\frac{T_d^2 s^2 - 6T_d s + 12}{T_d^2 s^2 + 6T_d s + 12} \right) \tag{33}$$

An equivalent open-loop transfer function is obtained from the SOGI PR controller without the diagonal component matrix representing the coupling elements.

$$\boldsymbol{G_{OL_{SOGI}}}(\boldsymbol{s}) = \begin{bmatrix} \dfrac{K_p s^2 + 2K_i s + K_p \omega^2}{Ls^3 + R_L s^2 + (Ls + R_L)\omega^2} & 0 \\ 0 & \dfrac{K_p s^2 + 2K_i s + K_p \omega^2}{Ls^3 + R_L s^2 + (Ls + R_L)\omega^2} \end{bmatrix} \cdot \left(\frac{T_d^2 s^2 - 6T_d s + 12}{T_d^2 s^2 + 6T_d s + 12} \right) \tag{34}$$

For the open-loop bode plot analysis, the parameters specified in Table 8.

Modeling parameters	
Filter Inductor (L)	777 µH
Filter resistor (R_L)	0.0021 Ω
Sampling time (T_s)	1/6300
Proportional gain (Kp)	1
Integral gain (Ki)	100

Table 8: Modeling parameters for the comparison between the SOGI and the modified PR structures

The open-loop response for the modified-PR and the SOGI-PR controller is presented in Figure 59, showing the equivalency of both controllers for the direct matrix. However, the coupling terms from the modified PR structure are only existent in the modified structure. The gain margin and the phase margin of both controllers are the same, reaching a gain margin of 14.2 dB, and a phase margin of 67,7 degrees. Even though the structure is different the diagonal transfer function provides the same open-loop response.

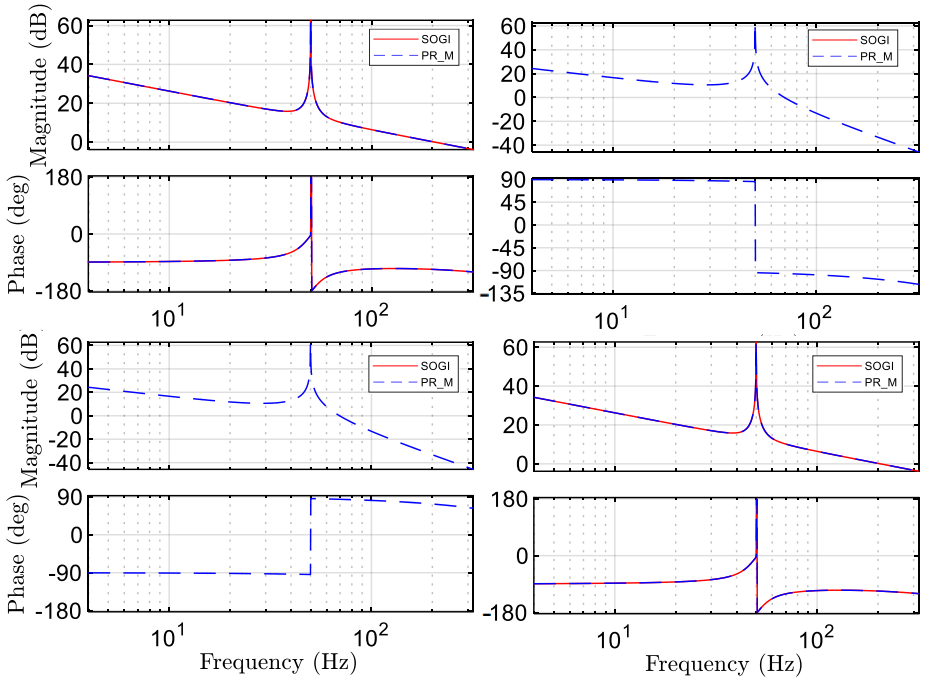

Figure 59: Open-loop bode plot of the SOGI PR controller and the modified PR structure

The closed-loop transfer function can be obtained using the feedback of the open-loop system.

$$G_{CL_m}(s) = \frac{G_{OL_m}(s)}{1 + G_{OL_m}(s)} \tag{35}$$

In this case, although the controllers generated an equal performance in the open-loop response shown in Figure 59, the closed-loop response of the system differs from each other. Both systems still have a 0dB gain at the resonant frequency, Figure 60. However, the modified PR controller presents a smaller gain at the higher frequencies. Apart from the difference in the gain at the resonant frequency at the positive sequence, the SOGI PR controller can regulate the negative sequence with the same structure. As shown in Figure 61 the SOGI-PR controller presents symmetrical behavior in the positive and the negative sequence. On the contrary, the modified PR structure provides an asymmetrical system reducing the gain at the negative sequence, thus reducing the possible oscillations due to a high gain in the negative sequence component.

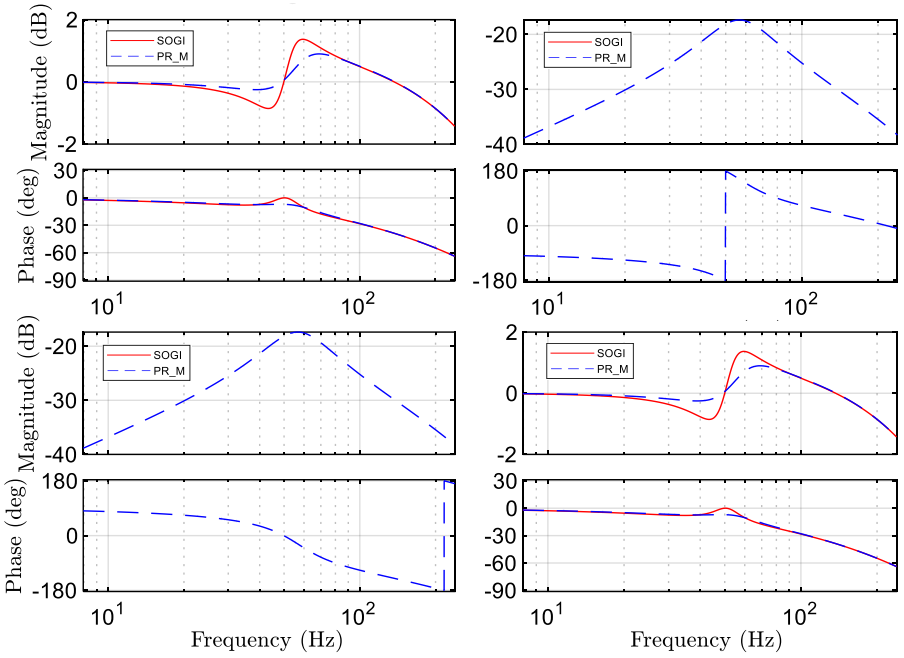

Figure 60: Closed-loop bode plot of the SOGI and the modified PR controller

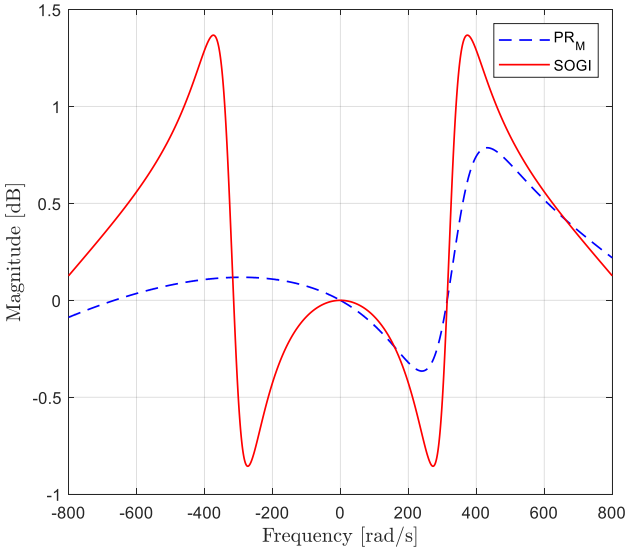

Figure 61: Positive and negative closed-loop bode plot of the SOGI and the modified PR controller.

To compare the effect of the negative sequence coupling during transients two cases scenario are set to show the dynamic response of each of the controllers. To highlight the effect of the coupling the system is tested under a weak grid connection. In the first stage, the system will be tested without any decoupling terms in the controller, meaning that the controller is the only factor regulating the current in the power converter. In a second stage, the decoupling terms are added into the control structure providing an additional factor during the step. In this simulation result, the PI regulator in the synchronous reference frame, the SOGI PR controller, and the modified PR controller, named proportional resonant with negative decoupling (PRN), are tested.

3.5. Simulation result

In this subsection simulation results will be presented to show the different behavior of the inner current controllers of a power converter, focusing on the different performances. A comparison between the different current controllers will be shown performing in a 100 kVA power converter connected to the grid, Table 9.

Total output power	100 kVA
Filter Parameters	
Converter Inductor (Lf)	777 µH
Transformer inductance $(L_s + L_p)$	400 µH
Damping resistor (R_d)	0.5 Ω
Capacitor (C_f)	66 µF
Grid impedance (Lg)	0.0251 Ω
Proportional gain (Kp)	1
Integral gain (Ki)	100
Simulation Parameters	
Switching frequency (fsw)	3150 Hz
Sampling frequency (fs)	6300 Hz
Vdc voltage level	800 V
Nominal phase voltage	230 V
Nominal frequency	50 Hz
Bandpass filter gain (k_r)	100
Central frequency (ω_r)	314.15 rad/s

Table 9: Simulation parameters for the 100kVA power converter.

Figure 62 presents the simulation setup for the tests, composed of a current controller and current reference generator in the control structure, and an LCL filter, an isolation transformer, and a grid impedance for the electrical part.

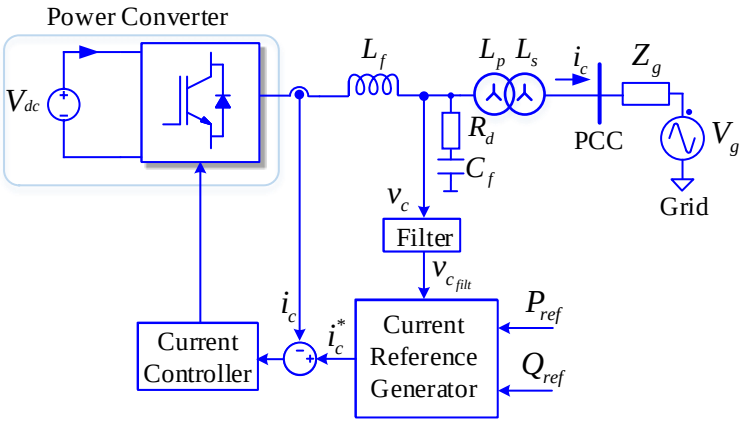

Figure 62: Simulation setup for the current control performance

The current reference generator block can be composed mainly of two different schemes depending if it is working on the synchronous or stationary reference frame. In the case of working with *dq*-components, the current reference can be either obtained from a PI regulating the active and reactive power to generate a current reference for the *d* and *q* component, or the current reference can be obtained from an open-loop calculation which transforms the power reference into current reference by using the algebraic equations (36) and (37), taking into account the grid voltage v_d and v_q.

$$i_d^{ref} = \frac{1}{v_d^2 + v_q^2}\left(v_d \cdot P^{ref} - v_q \cdot Q^{ref}\right) \tag{36}$$

$$i_q^{ref} = \frac{1}{v_d^2 + v_q^2}\left(v_q \cdot P^{ref} + v_d \cdot Q^{ref}\right) \tag{37}$$

Normally, the voltage measurement is filtered to reduce the harmonics and undesired components in the generated reference current. In the synchronous reference frame, it is common to use a low-pass filter to remove undesired harmonic components to the PLL output voltage. Whereas, on the stationary reference frame, generally a band-pass filter tunned at the grid frequency is used to eliminate undesired components. Figure 63 presents the control scheme to generate the references in the *αβ*-stationary reference frame.

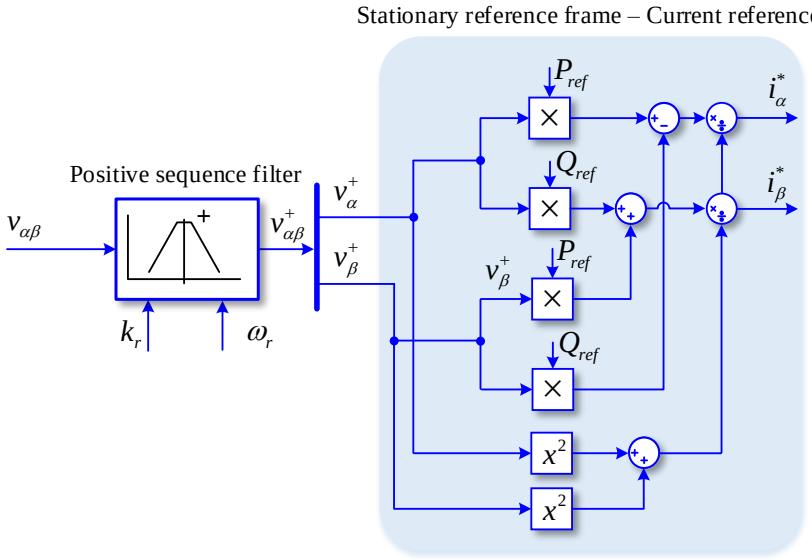

Figure 63: Current reference generator in the stationary reference frame

The band-pass filter coefficient k_r and ω_r adjust the central frequency and the bandwidth of the filtering. In this case, only the positive sequence of the grid voltage is desired to provide a pure sinusoidal waveform reference. The algebraic equations in the synchronous reference frame can be described as (38) and (39):

$$i^*_\alpha = \frac{P \cdot v_\alpha - Q \cdot v_\beta}{v^2_\alpha + v^2_\beta} \tag{38}$$

$$i^*_\beta = \frac{P \cdot v_\beta + Q \cdot v_\alpha}{v^2_\alpha + v^2_\beta} \tag{39}$$

3.5.1. Current control without decoupling terms

It is possible to see in Figure 64 that both the PI controller in the synchronous reference frame and the PRN controller in the stationary reference frame have an equivalent performance under a 0.6 p.u power step in the power converter. However, the SOGI structure presents a different transient performance due to its transfer function without quadrature terms, as shown in equation (11). This leads to the different dynamic behavior of the SOGI PR, as seen in the previous section, which makes it have a higher coupling between active and reactive power during the step. Although the tuning of the three controllers is the same, it is possible to see how under a weak grid interconnection, the controller presents a different dynamic compared to the other two, that match perfectly. On top of this, it is possible to detect the negative

sequence coupling in the SOGI PR controller as it is present in the figure as a 100 Hz oscillation both in the active and the reactive power.

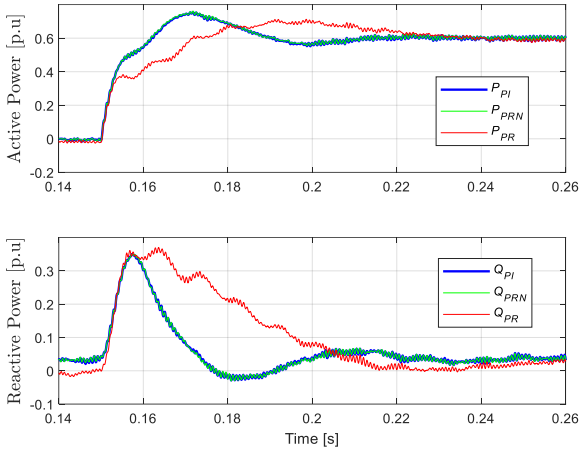

Figure 64: Power step with different current controllers without decoupling terms

3.5.2. Current control with decoupling terms

Even though the SOGI PR controller has a significantly different dynamic compared to the other two controllers during the power step, the addition of the decoupling terms at the output of the controller reduce the output coupling from the inductance, as presented in equations (16) and (17), increasing the time response of the controller without modifying its parameters. Figure 65 presents the control scheme for the decoupling terms. In this case, each current controller will add the decoupling terms at its output to minimize the effect of the filter inductance during the transient.

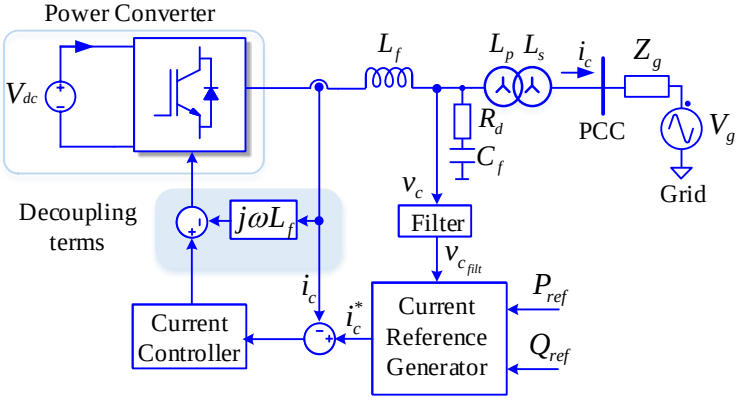

Figure 65: Control structure with decoupling terms

In Figure 66 the transient response of the different controllers can be seen. The performance of all the current controllers increases as they reach the setpoint much faster and avoiding power oscillations and coupling between active and reactive power. Comparing Figure 64 and Figure 66, it is possible to see how the settling time of the controller has been reduced from a time response of around 50 ms without decoupling terms, to a response of 10 ms. In addition to the settling time decrease, the controllers have also avoided the overshoot during the power step and the coupling between the active and reactive power is insignificant.

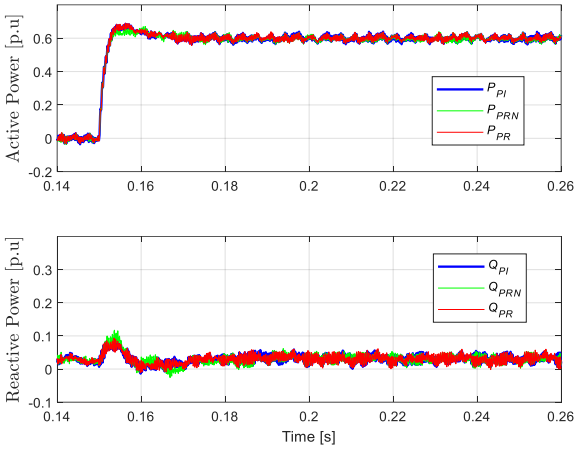

Figure 66: Power step with different current controllers with decoupling terms

3.6. Experimental results

The experimental setup follows the structure presented in Figure 62. A picture of the experimental setup is shown below, Figure 67. In this testbench, the SOGI-PR current controller and the proposed version of the resonant controller are tested and compared to each other, with and without the decoupling terms. In the first stage, the SOGI-PR controller will be tested under a 100 kW test, to show the performance of the controller and the coupling between the active and reactive power. Second, the reduced resonant controller will be tested under the same conditions with the same controller parameters. Finally, the decoupling terms will be added to the system to see the effect on the output power coupling.

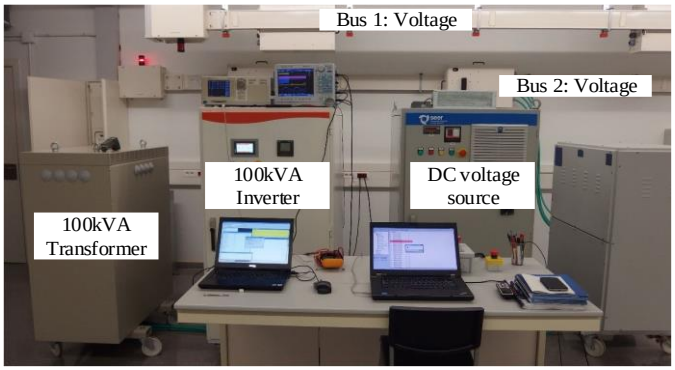

Figure 67: Experimental setup

The electrical parameters of the system are equal as in the simulation setup presented in Table 9, and the controller parameters used for the experimental results resonant controllers are presented in Table 10.

Table 10: Experimental parameters

Controller parameters	
Proportional controller	2.25
Integral controller	100
Bandpass filter gain (k_r)	100
Central frequency (ω_r)	314.15 rad/s

3.6.1. SOGI-PR current controller – experimental results

In Figure 68, the power step using the SOGI-PR controller can be observed. During the step, there is a huge transient in the current that affects the voltage at the point of connection. Due to this distortion, the settling time of the power of the controller is reduced.

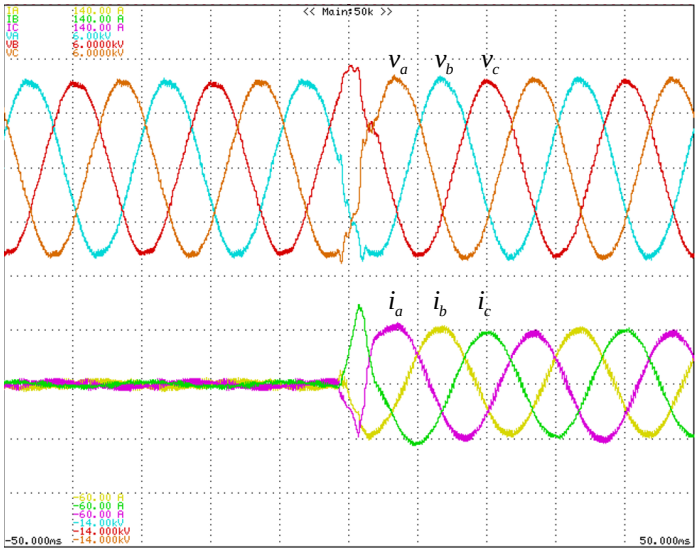

Figure 68: SOGI-PR structure performance in fron of 100kW active power step. (Voltage scale 200V/div, current scale 200A/div)

If the output power is calculated from the sinusoidal waveform obtained, Figure 69, it is clear that in this case, the coupling between the active and reactive power is high. Even though the response of the current controller is fast, the coupling between active and reactive power can be harmful to the voltage at the point of connection, as we can see from the experimental result.

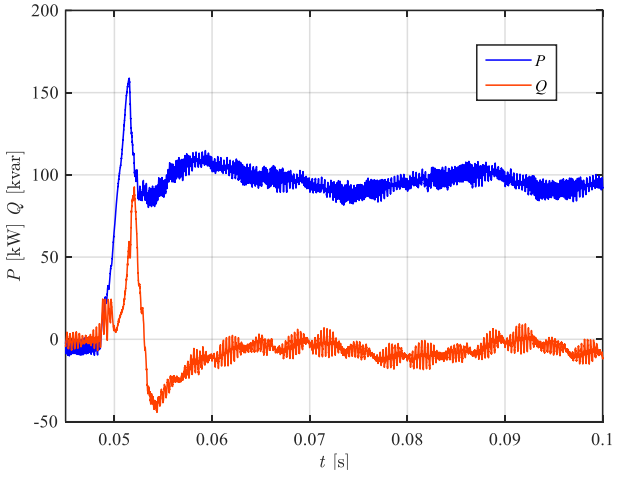

Figure 69: SOGI-PR structure performance in fron of 100 kW active power step – Power calculation.

3.6.2. Modified PR controller – experimental results

In Figure 70 the power step to 100 kW is done with the modified PR controller structure. It is clear from the obtained results, that the performance is satisfactory, reaching the reference fast and with a transient behavior that does not contain undesired over-currents and just a low variation in the voltage due to the line impedance.

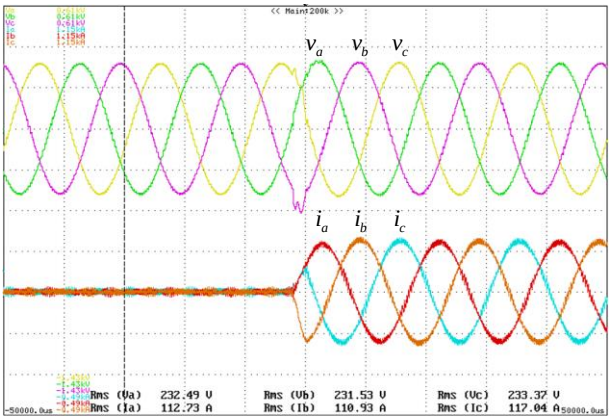

Figure 70: PRN controller performance in front of 100 kW active power step. (Voltage scale 200V/div, current scale 200A/div)

If the power calculation is done in this case, it is possible to see that there is a high reduction in the coupling on active and reactive power, as can be seen in Figure 71. The modified PR controller avoids the coupling in the system and provides better dynamic performance than the SOGI PR structure in a weak grid case, and without the external decoupling matrix.

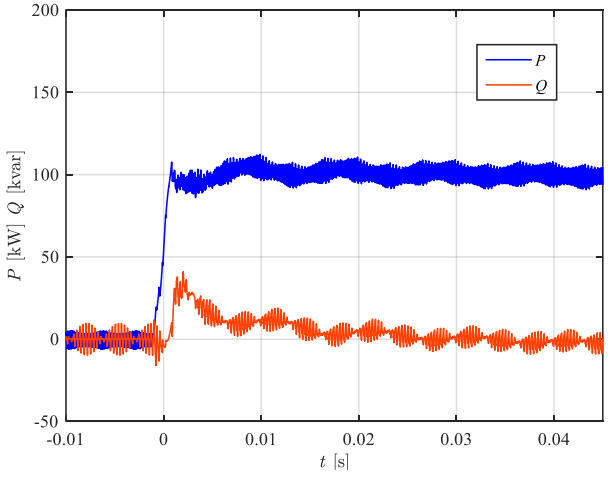

Figure 71: PRN controller performance in front of 100 kW active power step – Power calculation

3.6.3. Modified PR controller with decoupling terms – experimental results

Finally, the decoupling terms are added to the modified PR controller to counteract the effect of the inductance voltage variation. Figure 72 presents the results for a 100 kW power step.

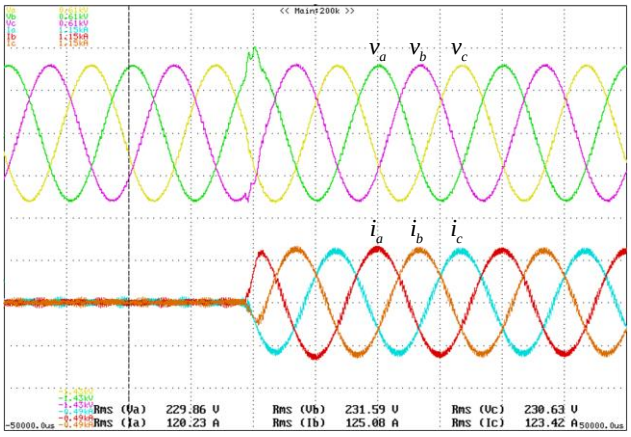

Figure 72: PRN structure with decoupling terms in front of 100kW active power step. (Voltage scale 200V/div, current scale 200A/div)

Comparing the power calculation to the previous case, it can be seen that the reactive power in Figure 73 is reduced until a value below the 10 kvar, while in the previous case the reactive power coupling during the power step almost reached the 40 kvar. The addition of the decoupling matrix into the modified-PR controller allows to increase the controller performance and reducing the coupling between the active and reactive power.

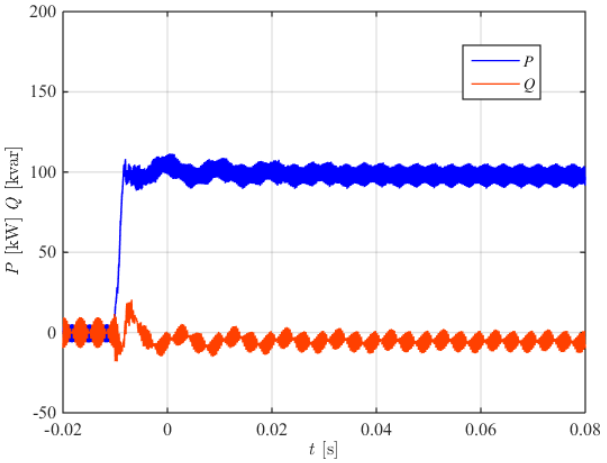

Figure 73: Reduced PR structure with decoupling terms performance in front of 100 kW active power step – Power calculation

3.7. Conclusions

The simulation and experimental results have shown the difference between the different controllers under test. On the one hand, the simulation results clarified the difference between the SOGI PR structure and the modified-PR structure in terms of the negative sequence coupling, and the matching behavior between the PI in the synchronous reference frame and the modified-PR structure in the stationary reference frame. Apart from the structure itself, the addition of the decoupling term in the control structure of the current controller also added a beneficial effect on the overall dynamic performance, highly reducing the settling time of the power step and the coupling between active and reactive power.

On the other hand, the experimental results presented the difference between the SOGI-PR controller and the modified-PR controller in a real environment. In the first case, the high coupling and the transient created by the SOGI structured are highly reduced with the modification of the current control structure. Although the similarity in the control structure, the benefits from the modified-PR controller are seen from the experimental results, and even improved with the addition of the decoupling terms. This strategy of the modified-PR structure with the decoupling terms can be impactful in cases where the grid is weak with a high interconnection impedance.

Chapter 4.

Auxiliar services in virtual synchronous machines

The increased integration of distributed generation units in the electrical grid is highly conditioned by the distributed power plant fulfillment of the grid codes. These requirements are designed to guarantee the stable operation of the electrical system working as the main operation principle to all the generation systems connected to the electrical network. Although there are differences among countries despite the grid codes, the requirements represent the performance and the response of the systems under different operating conditions, especially regarding the boundaries of voltage and frequency, regulation profiles, and transient response under grid contingencies.

The high penetration of renewable energy systems and the reduction of synchronous units implicates a reduction of the overall inertia in the system, thus significantly reducing the system's robustness in front of disturbances. This is particularly a delicate issue especially in isolated systems and microgrids, which needs further attention regarding the participation of all generation units in the frequency regulation.

In this chapter, frequency and voltage support functionalities will be presented focusing on the generic integration to a traditional power converter, and its implementation in the SPC structure. Then, each of the services will be put under test on the experimental testbench to present the behavior of the SPC-based power converter on a device.

To test all the possible services of the synchronous control, an experimental setup is built to perform all the necessary adjustments to the frequency and the voltage of the grid. The setup is composed of a 250kVA grid emulator to create a weak grid at the PCC, two 100kVA power converters, and the harmonic load. This connection is made through a sag generator creating voltage sags by the sequential connection of inductances and an autotransformer. Figure 74 shows the electrical interconnection of all the devices, where all of them are connected to the same PCC. The grid emulator is regulated by a back-to-back power converter to controls the frequency and the voltage amplitude of the grid.

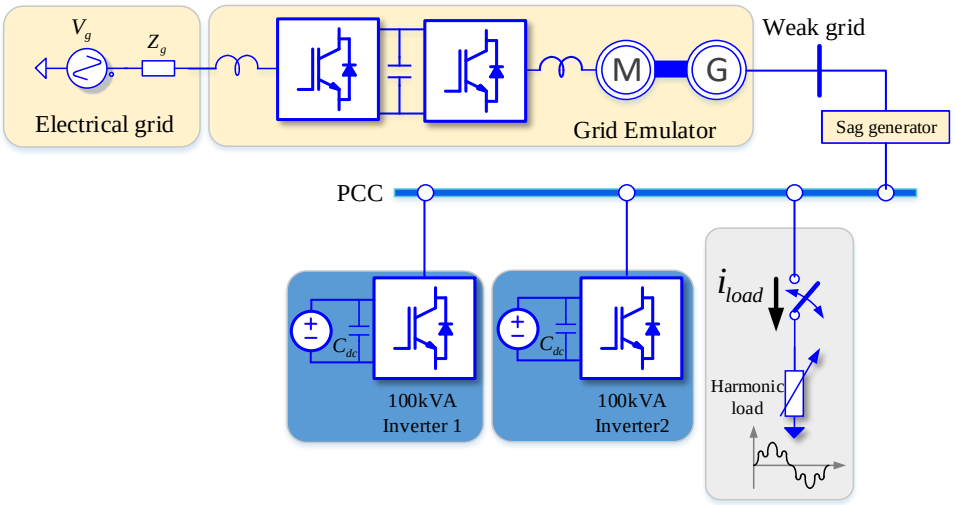

Figure 74: Electrical schematic of the experimental setup for the different synchronous power controller services.

4.1. Experimental setup

The experimental setup is shown in Figure 75. The synchronous generator is interconnected through the voltage-sag generator to the PCC of the power converters and the harmonic load.

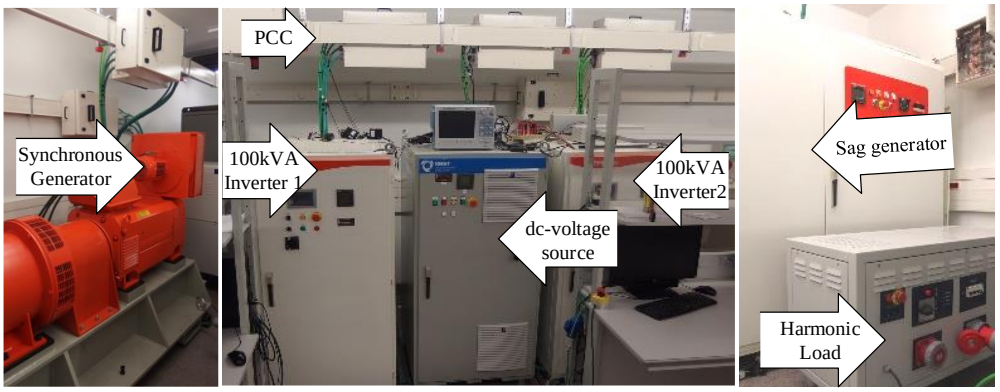

Figure 75: Experimental setup for the synchronous power controller services.

Each power converter is equipped with an SPC structure, enabling the power converter to have multiple functionalities, such as, primary frequency and voltage control, synthetic inertia emulation, power oscillation damping, and multiple virtual admittances for voltage support capabilities. The general schematic of the SPC is shown in Figure 76. The control system is composed of a frequency and voltage droop controller, the power loop controller (PLC), and

a virtual admittance. Each of the highlighted blocks is in charge of one or more specific services. In the case of the droop controllers, they are strictly linked to the voltage and frequency measurements at the PCC acting as the primary control actuators. The PLC includes more than one feature as it uses power balance synchronization. This regulator is capable of adding synthetic inertia and power oscillation damping to the power converter as it relates phase angle changes to active power variations, thus acting dynamically over any phase or frequency contingency at the PCC. Finally, the virtual admittance is capable of generating multiple current references at specified harmonic sequences, allowing the regulation of harmonic currents to compensate for distortions at the grid voltage and support the unbalance.

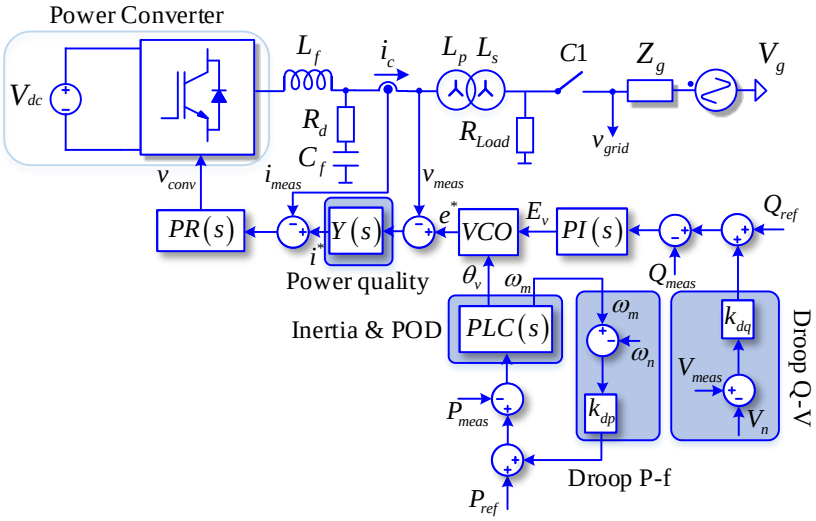

Figure 76: SPC-based power converter general control structure

4.2. Primary frequency control

All grid-connected generation systems are required to provide frequency support to the network, which is performed generally through the regulation of the active power. In this regard, the power converter has to include some additional control blocks to enable frequency support. The inertial response of the power converter can be implemented in two different ways, one is to be calculated as the derivative term of the system frequency, and the other to be implemented similarly to the one in synchronous generators. The power oscillation damping tries to reduce the oscillation of the system by adjusting the output power delivered by the system. In the case of the primary frequency control, it is generally characterized by droop control. This regulation principle uses a gain factor, R, to produce a modification in the output power delivery proportional to the difference between the nominal and the measured

frequency. Moreover, the droop control uses a dead band to only activate the service when the frequency exceeds a specific boundary.

The droop characteristic is provided by the national grid code, which can differ between the countries in the boundaries and the slope. However, in Figure 77 a generic representative case is shown, with a characteristic slope, dead band, and boundaries.

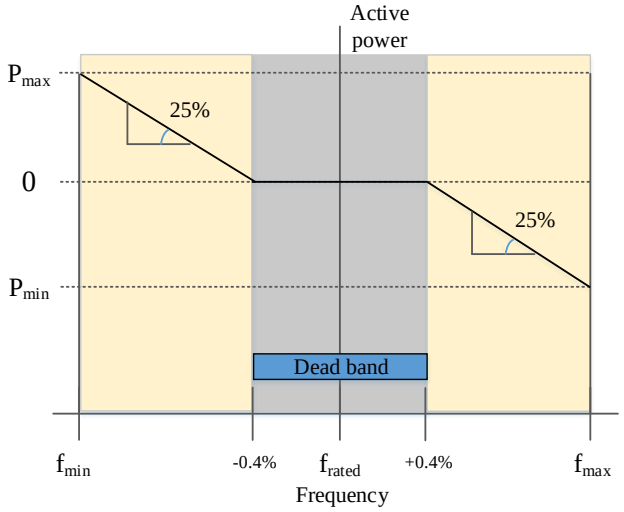

Figure 77: P-f droop control study case

The implementation of the frequency droop control is based on a dead band and a gain factor, which can be adjusted to set the slope of the system. The frequency deviation is the input to the droop control and the output is the active power reference to the power controller, Figure 78. Considering a linear variation in the frequency, the droop control should present no action within the dead band boundary, just after the frequency is over the limit the droop control will be operative.

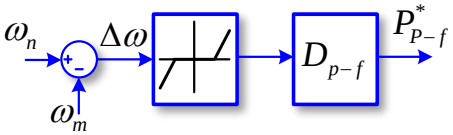

Figure 78: Implementation of the frequency droop characteristic in the proposed control algorithm.

In the case of the integration of the droop control in a VSM implementation, the control algorithm is similar to the one presented in Figure 78. Once the frequency surpasses the frequency boundary, the droop control starts generating the necessary power reference to support the grid, Figure 79. In this case, the frequency is increasing to a value of 50.4Hz which

makes the power converter absorb active power. As the droop is set to a 4% frequency deviation respect to the nominal frequency, for a 0.4Hz frequency deviation the power converter has to absorb around 20kW of active power to counteract the frequency movement.

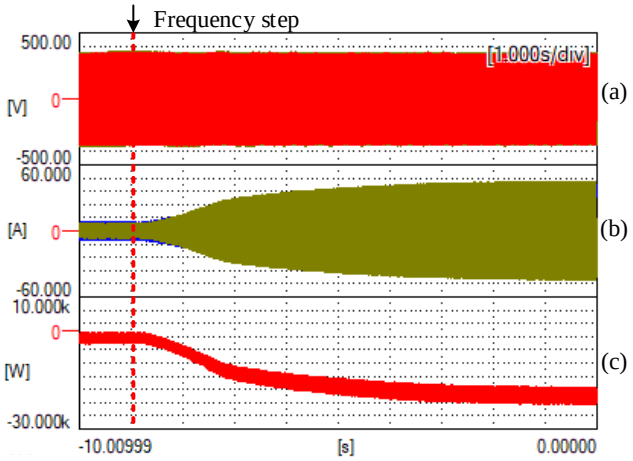

Figure 79: SPC frequency droop control. (a) PCC voltage (b) Power converter current (c) Active power

As it is possible to see from Figure 80, once the frequency deviation starts, the power converter absorbs active power to counteract the frequency deviation. It is clearly seen from the image that for a +0.4Hz frequency movement, the active power absorbed by the power converter reaches the -20kW as specified in the droop settings.

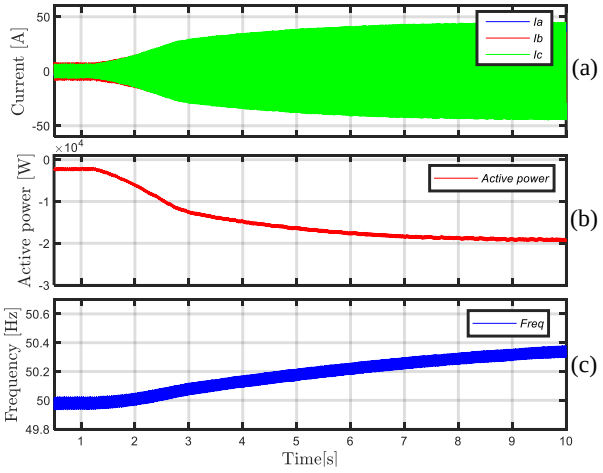

Figure 80: SPC Frequency droop control – Frequency step +0.4Hz (a) Power converter current (b) Active power (c) Grid frequency

4.2.1. Auxiliar service – Inertia emulation

The integration of new generation facilities mainly centered on renewable energy has forced the grid codes to start requesting additional features to the grid-connected generators to reach an optimal solution. Most likely, those new requests may become requirements shortly, so they should be considered for making these newly integrated systems suitable to comply with the new demands. In general, these requirements go in the line of resembling the behavior of traditional generators to counteract frequency variations in the network, thus dynamically supporting the electrical grid. Moreover, the capability of island mode may be a requirement in the near future to enable the operation of part of the system during partial outages.

The traditional synchronous generator can provide dynamic support to the frequency instantaneously, as a result of the mechanical energy in the shaft of the generator, which is delivered to the grid as electrical power during power or frequency changes. In this regard, this dynamic support contributed to the phase angle stability of the electrical network. Although it is not required in all grid codes, it is starting to be requested to ensure that all the generation systems linked to the electrical network will have to emulate the inertial response of a synchronous generator.

To generate an inertial response in a traditional power converter, one alternative is to measure the frequency and obtain its derivative term $d\omega/dt$ and use the moment of inertia, J, to generate the active power. The equation defining this control loop can be expressed as:

$$\Delta P_H = J \frac{d\Delta\omega}{dt} \tag{40}$$

Where ΔP_H represents the active power reference to be delivered to the system as inertia, J is the moment of inertia to be emulated, and $\Delta\omega$ is the frequency deviation of the system. This simple approach allows representing the behavior of inertia in a synchronous generator into traditional power controllers. However, the derivative term is highly dependant on the measure, leading to possible significant noises in the inertia power reference. In this regard, additional filtering is needed for the frequency measurement, which reduces the bandwidth of the controller. Thus, reducing the time response of the inertia when trying to limit the ROCOF and increasing the possibility to create system instability.

In contrast to the previous implementation, the use of the swing equation in most of the VSM approaches enables easier integration of the inertial response of the power converter. The dynamic equation of the swing equation was presented in (7), which allows setting the desired inertial response by adjusting the parameter *J*. Figure 81 shows the effect of different inertia factors during a constant ROCOF in the grid frequency, removing the inherent droop control added by the additional damping windings in the swing equation. Once the frequency deviation starts, the equation detects the derivative term of the frequency by using the power synchronization loop, and provides the specified amount of inertial response to the system. In

this specific case, the constant of inertia has been modified from a value of 2 to a value of 4. This increase in the value of the inertia constant also modifies the virtual power provided during the deviation.

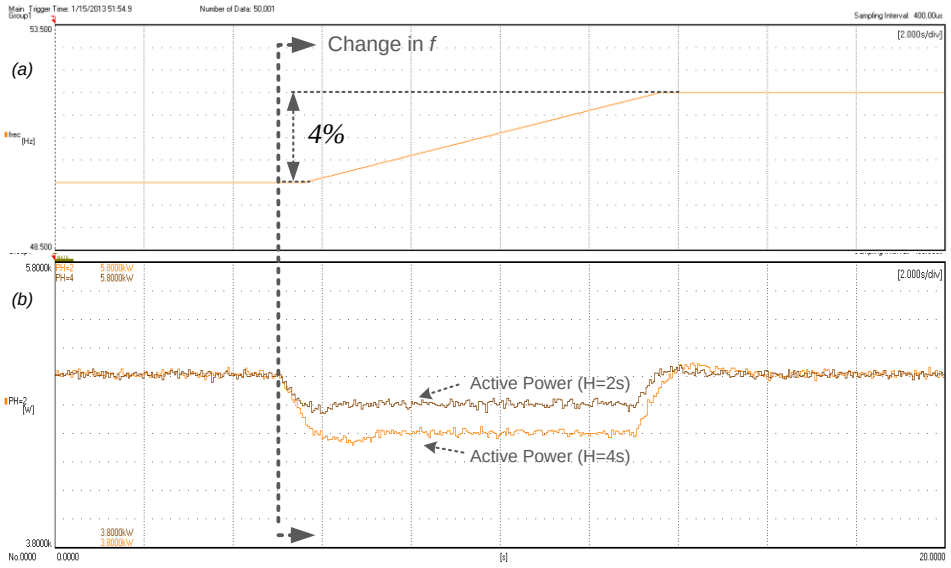

Figure 81: Inertial response of the swing equation in front of a constant ROCOF.

4.2.2. Auxiliar service - Power oscillation damping

The change in power balance, between power generated and demand, gives rise to frequency changes in the network. These transients generate oscillations in the frequency, which are harmful from the perspective of the grid. Therefore, it is being required by some grid codes to adapt the control of the power converter to be able to damp or not excite these oscillation modes during grid-connected operation. It is worth mentioning that the traditional synchronous generator does not have an optimal response in front of such transients as they generally have low damping factors. In this regard, synchronous generators are attached with a power system stabilizer (PSS) providing a positive contribution to the damping of the rotor, which can have frequency oscillation in ranges of 0.1 to 1Hz for interarea modes, and from 1 to 2Hz for local modes.

The synchronization based on power balance is able to adjust the parameters of the damping factor to any desired value as it is a virtual device, adding a positive contribution and an enhanced performance during the oscillation. Due to the power synchronization, the frequency deviation is automatically detected by the power controller, adjusting and adding power to counteract the oscillation effect. Fortunately, the fast response of power electronics can aid in the stability of the system by properly adjusting this control algorithm. By this, the power

converter is enabled not only to damp oscillations within one range but include a selective power oscillation damping for specific oscillation modes [65]. Figure 82 shows a 30kW load connection fed by the synchronous machine.

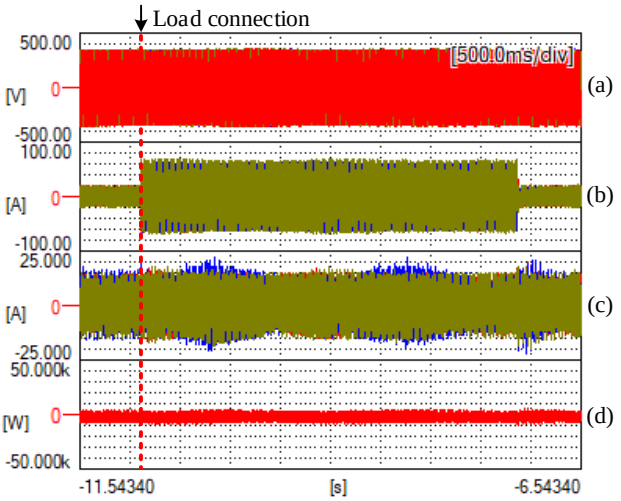

Figure 82: Oscillation damping of a synchronous machine with a 30kW load connection without the converter. (a) Grid voltage (b) Load current (c) Converter current (d) Converter active power

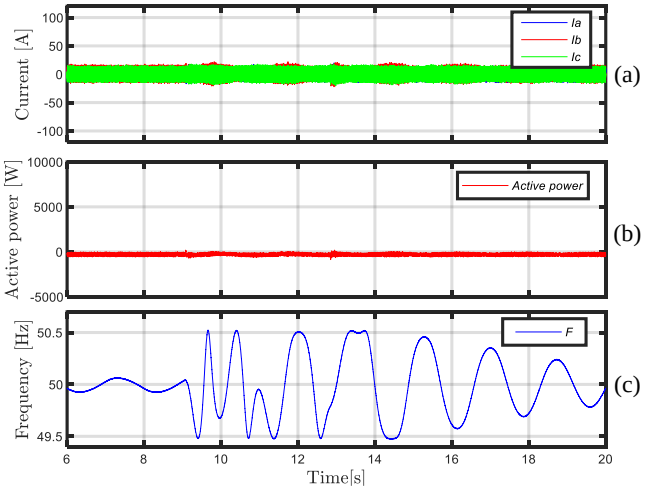

Figure 83: Frequency of the grid voltage during the mechanical oscillation of the synchronous generator (a) Converter current (b) Converter active power (c) Synchronous generator frequency.

If the system frequency in Figure 82 is analyzed it can be seen that although feeding the resistive load instantaneously, the sudden change of load generates an oscillation in a range of 1Hz in magnitude and 0.5Hz in oscillation frequency, Figure 83(c). This low damping capability is generated by the slow reaction of the mechanical shaft in front of a load connection, leading to a high change in the frequency.

In order to reduce the frequency oscillation of the electrical grid, the SPC-based power converter is enabled in the system. Figure 84 shows the dynamic behavior of the power converter during the load connection event. At the connection time, the SPC rapidly increases the active power delivered to the grid to reduce the oscillation in the frequency. Figure 85(a) and Figure 85(b) show the current and the active power injection during the load connection event, respectively. The power converter's fast action highly reduces the mechanical oscillation in the generator by providing the necessary power to the load, avoiding a fast current response of the synchronous generator, thus reducing the initial frequency oscillation. Furthermore, the power converter damps the oscillations of the generator by measuring the frequency deviation at the PCC and counteract by injecting a phase-shifted active power to reduce the frequency oscillation. It is possible to see from Figure 85(c) that the frequency oscillation has been highly decreased from a magnitude of 1Hz to a value around 0.1Hz, and the oscillation time has been reduced in time.

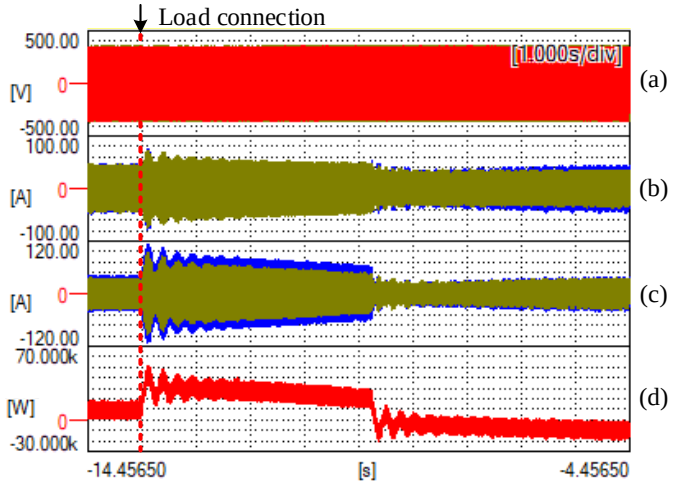

Figure 84: Mechanical oscillation damping of a synchronous machine with a 30kW load connection and the SPC-based power converter. (a) Grid voltage (b) Load current (c) Converter current (d) Converter active power

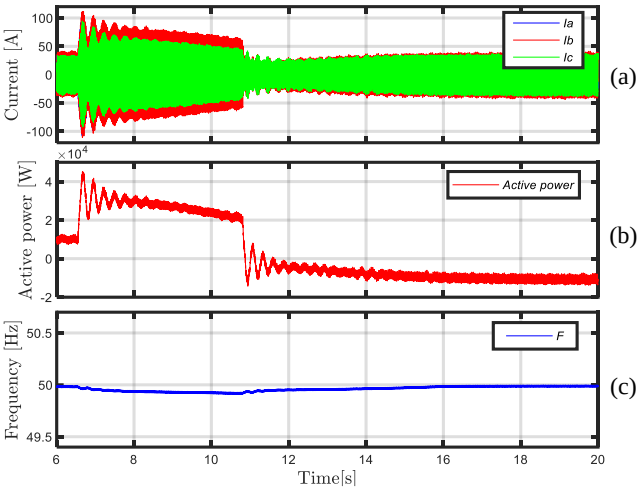

Figure 85: Frequency of the grid voltage during the mechanical oscillation of the synchronous generator with the SPC-based power converter. (a) Converter current (b) Converter active power (c) Synchronous generator frequency.

4.3. Voltage regulation

The reactive power and the voltage control are meant to respond during contingencies and shifts in generation and demand to ensure the voltage is within acceptable limits. This allows generation units to inject or absorb reactive power in accordance with the grid codes and the market rules. The voltage droop-based control is the most standard regulation in grid-connected units, as it allows a natural integration of the reactive power control in parallel operation.

4.3.1. Voltage droop control

In an equivalent way to the frequency regulation, the electrical grid needs support from the grid-connected generation units to regulate the voltage profile in the network. Considering the electrical network is predominantly inductive, the reactive power injection can influence the system at a certain point. This regulation can be implemented as a droop-based system composed of a gain and a dead band boundary. Despite the differences in regulation demanded by countries, the droop characteristic is based on the difference between the nominal voltage of the area and the measured voltage at the point of connection of each generation unit, Figure 86.

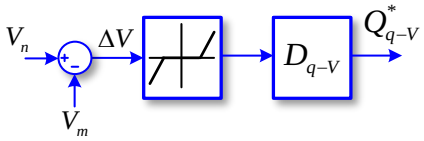

Figure 86: Implementation of the voltage droop control algorithm.

In Figure 87 a representative case of the voltage droop-based slope and the dead band is presented. Those parameters can be adjusted to the desired behavior of the droop control, which has to fulfill the grid requirements in each country.

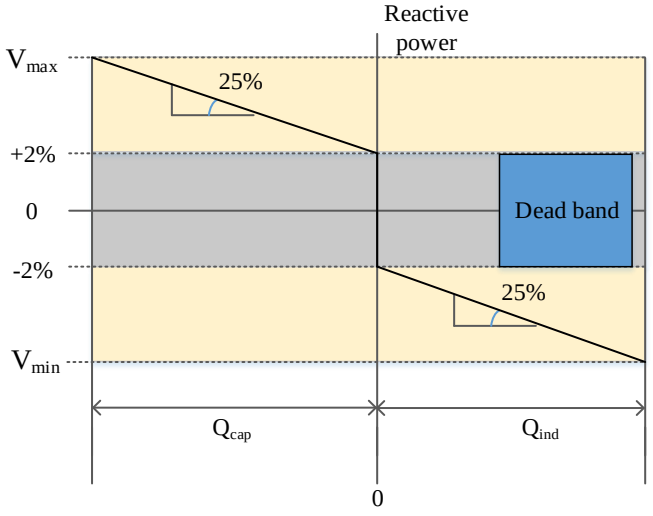

Figure 87: Q-V droop control study case

The implementation of the voltage droop control in a VSM is generally done by adjusting the electromotive force in the virtual machine. This variation in the voltage reference creates the necessary reference to either absorb or inject reactive power to the grid when necessary. As shown in Figure 88 the droop-based voltage controller is included in the SPC implementation of a virtual machine. After detecting the voltage magnitude has gone above the dead band boundary, the system starts injecting reactive power to reduce the amount of voltage drop generated at the PCC, thus supporting the grid voltage. Once the voltage returns to the nominal value, the reactive power delivered by the power converter is automatically reduced.

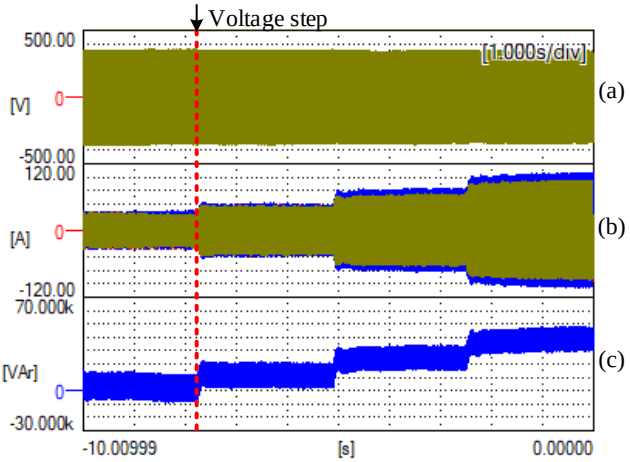

Figure 88: SPC voltage droop control (a) PCC voltage (b) Power converter current (c) Reactive power of the power converter.

This can be highlighted in Figure 89, which shows how the voltage magnitude is decreased at each step. In counteract, the reactive power injects inductive reactive power to increase the voltage level at the PCC. In this case, the voltage droop control is set with a 10% maximum voltage droop with a dead band of 5V. At t=2s the voltage crossed the dead band limit and the system starts injecting the necessary reactive power.

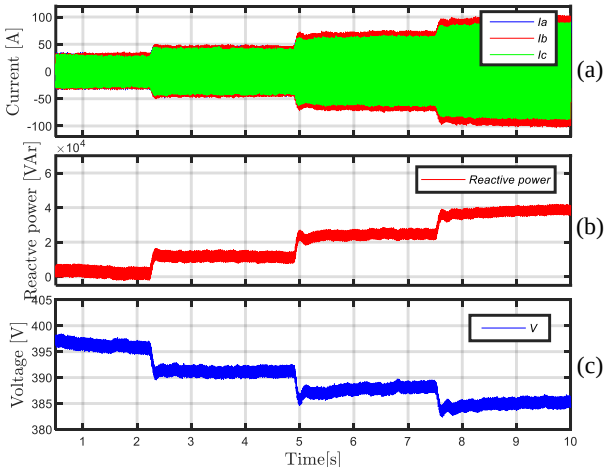

Figure 89: SPC voltage droop control over 10V voltage steps. (a) Power converter current (b) Reactive power of the power converter (c) Voltage magnitude at the PCC.

4.3.2. Low voltage ride-through (LVRT) - Balanced

Although during steady-state operation the voltage is normally within the safety limitations, there are dramatic changes that threaten the stability of the system. Due to these voltage changes, some distributed generators may disconnect from the system. The system operators require the distributed generators to remain connected during grid disturbances depending on their duration and depth. The LVRT requirement participates in the recovery of the grid voltage by supporting the grid with reactive current within a designated voltage profile. As an example, the German grid code requirements for a three-phase voltage sag profile and the required current injection are presented in Figure 90. Figure 90(a) represents the voltage drop sequence in time, and Figure 90(b) the required current depending on the depth. This profile is only specified for a three-phase balanced voltage sag.

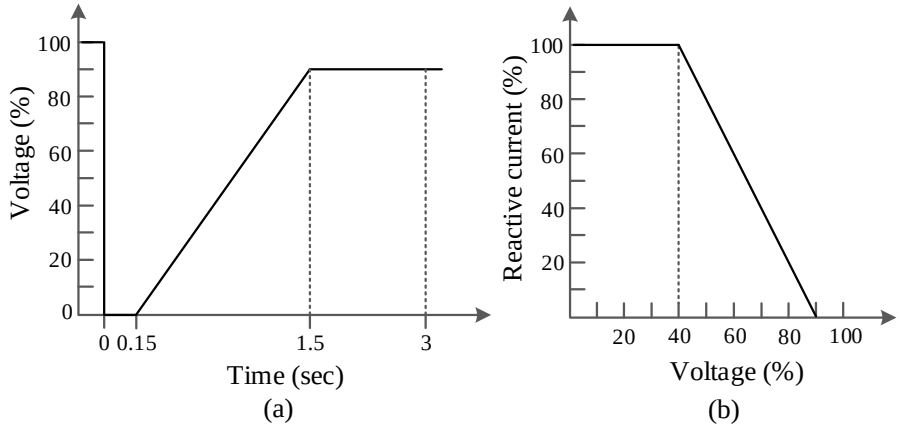

Figure 90: German grid code LVRT requirements

To virtual admittance is in charge of determining the amount of current injected during the voltage sag. In this case, the dramatic change in the voltage magnitude instantaneously generates a reactive current in the virtual admittance due to the difference to the *emf*, Figure 91.

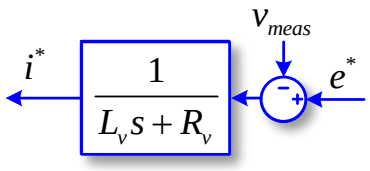

Figure 91: Virtual admittance implementation

A balanced voltage sag can be appreciated in Figure 92 where an SPC-based power converter has a dramatic change in the voltage at the PCC. At the beginning of Figure 92(a) the voltage is heavily decreased to half of the nominal value, forcing the converter to inject reactive power. It can be clearly seen from Figure 92(b) and Figure 92(c) that the voltage magnitude is dramatically modified when the power converter provides reactive power support. Figure 92(b) displays the voltage sag without reactive support, whereas Figure 92(c) has both system active.

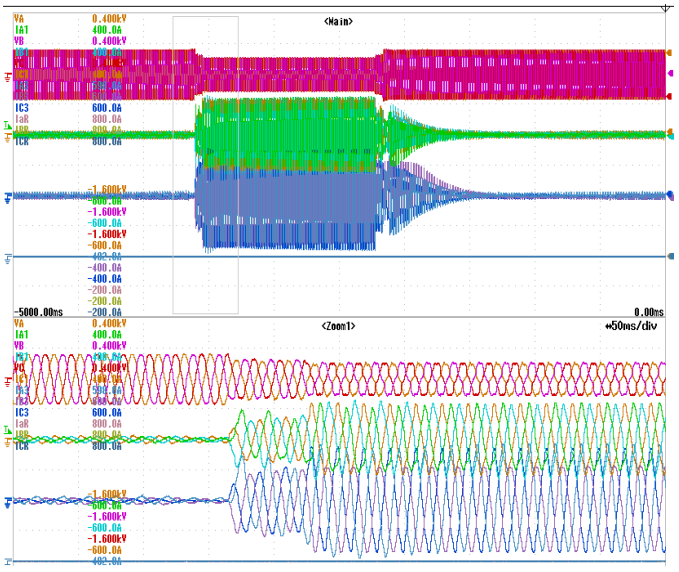

(a)

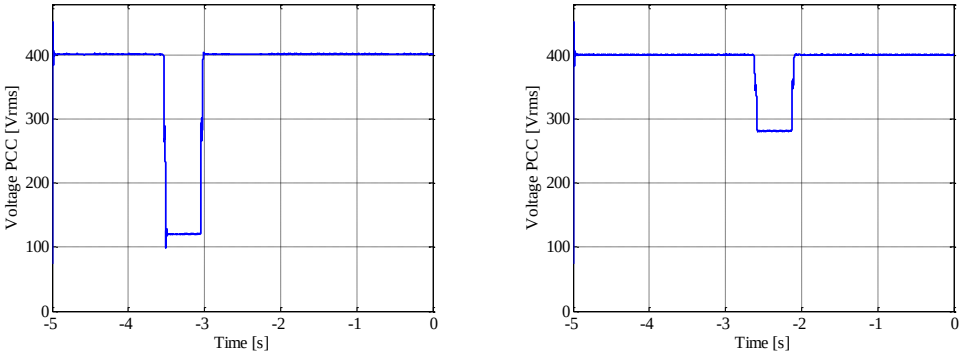

(b) (c)

Figure 92: Two 100kVA power converters under a balanced three-phase voltage sag. (a) Time domain result of the two power converter (b) Voltage magnitude without power converters (c) Voltage magnitude with the power converter support.

4.3.1. Low voltage ride-through (LVRT) - Unbalanced

It is well known that voltage sags are regarded as one of the frequency issues in the electrical grid, which not only consider three-phase faults but also one-phase faults, giving rise to an unbalanced system where the magnitude of the voltages may have important differences. To counteract these differences, the SPC approach enables a two-component virtual admittance, thus providing an automatic regulation for a balanced voltage sag or an unbalanced voltage sag. This structure is shown in Figure 93 where two bandpass filters are used to separate the positive- and negative-sequence component of the voltage error to be sent to the virtual admittance. This approach enables the system to regulate independently the amount of current injected for each sequence.

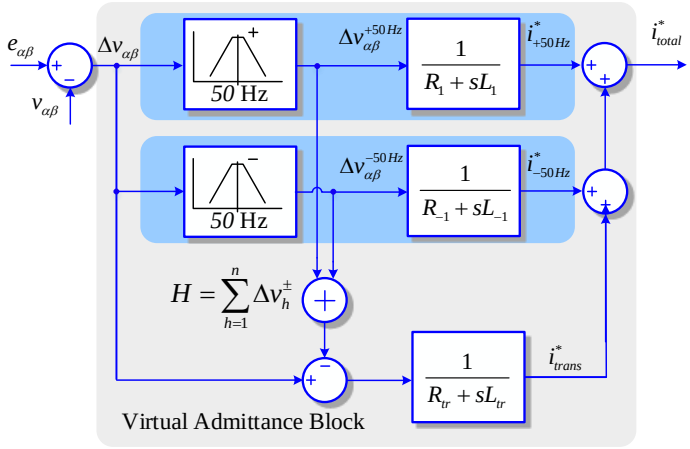

Figure 93: Positive and negative sequence virtual admittance for balanced and unbalanced voltage sags.

An unbalanced voltage sag is generated in Figure 94 using a voltage sag generator. In the first test, two SPC-based power converters are connected to the PCC where the fault is generated. In Figure 94(a) the voltage change is generated without the action of any of the power converters. It can be seen that the voltage of one of the phases has a great drop compared to the other two signals, where the negative sequence voltage reaches a value of 80V approximatelly. In a second step, both power converters are enabled and the same fault is executed. Figure 94(b) shows the effect of the power converter negative virtual admittance. The reactive current injected by both power converters highly reduces the voltage drop at one of the phases, thus supporting the system to be more balanced. In this case, the negative sequence current increases to 80A which decreases the value of the negative sequence voltage to 40V. It is possible to see from Figure 94(b) that, even though the voltage sag is unbalanced, the current injected during the voltage contingency uses both positive and negative current injection to support the grid.

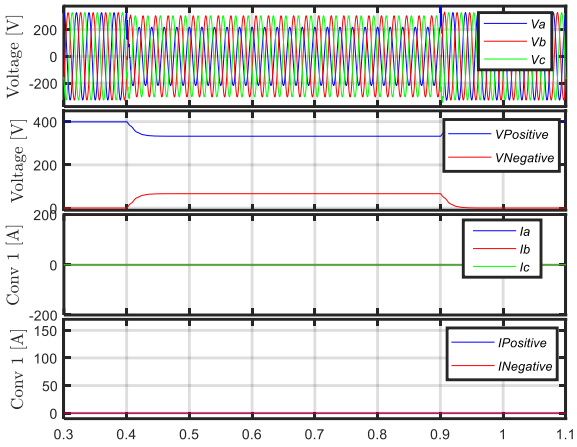

(a)

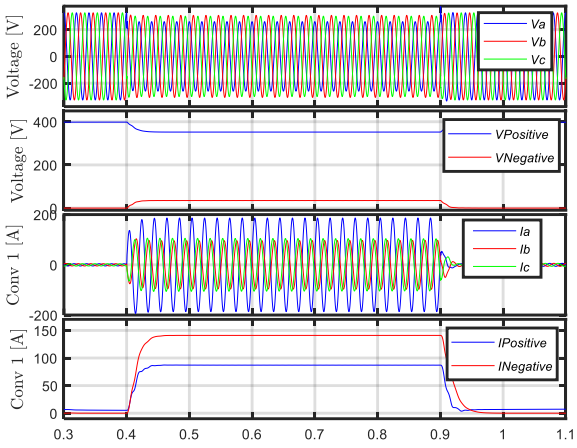

(b)

Figure 94: 100 kVA power converter under an unbalanced voltage sag (a) Without the power converter (b) With the power converter

4.4. Power quality

Frequency and voltage support are key to maintain the system under stable operating conditions. However, some additional services can be provided by power converters by using their high controllability. One common issue in many weak grids is the appearance of voltage harmonics, which are prone to be generated by a large number of devices. Among them, power electronic-based systems, like rectifiers, charging systems, or even computers, produce grid voltage harmonics. Furthermore, the combination of this distorted current to the line

impedance of the devices may give rise to severe damages to the equipment connected to the PCC.

This issue has been presented in the literature to find an appropriate approach to compensate for those harmonic distortions [91], [92]. Some solutions present either a virtual impedance or a virtual admittance approach to reduce the amount of voltage distortion at the PCC [93]. The SPC uses the virtual admittance selective harmonic control to automatically reduce the harmonic presence in the grid voltage, Figure 95.

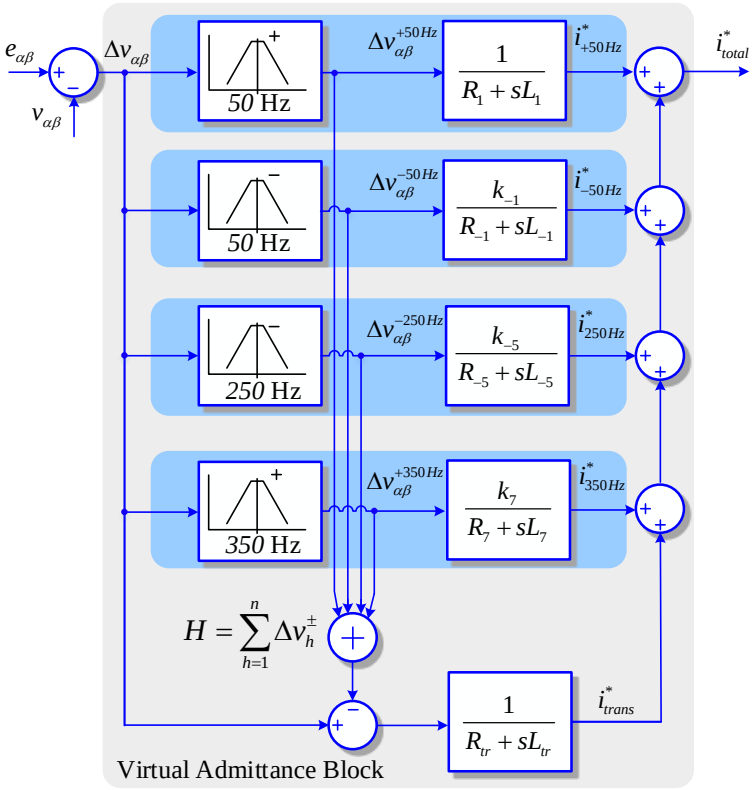

Figure 95: Selective harmonic control strategy based on parallel virtual admittance blocks.

This structure uses bandpass filters to extract the harmonic component from the voltage error between the electromotive force emulated and the grid voltage. Then, this separated component is used to generate a specific current reference for the selected harmonic, which can be at any frequency and phase angle. Figure 96(a) presents the connection of a harmonic load into the same PCC where the power converter is connected. At the time of the connection, the SPC-based converter starts injecting harmonic current to reduce the harmonic distortion at

the grid voltage. When the power converter is disabled, Figure 96(b), it is possible to see how the voltage is highly distorted by the harmonic load connected at the PCC.

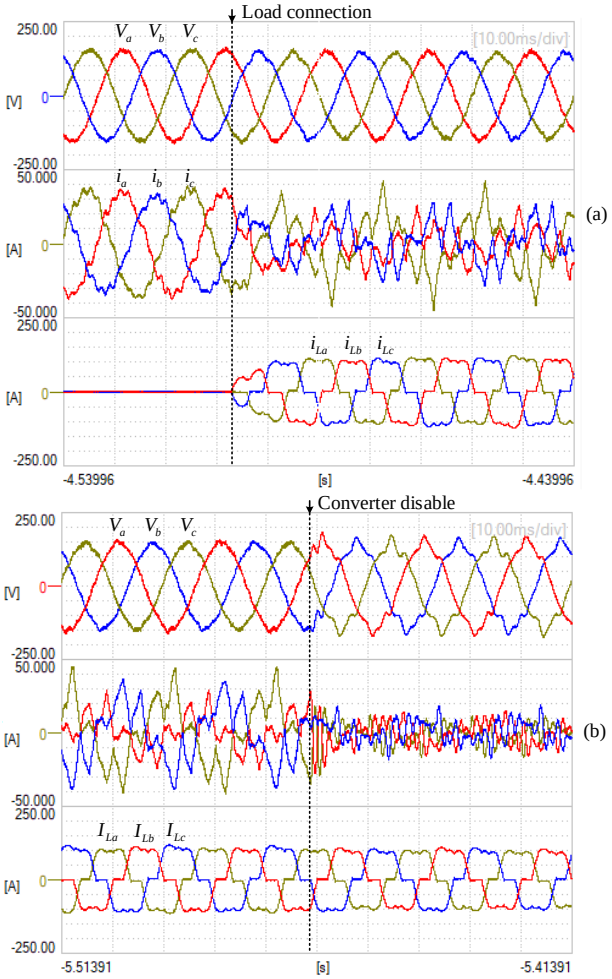

Figure 96: Connection of a harmonic load to the PCC of a 100 kVA SPC-based power converter (a) connection of the harmonic load to the system. (b) disconnection of the power converter

Chapter 5.

Synchronous control oriented to the device

During the last decade, the installation of renewable energy systems (RES), especially PV and wind power, has experienced major growth in Europe [94]. The RES shared 12,7% of overall energy consumption in Europe, and its target is to get to a participation of 27% by 2030 [95]. This increase in renewable energy penetration has forced newly integrated systems to provide grid-supporting functionalities, as dynamic support has been recently required by the system operators [96] and [97].

The integration of VSM into distributed power converters has been widely studied in the literature as well as its implementation in real experimental setups. It is well known that the VSM implementation provides a natural interaction with the electrical grid [69]. This is due to their power synchronization mechanism, which allows them to provide dynamic frequency and voltage control. Although the good performance of a VSM power converter in different applications, such as microgrids or small generation systems, the adaptation of this controller to a more extensive generation system is not straightforward.

In this chapter, the study of a single power converter with one of the VSM implementations is presented, focusing on the controllability of the device and its features. Regarding the cascaded loop control, a general modeling of synchronous power control for a single power converter is described.

During the last decade, common synchronization methods for connecting power converters to the electrical grid involved the synchronous reference frame phase-locked loop (SRF-PLL). The reason for this preference is the fast and precise detection of the grid phase angle and the grid voltage amplitude. Nevertheless, this implementation approach has limited capability to mitigate grid disturbances, such as unbalances, harmonic distortions, or noises in the measurement. For instance, any failure in the synchronization process results in an out-of-phase detection, hence making the system prone to instabilities.

In order to cope with these drawbacks, different control structures have been presented to break those limitations and enhance the stability and reliability of those grid-connected power

converters. The VSM approach has been one of the most interesting options, and although not all of them rely on the power synchronization concept, most of them add interesting features both for synchronization and steady-state operation. One of the most extended approaches is the SPC controller, which uses the swing equations and the virtual admittance to create a natural interaction of the power converter and the grid. Moreover, the control structure of the SPC makes the power converter act as a controlled current source, which inherently provides additional protection in case of overcurrents and of short-circuits.

Although the SPC implementation is well studied in the literature, advances in regards to its operability have been achieved. In this chapter an advanced virtual synchronous machine implementation is composed using the well-known SRF-PLL integrating a virtual admittance compensation loop, enhancing the current controller structure. On top of this, a sensorless approach to the SPC implementation has been proposed to enhance the traditional performance of the power converter, allowing to act as a compensation loop with grid-forming capabilities, while still using the traditional control of a grid-following system.

5.1. Cascaded loop control

The SPC has been extensively used to allow power converters to perform as a synchronous generator. In contrast to the PLL-based conventional grid-following control schemes, the SPC relies on power balancing to maintain the synchronism and the power exchange with the electrical grid. The SPC can be separated into three control loops with different bandwidths, meaning that they can be independently tuned to meet the desired stability requirements and to fulfill grid codes. In this respect, the current control loop, the virtual admittance, and the power loop controller have different settling times and bandwidths; thus they can be tuned separately as they are almost naturally decoupled. The settling time of the current control is typically around 1ms, the virtual admittance considering a 0.3 p.u of virtual inductance and 0.1 p.u of virtual resistance around the 15 ms, and finally, the power control loop has a settling time of 200 ms to 300 ms approximately.

The most inner control in the SPC is the current controller. The demanded requirements for this loop are to track the current reference generated by the virtual admittance block and to endure the inherent characteristics of the LCL output filter of the power converter. The model in the stationary reference frame of the LCL filter can be expressed as:

$$\begin{bmatrix} \dot{i}_c(t) \\ \dot{v}_f(t) \\ \dot{i}_g(t) \end{bmatrix} = \begin{bmatrix} -\frac{R_c}{L_c} & -\frac{1}{L_c} & 0 \\ \frac{1}{C_f} & -\frac{R_c R_f}{L_c} & -\frac{R_f}{L_g + L_{th}} & -\frac{R_f}{L_c} & R_f \frac{R_g + R_{th}}{L_g + L_{th}} & -\frac{1}{C_f} \\ 0 & \frac{1}{L_g + L_{th}} & -\frac{R_g + R_{th}}{L_g + L_{th}} \end{bmatrix} \begin{bmatrix} i_c(t) \\ v_f(t) \\ i_g(t) \end{bmatrix} + \begin{bmatrix} \frac{1}{L_c} \\ \frac{R_f}{L_c} \\ 0 \end{bmatrix} v_c(t) + \begin{bmatrix} 0 \\ \frac{R_f}{L_g + L_{th}} \\ -\frac{1}{L_g + L_{th}} \end{bmatrix} v_{th}(t) \qquad (41)$$

The time-domain variables are represented by the converter-side current, i_c, the capacitor voltage, v_f, the grid-side current, i_g, and the equivalent voltage at the grid side, v_{th}. The constant parameters described by, R_c, R_f, and R_g represent filter resistances. Whereas L_c and L_g are the filter inductances, and R_{th} and L_{th} are the equivalent resistance and inductance coefficients, calculated from the grid short-circuit ratio (SCR) and the quality factor $q = {R_{th}}/{\omega L_{th}}$. These grid parameters [98] can be expressed as:

$$R_{th} = \frac{V^2}{SCR \cdot P_n \sqrt{1+q^2}} \tag{42}$$

$$L_{th} = \frac{V^2 q}{SCR \cdot P_n \cdot \omega_g \sqrt{1+q^2}} \tag{43}$$

The LCL expression, obtained in (41), can be concisely represented as:

$$\dot{\mathbf{x}}_{lcl}(t) = \mathbf{A}_{lcl}\mathbf{x}_{lcl}(t) + \mathbf{B}_{lcl}u(t) \tag{44}$$

$$y_{lcl}(\mathrm{t}) = \mathbf{C}_{lcl}\mathbf{x}_{lcl}(\mathrm{t}) \tag{45}$$

Where it can be denoted that the output matrix is defined as $\boldsymbol{C}_{lcl} = [0\ 0\ 1]$. The digitalization of equation (73) can be expressed as:

$$\mathbf{x}_{lcl}(k+1) = \mathbf{A}_{lcl}\mathbf{x}_{lcl}(k) + \mathbf{B}_{lcl}u(k) \tag{46}$$

$$y_{lcl}(k) = \mathbf{C}_{lcl}\mathbf{x}_{lcl}(k) \tag{47}$$

The delay originated by the digital implementation of the controller highly affects the dynamic of the system, consequently, it is included in the controller design as a dummy variable, x_d, into the equation digital implementation definition.

$$\underbrace{\begin{bmatrix}\mathbf{x}_{lcl}(k+1)\\ x_d(k+1)\end{bmatrix}}_{\mathbf{x}_{in}(k+1)} = \underbrace{\begin{bmatrix}\mathbf{A}_{lcl} & \mathbf{B}_{lcl}\\ \mathbf{0} & 0\end{bmatrix}}_{\mathbf{A}_{in}}\underbrace{\begin{bmatrix}x_{lcl}(k)\\ x_d(k)\end{bmatrix}}_{\mathbf{x}_{in}(k)} + \underbrace{\begin{bmatrix}\mathbf{0}\\ 1\end{bmatrix}}_{\mathbf{B}_{in}}u(k) \tag{48}$$

$$y_{in}(k) = \underbrace{\begin{bmatrix}C_{lcl} & 0\end{bmatrix}}_{C_{in}}\underbrace{\begin{bmatrix}x_{lcl}(k)\\ x_d(k)\end{bmatrix}}_{x_{in}(k)} \tag{49}$$

To track the current reference, the internal model employed is used to define the proportional-resonant controller as:

$$\dot{\mathbf{x}}_{pr}(t) = \underbrace{\begin{bmatrix} 0 & 1 \\ -\omega_g^2 & 0 \end{bmatrix}}_{\mathbf{A}_{pr}} \mathbf{x}_{pr}(t) + \underbrace{\begin{bmatrix} 1 \\ 0 \end{bmatrix}}_{\mathbf{B}_{pr}} e_i(t) \tag{50}$$

Where the e_i, denotes the difference between the current reference, i^*, and the current measurement, i_g. The discretization of this equation can be expressed as:

$$\mathbf{x}_{pr}(k+1) = \mathbf{A}_{pr}\mathbf{x}_{pr}(k) + \mathbf{B}_{pr}e_i(k) \tag{51}$$

The current controller and the inverter model can be combined into a single space state equation modelled as following:

$$\begin{bmatrix} x_{in}(k+1) \\ \mathbf{x}_{pr}(k+1) \end{bmatrix} = \begin{bmatrix} \mathbf{A}_{in} & \mathbf{0} \\ -\mathbf{B}_{pr} & \mathbf{A}_{pr} \end{bmatrix} \begin{bmatrix} x_{in}(k) \\ \mathbf{x}_{pr}(k) \end{bmatrix} + \begin{bmatrix} \mathbf{B}_{in} \\ \mathbf{0} \end{bmatrix} u(k) + \begin{bmatrix} \mathbf{0} \\ \mathbf{B}_{pr} \end{bmatrix} r(k) \tag{52}$$

The virtual impedance is generally parametrized according to the required voltage support by the grid codes. The state-space of the virtual admittance can be represented as:

$$\dot{i}_g^*(t) = -\frac{R_v}{L_v} i_g^*(t) + \frac{1}{L_v} e(t) - \frac{1}{L_v} v_c(t) \tag{53}$$

Where the parameters R_v and L_v represent the virtual resistance and inductance in the system that can be adjusted to obtain the desired performance, i_g^* is the current reference for the current controller, e represents the internal electromotive force of the machine used as a voltage reference, and v_c is the grid voltage measurement.

The active and reactive power controllers are the fundamental elements to emulate the electromechanical loop of the synchronous generator. The active power is based on the electromechanical swing equations, previously presented in equation (7). And the reactive power controller is based on a proportional-integral loop, defined as:

$$E = \frac{k_p s + k_i}{s}\left(Q^* - Q_m\right) + E_n \tag{54}$$

Where E is the virtual electromotive force of the emulated machine, E_n is the nominal voltage of the grid, Q^* and Q_m are the reactive reference and the measurement, and the parameters k_p and k_i are the proportional and integral gain, respectively.

The resulting diagram of the SPC is shown in Figure 97.

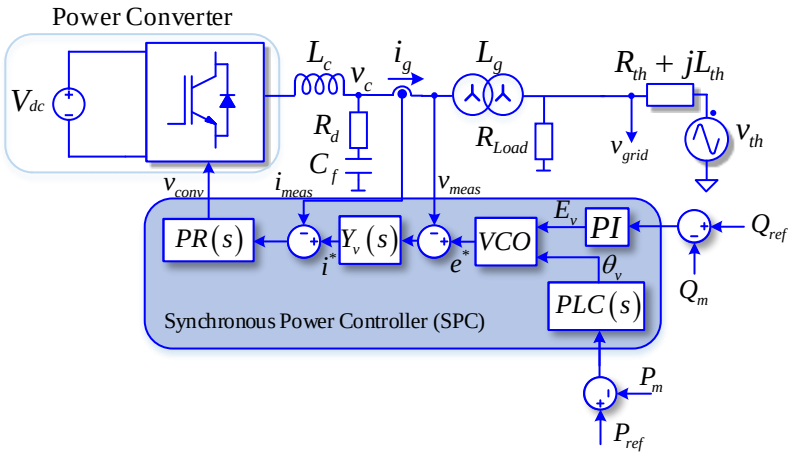

Figure 97: Cascaded SPC implementation

Although the core implementation has been widely implemented in different publications, several additional external loops have been integrated to cover the SPC operation in specific grid scenarios.

5.1.1. External controllers – Vdc limitation

In addition to the synchronous services presented in the previous section, some additional features have been added to the SPC control to expand its reliability and stability. In the case of weak dc-voltage links, such as PV systems, the dc-voltage might experience some dramatic changes due to unexpected events, such as line trips. To maintain the dc-bus voltage in those cases within the safety region of operation, a protection control loop has been added to the SPC controller, Figure 98.

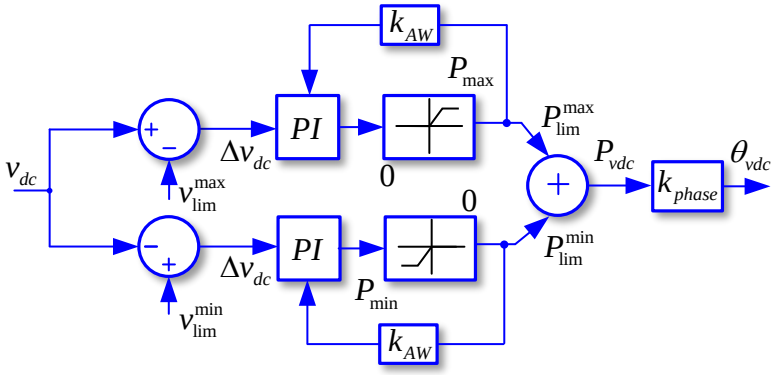

Figure 98: Proportional integral PI strategy for dc voltage protection.

This protection loop has two PI controllers devoted to directly modify the phase-angle in the electromotive force, e^*, thereby modifying the active power to keep the dc-bus voltage within the specified limits. The range for the limitation of the dc-voltage link can be adjusted by setting the parameters v_{lim}^{max} and v_{lim}^{min}. This range specifies the maximum and the minimum voltage allowed in the power converter dc-bus. In addition, a saturation block is added at the output of each PI controller to ensure that the protection loop is acting only when the voltage at the dc bus is out of the limits and or above its maximum capacity. This control loop has a fast response since it changes directly the voltage reference of the SPC, its dynamic being set by the parameter k_{phase}.

5.1.2. External controllers – Resynchronization algorithm

It is well known that the SPC strategy allows the power converter to be grid-forming, meaning that if there is no grid available for the power converter it is able to form its own grid. In this regard, the generation of the own grid allows the power converter to have a flexible grid-operation condition that can be disconnected from the utility grid when necessary. However, the system cannot be reconnected to the utility grid in the same manner due to the possible phase difference between the voltage created by the power converter and the phase in the grid. To synchronize the system to the electrical grid before its reconnection, two control loops are needed to ensure the synchronism of both elements, Figure 99. First, the frequency synchronization loop tries to match the grid voltage frequency with the islanded power converter frequency. Whereas the second loop ensures the phase-angle of both systems match to avoid a huge power spike during the reconnection time. The loop can be used in grid-connected mode, however as the system is in-phase with the grid voltage it does not provide any power

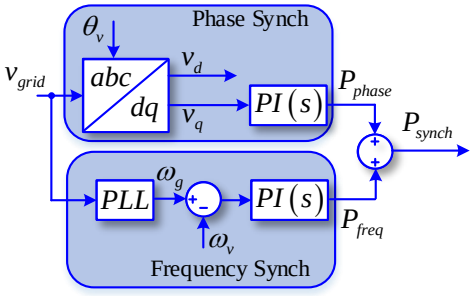

Figure 99: Resynchronization control scheme

The frequency loop includes an additional PLL to extract the frequency measurement of the grid voltage. The tunning of the PLL parameters K_{p_pll} and k_{i_pll} are based on the desired settling time and the nominal voltage of the grid.

$$k_{Ppll} = \frac{8}{V_n \cdot \tau_{pll}} \tag{55}$$

$$k_{Ipll} = \frac{32}{V_n \cdot \tau_{pll}^2} \tag{56}$$

This measurement is subtracted from the frequency detected by the active power controller in the SPC, ω_v, which describes the frequency of the virtual rotor of the synchronous machine. The power output obtained from the frequency synchronization loop is attached as an additional input to the power loop controller in the SPC, which accelerates or decelerates the virtual rotor to match both frequencies.

The phase synchronization loop uses the internal virtual phase, θ_v, to rotate the grid voltage, v_{grid}, into the synchronous reference frame. This rotation, using the Park transformation, detects the phase difference between both phases by terms of measuring the magnitude difference in the vector v_q. Once the frequency is under a certain boundary the phase synchronization is enabled to match the grid phase-angle to the internal voltage generated by the converter.

5.1.3. Real-time simulation

The real-time simulation results are composed of a Typhoon HIL 602+ that emulates a 200 kVA power converter connected to the grid, an NRGLab amplifier to increase the voltage level of the HIL simulation for the real measurement units, and a visualization control system to obtain all the data from the control board by using EtherCAT automation protocol (EAP) communications, as shown in Figure 100.

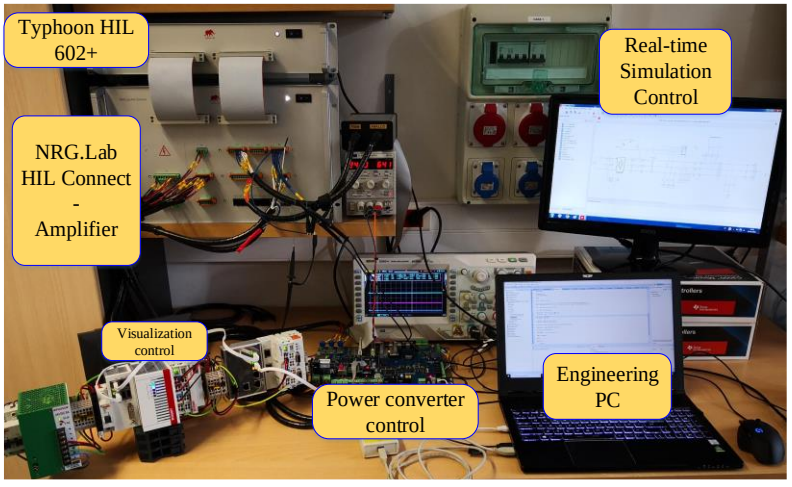

Figure 100: Real-time simulation setup

The electrical system and the control scheme are presented in Figure 101. In this case, the SPC-based power converter is attached by the external resynchronization control, and in addition, does not include a reactive power controller, meaning that the electromotive force is fixed to E_v parameter.

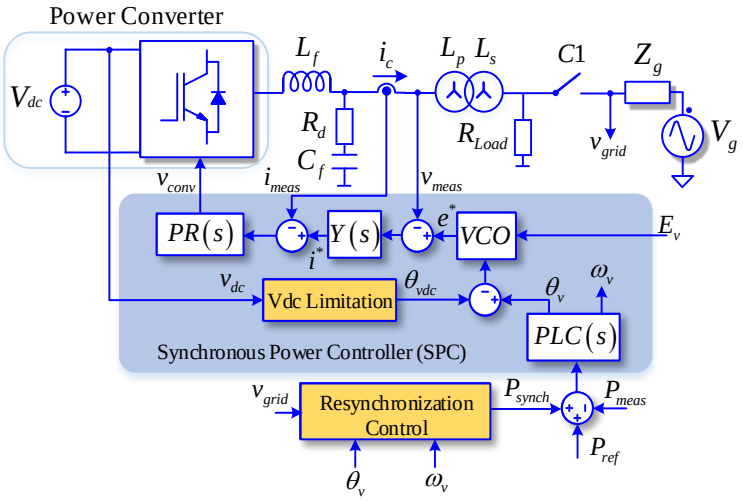

Figure 101: Resynchronization control, electrical and control schemes

The real-time simulation results are separated into two stages to show the resynchronization process of the SPC-based power converter. The first result is the transition of the power converter into the island mode operation with and without a load at the PCC. The second result is the resynchronization process, where the two added external loops will force the system to synchronize to the external voltage. The electrical parameters of the real-time simulation are presented in Table 11.

Symbol	Definition	Values
S	Converter nominal power	200 kVA
L_f	Inverter-side inductance	140 µH
C_f	Capacitance	240 µF
R_d	Damping resistance	25 mΩ
L_p+L_s	Grid-side inductor	84 µH
Z_g	Grid impedance	0.125 Ω
P_{dc}	dc source nominal power	200 kW
V_{dc}	dc nominal voltage	800 V

Table 11: Real-time simulation electrical parameters

Table 12 presents the control parameters for the real-time simulation results.

Symbol	Definition	Values
S_n	Nominal power	200 kVA
V_n	Nominal voltage	360 V
f_n	Nominal frequency	314.15 rad/s
H	Inertia factor	5
ξ	Damping factor	0.7
R_v	Virtual resistor	2 Ω
X_v	Virtual reactance	6 Ω
k_p^f	Proportional gain frequency loop	0.1
k_i^f	Integral gain frequency loop	0.5
k_p^{ph}	Proportional gain phase loop	0.5
k_i^{ph}	Integral gain phase loop	1

Table 12: Real-time simulation results control parameters

The first HIL result is based on the island transition of the SPC-based power converter. In this case, the system was operating connected to the grid without exchanging any power to the system. In Figure 102, at t = 47 s the circuit breaker C1 is opened, leaving the power converter without any external grid to connect to. It starts operating as a grid-forming unit by creating and regulating the voltage and frequency. Once the circuit breaker is opened, from t = 47 s to t = 62s, the system remained to form the grid without any load connection at the point of common coupling. This can be appreciated in Figure 102(a) where the current is transitioned to zero and from Figure 102(b) which maintains the same voltage level with the same frequency. However, at t = 62 s a load is connected to the system which consumes 100 kW directly fed from the power converter. As soon as the load is connected to the system, the frequency starts drooping following the frequency droop control dynamics.

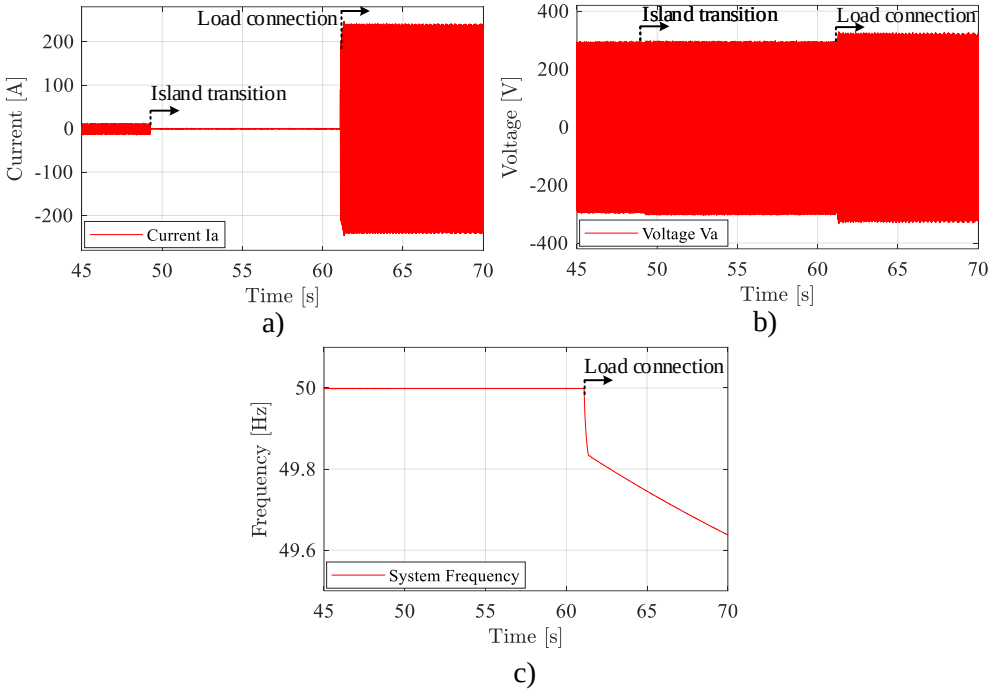

Figure 102: Island transition and load connection of a 200 kVA SPC-Based power converter (a) Current of phase A (b) Voltage at the converter side of phase A (c) System frequency deviation during the load event.

Figure 103 shows the total response of the system in front of the load connection event, where the frequency droops until a value of 48,9 Hz.

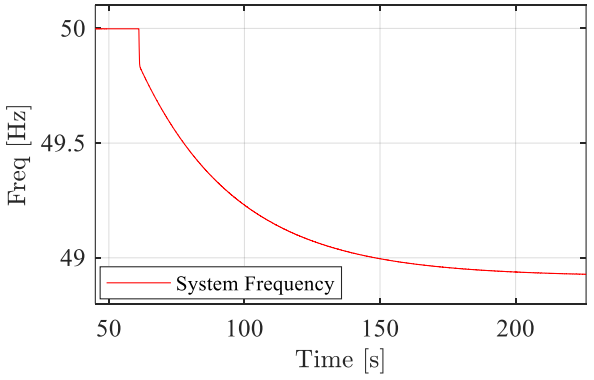

Figure 103: Total response of the system under the load event.

The SPC-based converter is capable of maintaining the frequency of the system even during the load event connection. However, for the reconnection procedure, it is not possible to match the phase of the grid and the phase of the electromotive force of the virtual machine if the frequency, phase and magnitude are not close. For this reason, the resynchronization process starts with frequency control to adjust the islanded frequency generated by the power converter. Figure 104 shows the resynchronization process of the SPC-based power converter. At t = 245s the frequency loop is activated, starting the acceleration of the virtual rotor in the virtual machine by adding power reference to the PLC. Even though it is a power reference, the power provided by the converter does not change as it is the only generator feeding the load, Figure 104(b) . Once the frequency reaches a certain boundary, the phase synchronization tries to match the phase angle of both voltages. It can be seen on Figure 104(a) that the phase synchronization does four different attempts to match the phase of the virtual rotor to the phase of the grid. Once the system can follow the phase of the grid, the system frequency automatically reaches the target frequency as the phase controller is the one adjusting the speed of the machine to match the phase of the grid. As the power converter is operating in a grid-forming condition, even though the active power reference is modified to resynchronize to the electrical grid, the active power delivered to the load remains constant, Figure 104(b).

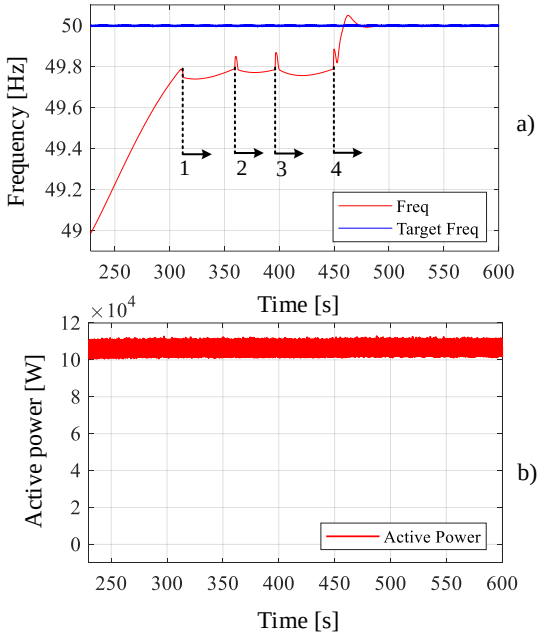

Figure 104: Resynchronization procedure to the electrical grid of the SPC-based power converter (a) System frequency and grid target frequency (b) Active power output from the power converter

5.1.4. Experimental results

The experimental setup is formed by a 200kVA power converter interconnected through an isolation transformer to the electrical grid. In addition, the dc-bus is provided by a 200kWh battery stack, and there is a variable load connected to the PCC. Figure 105 presents the electrical configuration of the experimental setup, which allows disconnecting the power converter from the electrical grid while the converter keeps feeding the local load. The experimental results are split into two stages. First, the transition to the island operation mode considering a load is already connected to the PCC. Second, the resynchronization process is enabled in the SPC-based power converter starting the synchronization process with the frequency and phase control loops.

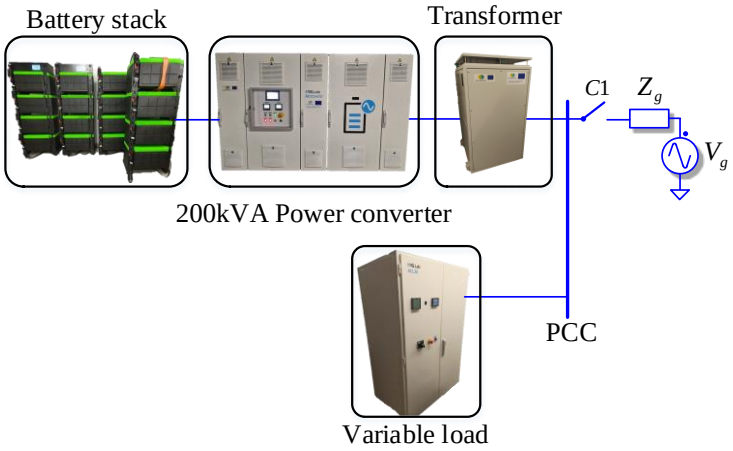

Figure 105: Experimental setup configuration.

In the first test, the power converter was injecting 30 kW previous to the opening of the circuit breaker C1. Figure 106 shows the behavior of the power converter during the grid disconnection. The zoom highlights the minor distortion in the voltage during the event.

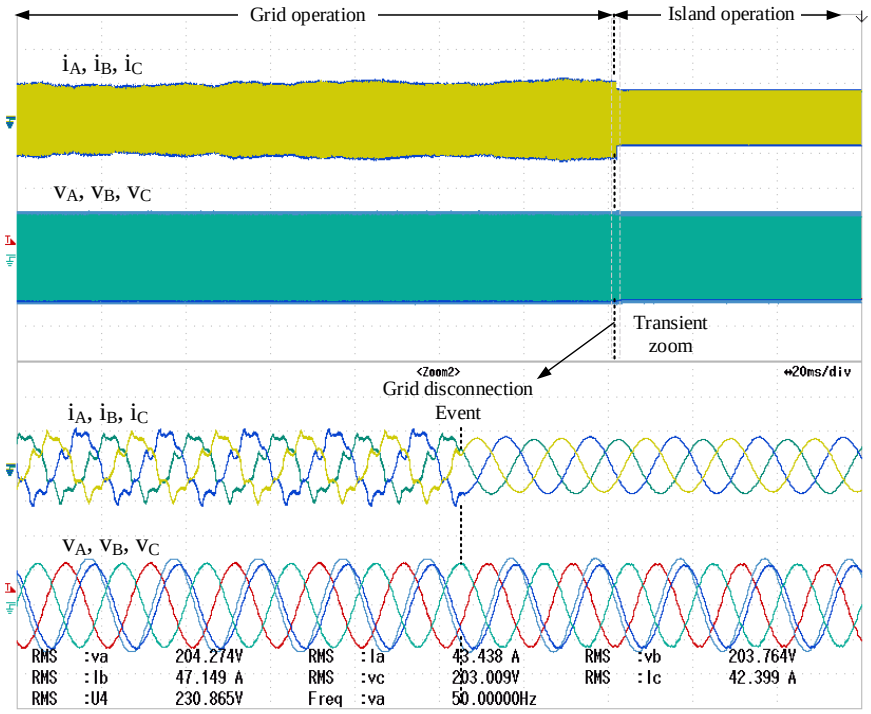

Figure 106: Transition to island operation with a 30 kW load connected.

At the instant of disconnection, the SPC leads the creation of the grid, regulating the amount of power fed to the load, the frequency, and the voltage magnitude during the island operating mode. In regards to the current before the disconnection, it is possible to see that it has a clear harmonic component lead by two aspects. First, the virtual admittance is compensating for voltage distortions which adds a harmonic component to the current for compensating the voltage. Second, the low inductance value of the converter filter inductance increases the noise due to the switching frequency increasing in this way the harmonic component at the output.

The slow dynamic of the resynchronization process is due to the variability of the phase and the frequency of the electrical grid. First, the frequency loop will accelerate the virtual rotor until it reaches the boundary of 0.2 Hz from the measured frequency. When this value is reached, the phase synchronization will adapt the phase angle of the power converter to adjust its electromotive force to the one in the grid. For safety operation, the power converter has to remain phase synchronized to the grid voltage for two minutes before the reconnection. Once the safety time has been reached the system will automatically close the circuit breaker as seen in Figure 107.

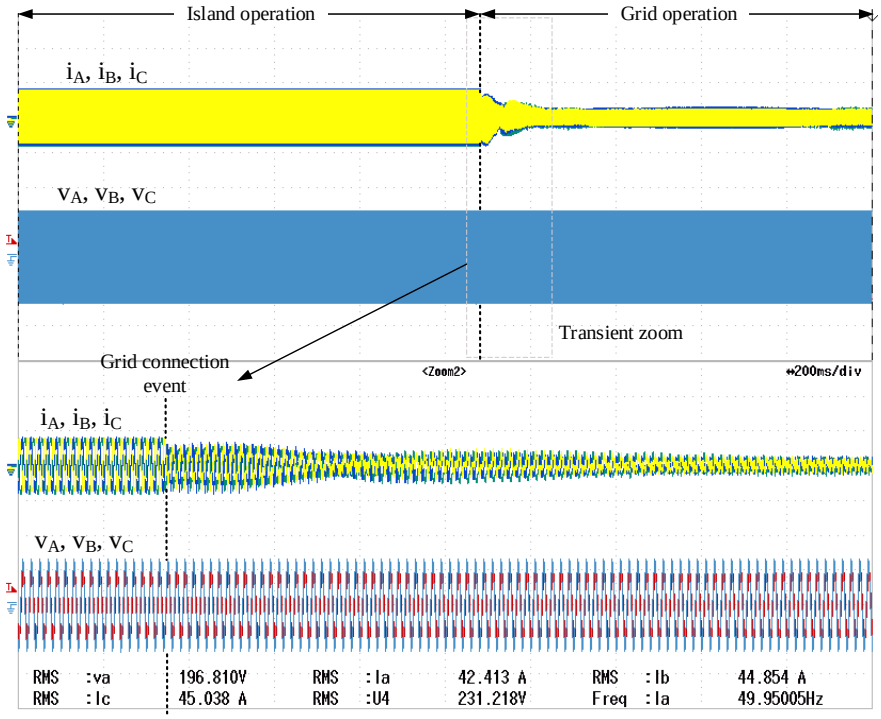

Figure 107: SPC-based power converter reconnection to the electrical grid.

It is possible to see that, during the transient, the power from the power converter resembles the connection of a synchronous machine in phase to the electrical grid. However, the increased damping factor highly reduces the oscillation during this reconnection. Furthermore, as the phase angle of the power converter and the grid are almost equal before the reconnection, the power deviation during the transient is reduced.

5.2. Grid-forming PLL strategy

It has been reviewed in the state of the art that the PLL has been widely used in the control of power converters. Despite the fast and precise detection of phase angle and amplitude of the grid voltage, the PLL has a limited capability in terms of harmonic distortions, unbalances, and grid-forming capabilities. This last issue is generally due to implementing the PLL strategy, which focuses on matching a voltage reference, and not generating a virtual one. Therefore, any failure in the voltage measurement leads to the total out-of-phase of the power converter, leading it to unstable operating points. In this regard, the literature presented some additional blocks to enhance the traditional operation of the PLL under some of those undesired environments [99] and [11].

Grid-forming converters generally use the VSM approach to generate a virtual electromotive force to provide the power converter with interesting features such as the island mode operation or the automatic power balancing. However, in commercial power converters, such control is not yet widely implemented as the control is focused on the reliability of the system and its capacity to inject the required power into the grid. This control structure can be described in Figure 108, which is a grid-following power converter. This structure needs a voltage source to be connected to, as it acts as a voltage-controlled current source in front of the grid.

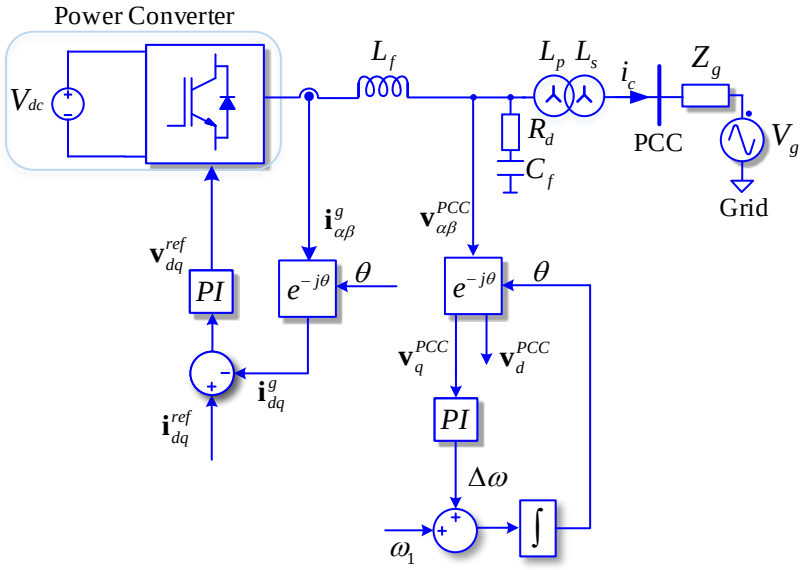

Figure 108: Three-phase power converter connected to the electrical grid using a traditional current controller and a PLL.

The current controller is generally implemented in the synchronous reference frame, which uses the phase angle detected by the PLL to rotate at the same speed as the electrical grid. The PLL outputs can be identified in the *dq* axis as the magnitude of the input voltage in the *d* axis, and the frequency deviation in the *q* axis, which is generally used to ensure the phase matching between the θ of the PLL and the grid phase angle. The voltage-based synchronization system has been used as a method of reaching the VSM in some of their implementations, as presented in Section II. However, most of the approaches used the PLL in case of disturbances or as a protection element.

In this way, the combination of a PLL and a virtual admittance enables the power converter to have a grid-forming capacity, as depicted in Figure 109. The addition of the virtual admittance into the structure of the converter control allows introducing a voltage error at the

input of the admittance. Considering that the SRF-PLL extracts the voltage magnitude and frequency of the grid by rotating the system at the same rotational speed, an internal electromotive force can be induced by generating a value for the voltage amplitude in the *d* axis and a phase difference in the *q* axis. With this method, by regulating the voltage magnitude $|V_n|$ the reactive power is controlled, whereas the difference in $\Delta\omega$ regulates the active power. Considering the control of this structure, the PLL will determine the needed compensation current to be perfectly synchronized to the electrical grid. In addition, if the voltage at the grid side is lost, the internally generated *emf* will generate the necessary current to maintain the electrical grid.

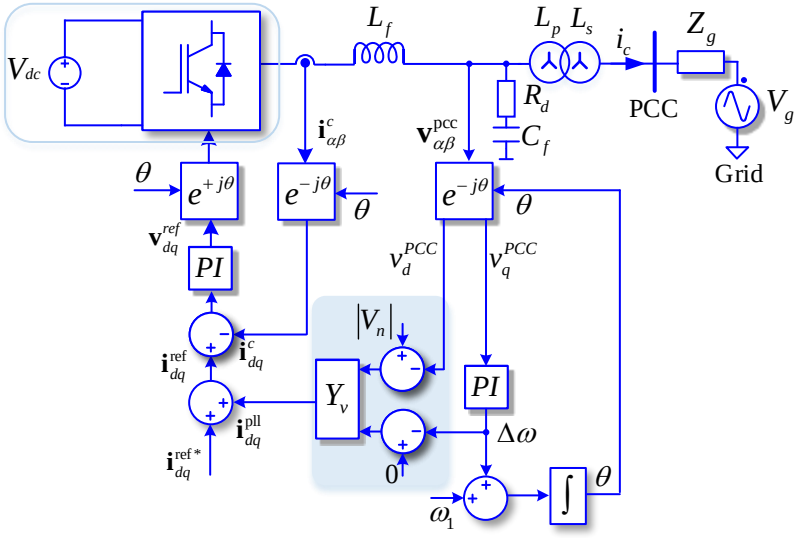

Figure 109: Virtual admittance structure for the SRF-PLL synchronization system.

The virtual admittance, Y_V, implementation in the stationary reference frame can be obtained from the Park transformation, leading to a coupling feedback loop between the *d* and *q* axes. This coupling is purely determined by the amount of inductance set in the virtual admittance, which defines negative and positive feedback from the quadrature signal to the voltage error of each axis, as shown in Figure 110.

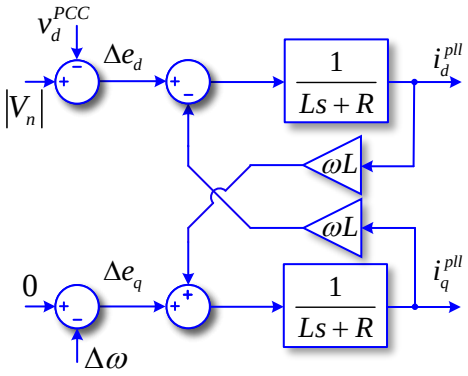

Figure 110: Representation of a virtual admittance in the synchronous reference frame.

5.2.1. Stability analysis

In this section, the power converter stability is studied when the admittance compensation loop is integrated into the control loop. To analyze the system stability, the simplified block diagram is presented in Figure 111. This model is composed of a PI controller for the current control, a time delay Padé approximation for the PWM delay, an LCL output filter of the power converter, a PLL to detect the phase and the magnitude of the grid, a virtual admittance to generate the compensating current, a grid impedance to emulate the grid interconnection, and a rotation function to switch the model from the synchronous to the stationary reference frame.

The terms $e^{+j\theta}$ and $e^{-j\theta}$ expresses the rotation shift between the different reference frames. When moving from the stationary to the synchronous reference frame $e^{-j\theta}$ is used to decelerate the system to a continuous signal, whereas $e^{+j\theta}$ is used to accelerate the system to a sinusoidal waveform at the specified frequency.

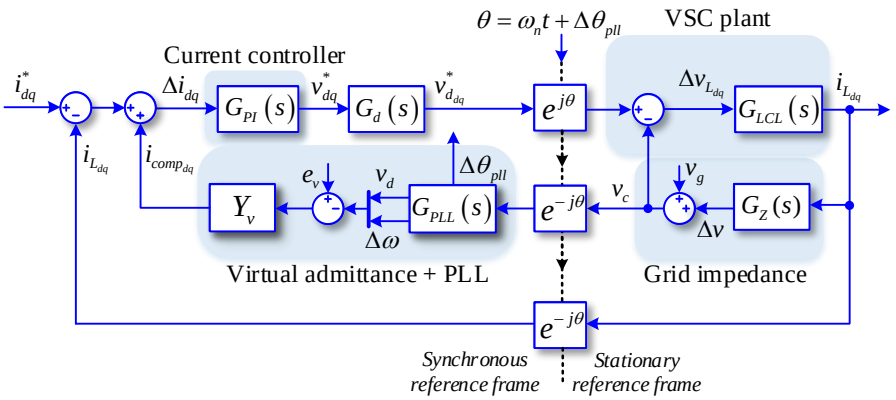

Figure 111: Extended block diagram for the virtual admittance with PLL and the rest of required blocks for the stability analysis .

In order to analyze the system properly, all the internal blocks have to be shifted into a unique reference frames. In this case, the synchronous reference frame is selected as it allows a simpler analysis of the PLL interaction. Even though the whole system can be shifted by rotating the system at the nominal frequency ω_n, the effect of the PLL due to the park transformation cannot be discarded as it is highly affecting the dynamic of the system as shown in Figure 112.

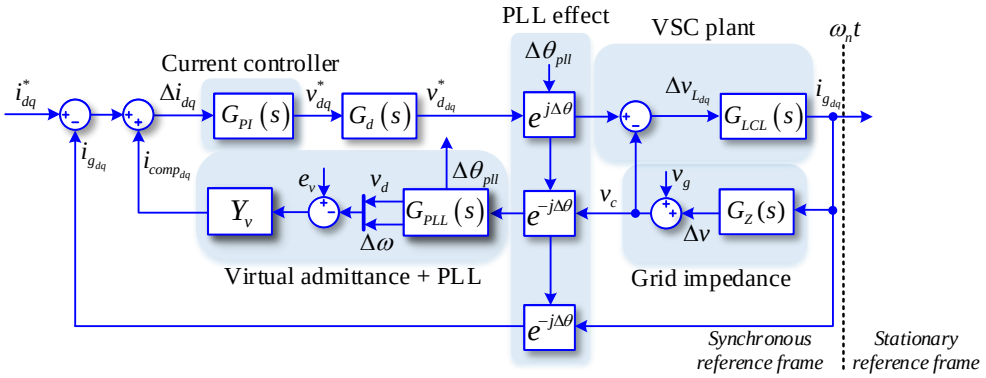

Figure 112: Synchronous reference frame model with the PLL effect on the Park transformation.

This PLL effect can be described as equation (57), which relates the input Δv_q to the output $\Delta\theta$.

$$G_{\Delta\theta}(s) = \frac{k_p^{pll} s + k_i^{pll}}{s^2 + k_p^{pll} s + k_i^{pll}} \tag{57}$$

This will be included in all Park transformations used throughout the analysis, coupling the synchronous reference frame on its quadrature signals as shown in (58).

$$\boldsymbol{e}^{j\theta} = \begin{bmatrix} 1 & -\Delta\theta \\ \Delta\theta & 1 \end{bmatrix} \tag{58}$$

In addition to the $\Delta\theta$ transfer function, to obtain the PLL transfer function for the frequency variation and the voltage magnitudes in the *dq*-reference frame, the following expressions can be used:

$$G_{\Delta\omega}(s) = \frac{k_p^{pll} s^2 + k_i^{pll} s}{s^2 + k_p^{pll} s + k_i^{pll}} \tag{59}$$

$$G_{\Delta Vd}(s) = v_d - \Delta v_q \Delta\theta \tag{60}$$

$$G_{\Delta Vq}(s) = v_q + \Delta v_d \Delta\theta \tag{61}$$

Where the parameters k_p^{pll} and k_i^{pll} define the dynamic response of the PLL. The transfer function of the voltage magnitude is directly defined by the value of the voltage in the *dq* axis plus the variation in the quadrature component, Δv_{dq}, multiplied by the PLL effect, $\Delta\theta$.

Following the same methodology, the rest of the transfer functions can be modeled in the synchronous reference frame. The transfer function of the PI controller can be defined as:

$$\boldsymbol{G_{PI}}(\boldsymbol{s}) = \begin{bmatrix} k_i + k_p s & 0 \\ 0 & k_i + k_p s \end{bmatrix} \cdot \frac{1}{s} \tag{62}$$

In a similar way to the analysis presented in Chapter 3, the time delay of the PWM can be described as in (30).

The plant system is composed of an LCL filter, which transfer function can be generally represented as the equation (63). The shift from the stationary to the synchronous reference frame of the inductances, capacitor, and damping resistor can be obtained by switching the Laplace coefficient, s, into a value of $s - j\omega$. The result for the transformation is shown in equations (64), (65), and (66).

$$\boldsymbol{G_{LCL}}(\boldsymbol{s}) = \frac{Y_1 \cdot (Z_c Y_2 + 1)}{Z_c (Y_1 + Y_2) + 1} \tag{63}$$

$$\boldsymbol{Y_1}(\boldsymbol{s}) = \begin{bmatrix} L_f s + R_f & -\omega L_f \\ \omega L_f & L_f s + R_f \end{bmatrix} \cdot \frac{1}{\left(\omega^2 + s^2\right) L_f^2 + 2 L_f R_f s + R_f^2} \tag{64}$$

$$\boldsymbol{Z_c}(\boldsymbol{s}) = \begin{bmatrix} C_f R_d s^2 + s + C_f R_d \omega^2 & -\omega \\ \omega & C_f R_d s^2 + s + C_f R_d \omega^2 \end{bmatrix} \cdot \frac{1}{C_f \left(\omega^2 + s^2\right)} \tag{65}$$

$$\boldsymbol{Y_2}(\boldsymbol{s}) = \begin{bmatrix} L_2 s + R_2 & -\omega L_2 \\ \omega L_2 & L_2 s + R_2 \end{bmatrix} \cdot \frac{1}{\left(\omega^2 + s^2\right) L_2^2 + 2 L_2 R_2 s + R_2^2} \tag{66}$$

The values of $[L_1, R_1]$ and $[L_2, R_2]$ express the first and second inductance parameters, whereas $[C_f, R_d]$ represents the capacitor value and the passive damping resistor of the filter. The grid impedance is added to the second inductance of the filter as an additional inductance and resistance.

$$\boldsymbol{Y_2^g}(\boldsymbol{s}) = \begin{bmatrix} \left(L_2 + L_g\right) s + R_2 + R_g & -\omega\left(L_2 + L_g\right) \\ \omega\left(L_2 + L_g\right) & \left(L_2 + L_g\right) s + R_2 + R_g \end{bmatrix} \cdot X_{den} \tag{67}$$

$$X_{den} = \frac{1}{\left(L_2 + L_g\right)^2 s^2 + 2\left(R_2 + R_g\right)\left(L_2 + L_g\right) s + \left(L_2^2 + 2 L_2 L_g + L_g^2\right)\omega^2 + \left(R_2 + R_g\right)^2} \tag{68}$$

Finally, the virtual admittance block, Y_v, can be modeled based on Figure 110 as:

$$\boldsymbol{Y}_v(\boldsymbol{s}) = \begin{bmatrix} L_v s + R_v & -\omega L_v \\ \omega L_v & L_v s + R_v \end{bmatrix} \cdot \frac{1}{\left(\omega^2 + s^2\right) L_v^2 + 2 L_v R_v s + R_v^2} \tag{69}$$

Where the parameters $[L_v, R_v]$ can be modified online to increase or decrease the action of the compensation loop.

The static parameters used for the analysis are described in Table 13.

Symbol	Definition	Values
S	Converter nominal power	100 kVA
L_f	Inverter-side inductance	777 µH
C_f	Capacitance	66 µF
R_d	Damping resistance	0.5 Ω
L_2	Grid-side inductor	294 µH
R_v	Initial virtual resistor	0.16 Ω
L_v	Initial virtual inductor	0.00152 H

Table 13: Parameters for the analysis of the virtual admittance PLL.

To analyze the stability and how the system reacts in front of different grid and control parameters, a pole movement analysis have been carried out. This study focused on three parameters modifications while the other are set as static to highlight their effect on the system's eigenvalues. In a first scenario, the system is analyzed with and without the virtual admittance compensation loop for a variation in the SCR of the grid, from 10 to 1.5, achieved by modifying the interconnection impedance. In this first case, the parameters of the PLL are defined as static parameters and the settling time, τ_s, is set to 40ms. In a second scenario, the grid SCR is set to a fix value and the control parameters of the PLL are modified by adjusting the settling time τ_s. In this case the system is also analyzed with and without the virtual admittance to demonstrate the increase on the stability and performance of the power converter. Finally, in the third scenario, the system is analyzed for two different SCR values, one with a SCR = 2 and the other one with SCR = 10, with a fix settling time of 40ms in the PLL.

Scenario1:

Figure 113 shows the pole movement due to the SCR change in the grid with a fix settling time of the PLL. The poles of the system without virtual admittance, red dots in the figure, move towards the unstable area when the SCR of the grid is reduced below the value of 1.6. As is it clearly seen in the figure, the system present a poorly damped pole when the SCR is close to 2, with a natural resonance frequency of 109 rad/s. In contrast, the virtual admittance

compensation, blue dots in the figure, moves those unstable poles to the stable region, Figure 113, increasing the damping in all the range and maintaining its value during the different values of SCR.

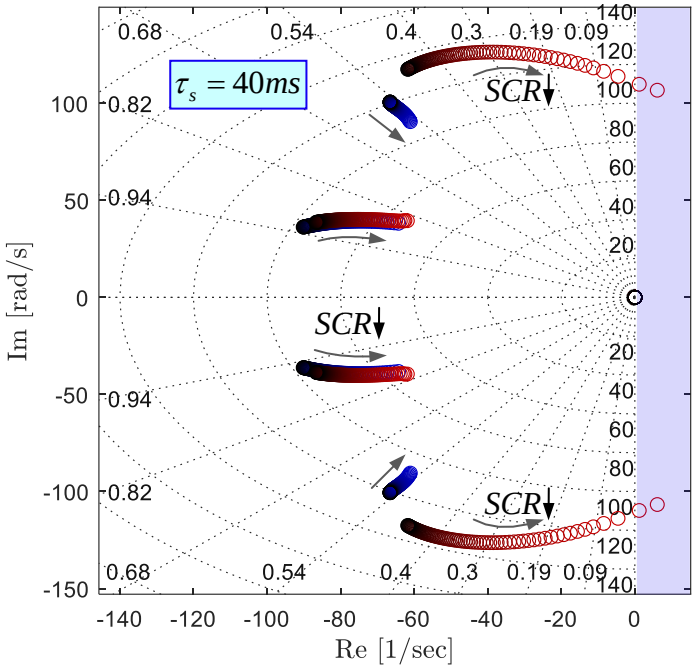

Figure 113: Eigenvalues movement for different SCR with fixed PLL = 40 ms, with virtual admittance (blue) without virtual admittance (red).

To highlight the difference between operation points, with and without the virtual admittance, two simulation results are analyzed. Figure 114(a) display the time domain result of the system in a SCR of 2 with a PLL settling time of 40 ms. In this case, it is clearly seen that the response of the system under a current step to $I_{dq} = 72\ A$ is highly underdamped, showing a slow dynamic response and a oscillation frequency around 109 rad/s as indicated in the poles result in Figure 113. The use of the virtual admittance increase the damping and the time response of the system during the step as shown in Figure 114(b). The current step response is damped and the dynamic response of the system is fast, reducing the possible oscillation of the system.

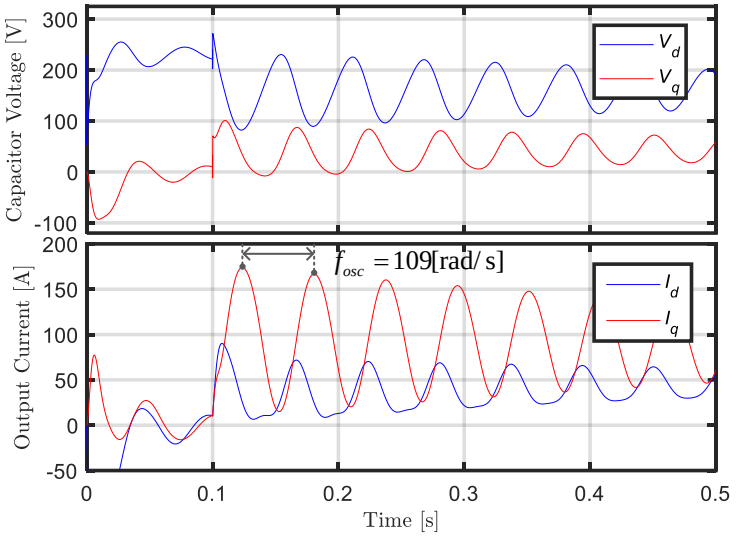

(a)

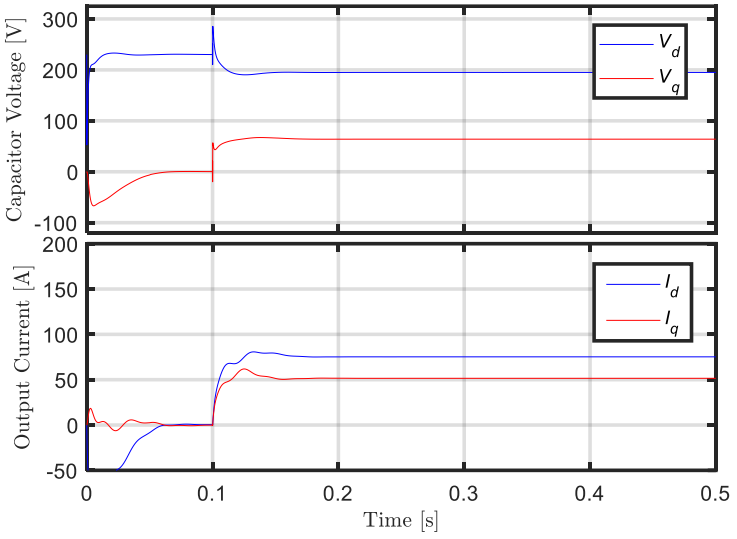

(b)

Figure 114: Current step Id=72 A and Iq = 72 A simulation results in a SCR = 2 grid connection with a 40 ms PLL settling time (a) without virtual admittance (b) with virtual admittance

Scenario 2:

The eigenvalues in Figure 115 represent the movement of the poles considering a settling time variation of the PLL in a grid with a SCR of 2. The settling time of the PLL is moved from a value of 50 to 200 ms, where as shown in Figure 115, it highly affects the stability of the system by moving the poles into the unstable zone. On the one side, the system without virtual admittance presents an unstable behavior close to the 50 ms settling time for the PLL, which has a very low damping coefficient with a slow dynamic response. On the other side, adding the virtual admittance into the system improves the overall stability of the system. Even though the dynamic is modified, the damping factor remain under the same value.

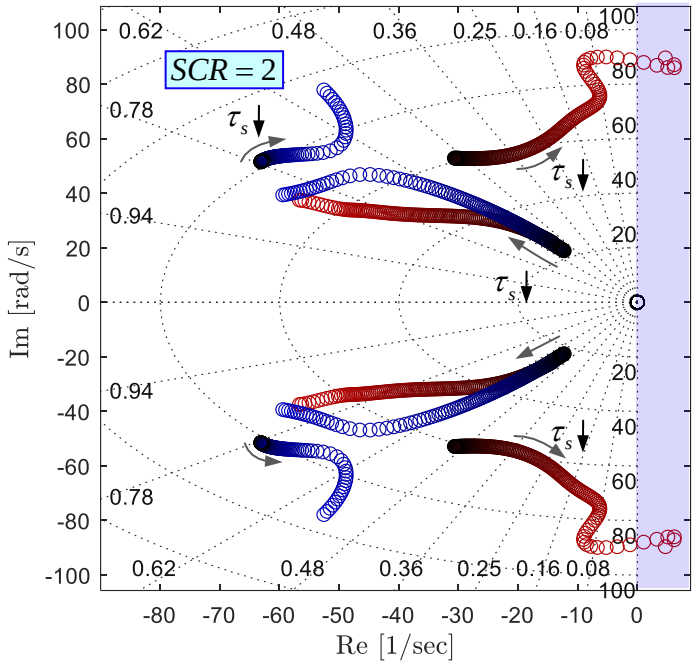

Figure 115: Eigenvalues for a fixed SCR = 2 and movement in the PLL settling time (τ_s) from 50 ms to 200 ms, with virtual admittance (blue) without virtual admittance (red).

To display the difference between the different operating points of the system, with and without virtual admittance, two simulation results have been obtained to highlight the benefits of the compensation loop. Figure 116(a) shows the system close to the unstable area, where the natural frequency of oscillation is around 95 rad/s with a highly underdamped response. If the settling time is increase to 200 ms, Figure 116(b), the stability of the system increase as the poles move towards the left side. Although the system is more stable, the dynamic response of the system is also reduced, giving rise to a higher settling time of the controller.

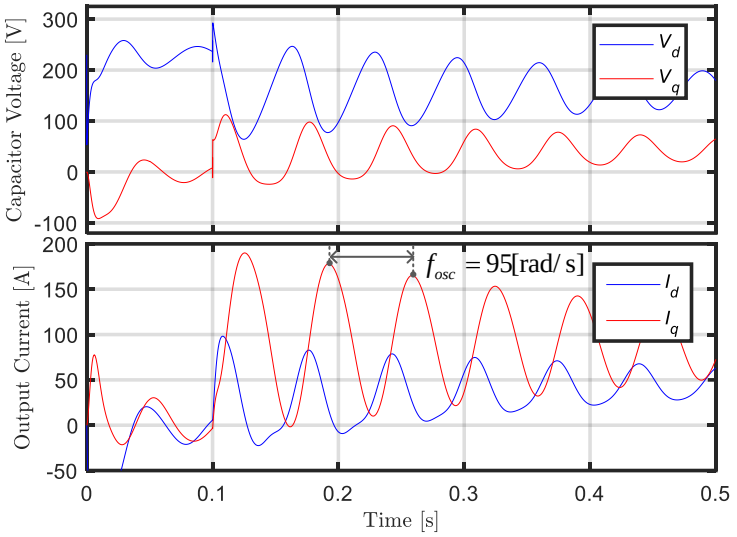

(a)

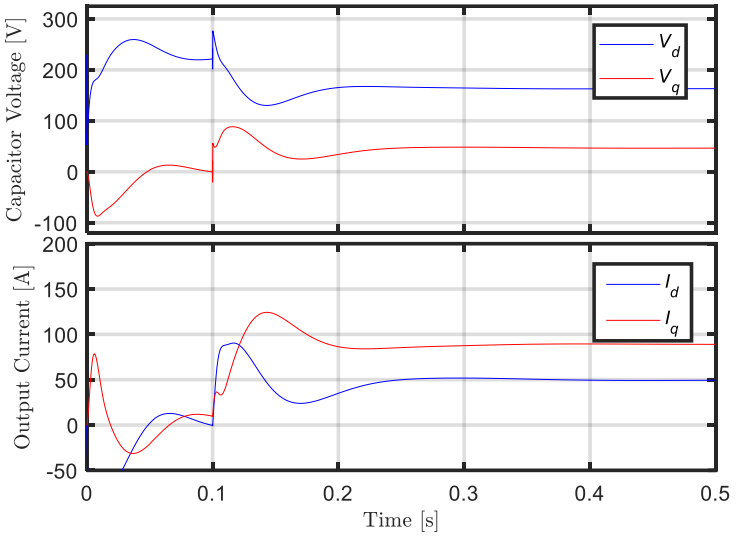

(b)

Figure 116: Time-domain simulation for a fixed SCR = 2 and movement in the PLL settling time (τ_s) without virtual admittance (a) 50 ms settling time (b) 200 ms settling time

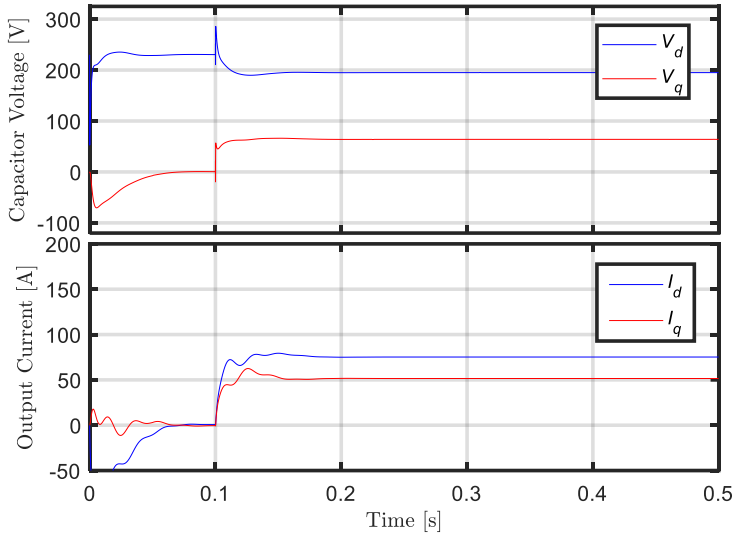

(a)

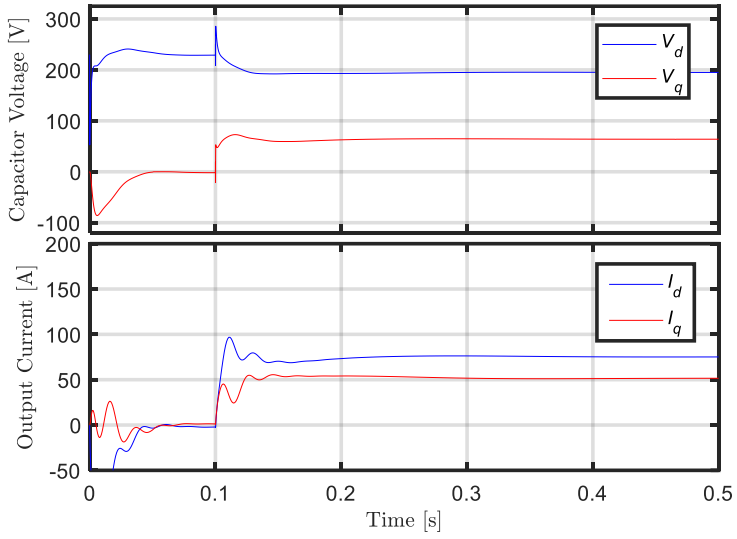

(b)

Figure 117: Time-domain simulation for a fixed SCR = 2 and movement in the PLL settling time (τ_s) with virtual admittance (a) 50 ms settling time (b) 200 ms settling time.

Once the virtual admittance is included into the converter control, the poles move to the left side of the map, Figure 115, increasing the damping and the dynamic response. This response is highligthed in Figure 117(a) and Figure 117(b), which increases the performance under the current step. Even though both systems presents an improved response compared to Figure 116, the decrease in the settling time in the PLL also affects the dynamic behavior of the current controller, presenting a slower response during the step.

Scenario 3:

Finally, Figure 118 illustrates the eigenvalues movement due to the modification of the gain in the virtual admittance, increasing both variables at the same time in different SCR of the grid. The nominal values for the virtual resistance and inductance have been selected based on traditional values for the subsynchronous impedance of a synchronous generator, with an the inductance around 0.3 p.u and a resistance of 0.1 p.u. It can be seen from the figure that for a low SCR, the virtual admittance has a beneficial effect on the damping and the speed of the eigenvalues, moving them to a more stable zone. In contrast, in a high SCR it impacts the damping of the pole but not as noticeable as in a weak grid condition.

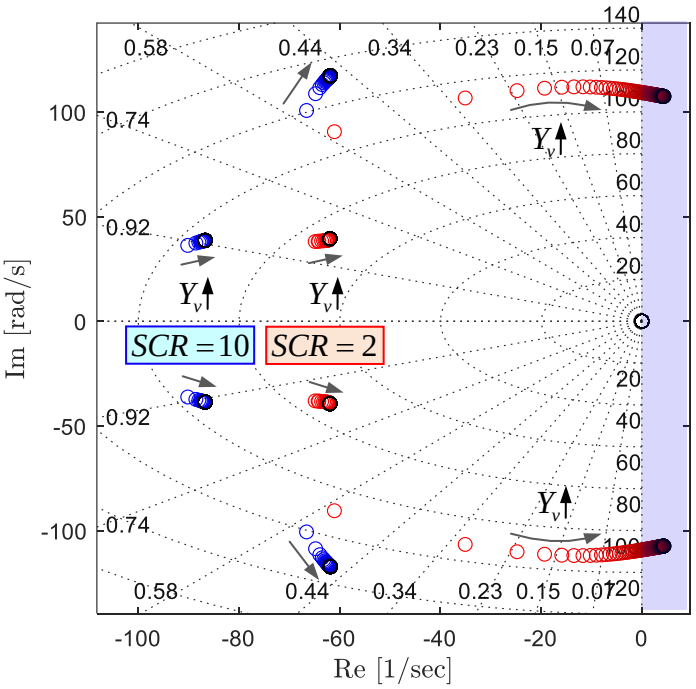

Figure 118: Eigenvalues for a fixed SCR = 2 (red) and SCR = 10 (blue) and a PLL settling time (τ_s) of 40 ms, with an increasing value of virtual admittance from a unitary value to 100 times larger.

The time-domain simulation presented in Figure 119 displays the difference between three virtual admittance gain factors. The parameters of the virtual admittance have been scaled from the nominal parameters to five larger, and finally increased ten times from the nominal value. It can be seen from Figure 119 that the difference in virtual admittance scale highly affects the damping of the system, where the larger the admittance the lower the damping of the system during the current step. Furthermore, as the virtual admittance uses voltage difference as an input it also supports the voltage magnitude level. This can be clearly seen from the difference between the capacitor voltage, V_d, compared to the one with a larger admittance, V_{d5}. In the case of V_d, the q current component is providing more voltage support than in the case of V_{d5}, resulting in the possibility to inject more active power during the step.

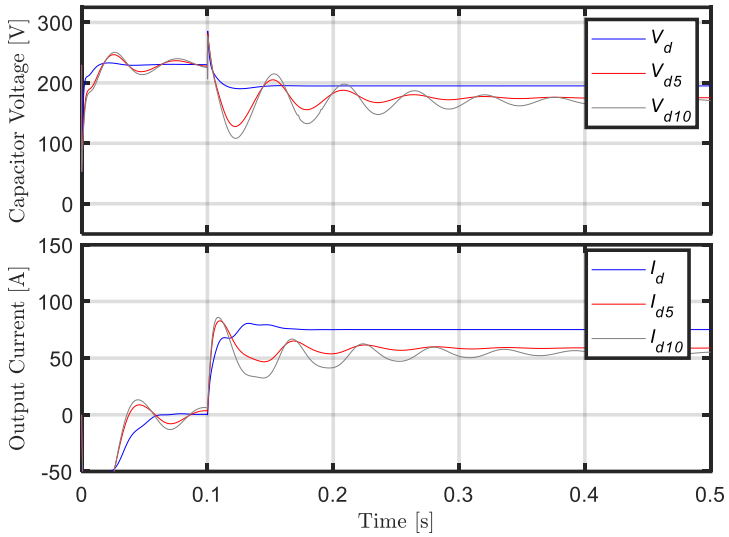

Figure 119: Time-domain simulation for a fixed SCR = 2 and a PLL settling time (τ_s) of 40 ms, with three different virtual admittance gains.

5.2.2. Experimental results

The experimental setup is composed of a 10 kVA power converter, two 2kW active loads, and a 10 kW dc power source. The system is connected through an isolation transformer and a circuit breaker to the utility grid, which can be opened to reproduce the island mode transition.

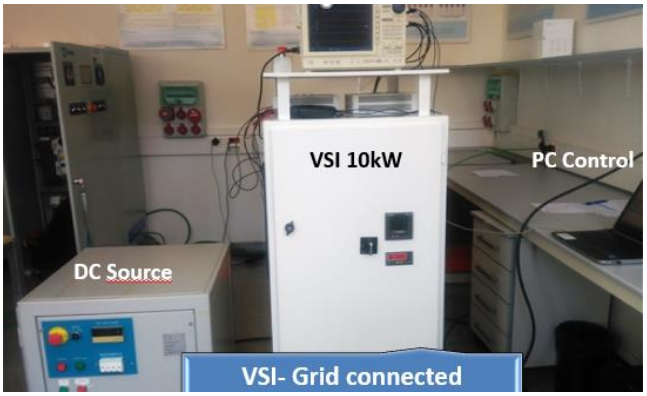

Figure 120: Experimental setup of a 10 kVA power converter.

The electrical scheme of the system is depicted in Figure 121.

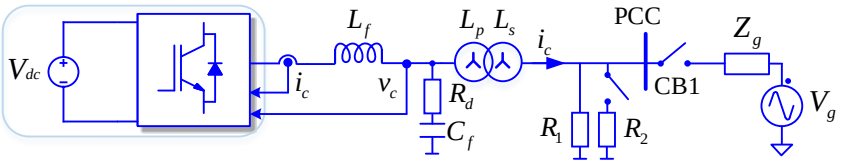

Figure 121: Electrical configuration of a 10 kVA power converter connected to the grid.

The results are separated into two sets of experiments. The first experiement consists of an island transition of the power converter to ensure the grid-forming capacity of the combined structure of the PLL and the virtual admittance. The grid-forming capacity will be put under test by adding loads during the island mode operation, which will force the converter to increase and decrease the power fed to the loads while maintaining the grid under a stable operation. The second experiment exposes a comparison between the system with and without virtual admittance during a voltage sag. The electrical parameters are presented in Table 14 and the control parameters in Table 15.

Symbol	Definition	Values
S	Converter nominal power	10 kVA
L_f	Inverter-side inductance	2.6 mH
C_f	Capacitance	5.5 µF
R_d	Damping resistance	0.1 Ω
L_p+L_s	Grid-side inductor	0.76 mH
Z_g	Grid impedance	0.125 Ω
P_{dc}	dc source nominal power	10 kW
V_{dc}	dc nominal voltage	750 V

Table 14: Electrical parameters of the 10kVA power converter

Symbol	Definition	Values
kp	Proportional gain	5
ki	Integral gain	1010
k_{p_PLL}	Capacitance	0.5
k_{i_PLL}	Damping resistance	10
R_v	Virtual resistance	1.6 Ω
L_v	Virtual reactance	15,2 mH
fsw	Switching frequency	10 kHz

Table 15: Control parameters of the 10 kVA power converter

Figure 122 presents the island transition of this combined control scheme. In the beginning, the power converter was not exchanging any power to the grid, and the 2 kW active power load was directly fed by the grid. Once the circuit breaker is opened, the combined controller of the PLL and the virtual admittance generate a current reference due to the loss of voltage at the PCC to maintain the grid. Figure 122 shows the moment of the circuit breaker opening and , as a consequence, the frequency of the system is slightly modified. Once the system is stable in island mode, Figure 123 shows the performance of the controller during connections and disconnections of active power loads. It is worth mentioning that each load connected to the grid increases the amount of current to be fed by the converter, but reduces the voltage amplitude.

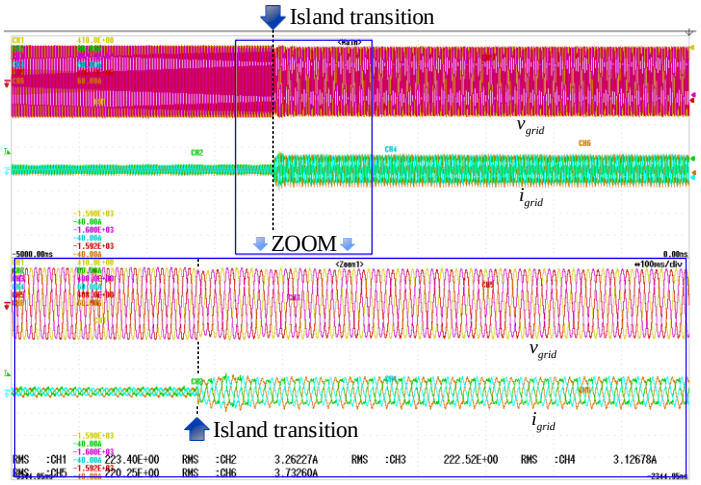

Figure 122: Island transition event with the combination of virtual admittance and PLL.

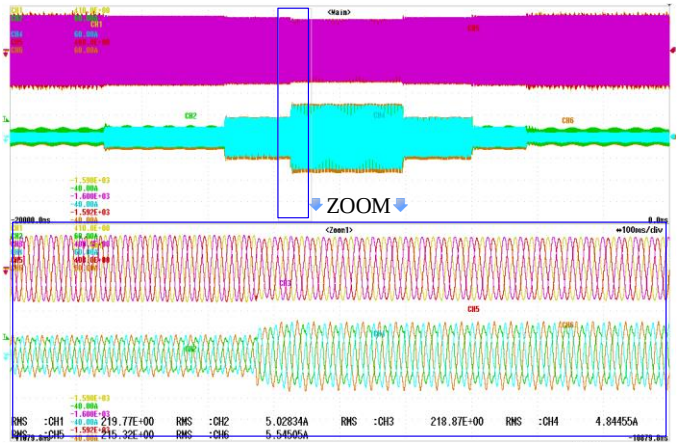

Figure 123: Load connections during island operation mode of the power converter.

In the second test, a voltage sag is generated at the PCC of the power converter suddenly changing the voltage measurement and affecting the current controller. As it is possible to see in Figure 124, the behavior of the traditional power converter control without the virtual admittance is presented. During the voltage drop, the power converter does not inject any reactive current into the system. Even though the power converter is not providing any support, with a zero power reference value, during the event, the inverter current presents an oscillation during the entrance and the exit of the voltage sag due to the effect of the PLL. In Figure 125 the system is attached with the virtual admittance. The voltage difference created by the

measured voltage magnitude and the nominal value of $|V_n|$ gives rise to a reactive compensation current to support the grid during the event.

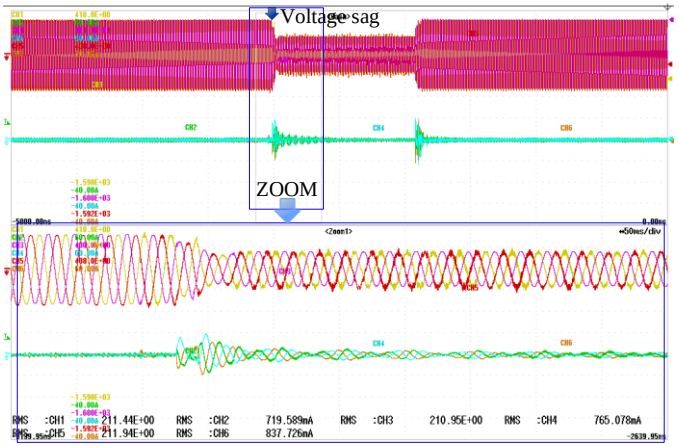

Figure 124: Voltage sag without the combined effect of the PLL and the virtual admittance

The amount of reactive power injected is directly determined by the virtual admittance gain, which can be settled to inject a specific amount of reactive power. It can be seen from Figure 124 that the voltage sag is around 50% of the nominal voltage. Thus, following the LVRT requirement of the German grid code, it has to inject around 80-90% of the reactive power during the event. It is possible to see from Figure 125 that channels 1-2 have a 90º inductive phase shift between the voltage and the current injected, meaning that the power converter is injecting inductive reactive power to support the grid during the voltage contingency.

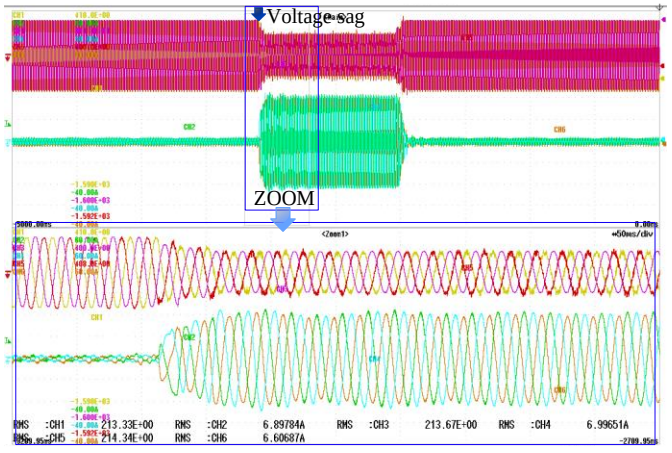

Figure 125: Voltage sag with the combined effect of the PLL and the virtual admittance

5.3. Sensorless grid-forming control

In the previous section, the addition of the virtual admittance in the traditional structure of a power converter was enough to converter its control from a grid-following to a grid-forming power converter, with features similar to the ones in a synchronous machine. The initial structure uses a synchronous reference frame PI controller and a PLL connected to the grid voltage measurement to regulate the output current by tracking the phase and the voltage amplitude of the system. This standard configuration is depicted in Figure 126, where the power converter is seen as a controlled current source, and the PLL is extracting the necessary phase and voltage magnitude from the grid voltage. The effect of the PLL over the current control has been widely studied in [100], where the effect of the synchronization system over the current and voltage transformations can be set as an admittance shaping between the systems.

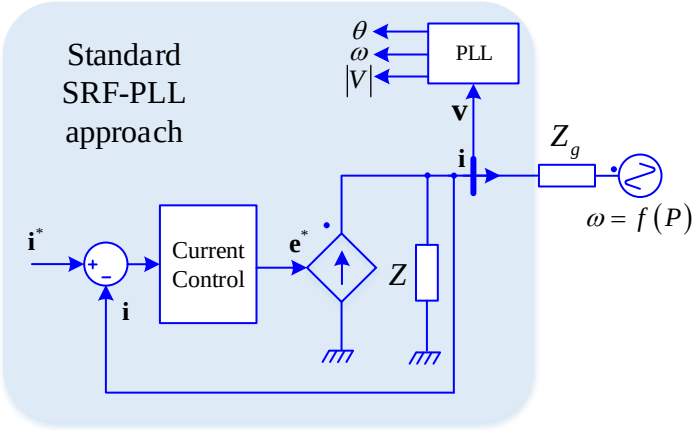

Figure 126: Traditional SRF-PLL implementation approach.

It has been demonstrated that, by attaching a virtual admittance to the approach, Figure 126, the system is able to obtain grid-forming features, such as the islanding operation or the voltage and frequency support during faults. In this regard, to reduce the effect of the Park transformation from the voltage measurement, it is switched to the voltage reference generated by the power converter. This approach reduces the number of voltage sensors needed for the system to be synchronized, as it directly uses the reference voltage at the converter side.

Although the system can operate by using the internal voltage to synchronize to the grid, there are some challenges in the startup as the output voltage of the controller is not in steady-state from initial conditions. On top of this, even with the modification of the measurement point, the system is still operating as a controlled current source from the point of view of the grid, Figure 127.

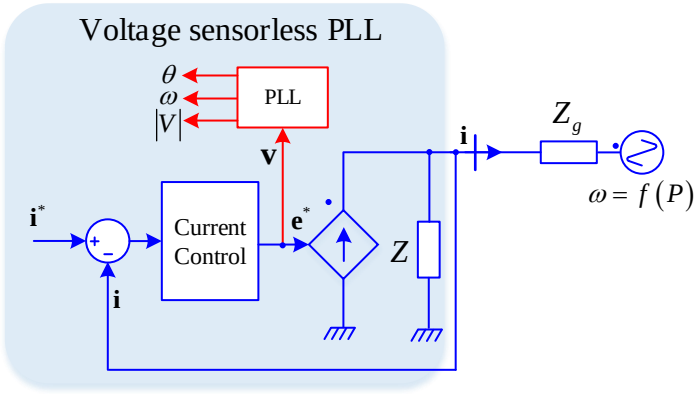

Figure 127: Voltage sensorless approach with standard SRF-PLL

The synchronization loop directly uses the *q* axis of the reference voltage of the controller to obtain the phase angle of the system. Considering that the reference voltage is already in the synchronous reference frame, the Park transformation is omitted from PLL implementation. Thus, it is possible to obtain the frequency of the grid as shown in Figure 128.

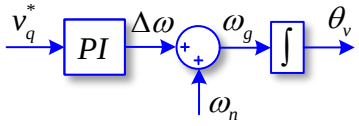

Figure 128: SRF-PLL without the Park transformation for the sensorless approach.

This concept of switching the voltage measurement into the current controller output leads to many different implementations of traditional power converter control schemes. First of all, the use of the control scheme presented in Figure 127 partially removes the voltage measurements required at the grid side, and presents a simple approach to a grid-supporting power converter strategy, by using the internal output voltage of the current controller to adjust the current control. If the virtual admittance approach is implemented in this case scenario, the power converter is enabled to provide grid-forming capabilities. Furthermore, a proper tunning to the PLL can resemble the dynamic effect of a virtual synchronous machine.

In this regard, by using the sensorless concept presented above, the integration of a VSM as a compensation system for the power converter is a feasible solution. One of the incoming requirements from the grid codes is the emulation of inertia and the power oscillation damping, which is generally present during frequency distortions on the electrical grid. The different VSM, especially those based on a power-based synchronization, have presented a simple yet effective approach to emulate those performances by using the swing equations. However, in

all those VSM implementations the swing equation was used as power controller in steady-state, and not specifically for transient events as the compensation proposal.

A simple approach to self-synchronize a current control is presented in Figure 129, which can include an additional compensation loop to adjust the current controller, leading to the self-synchronous current control strategy (SSCC). This basic control scheme presents only a unitary gain value in the v_q to use it as a variation in rotational speed. It is possible to obtain the frequency and the phase angle of the grid using this simple strategy without the need for any external voltage measurement unit.

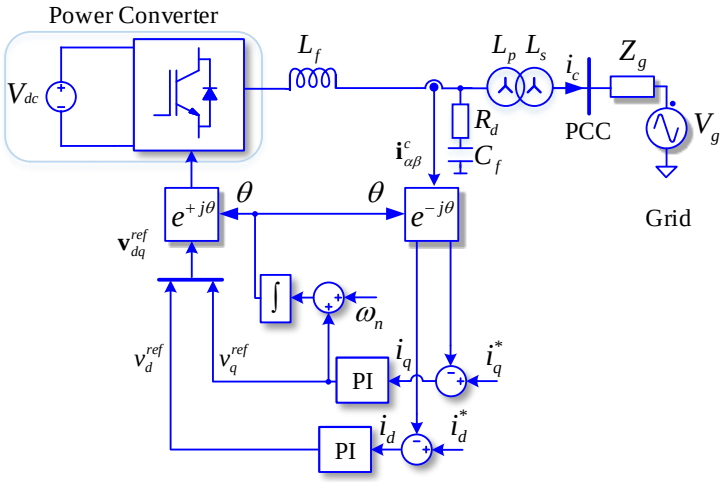

Figure 129: Self-synchronous current controller

This strategy allows a synchronous reference frame current controller to self-synchronize to the electrical grid without the need for any external voltage measurement. However, this strategy only synchronizes the system to the electrical grid and does not provide any kind of support during faults. This initial scheme in Figure 129 can be extended into a PI controller, that would match the SRF-PLL implementation with the virtual admittance but avoids the phase distortion due to Park transformation, Figure 130.

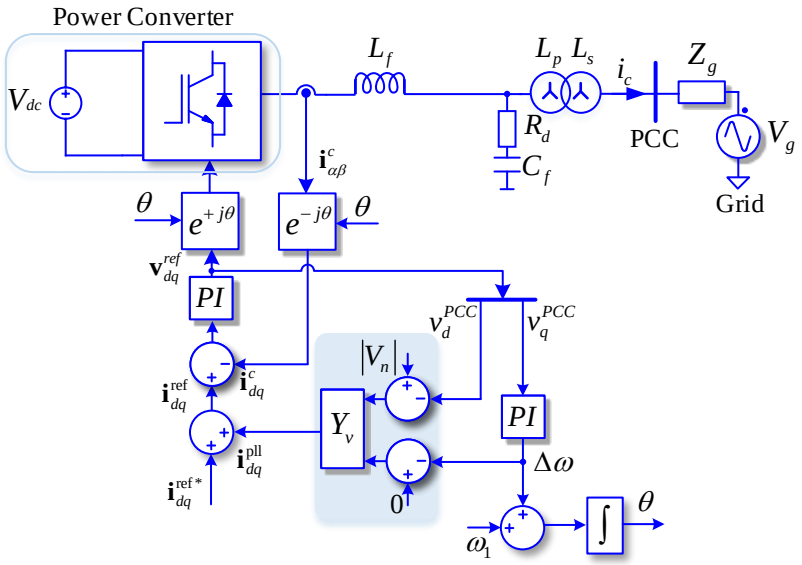

Figure 130: Sensorless PLL with a virtual admittance block diagram.

5.3.1. Stability analysis

In this section, the stability of the proposed sensorless approach is analyzed. The equivalent model can be conceived as Figure 131, which avoids the PLL effect due to the Park transformation on the voltage measurement as it directly obtains the voltage from the output of the PI in the synchronous reference frame. This improvement can highly reduce the effect of disturbances on the mesasurement devices, such as dc-components, reducing sensing filters, and avoiding additional delays due to the measurement stage.

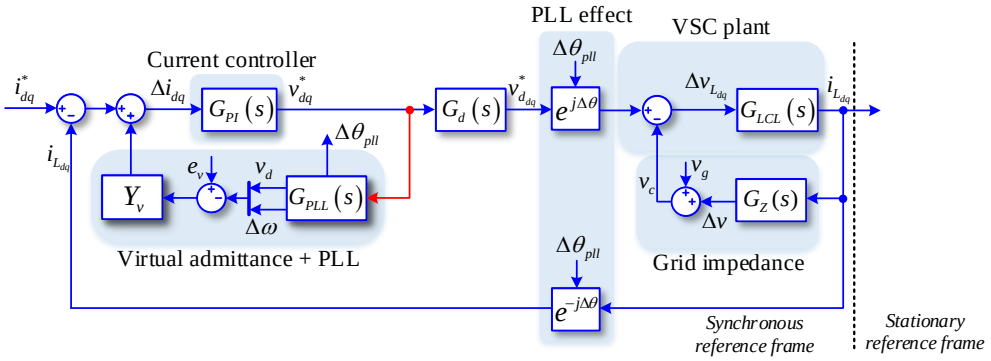

Figure 131: Synchronous reference frame model of the sensorless PLL with virtual admittance system and the rest of required blocks for the stability analysis

Figure 132 shows the difference in the eigenvalues movement between the use of the internal or the external voltage measurement on the virtual admittance compensation loop. On the one hand, the red dots highlight the effect of the external voltage during the decrease of the grid SCR, which moves towards a slower system but without crossing the unstable boundary. Furthermore, the system remains with a similar damping coefficient even in very low values of SCR. On the other hand, the blue dots presents the internal voltage measure which display almost identical behavior to the external measure when the grid is becoming weaker. Even though both system present similar behaviors the internal voltage generated by the current controller gains damping factor during variation in the grid SCR.

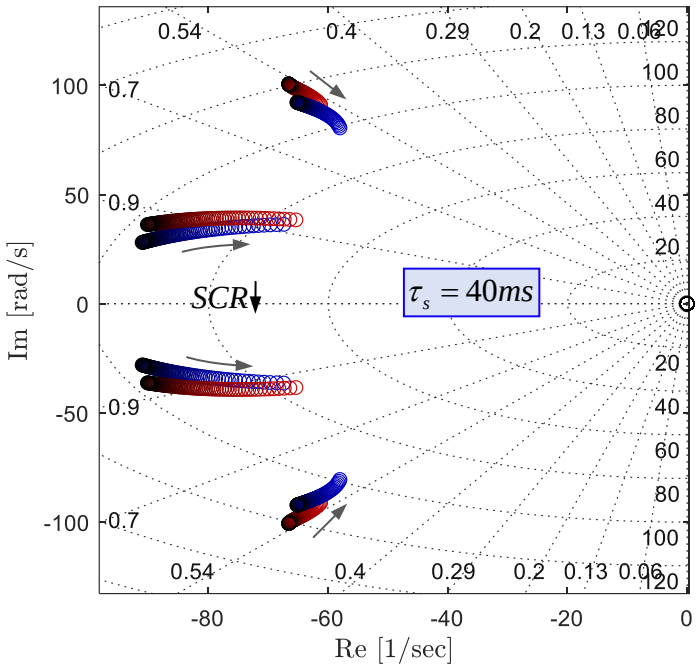

Figure 132: Eigenvalues movement for different SCR with fixed PLL = 40ms. With internal voltage measure (blue) with external voltage measure (red).

The difference is more significant when comparing the PLL settling time using internal or external voltage measurement. Figure 133 shows the eigenvalue movement for a fixed SCR and a movement in the settling time from 50 to 200 ms. It is seen in the figure that, even though the settling time heavily affects the damping factor and the speed of the system when the external voltage is used, the damping factor remains almost constant when using the internal voltage.

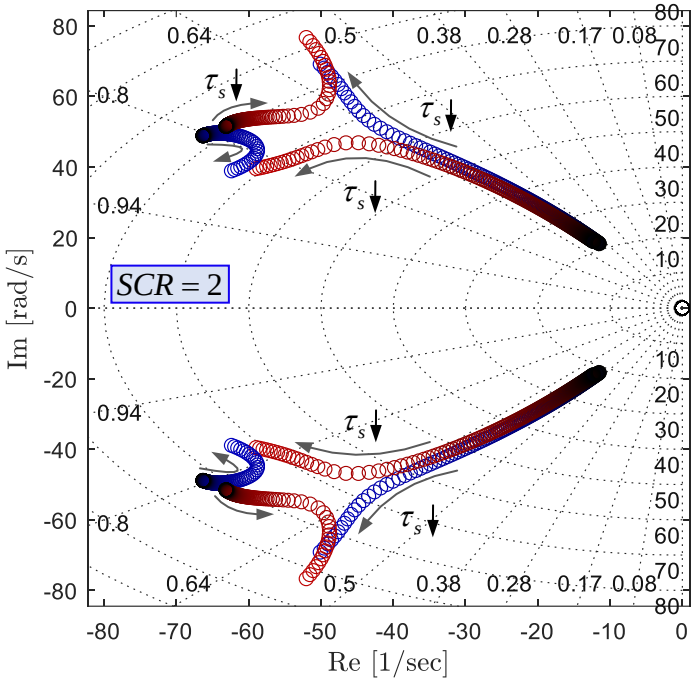

Figure 133: Eigenvalues for a fixed SCR = 2 and movement in the PLL settling time (τ_s) from 50ms to 200ms. With internal voltage measure (blue) with external voltage measure (red).

5.4. SPC sensorless grid-forming strategy

Although the PLL provides a good behavior, the system can be enhanced even further by using the power synchronization, utilizing the power delivered at the output of the converter. In this way, a sensorless VSM can be implemented in the current controller, not as a power controller but as a compensation system that provides an additional performance under faults.

The SPC controller can be adapted to fit in this sensorless control loop by adding the virtual admittance and the power loop control to set the dynamic response for the inertia and damping. Some modifications have to be made in the synchronous controller to attach the SPC to this SSCC structure. Figure 134 presents the combined control scheme of the SSCC and the SPC controller. The electromagnetic block of the SPC, the virtual admittance (VA), creates the compensation current depending on the movement of the output reference voltage to the power converter $\boldsymbol{v}_{\boldsymbol{dq}}^{*}$. If there is a mismatch between the previous voltage generated by the reference voltage, $\boldsymbol{e}_{\boldsymbol{dq}}$, and the controller voltage, $\boldsymbol{v}_{\boldsymbol{dq}}^{*}$, the system will create not only a current compensation but also a power deviation to adjust the reference voltage until the power error is eliminated.

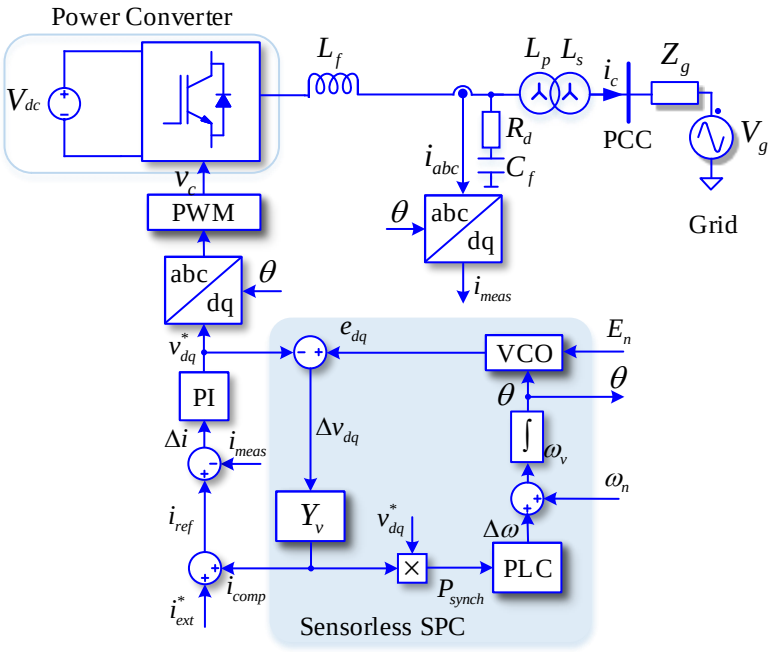

Figure 134: Self-synchronous current controller integrated with the SPC controller

This structure is active only during changes in the voltage reference output either produced by power reference changes in the controller or changes in the grid that makes the controller modify its output voltage to regulate the power output.

5.4.1. Simulation results

The simulation setup is composed of a 100 kVA power converter with an LCL filter, an isolation transformer, a grid interconnection impedance, and a circuit breaker to control the connection to the electrical grid, Figure 135. In the simulation results, the sensorless SPC implementation block presented in Figure 134 is used in three different scenarios. First, a power step with the compensation loop is made, followed by a load connection at the PCC, generating a phase shift in the voltage. Second, a voltage sag is generated at the grid side, where the power converter supports the grid during the fault. Finally, an island transition of the system will be done, by opening the circuit breaker connecting to the grid. The short-circuit ratio is intentionally decreased to a value of 3, to highlight the effect of the system under a weak-grid connection.

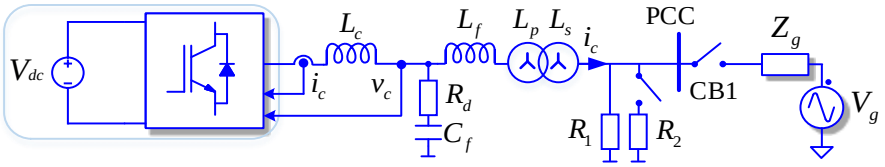

Figure 135: 100 kVA power converter simulation setup

The electrical parameters of the system, the controller parameters for the SPC controller, and the current controller are specified in Table 16 and Table 17, respectively.

Symbol	Definition	Values
S	Converter nominal power	100 kVA
L_c	Inverter-side inductance	777 uH
C_f	Capacitance	66 µF
R_d	Damping resistance	0.5 Ω
L_f	Grid-side inductor	294 mH
Z_g	Grid impedance	(0.531j + 0.053) Ω
P_{dc}	dc source nominal power	100 kW
V_{dc}	dc nominal voltage	750 V

Table 16: Electrical parameters of the 100 kVA power converter

Symbol	Definition	Values
kp	Proportional gain	5
ki	Integral gain	1010
H	Inertia constant	5
ξ	Damping factor	1
R_v	Virtual resistor	0.16 Ω
L_v	Virtual inductor	15.2 mH
fsw	Switching frequency	3150 Hz

Table 17: Control parameters of the 100 kVA power converter

A. Power step and load connection

Figure 136 presents an active power step in the system using the external current reference, I_{ext}, to provide 50 kW to the grid. At the moment of the step, due to the modification in the output voltage of the controller, the synchronous compensation system generates a current reference to limit the phase deviation, which is translated into active power exchange to the grid. This leads to generate the final current reference to the power converter, I_{Ref}, which follows the summation of both current references. In this case, the compensation system limits the maximum deviation angle on the reference voltage. The slow dynamic of the system reaching the steady-state after the 500 ms is due to the low SCR of the grid. As the SPC emulates the behavior of a synchronous generator, the weaker the grid the slower the dynamic response of the system. All the current references plotted in Figure 136 are obtained from the summation block before the current controller.

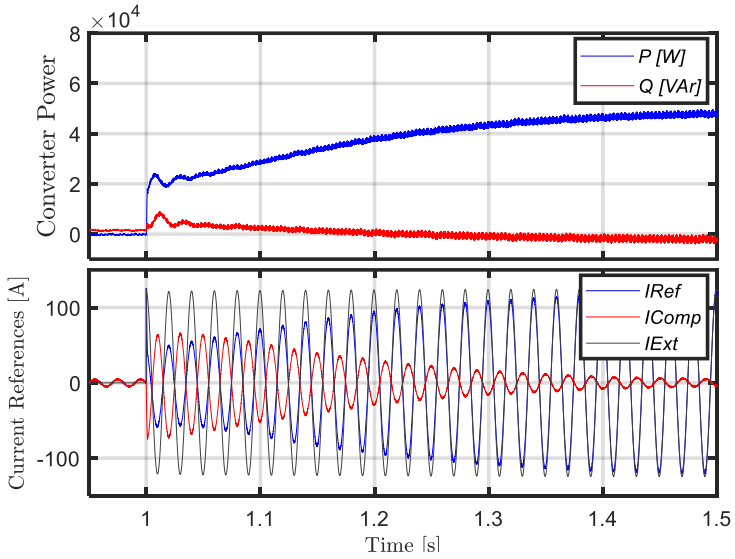

Figure 136: 50 kW power step in a weak grid with the compensation SPC algorithm.

Once the system has reached a steady-state, a load is connected to the PCC of the power converter. Due to the weak grid, this load connection creates a considerable phase shift in the grid voltage, Figure 137. The synchronous compensation system modifies the active power delivered by the power converter to offer dynamic support of inertia and damping during the event, without modifying the external reference.

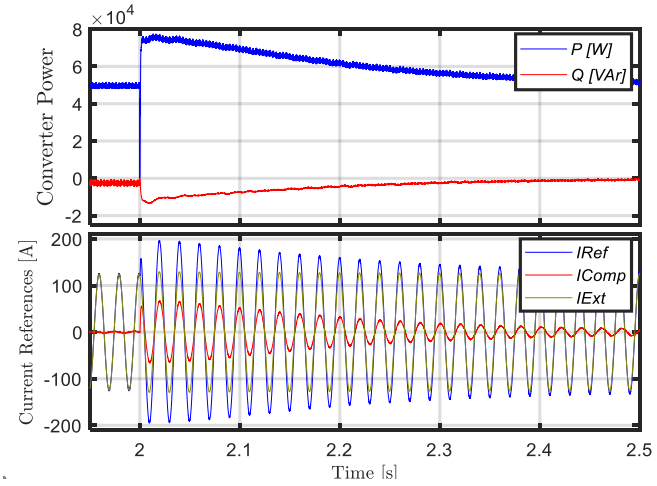

Figure 137: Active load connection at the PCC of the power converter.

B. Low-voltage ride through

In this simulation results, the system goes through a three-phase balanced voltage sag generated at the PCC of the power converter. The voltage is reduced to 80% of the nominal magnitude representing a reactive power injection of 20% of the nominal current of the power converter based on the LVRT German grid code. First, Figure 138 presents the system without the compensation system, just with the traditional control which does not provide any grid-supporting service during the event.

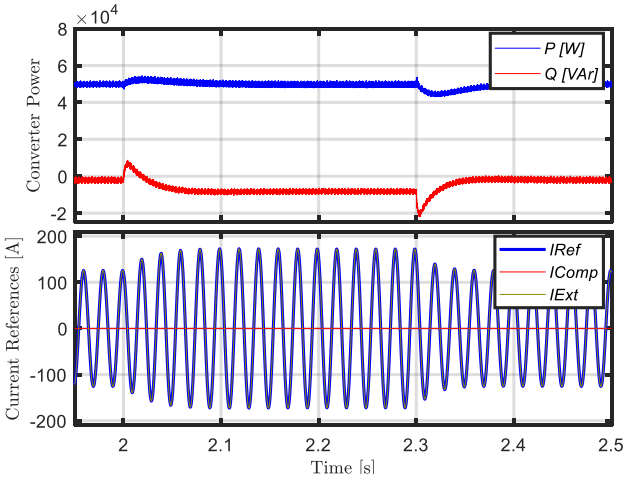

Figure 138: Voltage sag without the compensation system.

The result presented above, Figure 138, only has a PLL to synchronize to the system and the current control, which focuses on matching the grid voltage. Due to the voltage sag, the external current reference increases its setpoint to maintain the same active and reactive power delivered to the system, independently of the grid condition. In Figure 139, by including the the sensorless synchronous control, the system provide an automatic response to the voltage sag. Even though the output voltage of the controller decreases to the value of the grid, the reference from the SPC creates a setpoint for the voltage magnitude. This voltage difference computed by the virtual admittance gives rise to an immediate current response from the power converter to support the grid voltage. Although the system starts injecting reactive power, the active power is maintained from the external current reference, which increases its value to adjust to the new voltage magnitude.

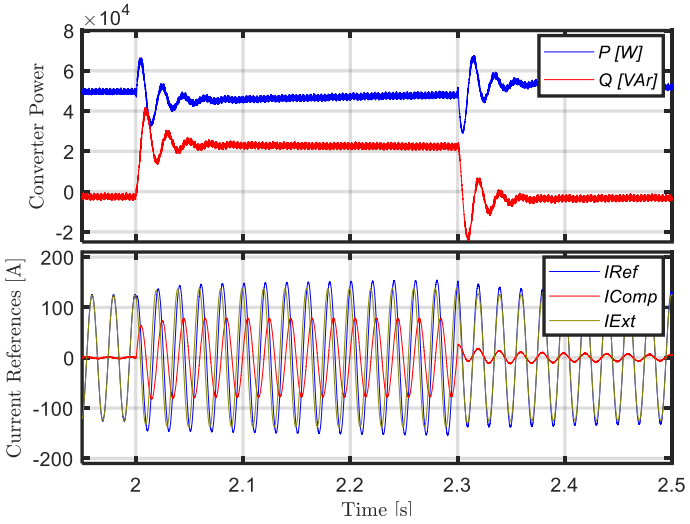

Figure 139: Voltage sag with the compensation system

To compare both support actions, Figure 140 presents the comparative results obtained from the voltage sag with and without the compensation loop. Without the compensation loop, the grid voltage magnitude decreases to a value of approximately 290 V, due to inexistent support provided by the system. Once the compensation loop is attached to the system, the reactive power injection during the fault increases the voltage magnitude up to 340 V, representing a 50 V improvement on the voltage level.

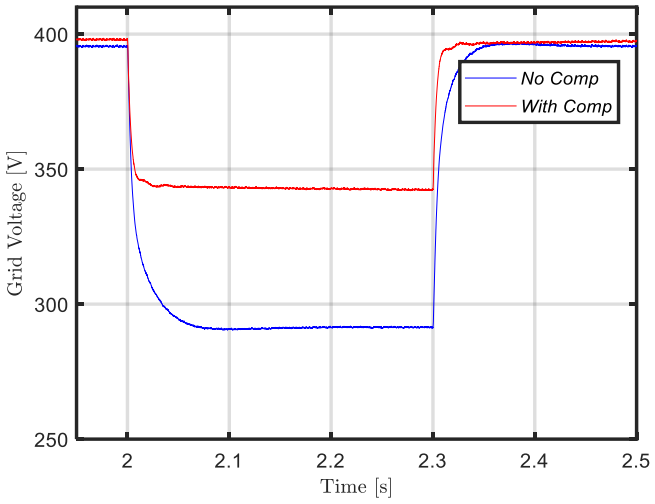

Figure 140: Voltage support during voltage sag with and without the compensation loop.

C. Island transition

The last simulation result is the island operation mode of the power converter. In this case, as shown in Figure 141, the power converter is transitioned to island mode at t = 1.5 s, where the circuit breaker is opened.

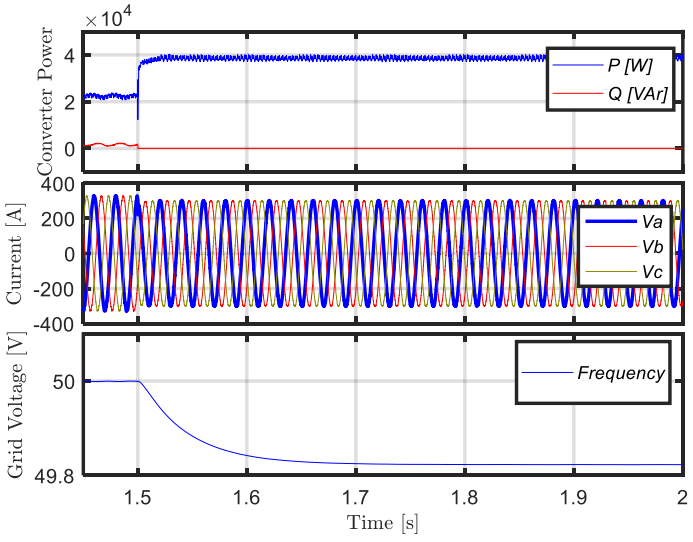

Figure 141: Island transition with the synchronous compensation loop.

At that instant, the sensorless-SPC compensation loop, Figure 134, computes the voltage error and sends a current reference to maintain the electrical island fed. As the power converter is the only system feeding the load connected, the frequency is reduced accordingly to the increase of power due to the load.

5.4.2. Experimental results

The experimental setup for the sensorless synchronous compensation loop is composed of a 10 kVA power converter, a 10 kW dc-source for the dc-voltage link, and an interconnection impedance to reduce the SCR of the system to a value close to 3, Figure 142. The grid interconnection cabinet is composed of inductances and an autotransformer that allows the generation of voltage sags, by selecting different combinations of inductances.

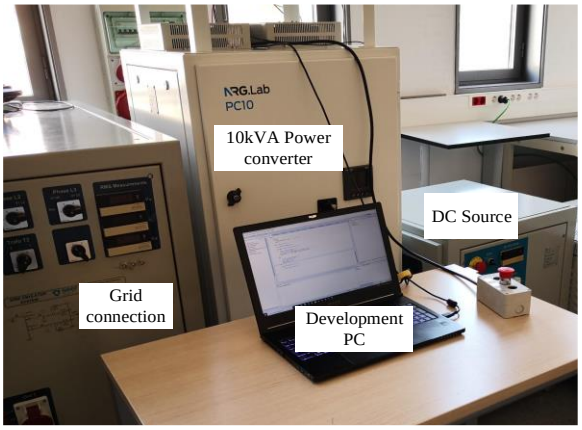

Figure 142: Sensorless synchronous compensation loop experimental setup.

The electric parameters are presented in Table 18, and the controller parameters in Table 19.

Symbol	Definition	Values
S	Converter nominal power	10 kVA
L_c	Inverter-side inductance	2.6 mH
C_f	Capacitance	5.5 µF
R_d	Damping resistance	0.1 Ω
L_f	Grid-side inductor	0.7 mH
Z_g	Grid impedance	1.570 Ω
P_{dc}	dc-source nominal power	10 kW
V_{dc}	dc-nominal voltage	750 V

Table 18: Electrical parameters of the 10 kVA experimental setup

Symbol	Definition	Values
R_v	Virtual resistor	0.1 p.u
L_v	Virtual inductance	0.3 p.u
k_p	Proportional gain current controller	5
k_i	Integral gain current controller	500
H	Inertia constant	5
ξ	Damping factor	1
f_{sw}	Switching frequency	10 kHz
f_{samp}	Sampling frequency	10 kHz

Table 19: Control parameters of the 10 kVA power converter

The experimental results are separated into two stages. The first one, a voltage sag is generated from the grid interconnection cabinet and the power converter is tested under three different scenarios. The second one, an island transition is made by opening the circuit breaker of the power converter, where different load will be connected to the system.

A. Low-voltage ride through

The first experimental result is based on the dynamic support of the power converter during a voltage sag at the PCC. Figure 143 presents the drastic voltage change of 50% in the system during the voltage sag without the use of any power converter connected to the system.

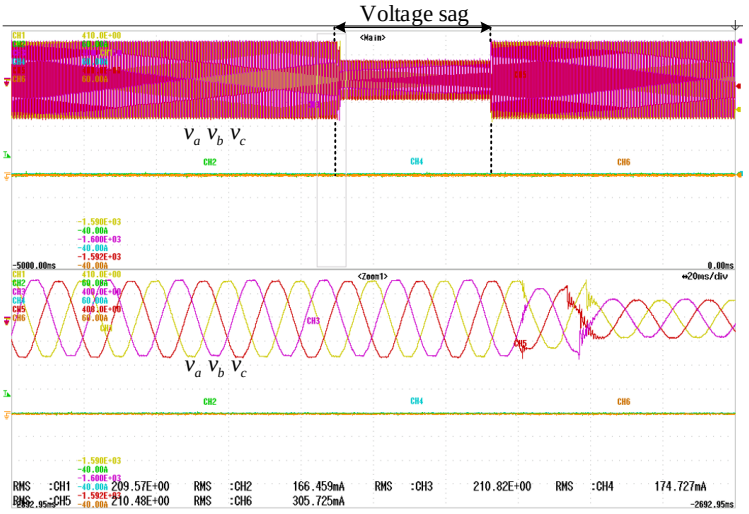

Figure 143: 50% voltage sag without the power converter connected to the grid.

Once the power is connected to the system and equipped with the compensation loop, it automatically generates a reactive current reference to withstand the voltage drop and provide the necessary support to increase the voltage as much as possible. In this case, the voltage is increased only by 15 V from the initial experimental results in Figure 143 due to the current limitation set to 10 A. If the current limitation is extended to 20 A, the dynamic voltage support generated by the power converter can be increased to approximately 30 V.

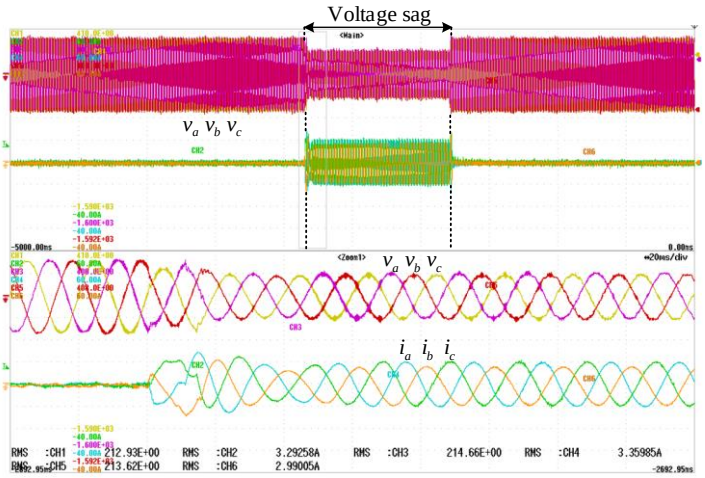

Figure 144: 50% voltage sag with the power converter equipped with the compensation loop limited to 10 A.

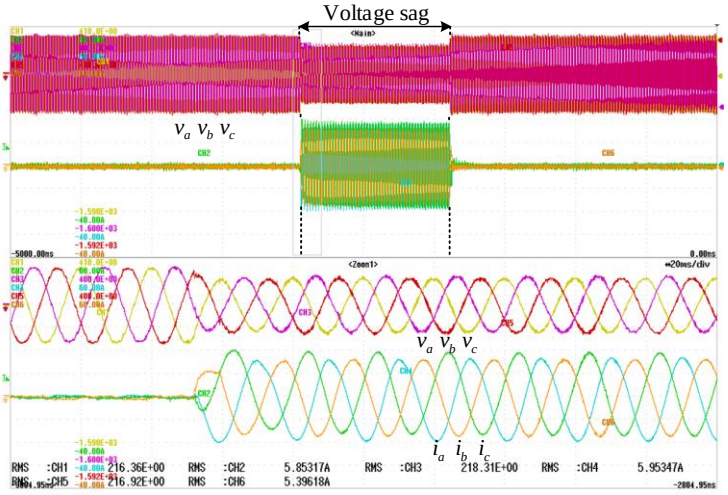

Figure 145: 50% voltage sag with the power converter equipped with the compensation loop limited to 20 A.

B. Island transition

In this experimental result, the power converter was forced to operate on island mode with a load connected to the PCC. Once the grid has been disconnected from the PCC, the power converter feeds the loads that remain connected to the islanded system. Figure 146 presents the island transition of the power converter, where it was not delivering any power to the grid before the event. After the circuit breaker is opened, the power converter feeds the 8 kW load instantaneously, as it is the only generator in the system. Due to this, the frequency and the voltage magnitude of the voltage created and regulated by the power converter are slightly modified.

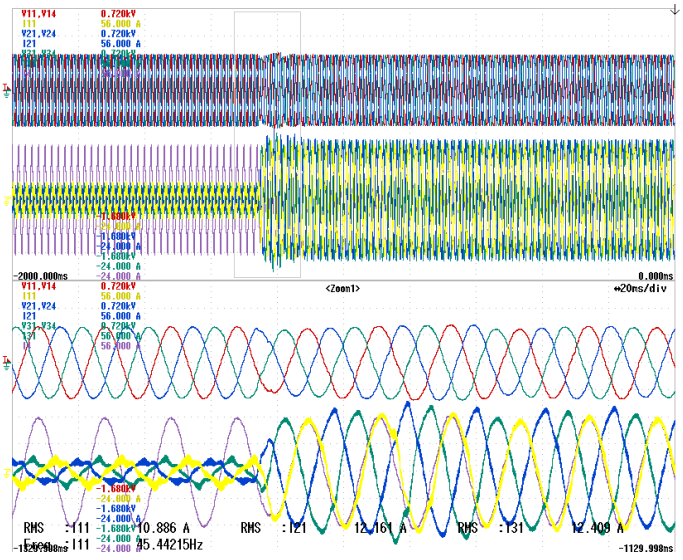

Figure 146: Island transition of the power converter feeding an 8 kW load.

Finally, after the steady-state has been reached for the transition of the island mode, some load transitions were done in the system. The first load step decreases the active load from 8 kW to 4 kW, as can be observed from the zoom highlight in Figure 147. In this plot, the changes in the active power demanded by the system highly affect the frequency, increasing its value when the power converter is less loaded. The active load keeps decreasing until reaching a value of 0, where the power converter can maintain the grid voltage generated.

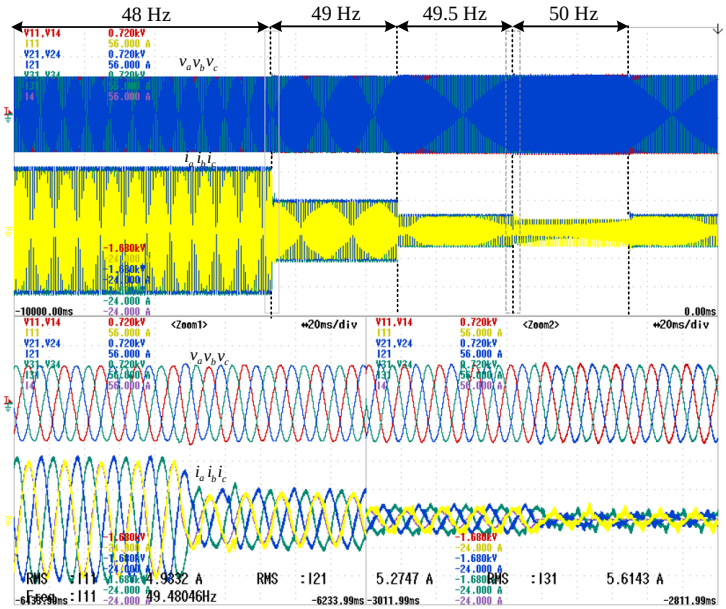

Figure 147: Island operation of the power converter with the synchronous compensation loop.

5.5. Conclusions

The synchronous control oriented to the device has been presented as a feasible way to include the functionalities of a synchronous machine into a power converter. In this regard, some additional control structures have been presented for the use of the SPC approach in the device to regulate and improve their reliability and the functionalities of the system, such as the Vdc limitation strategy or the resynchronization structure for an SPC-based power converter.

The use of this structure as a power controller highly improves the regulation of the power converter especially during faulty scenarios where the system naturally responds to any modification of the electrical grid. However, this natural response also has some drawbacks considering errors in measurements, especially in voltage, which can lead to high distortion in the current injected or even in dc components appearing into the system, creating possible failures and additional power losses in the system. In addition, the virtual admittance approach in the SPC may lead to some harmonic injection to compensate for voltage distortions, which can be reduced by using the multi virtual admittance approach.

The VSM machine approach is based on emulating the synchronous machine, and its capacity to provide a fast response during frequency or voltage events. In general, the traditional structure of the converter enabled only partial support using the droop-based regulation. The grid-forming PLL approach has been presented and tested in an experimental setup to show

the feasibility of the implementation. The virtual admittance enables the power converter to be a grid-forming generator, and with the proper tuning of the PLL, it may resemble the performance of a synchronous machine.

Although both of the implementations have been tested under experimental setups, both systems needed the use of an external voltage measurement to either synchronize to the system, using a PLL, or to generate the necessary error for the virtual admittance. In this regard, a voltage sensorless synchronous compensator has been presented based on the idea of the self-synchronous current controller. This simple concept avoids the use of a PLL and reduces the coupling effect due to the Park transformation in the synchronization loop, enabling the current controller to be synchronized to its output voltage. This implementation has been tested under simulation and experimental setups, where the system has presented a good performance under grid-connected and island operation modes.

Chapter 6.

Synchronous control oriented to the system

The power system was designed to regulate large centralized units to closely monitor and control in real-time the generation unit, ensuring the safe operation and reliability [8], [101]. The increased integration of RES presented new operation challenges to the already existing power system [102].

One of the main challenges of hugely increasing the renewable energy integration into the power system is the overwhelming amount of information that has to be processed in real-time by the operators. Moreover, the information regarding the reliability of the electronic interfaced system in a parallel operation condition, where hundreds or thousands of power converters would be simultaneously exchanging energy with the grid. It has been reported in the literature that power converter-based generation units are affecting the stability and reliability of the power system [3]. Even though the disturbances introduced by these systems are rarely considered due to their small participation in the power system, this is changing around the world due to the fast rise in RES integration, and the replacement of fossil-fueled power plants [103]. In this regard, there is a clear need to design and operate renewable power plants (RPP) to contribute to the stability of the power system, balancing generation and demand [104].

The renewable power plants, based on PV and wind, are composed of thousands of power converters whose control strategy plays a crucial role in the stability and reliability of the system [105]. Nowadays, the most common control scheme used for power converters in power plants is mainly based on a grid-following approach [87]. This operation mode allows the power converter to regulate the active and reactive power delivered to the electrical grid. Moreover, some simple grid supporting functionalities, such as a droop-based frequency regulation loop or a voltage regulation loop can be easily adapted to this control structure [106]. The power converters composing a renewable power plant are generally connected in parallel to the point of common coupling through step-up transformers. This additional impedance introduced by the transformer and the interconnection lines, make it difficult not only to ensure precise control on the active and reactive power delivered to the grid but also

to implement grid services. Furthermore, the grid conditions highly affect the interaction with each of the power converters which may give rise to undesired dynamics [107].

Renewable power plants are demanded to provide primary control services such as frequency or voltage regulation, however, they are now required to provide some dynamic services such as inertial response and power oscillation damping [108]–[111]. To implement those new required services two approaches can be used. The first approach is based on the replacement of the grid-following power converter control into a grid-forming power converter, where each power converter can emulate the performance of a synchronous generator, providing synthetic inertia and damping to an electrical grid. This implementation has been demonstrated possible in [112] and [113] for a single power converter. However, this approach may not be a cost-effective solution to the renewable power plant, as replacing the control system of all the power converters requires a huge development effort and a lot of resources. Moreover, a bad implementation of the VSM controller may give rise to power oscillations issues in the plant.

Nevertheless, the limitations of using multiple grid-forming power converters can be solved by adjusting the synchronous control into the power plant controller, not controlling individual units but the whole system. The second approach allows the use of conventional power converters, using simple grid-following strategies, in a renewable power plant, highly reducing the development effort and cost. However, the development of dynamic services for this central controller has not been properly addressed. In [114] a synchronous controller for a PV power plant was proposed, which separated the electromechanical loop and the electromagnetic loop of the SPC approach. The electromechanical loop was embedded in the central controller, whereas the electromagnetic loop was integrated into the power converter control, including the phase angle control and the electrical emulation. Even though this solution was able to regulate the phase angle of each power converter in a coordinated way, this implementation still needs a partial integration of a virtual synchronous machine in the local control of the converter. Thus requiring extended work to modify the control scheme of the power converter, which defeated the purpose of the proposal. Furthermore, the phase angle control is highly dependant on the power converter point of common coupling. Thus, for the same phase angle, each power converter does not necessarily exchange the same amount of power to the grid.

The following section presents the implementation of a virtual synchronous power plant controller (VSPPC) for the system. In this work, by means of emulating the electromechanical and electromagnetic dynamic equations of the synchronous machine, the system can provide primary services, as well as new required services, such as inertia or damping. If compared to the existing controllers, this approach does not require any modifications on the power converter control, which is a huge advantage in terms of installation cost and development work.

6.1. Power plant central controller

In general, the control of renewable power plants such as PV or wind focuses on maximizing the energy output of the system. The increased installation of those renewable power plants made it a necessity to actively regulate the power output, not only to precisely control the power set-points but also to adjust its operation to provide support in regulation and operation [115]. To achieve this goal, the control structure of a renewable power plant is composed of the inverter control (ICs) and the renewable power plant controller (RPPC). The ICs are the ones responsible of regulating the output current of the power converter under generic conditions. As previously presented in the power converter control section, there are many implementations for the ICs. However, the most extended one combines a current controller, a power controller, and a synchronization unit, Figure 148.

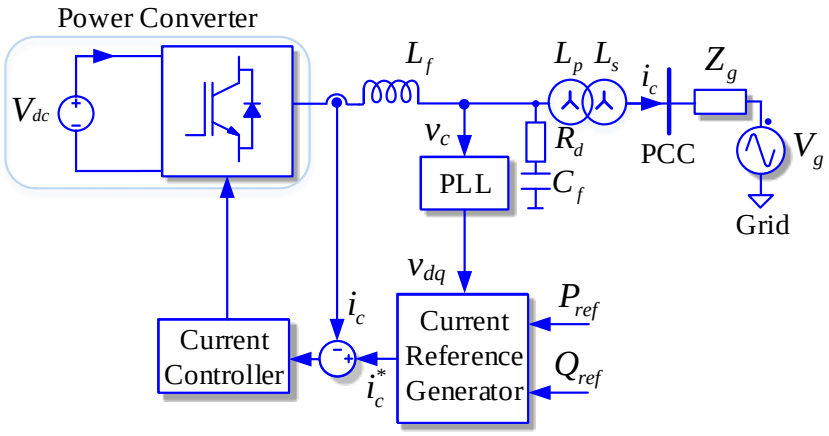

Figure 148: Control scheme of a grid-following power converter

Although the power converter is capable of exchanging power to the grid, the ICs are only able to regulate the power considering local measurements at the output. Thus, the accuracy of the power delivered at the point of connection of the power plant cannot be guaranteed by only using the ICs separately, especially when considering the effect of the equivalent impedance between the inverter to the point of common coupling.

The RPPC is used to ensure proper control of the power delivered by the entire power plant to the grid. It takes measurements from the point of connection to generate the necessary control outputs, which are processed and sent downwards to the ICs as references. Due to the fact that the RPPC is not able to be physically close to all the power converters, a communication link is vital to share and transfer the information from the RPPC to each of the ICs, Figure 149.

Grid services such as reactive power control, voltage and frequency regulation, and power factor control are nowadays implemented in most power plants PPC [116], providing primary

services to support the grid during steady-state operation. However, as the penetration of renewable energies increases, these newly introduced power plants are required to provide fast dynamic responses in addition to the primary regulation services.

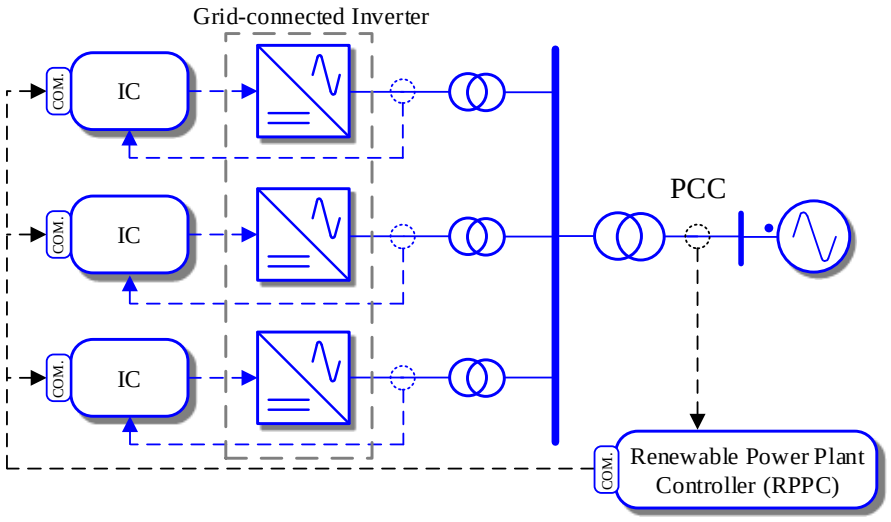

Figure 149: Simplified control system of a renewable power plant

To comply with such requirements, the use of grid-forming power converters based on the implementation of VSM has been proposed. This structure provides a natural interaction with the electrical grid, as well as providing fast dynamic services.

6.2. Phasor-domain structure

To cope with these new grid codes requirements, from a practical point of view, the virtual synchronous power plant controller presents a phasor-domain scheme that allows the implementation of the synchronous control in a central controller. The main idea behind this approach is to replicate the dynamic behavior of a synchronous generator not only in the device but in the system. This approach centralizes the operation and enables the VSPCC to support the grid and provide dynamic services, such as inertia or power oscillation damping, as a unique system to the grid instead of independent virtual machines.

The phasor-domain structure of the VSPPC is shown in Figure 150 and is composed of four main control loops: a power loop controller (PLC), a reactive power controller, a phase displacement calculator, and a power reference generator. The measurements of voltage and power for the inputs of the VSPPC are obtained at the PCC of the system, whereas the outputs of the VSPPC are references sent to the power converters. It is worth mentioning that providing power references at the output of the VSPPC allows the system to work with most of the commercial grid-following power converters on the market.

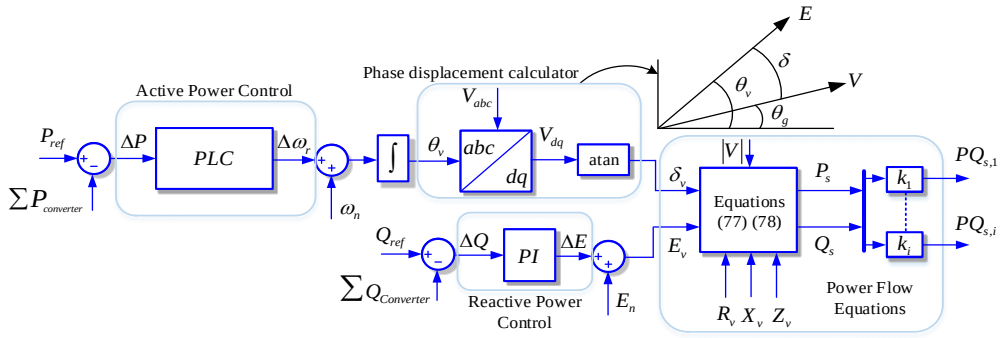

Figure 150: Control scheme of the proposed VSPPC

To emulate the dynamics of a synchronous generator there are two main blocks to be considered. The first one is the mechanical loop, which is in most of the cases presented by the swing equation. In this implementation, the electromechanical loop is presented in the PLC controller using the following transfer function:

$$G_P(s) = \frac{\Delta\omega}{\Delta P} = \frac{G_c}{s + \omega_c} \tag{70}$$

Where the cut-off frequency coefficient ω_c can be obtained by:

$$\omega_c = \frac{2 \cdot D}{\sqrt{\frac{X_v}{S_n} J \cdot \omega_g}} \tag{71}$$

And the gain coefficient G_c:

$$G_c = \frac{1}{J \cdot \omega_c \cdot \omega_g} \tag{72}$$

In the equations, S_n refers to the rated power of all the power sources, ω_g refers to the nominal grid frequency, X_v is the virtual reactance value, and J and D are the inertia and the damping coefficients respectively, that can be adjusted to modify the dynamic behavior of the electromechanical loop.

The output of this active power controller is $\Delta\omega$, which represents the additional rotational speed needed in the system to adjust the phase angle of the synchronous machine to exchange the desired power deliver. This rotational speed is added to the nominal grid frequency and is integrated to obtain the internal synchronous phase angle.

$$\theta_v = \int \Delta\omega_r + \omega_n \tag{73}$$

This virtual phase angle, θ_v, represents the internal emf phase angle of the virtual machine, which is used to transform the grid voltage from the stationary to the synchronous reference frame. Thus giving rise to a voltage difference component between both phases in the *dq*-reference frame.

$$\begin{bmatrix} V_d \\ V_q \\ 0 \end{bmatrix} = \sqrt{\frac{2}{3}} \cdot \begin{bmatrix} \cos(\theta_v) & \cos(\theta_v) & \cos(\theta_v) \\ -\sin(\theta_v) & -\sin(\theta_v) & -\sin(\theta_v) \\ 1/\sqrt{2} & 1/\sqrt{2} & 1/\sqrt{2} \end{bmatrix} \cdot \begin{bmatrix} v_a \\ v_b \\ v_c \end{bmatrix} \tag{74}$$

Where the phase displacement value, δ_v, can be obtained by using the arctangent function on the trigonometric components of the synchronous reference frame voltage values, V_q and V_d, mathematically expressed in (74).

The reactive power is also controllable from the VSPPC adjusting the value of the magnitude in the electromotive force. The transfer function in charge of regulating the magnitude of the voltage can be expressed as:

$$G_q(\mathrm{s}) = \frac{\Delta E}{Q^* - Q_m} = \frac{K_p \cdot s + K_i}{s} \tag{75}$$

Where the proportional parameter, k_p, and the integral parameter, k_i, regulate the amount of voltage variation, ΔE. In this equation, ΔE is the output of the reactive controller and the change on the electromotive force magnitude, whereas Q^* and Q_m are the reference and the measurement of reactive power respectively. These values can be used for voltage regulation services according to regulatory requirements. The voltage magnitude of the virtual *emf* can be determined as (76), where E_n is the nominal voltage of the grid, and ΔE is the voltage variation to regulate the reactive power exchange.

$$E_v = E_n + \Delta E \tag{76}$$

As presented before from equations (73) and (76), it is possible to obtain the parameters θ_v and E_v, respectively [114]. However, this approach is not feasible, mainly because most commercial power converters usually receive only active and reactive power references, and not voltage magnitude and phase angle. The well-known power flow equations are used to adjust this magnitude and phase angle and transform them into a power reference.

$$P_s = \frac{V_{PCC}}{R_v^2 + X_v^2}\left[R_v\left(V_{PCC} - E_v\cos(\delta_v)\right) + X_v E_v \sin(\delta_v)\right] \tag{77}$$

$$Q_s = \frac{V_{PCC}}{R_v^2 + X_v^2}\left[-R_v E_v \sin(\delta_v) + X_v\left(V_{PCC} - E_v\cos(\delta_v)\right)\right] \tag{78}$$

By means of using the power flow equations between two power sources through an impedance, allowing the system to emulate any desired virtual impedance by adjusting the

parameters R_v and X_v, which reflect the resistance and the reactance of the interconnection to the grid. The advantage of emulating this virtual impedance at the plant level is that the response of the power converter is not linked to any physical line impedance, as the power reference is controlled with respect to the PCC, eliminating any possible inter-converter oscillation.

The sharing of power to each power converter depends on the proportional gains k_{pi} and k_{qi}, acting as weight factors to distribute the power exchange duties of each power converter. One way to easily set the gains for each converter is to use the ratio between the nominal power of the power plant and the converter nominal power, as shown in (79).

$$k_{pi} = k_{qi} = \frac{S_i}{\sum_{i=1}^{N} S_i} \tag{79}$$

Where S_i is the nominal power of each power converter and N is the number of power converters composing the power plant. As the composition of the power plant may be different in terms of nominal power capacity, this simple distribution of power allows setting an equivalent percentage weight factor based on the nominal power of the power converter.

6.3. Performance analysis

One of the main advantages of the VSPPC is the use of the virtual impedance at the plant level, allowing the unification of the dynamic response of the power plant in front of any disturbance. To further compare the advantages of the VSPPC, this section compares the conventional control scheme based on synchronous generators with the performance of the VSPPC. The electrical parameters of the power converter are presented in Table 20, while the control scheme of the power converter was shown previously in Figure 148. It is composed of a synchronous reference frame current controller, a PLL, and a current reference generator. The parameters for the PLL were set to have a 100 ms time response by using the following parametrization.

$$k_{Ppll} = \frac{8}{V_n \cdot \tau_{pll}} \tag{80}$$

$$k_{Ipll} = \frac{32}{V_n \cdot \tau_{pll}^2} \tag{81}$$

In the case of the current controller, the parameters were set to $k_{pCC} = 5$ and $k_{iCC} = 1010$, which leads to a controller settling time of 2ms. To transform the power reference from the VSPPC to the current reference the instantaneous power theory has been used, which can be specified as in equations (38) and (39). All the parametrization set to the different elements in

the power converter internal control provides a settling time response under a power step of around 40ms. These parameters can be observed in Table 20.

Symbol	Quantity	Values
P	Converter nominal power	2 kW
L_f	Inverter-side inductance	5 mH
C_f	Capacitance	5 µF
R_d	Damping resistance	1 Ω
L_p+L_s	Grid-side inductor	2 mH
Z_L	Additional inductor	0.0942 Ω
Z_g	Grid impedance	1,57 Ω
P_{dc}	dc source nominal power	20 kW
V_{dc}	dc nominal voltage	750 V

Table 20: Parameters of the power converter

Whereas, Table 21 presents the parameters for the VSPPC plant controller.

Symbol	Quantity	Values
S_n	Nominal power	8 kVA
V_n	Nominal voltage	400 V
f_n	Power plant nominal frequency	314.15 rad/s
H	Power plant inertia factor	5
ξ	Power plant damping factor	0.7
R_v	Power plant virtual resistor	2 Ω
X_v	Power plant virtual reactance	6 Ω
k_{pQ}	Reactive power proportional gain	1e-6
k_{iQ}	Reactive power integral gain	1e-6

Table 21: Parameters of the plant controller

It is worth mentioning that these parameters are the ones used in the experimental results section.

For comparison purposes, two power plant control schemes are presented. Figure 151 describes the conventional control scheme where all the units are composed of an SPC-based grid-forming controller.

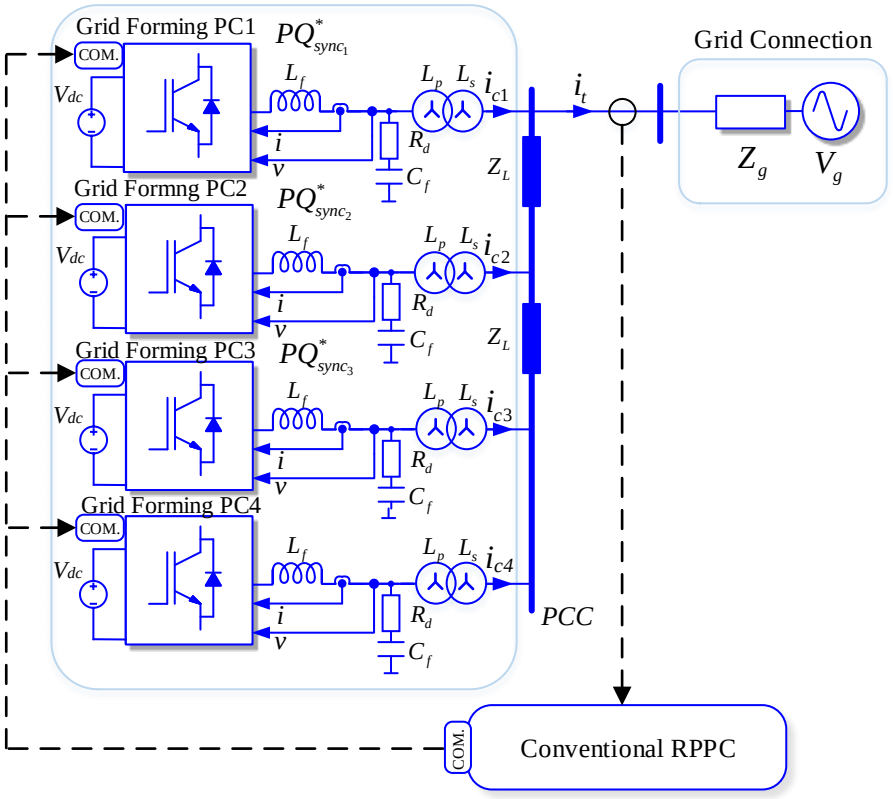

Figure 151: Setup for performance comparison using VSM implementations for the independent power converter control.

Similarly, Figure 152 presents the configuration for the proposed VSPPC, where the power converter control is composed of a simple grid-following controller. Both systems will be tested under a sudden phase shift of the grid to compare the effect of the controllers in parallel and the synchronous central controller.

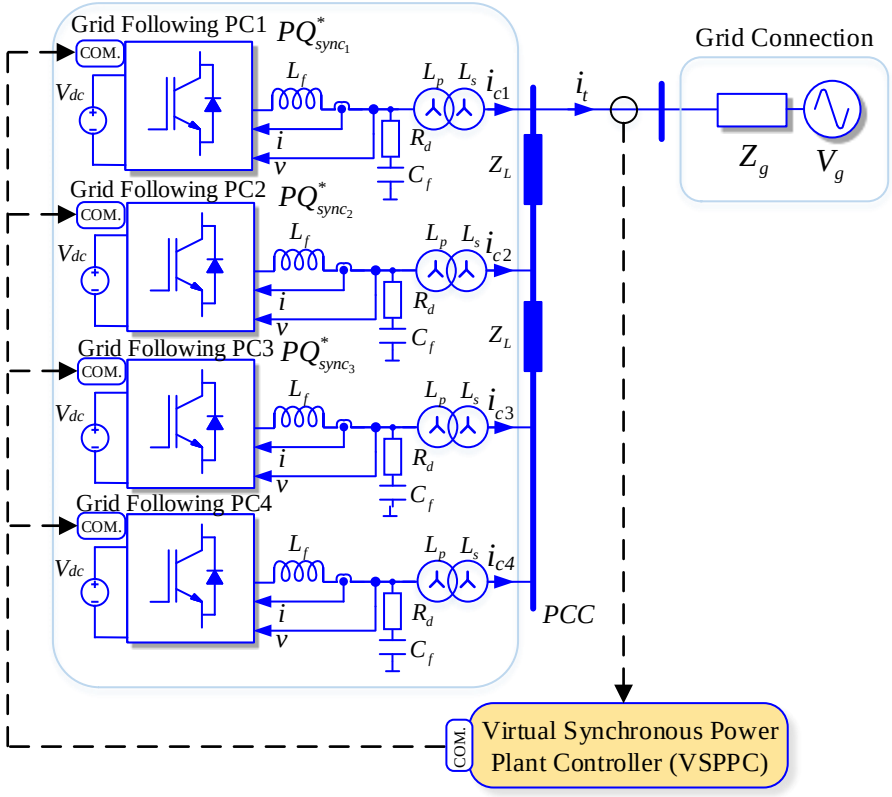

Figure 152: Setup for performance comparison using the proposed VSPPC

The results for both control schemes described above can be seen in Figure 153. In Figure 153(a) the results present a considerable dynamic difference between the active power of each power converter, ending in oscillations between the power converters. This internal oscillation leads to a reduction of the equivalent inertia constant and the damping factor of the whole plant, thus affecting the response of the power plant during the phase shift event at the grid side. In fact, the measurement of active power at the point of connection of the plant resembles a second-order function rather than an inertial response.

The undesired dynamics of each power converter obtained from the conventional control scheme are due to the line impedance differences that exist from each power converter with respect to the PCC, generally due to the different line lengths and transformers. As the power converters are only able to measure the voltage at its own point of connection, the line impedance between the converter and the PCC of the power plant plays a crucial role in the final response of the converter.

In the other case, Figure 153(b) shows the implementation of the VSPPC as the central controller, which uses a centralized virtual impedance in the system. By using this controller, the line impedance of each power converter can be neglected, obtaining an equally distributed power among units and presenting an inertia-like response in the active power at the PCC.

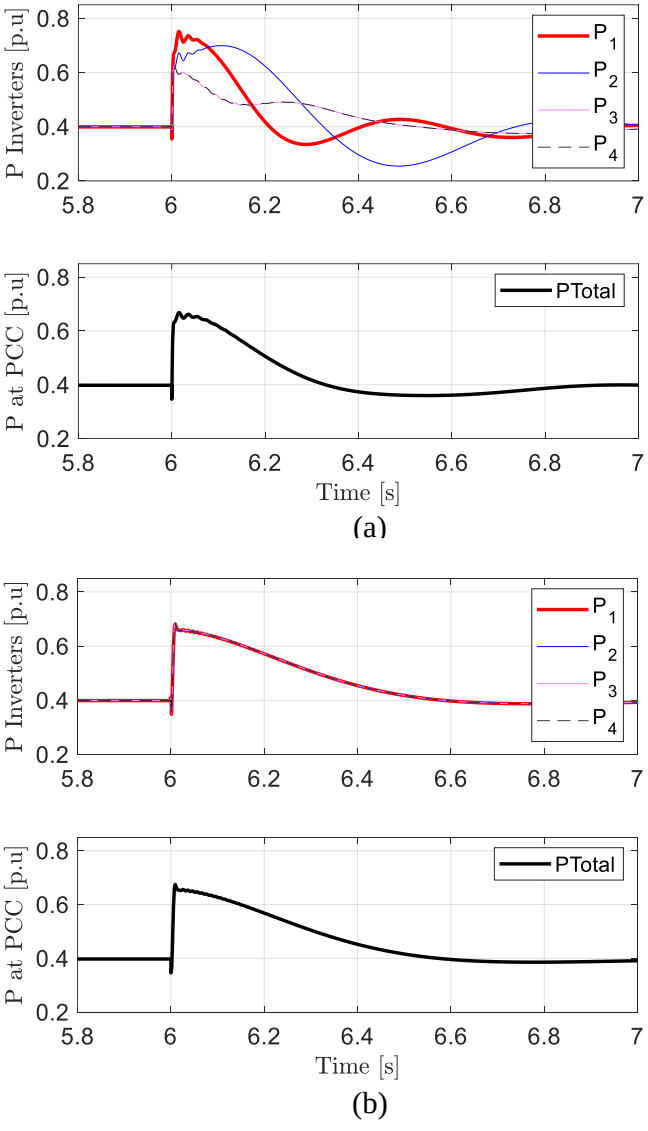

Figure 153: Control performance of (a) the conventional control scheme (b) the proposed VSPPC.

The aforementioned observation of the oscillation between power converters can be confirmed by analyzing the pole-zero map presented in Figure 154, whose parameters are shown in Table 20 for the electrical system, and in Table 21 for the controller parameters. Although the same parameters are used, the difference in line impedance causes the poles to move away from each other.

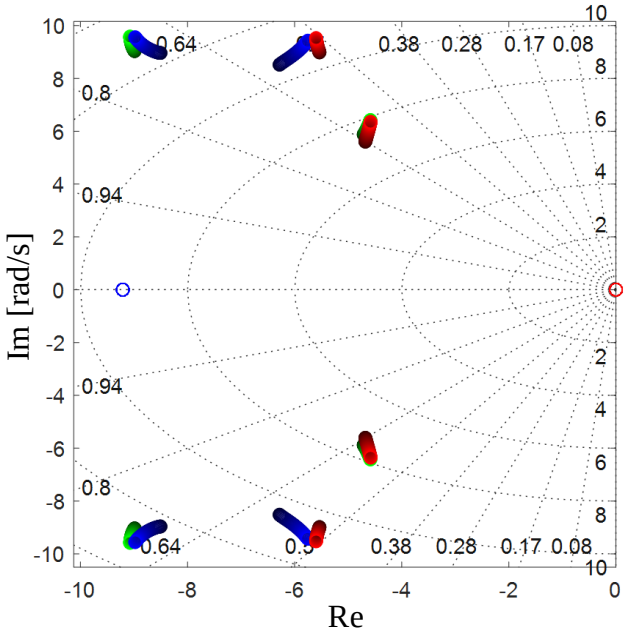

Figure 154: Pole-zero map for different values of SCR of the conventional controller

In contrast to this pole-zero map, considering each power converter with an SPC controller, Figure 155 shows the proposed VSPPC pole-zero map. In this case, the VSPPC only implements one mechanical equation and the impedance is emulated at the central level and not in each power converter. This is seen in the pole-zero map as it has only one pair of complex poles for all the cases. Therefore, even though the line impedance may give rise to undesired dynamics, the VSPPC central controller can avoid them by emulating a single machine with a unique interconnection point to the grid.

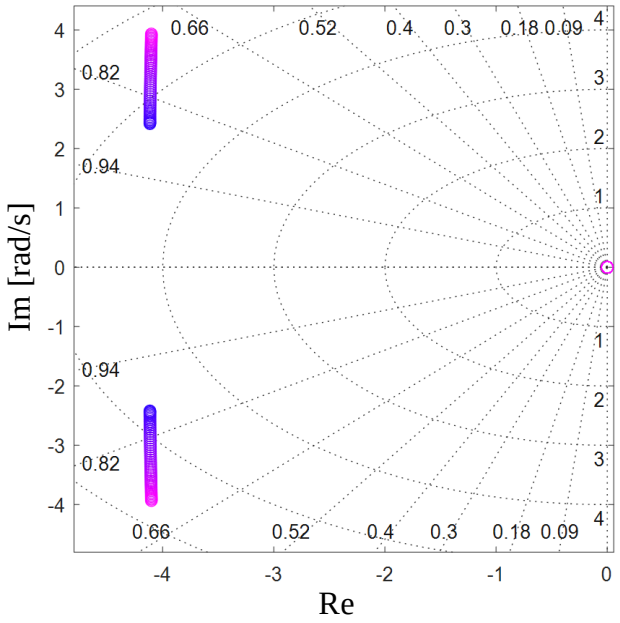

Figure 155: Pole-zero map for different values of short circuit ratio of the proposed VSPPC

6.4. Phasor-domain structure

To validate the presented VSPPC approach, a set of experiments have been executed in the laboratory. The emulated renewable power plant is emulated by four power converter units (Danfoss: FC-302P2K2T5E20H1) controlled by a microcontroller TMS320C28335. The dc-link of all the converters is generated by using a 20 kW dc-voltage source (MagnaPower: TSD1000-20). The converters are connected to the electrical grid through a 30 kVA transformer, Figure 156. For the central controller the VSPPC code is implemented in a control board based on a TMS320C28335 digital signal processor (DSP) which is able to communicate with each power converter microprocessor by using CAN communication at 125 kbps. The list of parameters for the power converter and the central controller are presented in Table 20 and Table 21, respectively.

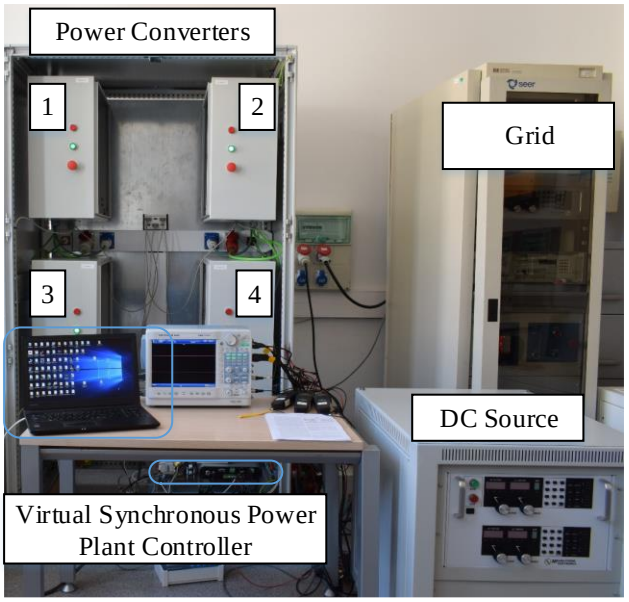

Figure 156: Experimental setup

The following experiments have been carried out using the previously described system:

- A power step change to verify the proposed VSPPC dynamic response.
- Connection and disconnection of different power converter units to validate the robustness of the VSPPC controller under undesired operations of power converters.
- Connection of a synchronous generator to ensure the damping capacity of the VSPPC.
- A load connection at the PCC to compare the dynamic response of the proposed VSPPC in front of different SPC in each power converter.

6.4.1. Performance in front of power changes

In Figure 157, the experimental results under a step-change in the active power are presented for the proposed VSPPC. It can be seen that the active power measurement at the PCC of the emulated power plant exhibits a stable operation, outperforming the one of a synchronous generator. This enhanced behavior is accomplished by the damping coefficient, which can be tuned to the desired performance specifications, and the virtual impedance, where the virtual resistor has been intentionally increased to provide additional electrical damping without increasing the power losses. Regardless of the difference in the line impedance, the four power converters distribute equally the active power. In addition to the overall dynamic, the zoomed-in wave-forms also confirm the proper quality of the current injected by the power converter.

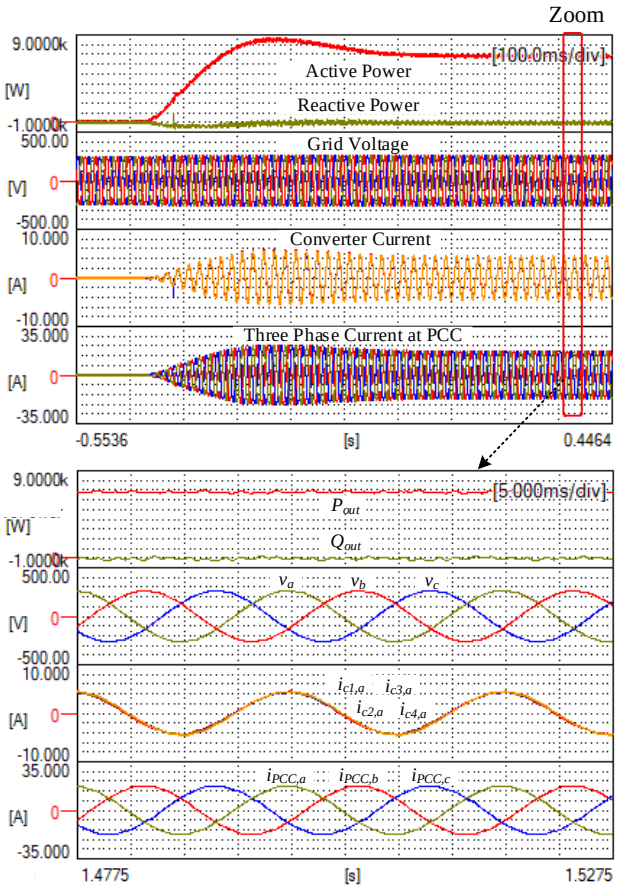

Figure 157: Response of the RPP with VSPPC under a step-change in reference power.

6.4.2. Connection and disconnection of generation units with the VSPPC

Figure 158 shows the experimental response of the VSPPC during the event of a disconnection of a power converter. The experiment starts with a constant power injection of active power equally shared among the power converters. At around t = 0.0431 s, one of the power converters is disconnected from the RPP. This disconnection gives rise to a transient mismatch between generation and consumption, reference and measurement, that should be corrected. As soon as the VSPPC detects this mismatch in power, it tries to regulate the power to return to the steady-state reference tracking. The dynamic response shown by the VSPPC is due to the inertia and damping coefficient set in the central controller.

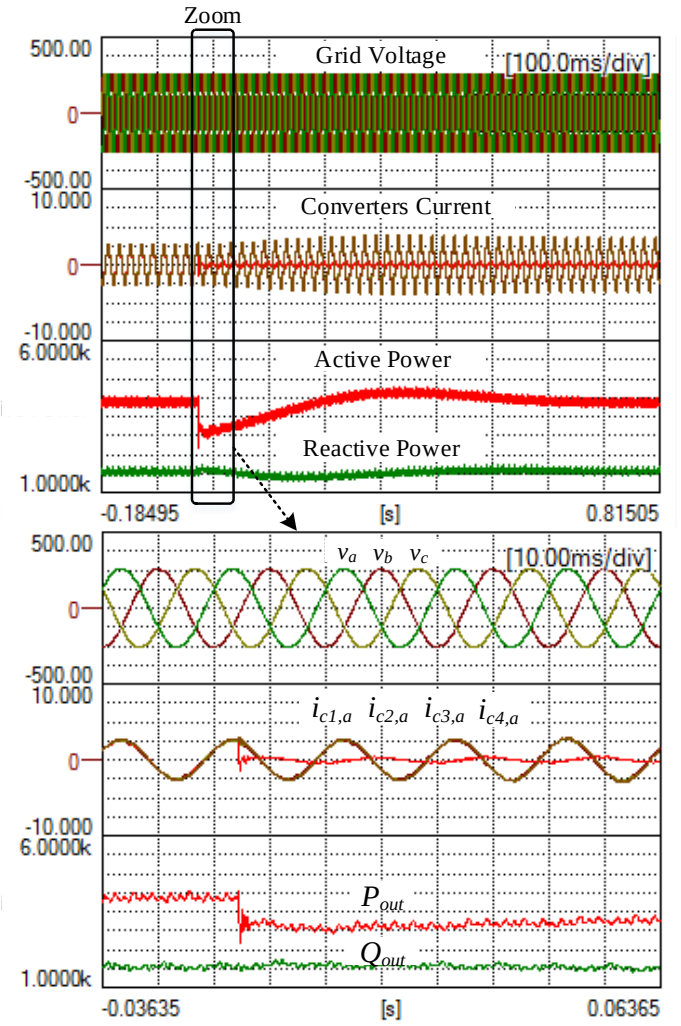

Figure 158: Experimental response of the VSPPC to a disconnection of one power converter.

In Figure 159 a similar response is shown when a power converter is connected to the VSPPC system. In this case, the experiment also starts with a constant injection of power. At around t= 2.45s, a power converter unit is connected to the RPP. The power mismatch during the connection is controlled by the VSPPC controller, which adapts the power reference of the system to equally distribute the power among all the units connected to the system in that instant.

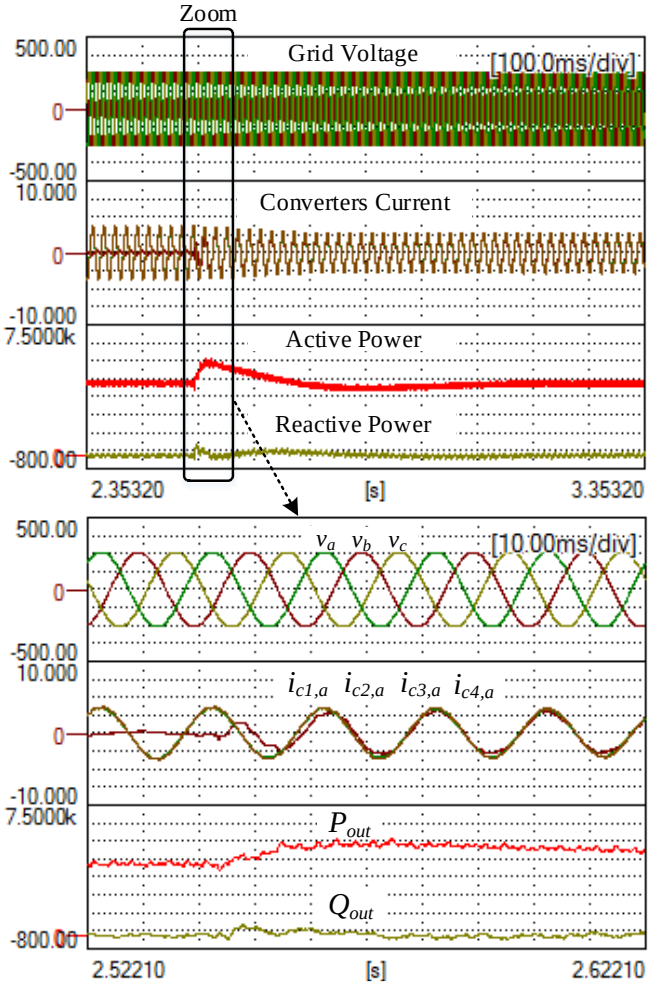

Figure 159: Experimental response of the VSPPC during the connection of one power converter to the system

6.4.3. Power oscillation damping with the VSPPC

To observe the damping capability of the proposed VSPPC, a 20kVA synchronous generator is connected to the PCC of the emulated power plant as depicted in Figure 160. This generator is naturally underdamped which leads to a two-case scenario.

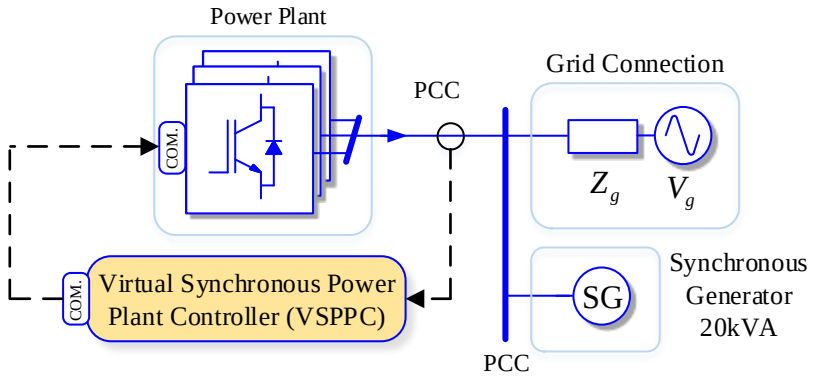

Figure 160: System configuration for the power oscillation damping.

In the first case, due to the low damping of the VSPPC and the synchronous generator, the active power measured at the PCC during the transient is highly oscillatory, giving rise to an undesired performance of the overall system, Figure 161.

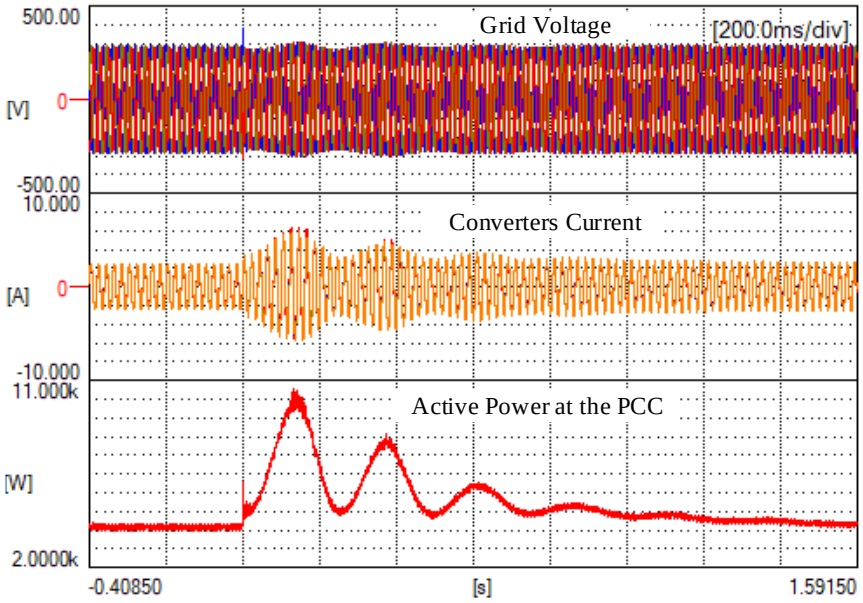

Figure 161: Damping performance of the VSPPC with $G_c = 4.796e^{-4}$ and $\omega_c = 8.186$.

In the second case, as the damping of the VSPPC is increased, the power oscillation at the PCC is attenuated, as can be observed from Figure 162. This result shows that the VSPPC can

provide additional damping to power oscillations, but also that its damping factor can be adjusted though G_c and ω_c.

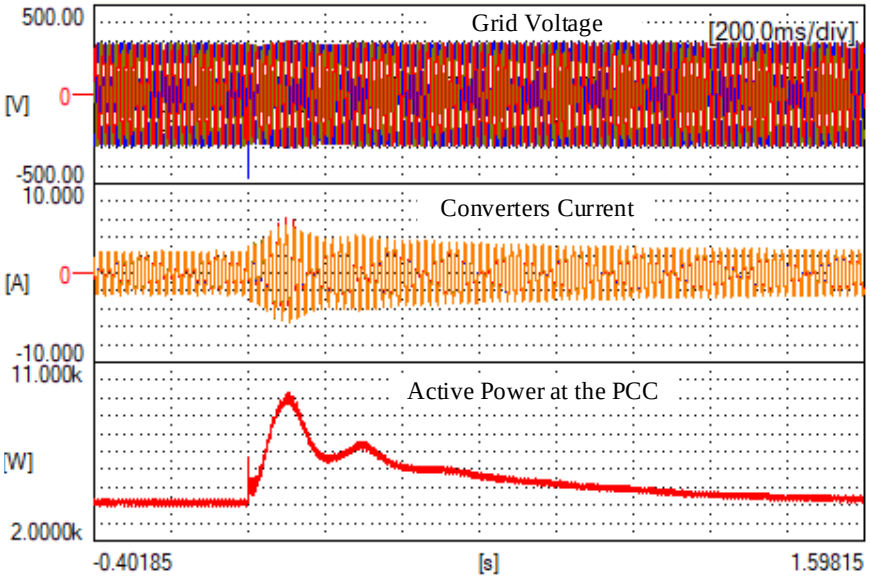

Figure 162: Damping performance of the VSPPC with $G_c = 2.71e^{-4}$ and $\omega_c = 14.326$.

6.4.4. Performance in front of power changes

In Figure 163, the comparison between the conventional controller using SPC-based power converters and the proposed VSPPC under a load step is presented. It is shown that, in both cases, the power converters inject a specific amount of active power to support the grid during the event. Such response implies that both control schemes provide inertia to the grid, scaled to the power plant. However, in Figure 163(a) the response of the conventional controller with power converters with embedded SPC implementations is not preferable considering unequal power-sharing during the event, giving rise to a distortion in the overall inertia and damping of the power plant.

On the other hand, in the case of the VSPPC, Figure 163(b) displays an identical response of all power converters. It is reasonable to conclude that the VSPPC offers better dynamic performance compared to a distributed synchronous control, and it does not require any modifications to the power converter control, making the VSPPC an effective solution for power plant controllers.

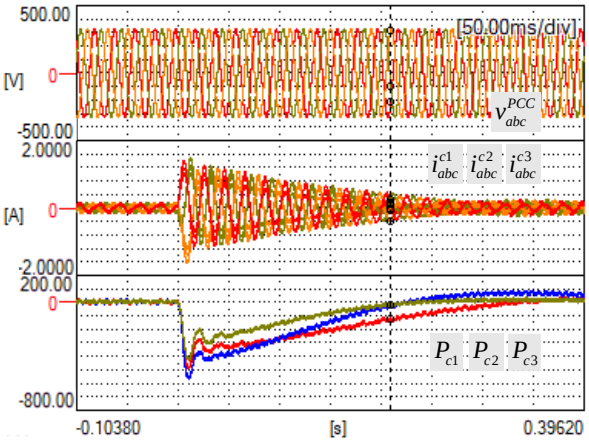

(a)

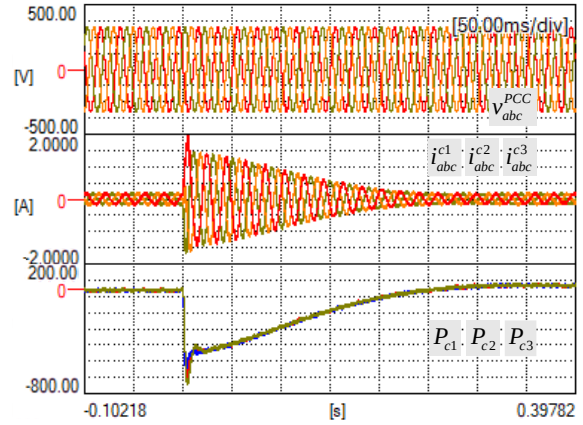

(b)

Figure 163: Experimental results of the emulated power plant under a load step with (a) the conventional controller using SPC in each converter (b) the proposed VSPPC.

6.5. Conclusions

The synchronous control oriented to the system has been presented and the VSPPC has been proposed as a solution to be used in a system composed of multiple units, such as a renewable power plant, providing dynamic support services as inertia and power oscillation damping. The structure of the VSPPC is based on the well-known SPC, which emulates some of the pilar characteristics of the synchronous generator. However, in addition to the motion equations and the central virtual impedance, the phase displacement calculator has a key effect on power regulation.

The main advantages of the usage of the VSPPC are twofold. The most important one is that the VSPPC is compatible with most of the control strategies used nowadays in the majority of power converters, reducing the cost of using smarter converters in the system. The second one is that the power injected into the grid is not specifically linked to the local voltage measurement as in the device approach, therefore reducing the current distortion due to errors in the voltage measurement.

This work has proven that the aggregation of grid-forming converters does not provide optimal performance in the power plant. One of the most relevant contributions of this work is the capability of controlling the mechanical behavior of the power plant, coordinating all the units to work as a unique synchronous machine. Thus, the power oscillation damping functionalities are boosted, and better dynamic performance is achieved by the whole synchronous system. The simulation results and the experimental results demonstrated that the VSPPC can provide fast frequency services as well as an increased control performance.

Chapter 7.

Conclusions

The work presented in this Ph.D. thesis addresses the control of renewable energy resources interfaced by power converters. Throughout all the document, modification and enhancements to power converter controllers have been demonstrated, following the natural transition of grid-following power converter into generation units with the capability to form a grid. After summarizing all the research material throughout the thesis, the conclusions of this work are exposed henceforth.

- One of the first objectives of the thesis was the modification of the traditional current controller implementation in the stationary reference frame. To achieve the first contribution, the traditional SOGI controller is adapted into a modified resonant structure. The reduction of integrators enables an easier separation of control capability for the fundamental and harmonic sequences. This work also provides a solution for power converter control in the $\alpha\beta$-reference frame to provide a behavior similar to the one in dq-reference frame, in terms of power coupling during active and reactive power steps. The addition of the modified resonant structure and the decoupling matrix in the $\alpha\beta$-reference frame, as well as its experimental validation, is presented in Chapter 3.

- The integration of a grid-forming control strategy based on the SPC has been shown in the document, on Chapter 4 and Chapter 5. The work exposes the beneficial effects not only in the dynamic support capabilities from grid-following power converters, such as frequency and voltage regulation, but also from the inherent regulation of the electromechanical loop. The integration of inertia and damping, through the swing equation and the virtual admittance, enable a high versatility in the power converter operation. This regulation goes from adding synthetic inertia and power oscillation damping to the system, dynamic support during balanced or unbalanced voltage sags, as well as a parallel virtual admittance strategy for voltage harmonic compensation.

- During the research of grid-forming power converter strategies, to enable a more natural interconnection of renewable energy systems to the grid, it became clear that the transition of grid-following to a grid-forming control required a high

implementation process. This transition is based on the modification of the voltage loop into a system that includes an electromechanical and electromagnetic emulation. However, the proposal in Chapter 5 presents a simple approach based on a virtual admittance implementation, enabling the system to operate as a grid-forming strategy by using the traditional converter control structure. Although the local measurements are vital to properly operate the system during the steady-state, a sensor-less synchronous system is feasible by using the reference voltage at the output of the current controller. This implementation reduces the voltage measurements required in the system, thus providing a self-synchronized controller. High interest may spark in household PV or battery storage systems with this implementation, as it ensures an enhanced natural interaction during contingencies.

- Although distributed generation units are having an immense impact, considering the increase of PV installed in residential areas and storage systems, big renewable energy power plants have also been on the rise during the last decade. With the improvements in communication technology, cloud-based systems and high-speed data sharing through the internet as leading factors, the communication delays are being heavily decreased even for field-bus technologies. This improvement allows the virtual synchronous power plant control to become a feasible reality. The approach presented in the thesis focuses on an area of generation units connected to the same PCC, enabling a harmonized behavior between units, with the aim of performing a coordinated action during grid contingencies. Chapter 6 provides a solution to the virtual synchronous power plant controller based on a phase domain approach, where power reference control signals provide an easily expandable system that enables hundreds or thousands of units to operate as a virtual synchronous machine without modifying the traditional control of the grid-following converter.

Overall, the synchronous control, oriented to the device and to the system, has been studied and analyzed throughout the document, where both simulation and experimental validation has been presented for all the study cases.

Although the insights on the virtual synchronous machine control gained during the research, there were some ideas that were not explored. The more notorious of them were found to be an interesting thought, and thus are described in the future work section.

7.1. Future works

One of the most important aspects that should be pursued in future endeavors is how the integration of renewable energy systems will affect the stability of the electrical grid when most of the systems are transitioned to grid-forming strategies. This consideration has an especial effect when both the stochastic behavior of renewable energy systems and the wide

grid-forming strategies collide, although there might be some drawbacks if there is not a standard to follow. The sensorless grid-forming power strategy, which uses the reference voltage of the current controller as the synchronization voltage, may be of interest if integrated just as a compensator for grid contingencies or huge imbalances on the power delivered. However, there is still room for further analysis on the parallelization of this system, as well as modifications including other electromagnetic emulations.

Another interesting topic focuses on the communication delay in the system-oriented synchronous control. Although there is much improvement in communication technologies, the loss of communication to the central synchronous unit has to be handled without harming the operation of the entire power plant. This presents a huge challenge in the harmonious operation of the system, especially considering the sudden disconnection of generation units or the partial loss of energy generation due to the unpredictable generation profile.

Another important aspect is the upcoming changes in the grid codes all around the world, which will restrict the operation of renewable energy generation and require more flexibility services. In this regard, the black-start energization of big islands, such as the United Kingdom or Australia, has been a hot topic for the last few years. Although the conventional power plants are in charge of energizing the electrical grid during the black-start process, the rising integration of grid-forming power converters makes it a feasible reality to start the energization process on the distribution system, which is certainly something worth investigating in the future

References

[1] D. Henner and REN21, *Ren21*. 2017.

[2] ENTSO-E, “Need for synthetic inertia (SI) for frequency regulation - ENTSO-E guidance document for national implementation for network codes on grid connection,” no. March 29, 2017.

[3] REE, Terna, TransnetBW, 50Hertz Transmission, Swissgrid, and Energinet.dk., “Frequency Stability Evaluation Criteria for the Synchronous Zone of Continental Europe,” *RG-CE Syst. Prot. Dyn. Sub Gr.*, p. 25, 2016.

[4] ENTSO-E, “Rate of Change of Frequency (RoCoF) withstand capability,” no. January, p. 9, 2018, [Online]. Available: https://docstore.entsoe.eu/Documents/Network codes documents/NC RfG/IGD_RoCoF_withstand_capability_final.pdf.

[5] P. Denholm, T. Mai, R. W. Kenyon, B. Kroposki, and M. O. Malley, “Inertia and the Power Grid : A Guide Without the Spin,” no. May, 2020, [Online]. Available: https://www.nrel.gov/docs/fy20osti/73856.pdf.

[6] B. S. Strategy, “Final 2021_22Black Start Strategy and Procurement Methodology _Published,” no. May, pp. 0–37, 2021.

[7] Y. Lin *et al.*, “Research Roadmap on Grid-Forming Inverters,” *Nrel*, 2020.

[8] P. Kundur, *Power System Stability and Control*. McGraw-Hill Education, 1994.

[9] J. Machowski, J. W. Bialek, and J. R. Bumby, “Power System Dynamics. Stability and Control,” Jan. 2012.

[10] A. Bergen and V. Vittal, *Power Systems Analysis*. 2006.

[11] P. Rodriguez, J. Pou, J. Bergas, J. I. Candela, R. P. Burgos, and D. Boroyevich, “Decoupled Double Synchronous Reference Frame PLL for Power Converters Control,” *IEEE Trans. Power Electron.*, vol. 22, no. 2, pp. 584–592, 2007, doi: 10.1109/TPEL.2006.890000.

[12] J. Matas, H. Martín, J. de la Hoz, A. Abusorrah, Y. Al-Turki, and H. Alshaeikh, “A New THD Measurement Method With Small Computational Burden Using a SOGI-FLL Grid Monitoring System,” *IEEE Trans. Power Electron.*, vol. 35, no. 6, pp. 5797–5811, 2020, doi: 10.1109/TPEL.2019.2953926.

[13] S. Golestan, J. M. Guerrero, J. C. Vasquez, A. M. Abusorrah, and Y. Al-Turki, “Harmonic Linearization and Investigation of Three-Phase Parallel-Structured Signal Decomposition Algorithms in Grid-Connected Applications,” *IEEE Trans. Power*

Electron., vol. 36, no. 4, pp. 4198–4213, 2021, doi: 10.1109/TPEL.2020.3021723.

[14] H. Beck and R. Hesse, "Virtual synchronous machine," in *2007 9th International Conference on Electrical Power Quality and Utilisation*, 2007, pp. 1–6, doi: 10.1109/EPQU.2007.4424220.

[15] D. T. R. Heese, H.-P. Beck, "Conditioning device for energy supply networks WO2009022198A2.," no. 12, 2009.

[16] R. Hesse, D. Turschner, and H. Beck, "Micro grid stabilization using the virtual synchronous machine (VISMA)," *Renew. energy \& power Qual. J.*, vol. 1, pp. 676–681, 2009.

[17] Y. Chen, R. Hesse, D. Turschner, and H. Beck, "Dynamic Properties of the Virtual Synchronous Machine (VISMA)," *Proc. ICREPQ*, pp. 1–5, 2011.

[18] Y. Chen, R. Hesse, D. Turschner, and H. Beck, "Improving the grid power quality using virtual synchronous machines," in *2011 International Conference on Power Engineering, Energy and Electrical Drives*, 2011, pp. 1–6, doi: 10.1109/PowerEng.2011.6036498.

[19] Y. Chen, R. Hesse, D. Turschner, and H. Beck, "Investigation of the Virtual Synchronous Machine in the island mode," in *2012 3rd IEEE PES Innovative Smart Grid Technologies Europe (ISGT Europe)*, 2012, pp. 1–6, doi: 10.1109/ISGTEurope.2012.6465648.

[20] Y. Chen, R. Hesse, D. Turschner, and H. Beck, "Comparison of methods for implementing virtual synchronous machine on inverters," *Renew. energy \& power Qual. J.*, pp. 734–739, 2012.

[21] J. Driesen and K. Visscher, "Virtual synchronous generators," in *2008 IEEE Power and Energy Society General Meeting - Conversion and Delivery of Electrical Energy in the 21st Century*, 2008, pp. 1–3, doi: 10.1109/PES.2008.4596800.

[22] K. Visscher and S. W. H. De Haan, "Virtual synchronous machines (VSG's) for frequency stabilisation in future grids with a significant share of decentralized generation," in *CIRED Seminar 2008: SmartGrids for Distribution*, 2008, pp. 1–4.

[23] M. P. N. van Wesenbeeck, S. W. H. de Haan, P. Varela, and K. Visscher, "Grid tied converter with virtual kinetic storage," in *2009 IEEE Bucharest PowerTech*, 2009, pp. 1–7, doi: 10.1109/PTC.2009.5282048.

[24] T. Loix, S. De Breucker, P. Vanassche, J. Van den Keybus, J. Driesen, and K. Visscher, "Layout and performance of the power electronic converter platform for the VSYNC project," in *2009 IEEE Bucharest PowerTech*, 2009, pp. 1–8, doi: 10.1109/PTC.2009.5282160.

[25] T. V Van *et al.*, "Virtual synchronous generator: An element of future grids," in *2010 IEEE PES Innovative Smart Grid Technologies Conference Europe (ISGT Europe)*, 2010, pp. 1–7, doi: 10.1109/ISGTEUROPE.2010.5638946.

[26] V. Karapanos, Z. Yuan, S. W. H. Haan, and K. Visscher, *A Control Algorithm for the Coordination of Multiple Virtual Synchronous Generator Units*. 2011.

[27] V. Karapanos, S. de Haan, and K. Zwetsloot, "Real time simulation of a power system with VSG hardware in the loop," in *IECON 2011 - 37th Annual Conference of the IEEE Industrial Electronics Society*, 2011, pp. 3748–3754, doi: 10.1109/IECON.2011.6119919.

[28] V. Van Thong *et al.*, "Virtual synchronous generator: Laboratory scale results and field demonstration," in *2009 IEEE Bucharest PowerTech*, 2009, pp. 1–6, doi: 10.1109/PTC.2009.5281790.

[29] M. Albu *et al.*, "Measurement and remote monitoring for virtual synchronous generator design," in *2010 IEEE International Workshop on Applied Measurements for Power Systems*, 2010, pp. 7–11, doi: 10.1109/AMPS.2010.5609328.

[30] Q. Zhong and G. Weiss, "Static synchronous generators for distributed generation and renewable energy," in *2009 IEEE/PES Power Systems Conference and Exposition*, 2009, pp. 1–6, doi: 10.1109/PSCE.2009.4840013.

[31] Q.-C. WEISS, George; ZHONG, "STATIC SYNCHRONOUS GENERATORS," 2015.

[32] Q. Zhong and G. Weiss, "Synchronverters: Inverters That Mimic Synchronous Generators," *IEEE Trans. Ind. Electron.*, vol. 58, no. 4, pp. 1259–1267, 2011, doi: 10.1109/TIE.2010.2048839.

[33] P.-L. Nguyen, Q. Zhong, F. Blaabjerg, and J. M. Guerrero, "Synchronverter-based operation of STATCOM to Mimic Synchronous Condensers," in *2012 7th IEEE Conference on Industrial Electronics and Applications (ICIEA)*, 2012, pp. 942–947, doi: 10.1109/ICIEA.2012.6360859.

[34] E. Brown and G. Weiss, "Using synchronverters for power grid stabilization," in *2014 IEEE 28th Convention of Electrical & Electronics Engineers in Israel (IEEEI)*, 2014, pp. 1–5, doi: 10.1109/EEEI.2014.7005736.

[35] W. Ming and Q. Zhong, "Synchronverter-based transformerless PV inverters," in *IECON 2014 - 40th Annual Conference of the IEEE Industrial Electronics Society*, 2014, pp. 4396–4401, doi: 10.1109/IECON.2014.7049164.

[36] Q. Zhong, "Four-quadrant operation of AC machines powered by inverters that mimic synchronous generators," in *5th IET International Conference on Power Electronics, Machines and Drives (PEMD 2010)*, 2010, pp. 1–6, doi: 10.1049/cp.2010.0040.

[37] C. Zhang *et al.*, "An improved synchronverter model and its dynamic behaviour comparison with synchronous generator," in *2nd IET Renewable Power Generation Conference (RPG 2013)*, 2013, pp. 1–4, doi: 10.1049/cp.2013.1879.

[38] R. Aouini, K. Ben Kilani, B. Marinescu, and M. Elleuch, "Virtual synchronous generators dynamic performances," in *2014 International Conference on Electrical Sciences and Technologies in Maghreb (CISTEM)*, 2014, pp. 1–6, doi: 10.1109/CISTEM.2014.7077025.

[39] Q. Zhong, P. Nguyen, Z. Ma, and W. Sheng, "Self-Synchronized Synchronverters: Inverters Without a Dedicated Synchronization Unit," *IEEE Trans. Power Electron.*, vol. 29, no. 2, pp. 617–630, 2014, doi: 10.1109/TPEL.2013.2258684.

[40] C. Li, J. Xu, and C. Zhao, "A Coherency-Based Equivalence Method for MMC Inverters Using Virtual Synchronous Generator Control," *IEEE Trans. Power Deliv.*, vol. 31, no. 3, pp. 1369–1378, 2016, doi: 10.1109/TPWRD.2015.2499262.

[41] S. Dong, Y. Chi, and Y. Li, "Active Voltage Feedback Control for Hybrid Multiterminal HVDC System Adopting Improved Synchronverters," *IEEE Trans. Power Deliv.*, vol. 31, no. 2, pp. 445–455, 2016, doi: 10.1109/TPWRD.2015.2420657.

[42] L. Lu and C. Chu, "Consensus-based distributed droop control of synchronverters for isolated micro-grids," in *2015 IEEE International Symposium on Circuits and Systems (ISCAS)*, 2015, pp. 914–917, doi: 10.1109/ISCAS.2015.7168783.

[43] G. C. Konstantopoulos, Q. Zhong, B. Ren, and M. Krstic, "Boundedness of Synchronverters," in *2015 European Control Conference (ECC)*, 2015, pp. 1050–1055, doi: 10.1109/ECC.2015.7330679.

[44] Z. Wei, C. Jie, and G. Chunying, "Small signal modeling and analysis of synchronverters," in *2015 IEEE 2nd International Future Energy Electronics Conference (IFEEC)*, 2015, pp. 1–5, doi: 10.1109/IFEEC.2015.7361434.

[45] V. Natarajan and G. Weiss, "Synchronverters With Better Stability Due to Virtual Inductors, Virtual Capacitors, and Anti-Windup," *IEEE Trans. Ind. Electron.*, vol. 64, no. 7, pp. 5994–6004, 2017, doi: 10.1109/TIE.2017.2674611.

[46] Q.-C. Zhong, G. C. Konstantopoulos, B. Ren, and M. Krstic, "Improved Synchronverters with Bounded Frequency and Voltage for Smart Grid Integration," *IEEE Trans. Smart Grid*, vol. 9, no. 2, pp. 786–796, 2018, doi: 10.1109/TSG.2016.2565663.

[47] J. Caicedo, A. R. de Castro, B. França, and M. Aredes, "Resonant harmonic compensation for synchronverter, integrating wind and photovoltaic power generation into an electrical grid, case study: Nonlinear and unbalanced load," in *2017 Brazilian Power Electronics Conference (COBEP)*, 2017, pp. 1–6, doi: 10.1109/COBEP.2017.8257275.

[48] J. Roldan-Perez, A. Rodríguez-Cabero, and M. Prodanovic, "Harmonic virtual impedance design for a synchronverter-based battery interface converter," in *2017 IEEE 6th International Conference on Renewable Energy Research and Applications (ICRERA)*, 2017, pp. 774–779, doi: 10.1109/ICRERA.2017.8191164.

[49] Z. Shuai, W. Huang, C. Shen, J. Ge, and Z. J. Shen, "Characteristics and Restraining Method of Fast Transient Inrush Fault Currents in Synchronverters," *IEEE Trans. Ind. Electron.*, vol. 64, no. 9, pp. 7487–7497, 2017, doi: 10.1109/TIE.2017.2652362.

[50] S. Dong and Y. C. Chen, "Adjusting Synchronverter Dynamic Response Speed via Damping Correction Loop," *IEEE Trans. Energy Convers.*, vol. 32, no. 2, pp. 608–619, 2017, doi: 10.1109/TEC.2016.2645450.

[51] L. Zhang and H. Nee, "Multivariable feedback design of VSC-HVDC connected to weak ac systems," in *2009 IEEE Bucharest PowerTech*, 2009, pp. 1–8, doi: 10.1109/PTC.2009.5282110.

[52] L. Zhang, L. Harnefors, and H. Nee, "Power-Synchronization Control of Grid-

Connected Voltage-Source Converters," *IEEE Trans. Power Syst.*, vol. 25, no. 2, pp. 809–820, 2010, doi: 10.1109/TPWRS.2009.2032231.

[53] D. Dong, B. Wen, D. Boroyevich, P. Mattavelli, and Y. Xue, "Analysis of Phase-Locked Loop Low-Frequency Stability in Three-Phase Grid-Connected Power Converters Considering Impedance Interactions," *IEEE Trans. Ind. Electron.*, vol. 62, no. 1, pp. 310–321, 2015, doi: 10.1109/TIE.2014.2334665.

[54] M. Durrant, H. Werner, and K. Abbott, "Model of a VSC HVDC terminal attached to a weak AC system," in *Proceedings of 2003 IEEE Conference on Control Applications, 2003. CCA 2003.*, 2003, vol. 1, pp. 178–182 vol.1, doi: 10.1109/CCA.2003.1223288.

[55] L. Harnefors, M. Bongiorno, and S. Lundberg, "Input-Admittance Calculation and Shaping for Controlled Voltage-Source Converters," *IEEE Trans. Ind. Electron.*, vol. 54, no. 6, pp. 3323–3334, 2007, doi: 10.1109/TIE.2007.904022.

[56] D. Jovcic, L. A. Lamont, and L. Xu, "VSC transmission model for analytical studies," in *2003 IEEE Power Engineering Society General Meeting (IEEE Cat. No.03CH37491)*, 2003, vol. 3, pp. 1737-1742 Vol. 3, doi: 10.1109/PES.2003.1267418.

[57] L. Zhang, L. Harnefors, and H. Nee, "Modeling and Control of VSC-HVDC Links Connected to Island Systems," *IEEE Trans. Power Syst.*, vol. 26, no. 2, pp. 783–793, 2011, doi: 10.1109/TPWRS.2010.2070085.

[58] L. Harnefors, "Control of a voltage source converter using a synchronous machine evolution," 2010.

[59] L. Zhang, *Modeling and Control of VSC-HVDC Links Connected to Weak AC Systems*. 2005.

[60] L. Zhang, H. Nee, and L. Harnefors, "Analysis of Stability Limitations of a VSC-HVDC Link Using Power-Synchronization Control," *IEEE Trans. Power Syst.*, vol. 26, no. 3, pp. 1326–1337, 2011, doi: 10.1109/TPWRS.2010.2085052.

[61] K. M. Alawasa and Y. A. I. Mohamed, "Impedance and Damping Characteristics of Grid-Connected VSCs With Power Synchronization Control Strategy," *IEEE Trans. Power Syst.*, vol. 30, no. 2, pp. 952–961, 2015, doi: 10.1109/TPWRS.2014.2332179.

[62] R. Rogersten, L. Zhang, and P. Mitra, "Applying power-synchronization control in a multi-terminal DC system," *IEEE Power Energy Soc. Gen. Meet.*, vol. 2014, Oct. 2014, doi: 10.1109/PESGM.2014.6939159.

[63] P. Mitra, L. Zhang, and L. Harnefors, "Offshore Wind Integration to a Weak Grid by VSC-HVDC Links Using Power-Synchronization Control: A Case Study," *IEEE Trans. Power Deliv.*, vol. 29, no. 1, pp. 453–461, 2014, doi: 10.1109/TPWRD.2013.2273979.

[64] R. RODRÍGUEZ CORTÉS, Pedro; CANDELA GARCÍA, José Ignacio; ROCABERT DELGADO, Joan y TEODORESCU, "CONTROLADOR DE POTENCIA SÍNCRONA DE UN SISTEMA DE GENERACIÓN BASADO EN CONVERTIDORES ESTÁTICOS DE POTENCIA," 2007.

[65] P. Rodriguez, I. Candela, J. Rocabert, and R. Teodorescu, "Virtual Controller of Electromechanical Characteristics for Static Power Converters," *International Patent Application*. 2012.

[66] ABENGOA Solar NewTechnologies, "Virtual admitance controller based on static power converters," *International patent application WO 2012/117133*. 2012.

[67] P. Rodriguez, I. Candela, and A. Luna, "Control of PV generation systems using the synchronous power controller," *2013 IEEE Energy Conversion Congress and Exposition*. pp. 993–998, 2013, doi: 10.1109/ECCE.2013.6646811.

[68] A. Tarrasó, J. I. Candela, J. Rocabert, and P. Rodriguez, "Grid voltage harmonic damping method for SPC based power converters with multiple virtual admittance control," in *2017 IEEE Energy Conversion Congress and Exposition (ECCE)*, 2017, pp. 64–68, doi: 10.1109/ECCE.2017.8095762.

[69] W. Zhang, A. Luna, I. Candela, J. Rocabert, and P. Rodriguez, "An active power synchronizing controller for grid-connected power converters with configurable natural droop characteristics," in *2015 IEEE 6th International Symposium on Power Electronics for Distributed Generation Systems (PEDG)*, 2015, pp. 1–7, doi: 10.1109/PEDG.2015.7223055.

[70] W. Zhang *et al.*, "Comparison of different power loop controllers for synchronous power controlled grid-interactive converters," *2015 IEEE Energy Convers. Congr. Expo. ECCE 2015*, pp. 3780–3787, 2015, doi: 10.1109/ECCE.2015.7310194.

[71] C. Li, R. Burgos, I. Cvetkovic, D. Boroyevich, L. Mili, and P. Rodriguez, "Analysis and design of virtual synchronous machine based STATCOM controller," *2014 IEEE 15th Work. Control Model. Power Electron. COMPEL 2014*, pp. 1–6, 2014, doi: 10.1109/COMPEL.2014.6877134.

[72] D. Remon, A. M. Cantarellas, E. Rakhshani, I. Candela, and P. Rodriguez, "An active power synchronization control loop for grid-connected converters," *IEEE Power Energy Soc. Gen. Meet.*, vol. 2014-Octob, no. October, pp. 1–5, 2014, doi: 10.1109/PESGM.2014.6939250.

[73] D. Remon, A. M. Cantarellas, E. Rakhshani, I. Candela, and P. Rodriguez, "An active power self-synchronizing controller for grid-connected converters emulating inertia," in *2014 International Conference on Renewable Energy Research and Application (ICRERA)*, 2014, pp. 424–429, doi: 10.1109/ICRERA.2014.7016421.

[74] C. Li, R. Burgos, I. Cvetkovic, D. Boroyevich, L. Mili, and P. Rodriguez, "Evaluation and control design of virtual-synchronous-machine-based STATCOM for grids with high penetration of renewable energy," *2014 IEEE Energy Convers. Congr. Expo. ECCE 2014*, pp. 5652–5658, 2014, doi: 10.1109/ECCE.2014.6954176.

[75] W. Zhang, D. Remon, I. Candela, A. Luna, and P. Rodriguez, "Grid-connected converters with virtual electromechanical characteristics: experimental verification," *CSEE J. Power Energy Syst.*, vol. 3, no. 3, pp. 286–295, 2017, doi: 10.17775/CSEEJPES.2015.00790.

[76] D. Remon, A. M. Cantarellas, J. D. Nieto, W. Zhang, and P. Rodriguez, "Aggregated

model of a distributed PV plant using the synchronous power controller," *IEEE Int. Symp. Ind. Electron.*, vol. 2015-Septe, pp. 654–659, 2015, doi: 10.1109/ISIE.2015.7281546.

[77] D. Remon, A. M. Cantarellas, and P. Rodriguez, "Equivalent Model of Large-Scale Synchronous Photovoltaic Power Plants," *IEEE Trans. Ind. Appl.*, vol. 52, no. 6, pp. 5029–5040, 2016, doi: 10.1109/TIA.2016.2598718.

[78] D. Remon, A. M. Cantarellas, W. Zhang, I. Candela, and P. Rodriguez, "Enhancement of the stability of a distribution system through synchronous PV," *IEEE Power Energy Soc. Gen. Meet.*, vol. 2016-Novem, pp. 1–5, 2016, doi: 10.1109/PESGM.2016.7741525.

[79] D. Remon, A. M. Cantarellas, J. Martinez-Garcia, J. M. Escaño, and P. Rodriguez, "Hybrid solar plant with synchronous power controllers contribution to power system stability," *2017 IEEE Energy Convers. Congr. Expo. ECCE 2017*, vol. 2017-Janua, pp. 4069–4076, 2017, doi: 10.1109/ECCE.2017.8096709.

[80] E. Rakhshani, D. Remon, A. M. Cantarellas, J. M. Garcia, and P. Rodriguez, "Virtual Synchronous Power Strategy for Multiple HVDC Interconnections of Multi-Area AGC Power Systems," *IEEE Trans. Power Syst.*, vol. 32, no. 3, pp. 1665–1677, 2017, doi: 10.1109/TPWRS.2016.2592971.

[81] S. D'Arco, J. A. Suul, and O. B. Fosso, "Control system tuning and stability analysis of Virtual Synchronous Machines," in *2013 IEEE Energy Conversion Congress and Exposition*, 2013, pp. 2664–2671, doi: 10.1109/ECCE.2013.6647045.

[82] S. D'Arco, J. A. Suul, and O. B. Fosso, "Small-signal modelling and parametric sensitivity of a Virtual Synchronous Machine," in *2014 Power Systems Computation Conference*, 2014, pp. 1–9, doi: 10.1109/PSCC.2014.7038410.

[83] S. D'Arco, J. A. Suul, and O. B. Fosso, "A Virtual Synchronous Machine implementation for distributed control of power converters in SmartGrids," *Electr. Power Syst. Res.*, vol. 122, pp. 180–197, 2015, doi: https://doi.org/10.1016/j.epsr.2015.01.001.

[84] S. D'Arco, J. A. Suul, and O. B. Fosso, "Small-signal modeling and parametric sensitivity of a virtual synchronous machine in islanded operation," *Int. J. Electr. Power Energy Syst.*, vol. 72, pp. 3–15, 2015, doi: https://doi.org/10.1016/j.ijepes.2015.02.005.

[85] S. D'Arco and J. A. Suul, "A synchronization controller for grid reconnection of islanded virtual synchronous machines," in *2015 IEEE 6th International Symposium on Power Electronics for Distributed Generation Systems (PEDG)*, 2015, pp. 1–8, doi: 10.1109/PEDG.2015.7223046.

[86] P. Rodriguez, A. Luna, M. Ciobotaru, R. Teodorescu, and F. Blaabjerg, "Advanced Grid Synchronization System for Power Converters under Unbalanced and Distorted Operating Conditions," in *IECON 2006 - 32nd Annual Conference on IEEE Industrial Electronics*, 2006, pp. 5173–5178, doi: 10.1109/IECON.2006.347807.

[87] J. Rocabert, A. Luna, F. Blaabjerg, and P. Rodríguez, "Control of Power Converters

in AC Microgrids," *IEEE Trans. Power Electron.*, vol. 27, no. 11, pp. 4734–4749, 2012, doi: 10.1109/TPEL.2012.2199334.

[88] R. Teodorescu, F. Blaabjerg, M. Liserre, and P. C. Loh, "Proportional-resonant controllers and filters for grid-connected voltage-source converters," *IEE Proc. - Electr. Power Appl.*, vol. 153, no. 5, pp. 750–762, 2006, doi: 10.1049/ip-epa:20060008.

[89] A. Tarraso, J. I. Candela, J. Rocabert, and P. Rodriguez, "Proportional-resonant current controller with orthogonal decoupling on the αβ-reference frame," in *IECON 2017 - 43rd Annual Conference of the IEEE Industrial Electronics Society*, 2017, pp. 1453–1458, doi: 10.1109/IECON.2017.8216247.

[90] D. N. Zmood, D. G. Holmes, and G. H. Bode, "Frequency-domain analysis of three-phase linear current regulators," *IEEE Trans. Ind. Appl.*, vol. 37, no. 2, pp. 601–610, 2001, doi: 10.1109/28.913727.

[91] Y. Hu, Y. Shao, R. Yang, X. Long, and G. Chen, "A Configurable Virtual Impedance Method for Grid-Connected Virtual Synchronous Generator to Improve the Quality of Output Current," *IEEE J. Emerg. Sel. Top. Power Electron.*, vol. 8, no. 3, pp. 2404–2419, 2020, doi: 10.1109/JESTPE.2019.2918386.

[92] X. Zhang, X. Ruan, and Q. Zhong, "Improving the Stability of Cascaded DC/DC Converter Systems via Shaping the Input Impedance of the Load Converter With a Parallel or Series Virtual Impedance," *IEEE Trans. Ind. Electron.*, vol. 62, no. 12, pp. 7499–7512, 2015, doi: 10.1109/TIE.2015.2459040.

[93] X. Liang and C. A.-B.- Karim, "Harmonics and Mitigation Techniques Through Advanced Control in Grid-Connected Renewable Energy Sources: A Review," *IEEE Trans. Ind. Appl.*, vol. 54, no. 4, pp. 3100–3111, 2018, doi: 10.1109/TIA.2018.2823680.

[94] European Commission, "Green Paper - A 2030 framework for climate and energy policies," *COM(2013) 169 Final*, pp. 1–16, 2013, [Online]. Available: http://ec.europa.eu/clima/policies/strategies/2030/documentation_en.htm.

[95] European Council, "European Council (23 and 24 October 2014) Conclusions, EUCO 169/14, CO EUR 13, CONCL 5," *Eur. Counc.*, no. October, pp. 1–15, 2014.

[96] RSA Grid Code Secretariat, "Grid Connection Code for Renewable Power Plants Connected to the Electricity Transmission System or the Distribution System in South Africa," vol. 8, no. July, p. 17, 2014.

[97] H. Berndt, M. Hermann, H. Kreye, R. Reinisch, U. Scherer, and J. Vanzetta, "TransmissionCode 2007 Network and System Rules of the," no. August, 2007.

[98] N. J. Kundur, P. and Balu, *Power System Stability and Control*. McGraw-Hill, 1994.

[99] M. Karimi-Ghartemani and M. R. Iravani, "A method for synchronization of power electronic converters in polluted and variable-frequency environments," *IEEE Trans. Power Syst.*, vol. 19, no. 3, pp. 1263–1270, 2004, doi: 10.1109/TPWRS.2004.831280.

[100] X. Wang, L. Harnefors, F. Blaabjerg, and P. C. Loh, "A unified impedance model of voltage-source converters with phase-locked loop effect," *ECCE 2016 - IEEE Energy*

Convers. Congr. Expo. Proc., 2016, doi: 10.1109/ECCE.2016.7854800.

[101] A. Gómez Expósito, A. J. Conejo, and C. Cañizares, *Electric energy systems : analysis and operation*. Boca Raton: CRC Press, 2009.

[102] M. De Prada-Gil, J. L. Domínguez-García, L. Trilla, and O. Gomis-Bellmunt, "Technical and economic comparison of various electrical collection grid configurations for large photovoltaic power plants," *IET Renew. Power Gener.*, vol. 11, no. 3, pp. 226–236, 2017, doi: 10.1049/iet-rpg.2016.0304.

[103] D. Remon, C. A. Cañizares, and P. Rodriguez, "Impact of 100-MW-scale PV plants with synchronous power controllers on power system stability in northern Chile," *IET Gener. Transm. Distrib.*, vol. 11, no. 11, pp. 2958–2964, 2017, doi: 10.1049/iet-gtd.2017.0203.

[104] F. Jibji-Bukar and O. Anaya-Lara, "Frequency support from photovoltaic power plants using offline maximum power point tracking and variable droop control," *IET Renew. Power Gener.*, vol. 13, no. 13, pp. 2278–2286, 2019, doi: 10.1049/iet-rpg.2019.0211.

[105] D. Yang, X. Wang, F. Liu, K. Xin, Y. Liu, and F. Blaabjerg, "Adaptive Reactive Power Control of PV Power Plants for Improved Power Transfer Capability Under Ultra-Weak Grid Conditions," *IEEE Trans. Smart Grid*, vol. 10, no. 2, pp. 1269–1279, Mar. 2019, doi: 10.1109/TSG.2017.2762332.

[106] E. Serban, M. Ordonez, and C. Pondiche, "Voltage and Frequency Grid Support Strategies Beyond Standards," *IEEE Trans. Power Electron.*, vol. 32, no. 1, pp. 298–309, 2017, doi: 10.1109/TPEL.2016.2539343.

[107] T. Knüppel, J. N. Nielsen, K. H. Jensen, A. Dixon, and J. Østergaard, "Power oscillation damping capabilities of wind power plant with full converter wind turbines considering its distributed and modular characteristics," *IET Renew. Power Gener.*, vol. 7, no. 5, pp. 431–442, 2013, doi: 10.1049/iet-rpg.2012.0030.

[108] R. K. Varma and M. Akbari, "Simultaneous Fast Frequency Control and Power Oscillation Damping by Utilizing PV Solar System as PV-STATCOM," *IEEE Trans. Sustain. Energy*, vol. 11, no. 1, pp. 415–425, 2020, doi: 10.1109/TSTE.2019.2892943.

[109] G. N. Baltas, N. B. Lai, L. Marin, A. Tarrasó, and P. Rodriguez, "Grid-Forming Power Converters Tuned Through Artificial Intelligence to Damp Subsynchronous Interactions in Electrical Grids," *IEEE Access*, vol. 8, pp. 93369–93379, 2020, doi: 10.1109/ACCESS.2020.2995298.

[110] J. Fang, P. Lin, H. Li, Y. Yang, and Y. Tang, "An Improved Virtual Inertia Control for Three-Phase Voltage Source Converters Connected to a Weak Grid," *IEEE Trans. Power Electron.*, vol. 34, no. 9, pp. 8660–8670, 2019, doi: 10.1109/TPEL.2018.2885513.

[111] M. Abdollahi, J. I. Candela, J. Rocabert, M. A. Elsaharty, and P. Rodriguez, "Novel Analytical Method for Dynamic Design of Renewable SSG SPC Unit to Mitigate Low-Frequency Electromechanical Oscillations," *IEEE Trans. Power Electron.*, vol. 35, no. 7, pp. 7532–7544, 2020, doi: 10.1109/TPEL.2019.2956397.

[112] P. Rodríguez, C. Citro, J. I. Candela, J. Rocabert, and A. Luna, "Flexible Grid

Connection and Islanding of SPC-Based PV Power Converters," *IEEE Trans. Ind. Appl.*, vol. 54, no. 3, pp. 2690–2702, 2018, doi: 10.1109/TIA.2018.2800683.

[113] W. Zhang, A. M. Cantarellas, J. Rocabert, A. Luna, and P. Rodriguez, "Synchronous Power Controller with Flexible Droop Characteristics for Renewable Power Generation Systems," *IEEE Trans. Sustain. Energy*, vol. 7, no. 4, pp. 1572–1582, 2016, doi: 10.1109/TSTE.2016.2565059.

[114] C. Verdugo, A. Tarraso, J. I. Candela, J. Rocabert, and P. Rodriguez, "Centralized Synchronous Controller based on Load Angle Regulation for Photovoltaic Power Plants," *IEEE J. Emerg. Sel. Top. Power Electron.*, pp. 1–1, 2020, doi: 10.1109/jestpe.2020.2995339.

[115] V. Gevorgian and B. O. Neill, "Demonstration of Active Power Controls by Utility-Scale PV Power Plant in an Island Grid," *6th Sol. Integr. Work.*, no. February, 2016.

[116] E. Bullich-Massagué, R. Ferrer-San-josé, M. Aragüés-Peñalba, L. Serrano-Salamanca, C. Pacheco-Navas, and O. Gomis-Bellmunt, "Power plant control in large-scale photovoltaic plants: Design, implementation and validation in a 9.4 MW photovoltaic plant," *IET Renew. Power Gener.*, vol. 10, no. 1, pp. 50–62, 2016, doi: 10.1049/iet-rpg.2015.0113.